The Role of TBX22 in Craniofacial Development

Aya Hoshino

Thesis submitted in partial fulfilment of the degree of Doctor of Philosophy at University College London

January 2011

Neural Development Unit

Institute of Child Health

University College London

30 Guilford Street

London WC1N 1EH

I, Aya Hoshino confirm that the work presented in this thesis is my own. Where information has been derived from other sources, I confirm that this has been indicated in the thesis.

ABSTRACT

Cleft lip and/or cleft palate are a heterogeneous group of disorders that rank among the commonest birth defects known, affecting 1 in 700 births worldwide. The underlying cause is poorly understood, with a complex interaction of genes and environmental factors being implicated. Nevertheless, several important genetic causes have been identified, including that of X-linked cleft palate and ankyloglossia (CPX). CPX is a semi-dominant condition caused by mutations in *TBX22* which encodes a T-box containing transcription factor. *TBX22/Tbx22* is highly conserved and expressed in the developing palatal shelves as well as at the base of the tongue, medial and lateral nasal prominences and periocular mesenchyme in both human and mouse embryos.

This project set out to better understand the functional role of TBX22 using *Tbx22* null mouse model that is characterised by overt or submucous cleft palate, ankyloglossia and choanal atresia. Microarray analysis of E13.5 palatal shelves dissected from wild type and *Tbx22* null mice revealed a global upregulation of muscle genes such as myosin and muscle actin in the null palatal shelves. Key myogenic regulatory factors *MyoD* and *myogenin* were moderately upregulated. Increased expression was independently confirmed using real-time PCR. *In vitro* analysis in a mammalian cell line using luciferase reporter assays and chromatin immunoprecipitation showed that TBX22 could repress the *MyoD* promoter and was capable of interacting with its promoter regions. This may provide a link between lack of *Tbx22* and upregulation of muscle markers. These results support a hypothesis that *MyoD* is a possible direct target gene of TBX22. In addition, decreased cell proliferation in the *Tbx22* null palatal shelves was observed, along with reduced expression of *Cyclin D2*. This indicates that TBX22 has a role in the regulation of cell proliferation during palate development as well as a previously identified role in osteoblast differentiation and maturation.

ACKNOWLEDGEMENTS

First and foremost I would like to thank my supervisors Dr Philip Stanier and Prof. Gudrun Moore for their supervision and support throughout this project. I especially owe thanks to Dr Philip Stanier for his assistance and encouragement during the writing of this thesis.

I would like to express thanks to Dr Erwin Pauws for his guidance and advice on technical aspects of the experimental part of this study, and for his assistance during the writing of this thesis.

I would like to acknowledge and thank the members of Neural Development Unit to whom at some stage of the work I have come to for help.

I would like to thank the Child Health Research Appeal Trust and Overseas Research Students Awards for funding this project.

Finally, and most of all, I thank my parents for their support and encouragement. I would also like to make special mention of Kana, Kouta and all my friends in Japan who have supported me throughout.

CONTENTS

LIST OF FIGURES

LIST OF TABLES

ABBREVIATIONS

BMP	Bone morphogenetic protein
cDNA	Complementary DNA
CL	Cleft lip
CL/P	Cleft lip and/or cleft palate
CLP	Cleft lip with or without cleft palate
CLPED1	CLP with ectodermal dysplasia
CNC	Cranial neural crest
CO_2	Carbon dioxide
CP	Cleft palate
CPO	Cleft palate only
CPX	X-linked cleft palate with ankyloglossia
cRNA	Complementary RNA
C-terminal	Carboxy-terminal
DEPC	Diethylpyrocarbonate
DMEM	Dulbecco's modified eagle's medium
DMSO	Dimethyl sulphoxide
DNA	Deoxyribonucleic acid
dNTPs	Deoxyribonucleotide triphosphates
EDTA	Ethylenediaminetetraacetic acid
EEC	Ectodactyly, ectodermal dysplasia and CLP
EMT	Epithelial-mesenchymal transformation
FBS	Foetal bovine serum
FCS	Foetal calf serum
FGF	Fibroblast growth factor
g	Times gravity
GAPDH	Glyceraldehyde 3 phosphate dehydrogenase
H_2O	Water
HA	Hyaluronic acid
HEK 293T	Human embryonic kidney 293 T cells
kb	Kilobase
MEE	Medial edge epithelium

MES	Midline epithelial seam
MMP	Matrix metalloprotease
MRF	Myogenic regulatory factor
mRNA	Messenger RNA
N-terminal	Amino-terminal
PBS	Phosphate buffered saline
PCR	Polymerase chain reaction
PFA	Paraformaldehyde
RNA	Ribonucleic acid
rpm	Revolutions per minute
rRNA	Ribosomal ribonucleic acid
RT-PCR	Reverse transcription polymerase chain reaction
SDS	Sodium dodecyl sulphate
SUMO	Small ubiquitin-like modifier
TAE	Tris acetate EDTA
TBE	T-box element
TBX	T-box transcription factor
TCS	Treacher Collins syndrome
TE	Tris EDTA
TGF	Transforming growth factor
v/v	Volume/volume
VDWS	Van der Woude syndrome
VPI	Velopharyngeal insufficiency

CHAPTER 1: INTRODUCTION

1 INTRODUCTION

1.1 Overview of craniofacial development

The craniofacial structures of the mammalian embryo are composed of cells derived from all three germ layers which are endoderm, mesoderm and ectoderm (Sperber et al., 2001). By the middle of the third week of development, each of these layers starts to follow specific developmental instruction to form the five craniofacial primordia or prominences. These are the frontonasal prominence, a pair of maxillary and a pair of mandibular prominences, which become distinct structures during early in the fourth week of development (Figure 1.1). The maxillary and mandibular prominences are both derived from the first branchial arch, a structure that is populated with cranial neural crest (CNC) cells that migrate from the anterior neural folds. The first branchial arch and particularly the CNC population is especially important in the morphogenesis of the face as the developing maxillary and mandibular prominences will go on to form the upper and lower jaw. Meanwhile, the frontonasal prominence forms the forehead and the horseshoe-shaped medial and lateral nasal processes surrounding the nasal pits, which are the future nares.

The midline fusion of the mandibular prominences occurs first to form the lower lip and lower jaw (mandible) as well as the chin and the lower cheeks. The upper lip and upper jaw (maxilla), nose and primary palate are then formed during fusion of the medial and lateral nasal and maxillary prominences, which also separate the nasal pits from the stomodeum. The maxillary prominences eventually form the maxilla, zygomatic bone and the secondary palate. The maxillary and mandibular prominences also merge laterally to form the corners of the mouth. As embryonic development continues, the cells of CNC origin eventually give rise to the bone, cartilage and ligaments while mesenchymal cells of mesodermal origin give rise to the muscles and vascular endothelia.

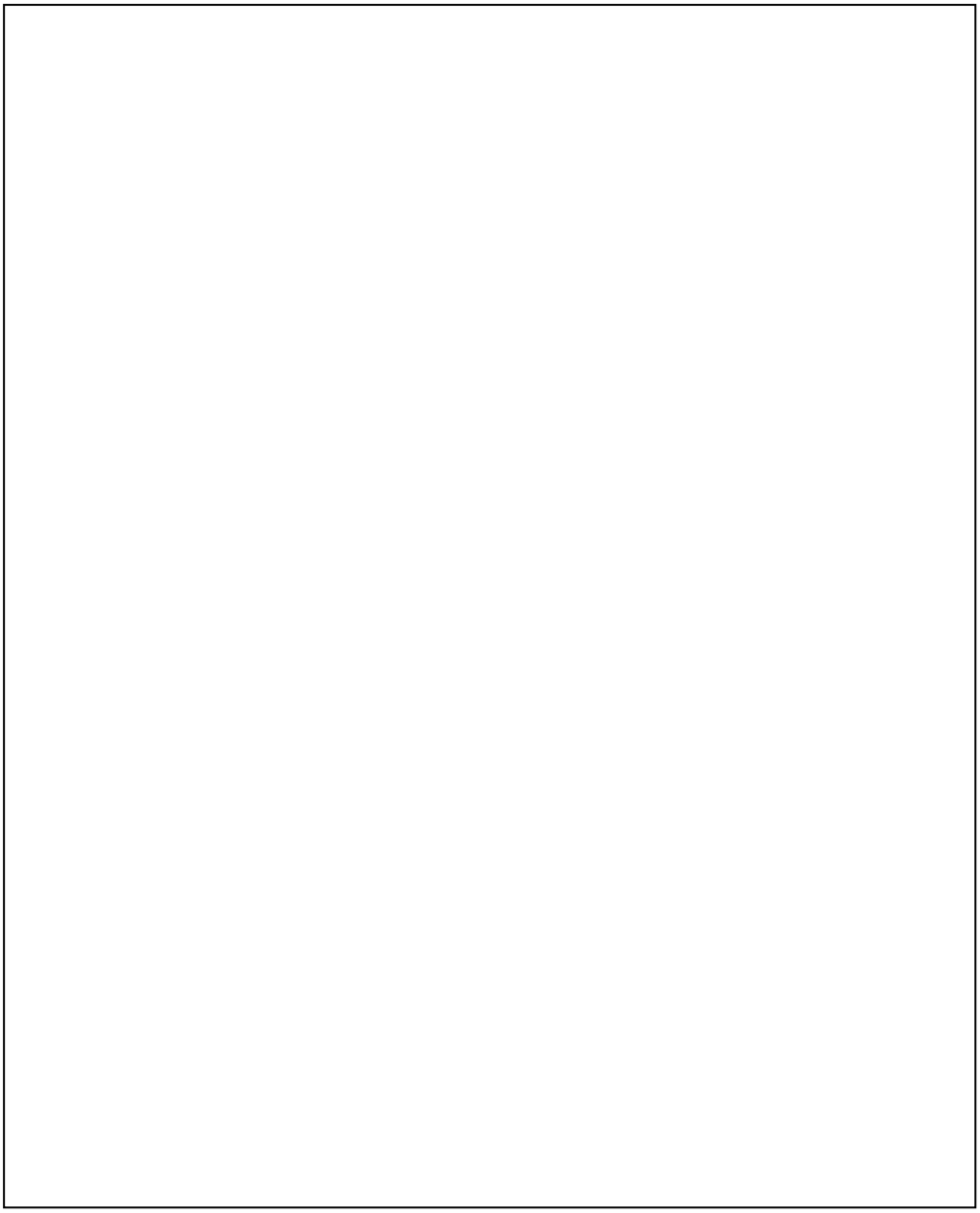

Figure 1.1 Schematic depiction of facial morphogenesis
Schematic depiction of facial morphogenesis at the fourth, fifth, sixth and seventh weeks of human development (Sperber et al., 2001). The figure is not shown due to copyright issues.

1.2 Origin of the cranial neural crest

The CNC cells are an important cellular component of the developing head. The CNC arises as a transient ectodermal component that is formed during anterior neurulation. It contains a population of pluripotent cells that migrate into the branchial arches and the frontonasal process (Figure 1.2), some of which differentiate into ectomesenchyme and eventually give rise to the craniofacial skeletal and connective tissues (Weston et al., 2004; Smith and Schoenwolf, 1997; Hall, 1999; LaBonne and Bronner-Fraser, 1999).

CNC migration follows stereotypical directional routes which are regulated by various cues of both intrinsic genetic factors and extrinsic signals which in turn establish unique positional identity of the CNC subpopulations (Minoux and Rijli, 2010). The migration process itself is facilitated by chemoattractant and repellent factors. The most important intrinsic factors for establishing positional identity are homeobox (Hox) genes and distal-less homeobox (*Dlx*) genes. Specific patterns of *Hox* gene expression in each branchial arch gives inter-arch rostro-caudal identity (Hunt et al., 1991). *Dlx* genes, on the other hand, are involved in specification of intra-arch dorso-ventral identity (Depew et al., 2005). External signals such as endothelin 1, FGF, BMP and SHH are as important in establishing and maintaining the CNC (reviewed in Minoux and Riji, 2010).

The appropriate positioning and segregation of the CNC into each branchial arch combined with intrinsic and extrinsic signals are then translated into differentiation of cells to distinct cell types later on, including bone, cartilage, cranial ganglia and the connective tissue of the head and neck. For example, the palatal shelves are mainly composed of mesenchymal cells derived from the ectomesenchymal CNC cells, which eventually differentiate into osteoblasts and form palatal bones (Figure 1.3) (Ito et al., 2003). Thus normal palatogenesis is reliant on appropriate CNC migration, proliferation and differentiation. The importance of neural crest development is highlighted by a mouse model for Treacher-Collins syndrome, where haploinsufficiency for *Tcof1* results in altered CNC cell formation and proliferation causing craniofacial malformations including cleft palate (Dixon et al.,

2006). Another study reports that A/WySn mouse strain is cleft-liable (CL/P) as a result of a defect in CNC migration and lower mitotic activity (Young et al., 2007).

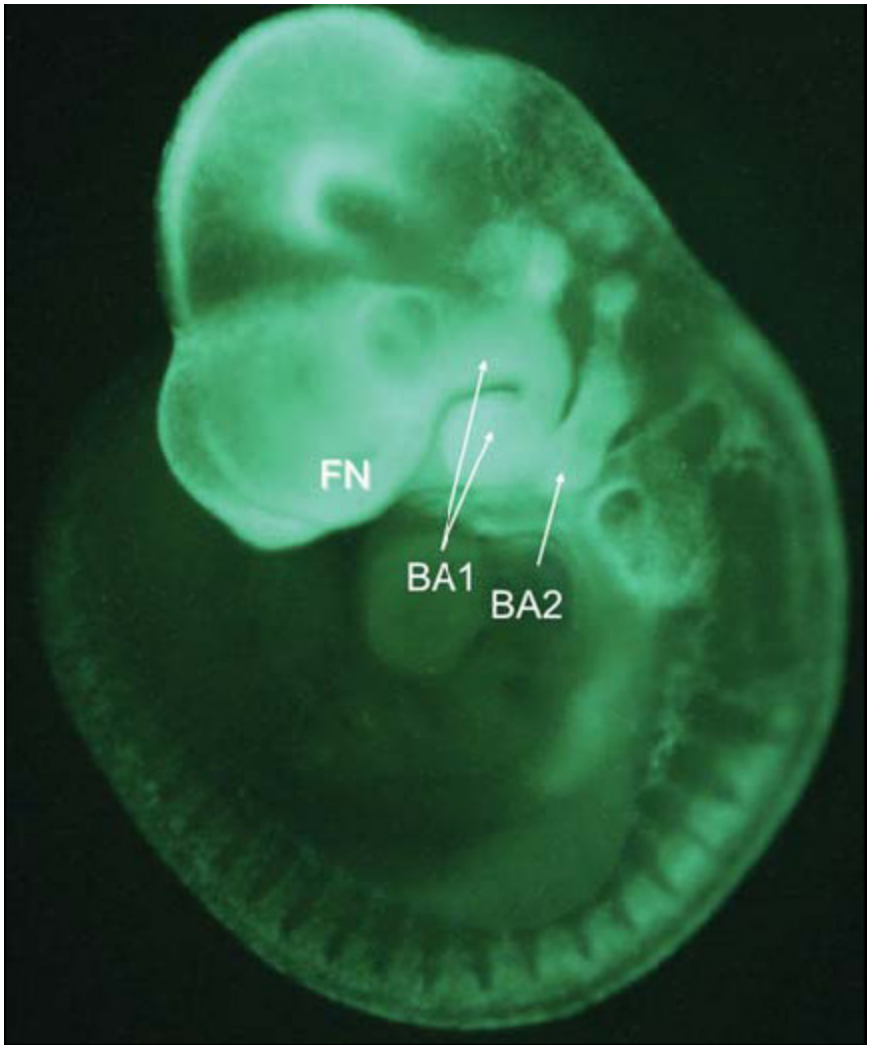

Figure 1.2 Migration of cranial neural crest cells during early development
Neural crest cells are labelled with enhanced green fluorescent protein (EGFP) in *Wnt1-Cre/Z-EG* transgenic mouse embryo at E9.5. EGFP expression is observed in the first and second branchial arches (BA1 and BA2) and in the frontonasal region (FN) (Greene and Pisano, 2010). Permission to reproduce this material has been granted by John Wiley & Sons.

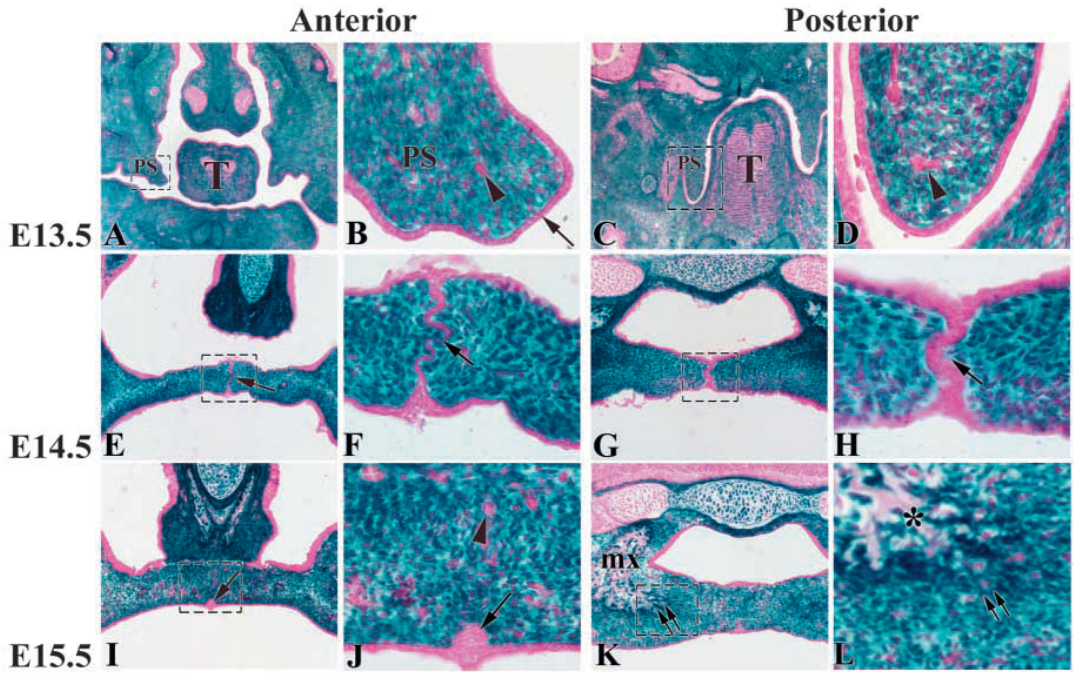

Figure 1.3 Contribution of CNC cells during palate development
CNC-derived palatal mesenchymal cells are marked by β-galactosidase (blue) in *Wnt1-Cre;R26R* mice. B, D, F, H, J and L are magnified pictures of A, C, E, G, I and K. CNC-derived cells contribute significantly to the palatal mesenchymal cells along the anterior to posterior regions. There are few non-CNC-derived cells (pink) within the developing palate (arrowhead). Arrows in E, F and H indicate the midline epithelium at E14.5. Arrows in I and J indicate remaining of the midline epithelium and double arrows in K and L indicate aggregated CNC cells at E15.5. The palatal epithelium is non-CNC-derived, indicating a distinct embryonic origin. MX, maxilla; PS, palatal shelf; T, tongue; *, the forming palatal bone (Ito et al., 2003). Permission to reproduce this material has been granted by The Company of Biologists.

1.3 Palate development

In mouse, palate development starts at around embryonic day (E) 10.5 and is completed by E16.5, which roughly corresponds to the end of the fifth week until the twelfth week of gestation in human.

The mammalian palate consists of the primary and the secondary palate; the former is derived from the intermaxillary segment and contributes to an anterior small part of the hard palate, whereas the latter is formed from the maxillary prominences and represents the majority of the hard and soft palates (Sadler, 2004). In embryology, the secondary palate is a primordium of the future hard and soft palates which separates the oral cavity from the nasal cavity in many adult vertebrates. Development of the palate in the embryonic stage involves several steps including the development and migration of CNC, the formation of the secondary palate and ossification in the anterior to midposterior palate to form the palatal bones as well as the formation of soft palate, as described below.

1.3.1 Formation of the primary palate

Development of the primary palate starts at around E10.5 in mouse (Diewert and Wang, 1992). It is formed from a mesenchymal mass called the intermaxillary segment derived from merging of medial nasal prominences. The intermaxillary segment contributes to the central upper lip as well as the primary palate which are initially continuous. The intermaxillary segment then grows into the stomodeum to form the primary palate which later fuses with the secondary palate (Hinrichsen, 1985). The primary palate consists of a premaxillary part of the maxilla anterior to the incisive foramen and represents a small part of adult hard palate.

1.3.2 Formation of the secondary palate

The development of the secondary palate starts at around E11.0. It involves the budding and vertical growth of a pair of palatal shelves from the maxillary prominences that elevate horizontally above the tongue and fuse to form a continuous palate (Figure 1.4). The three fundamental steps required for normal

palate development are described in this section, along with the gene pathways known to be involved in the process that have been greatly informed and facilitated by the use of many transgenic animal models.

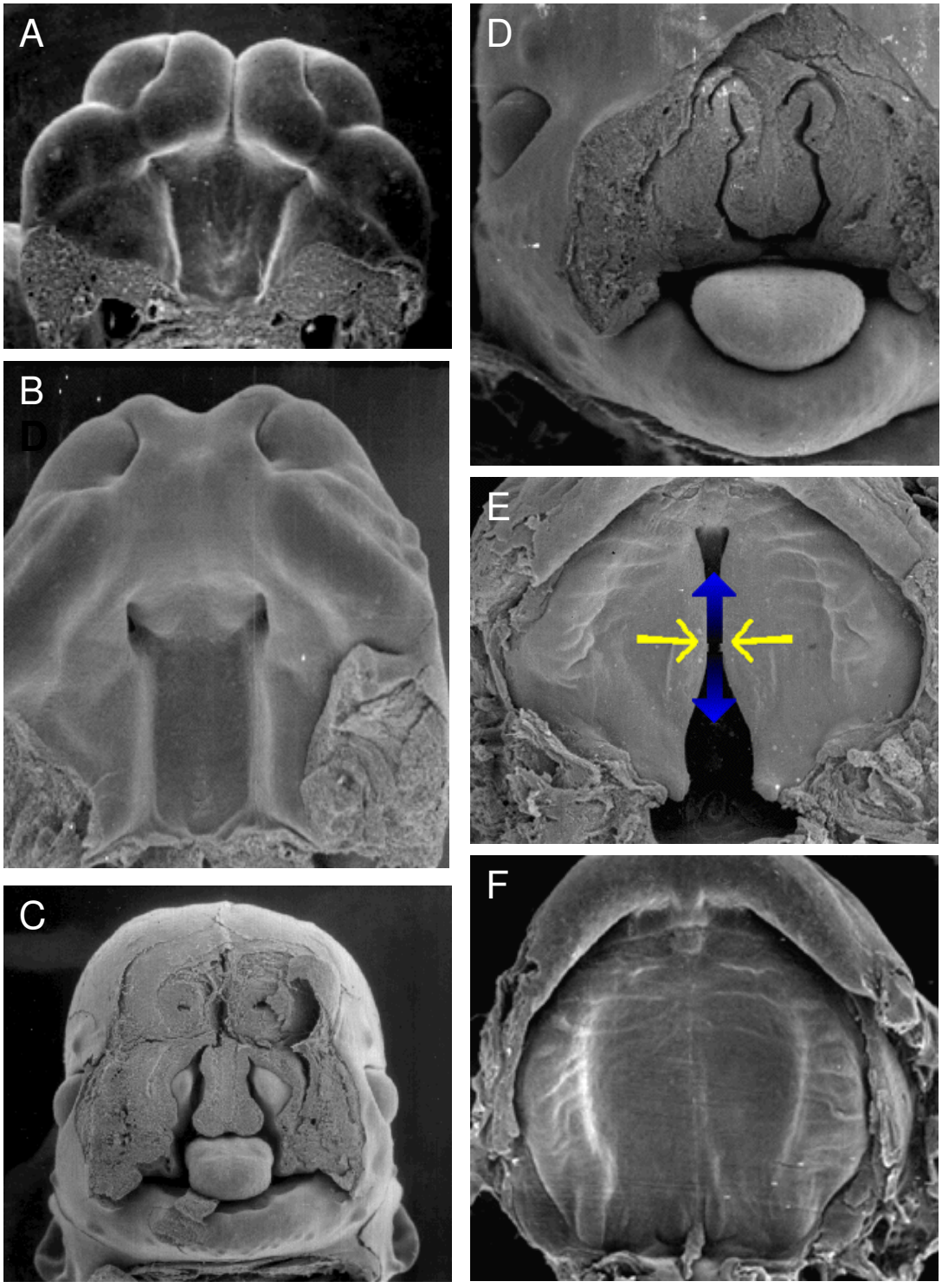
A
B
D
C
D
E
F

Figure 1.4 Development of the secondary palate
The palatal shelves appear from the maxillary prominences at E11.0 (the sixth week in human development) (A). The shelves grow laterally either side of the tongue from E12.0 to E14.0 (the seventh to eighth weeks in human development) (B, C). The shelves elevate above the tongue at around E14.5 to E15.0 (the ninth week in human development) (D). The shelves initially grow horizontally towards each other close to the midpoint (yellow arrows) and fuse anteriorly and posteriorly (blue arrows) between E15.0 to E16.5 (the ninth to tenth weeks in human development) (E, F). These images are used with permission from Professor Kathy Sulilk from http://www.med.unc.edu/embryo_images/unit-hednk/hednk_htms/.

1.3.2.1 Palatal shelf growth

Two palatal shelf outgrowths appear from the maxillary prominences at E11.0 and extend downward on each side of the tongue between E12.0 to E14.0. At this stage, the tongue sterically limits the lateral movement of the palatal shelves. The palatal mesenchymal cells are rapidly proliferating in the growing shelves, and many signalling pathways are implicated in the shelf growth.

In fact, defects in the growth of the palatal shelves are the most common causes of cleft palate in transgenic animal models. Examples include *Msx1*, *Fgf10*, *Fgfr2b*, *Tgfβr2*, *Pdgfc*, *Sim2* and *Lhx8* mutant mice (Satokata and Maas, 1994; Rice et al., 2004; Ito et al., 2003; Ding et al., 2004; Shamblott et al., 2002; Zhao et al., 1999). *Msx1* mutant mice exhibit a cleft palate caused by a reduced proliferation of the palatal mesenchyme (Satokata and Maas, 1994; Zhang et al., 2002). The cleft palate phenotype can be rescued by *Bmp4* which is thought to act downstream of *Msx1* (Zhang et al., 2002). Null mutations in *Fgf10* and its receptor *Fgfr2b* result in cleft palate due to reduced cell proliferation in both the palatal epithelium and mesenchyme, which is caused by altered SHH signalling downstream of *Fgf10*/*Fgfr2b* (Rice et al., 2004). In fact, a loss of either the ligand or receptor results in loss of *Shh* and *Ptc* expression. In addition to the altered cell proliferation, apoptosis is elevated in the mutant epithelium which may also contribute to the growth defects. Also, a loss of *Fgf10* in epithelia causes inappropriate fusion of the shelves to the surfaces of the tongue and mandible (Rice et al., 2004; Alappat et al., 2005). The palatal shelves of *Tgfβr2*, *Pdgfc*, *Sim2* and *Lhx8* mutant mice grow vertically and elevate normally but the shelves fail to contact in the midline as a result of retarded horizontal growth (Ito et al., 2003; Ding et al., 2004; Shamblott et al., 2002; Zhao et al., 1999). Cleft palate as well as calvaria defects are caused by conditional inactivation of *Tgfβr2* in neural crest cells (Ito et al., 2003). *Pdgfc* mutant mice have a complete cleft of the secondary palate which results in perinatal death (Ding et al., 2004). In this case, the defect may have been caused by disruption of CNC cell migration into the palatal shelves as Pdgf signalling is important for this process (Eberhart et al., 2008). Disruption of *Sim2* results in craniofacial malformations including a cleft of the secondary palate (Shamblott et al., 2002). The mutant mice are postnatal lethal due to aerophagia which is

characterised by accumulation of air in the gastrointestinal tract. *Lhx8* mutant mice develop an isolated cleft of the secondary palate without other craniofacial defects, indicating that the cleft palate is caused by an intrinsic factor (Zhao et al., 1999). Interestingly, deletion of TGF-β type I receptor *Alk5* in the ectoderm and neural crest cells results in an increased apoptosis in the branchial arch and palatal mesenchyme as well as over proliferation in the shelves, leading to cleft palate and severe craniofacial defects (Dudas et al., 2006).

Taken together, normal shelf growth can often be affected by altered cell proliferation and/or apoptosis in the palatal mesenchyme which results in hypoplastic or retarded palatal shelves. As a consequence, they fail to fuse at the midline simply by not making contact and thereby result in a cleft palate.

1.3.2.2 Palatal shelf elevation

Palatal shelf elevation is a rapid process. The anterior region flips first, followed by the posterior region (Ferguson, 1988). The exact mechanism of elevation is unknown but some possibilities have been suggested. One of them is an intrinsic force generated within the palatal shelf. There is an accumulation of the extra cellular matrix (ECM) prior to and during the shelf elevation (Larsson, 1960) as well as increased hyaluronic acid which forms hydrated gels that expands the ECM (Ferguson, 1988). The highest concentration of hyaluronic acid is observed in the posterior two third of palatal shelves (Brinkley and Vickerman, 1982; Brinkley and Morris-Wiman, 1984). This causes the ECM to swell and the resultant intrinsic force moves the palatal shelves into the horizontal position (Ferguson, 1988). It is also suggested that alignment of type I collagen and mesenchymal cells within the shelves facilitate shelf elevation (Brinkley and Morris-Wiman, 1984; Greene and Pratt, 1976). Apart from intrinsic factors required for shelf elevation to occur normally, the tongue needs to descend first in order to provide space for the horizontal apposition of the palatal shelves. In *Hoxa2*$^{-/-}$ and *Foxf2*$^{-/-}$ animals, the shelves fail to elevate due to mechanical obstruction by the tongue (Wang et al., 2003; Rijli et al., 1993; Barrow and Capecchi, 1999). In the case of *Hoxa2*$^{-/-}$ mice, the tongue anomaly is caused by the failure in the insertion of the hyoglossus muscle into the hyoid bone which in turn sterically limits the shelf movement,

resulting in a cleft. Interestingly, this phenotype is actually rescued by an additional mutation in *Hoxa1* because of its further effect on the hyoid bone, although the overall phenotype is more severe (Barrow and Capecchi, 1999). Similarly, mechanical obstruction by the tongue also causes a cleft phenotype in *Foxf2*$^{-/-}$ (Wang et al., 2003). There are no obvious defects in these mice other than the tongue which does not descend. In addition, the shelves also fail to elevate when they fuse with the tongue or the mandible instead of each other as shown by loss of function mutations in *Jagged2* (Jiang et al., 1998) and *Fgf10* (Alappat et al., 2005). In *Jagged2*$^{-/-}$ mice, the elevation defect is caused because the palatal epithelial cells aberrantly fuse to the tongue and mandible rather than a mechanical obstruction by the tongue. Interestingly, down regulation of *Jagged2* throughout the palatal epithelium, as well as ectopic expression of *Tgfβ3* in the oral epithelium of the palate, have been observed in *Fgf10*$^{-/-}$ mice in which shelf elevation was physically prevented due to adhesion of the shelves to the tongue and mandible (Alappat et al., 2005). Similarly, *Irf6* loss of function mutations in mice results in cleft palate due to epithelial adhesion in the oral cavity which prevents the palatal shelves from elevation (Ingraham et al., 2006; Richardson et al., 2006; Stottmann et al., 2010). Lastly, mutations in *Osr2* (Lan et al., 2004) and *Pdgfc* (Ding et al., 2004) cause cleft palate due to delayed elevation that is caused by abnormal mesenchymal cell proliferation.

Taken together, in terms of defective shelf elevation observed *in vivo*, it is often caused either by mechanical obstruction by the tongue or inappropriate fusion of shelves to the oral surface.

1.3.2.3 Palatal shelf fusion

Following elevation of the palatal shelves, they continue to grow horizontally towards each other until eventually the medial edge epithelial (MEE) cells contact and fuse between E14.5 to E15.0. This palatal fusion occurs in a zip-like manner toward anterior and posterior directions starting from the point of first contact which is between the third and the fourth rugae (Biddle, 1980; Sakamoto et al., 1989). The contact of MEE cells forms a midline epithelial seam (MES), which disappears by E15.5 to allow mesenchymal confluence to be achieved. However, in

some transgenic mouse models of cleft palate, the palatal shelves elevate and contact but the MES fails to disappear during the fusion process and thus mesenchymal continuity is not achieved, leading to an increased incidence of cleft palate. The exact mechanism of MES disappearance is controversial and three major hypotheses have been proposed as follows:

i) Apoptosis of MES has been indicated by various studies based on morphological and molecular analyses such as the TUNEL assay (Cuervo and Covarrubias, 2004; Martinez-Alvarez et al., 2000). *In vitro* experiments using cultured palatal shelves however resulted in somewhat different conclusions. In one study, palatal shelves failed to fuse in the presence of apoptosis inhibitors (Cuervo and Covarrubias, 2004) suggesting apoptosis was required, while in another study palatal shelf fusion occured in the presence of the inhibitors suggesting that apoptosis is not a prerequisite for fusion (Takahara et al., 2004). These contradictory results from different laboratories indicated that the *in vitro* systems used may not accurately reflect the *in vivo* situation. A more recent study used conditional transgenics (Cre-LoxP) to mark epithelial cells with β-galactosidase allowing *in vivo* genetic fate-mapping of the MEE (Vaziri et al., 2005). Analysis of these transgenic mice revealed that the β-galactosidase positive cells in the MES eventually aggregated and disappeared from the fusing palate. In addition, the cells in the seam were also positive for the apoptotic marker activated Caspase-3, underscoring the importance of apoptosis in the disappearance of MES. In terms of defective shelf fusion, *Tgfβ3* deficient mice are probably investigated most. The palate develops normally in the mutant up to the point where the shelves make contact at the midline (Kaartinen et al., 1995; Proetzel et al., 1995). However, the MES persists after fusion and fails to degenerate. Apoptosis clearly seems to be important in the seam degeneration as it is reduced in this mutant mouse model (Martinez-Alvarez et al., 2000) which also exhibits an excess proliferation in the MES (Cui et al., 2003).

ii) Epithelial to mesenchymal transformation (EMT) refers to a transdifferentiation of epithelial cells into mesenchymal cells. EMT has originally been proposed following observations in ultrastructural and lipophilic dye cell labelling studies *in vitro* (Shuler et al., 1992; Fitchett and Hay, 1989; Griffith and Hay, 1992). The disadvantages of using lipophilic markers included an inefficient uptake of dye by the MEE cells as well as nonspecific uptake by non-epithelial cells. As an *in vivo* approach, the Cre-LoxP system was used to label and fate map MEE cells (Jin and Ding, 2006). In their system, the cells positive for β-galactosidase were detected even after palatal fusion and some cells had typical morphology of mesenchymal cell, demonstrating the occurrence of EMT which contradicts the finding by Vaziri et al. (2005). Jin and Ding (2006) suggested that this might be because of the different *Cre* transgenic lines used in the two studies.

iii) Migration of the MEE cells along the midline to the nasal and oral epithelia has also been supported by lipophilic dye cell labelling (Carette and Ferguson, 1992) and *in vivo* fate mapping studies (Jin and Ding, 2006). However, it is not clear whether the thinning of the MES was caused by the movement of epithelial cells into the periphery or rather the epithelial cells are driven by the proliferating mesenchymal cells in the fusing palate.

In summary, the fate of MEE cells is still not conclusive but it is likely that a combination of the three mechanisms detailed above may be involved in the disappearance of the MES during the fusion process.

1.3.3 Formation of the hard and soft palates

The craniofacial bones are formed by two different processes called intramembranous and endochondral ossifications (Miloro et al., 2004). Both processes are essential during the embryonic development of bone tissue. In particular, the maxillary and palatine bones in the hard palate undergo intramembranous ossification, which does not involve a cartilaginous intermediate

as it does in endochondral ossification. In essence, intramembranous ossification starts with the condensation of mesenchyme followed by the differentiation of immature cells into osteoblasts that deposit mineralised extracellular matrix to form bone tissues. This process is regulated by a complex network of transcription factors and extracellular growth factors.

The ossification process is initiated at around E15.0 in the mouse palate after shelf fusion is complete. At this point, the undifferentiated mesenchymal cells start to condense to form dense aggregate known as intramembranous ossification centre. Once the ossification centre is formed, the mesenchymal cells stop proliferating and start to differentiate into osteoprogenitor cells, a precursor of osteoblasts. Osteoprogenitor cells express *Runx2*, also known as *Cbfa1*, which is a master regulatory transcription factor for the differentiation of the osteoblast lineage (Ducy et al., 1997; Komori et al., 1997; Ducy et al., 2000). Apart from its role during differentiation, RUNX2 also regulates the expression of osteoblast specific proteins such as *Osteocalcin* in terminally differentiated osteoblasts (Ducy and Karsenty, 1995), and its binding sites are present in the regulatory regions of genes involved in the synthesis of bone extracellular matrix (Ducy et al., 2000). *Osterix* is another key controller of osteoblast differentiation which acts downstream of *Runx2* (Nakashima et al., 2002). In fact, bone formation fails to take place without these factors as demonstrated by *Runx2* and *Osterix* deficient mice (Komori et al., 1997; Otto et al., 1997; Nakashima et al., 2002). Growth factors such as bone morphogenetic proteins (BMPs) and fibroblast growth factors (FGFs) are also essential in the differentiation of osteoprogenitor cells into mature osteoblasts (Chen et al., 2004; Agata et al., 2007). For instance, BMP2 is a strong inducer of osteoblastic differentiation in mesenchymal cells (Ryoo et al., 2006), while FGF2 is known to be important in the induction of osteoblast proliferation, although its role in differentiation seems to be stage-specific (Fakhry et al., 2005; Kalajzic et al., 2003). During differentiation and maturation processes, osteoblasts express characteristic markers including Osterix, type I collagen, bone sialoprotein, alkaline phosphatase, osteopontin, osteocalcin and osteonectin. Mature osteoblasts are bone forming cells entirely responsible for the deposition of bone extracellular matrix called osteoid which is mainly composed of type I collagen, and for the regulation of osteoclasts involved in bone resorption. During the mineralisation process, active

osteoblasts line the periphery of the ossification centre and continue to secrete osteoid as well as calcium, magnesium and phosphate ions. Eventually, these inorganic chemicals are combined within the osteoid and mineralised to become bone tissue. Some osteoblasts are trapped and incorporated within the osteoid during the process. These cells are called osteocytes. In the mouse palate, mineralisation within the ossification centre is observed from E15.5 onwards (Pauws et al., 2009a). Intramembranous ossification in the maxilla occurs anteriorly and posteriorly to the infraorbital foramen region, then ossification spreads through the secondary palate. This process results in the formation of the palatine process of the maxilla and the palatine bone accounting for the anterior three fourths and the posterior fourth of the bony hard palate, respectively (Figure 1.5).

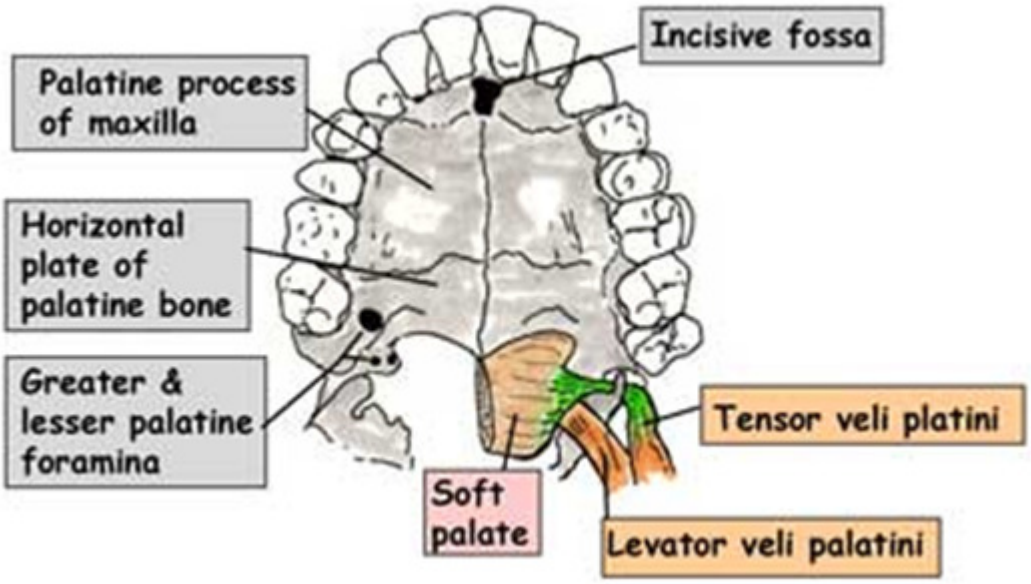

Figure 1.5 Schematic diagram of the hard and soft palates in human
Schematic diagram showing the hard and soft palates in human. Adopted from Instant anatomy, RH Whitaker, NR Borley, 4th edition, Wiley-Blackwell 2010. Permission to reproduce this material has been granted by John Wiley & Sons.

The posterior third of the secondary palate lacks ossification and consists mainly of muscle fibres covered in mucous membrane thereby developing into the soft palate. It mainly serves as a mobile flap to close off nasal cavity during swallowing as well as to direct the airflow during speech and breathing (Stal and Lindman, 2000).

The majority of craniofacial muscles including the muscles of the soft palate are derived from the branchial arch cells of cranial paraxial mesodermal origin (Zhang et al., 1999). In addition, progenitors of other cell lineages including endothelial cells, smooth muscles and connective tissues have been identified in this mesenchymal population (Noden and Francis-West, 2006). In humans, five types of muscles (tensor veli palatini, levator veli palatini, palatopharyngeus, palatoglossus and uvula) are found within the soft palate and attach to nearby hard tissue structures (Figure 1.6). Of these, tensor veli palatini and levator veli palatini insert onto, and palatopharyngeus, palatoglossus and uvula originate from the palatine aponeurosis which is a fibrous lamella found at the posterior border of the hard palate. The same muscles compose the soft palate in mouse but the uvula at the posterior end is absent (Zhang et al., 1999). During the soft palate development, muscles first emerge as mesenchymal condensations both in mouse and human (Cohen et al., 1993; Trotman et al., 1995). The condensation in the mouse palatal shelves starts at E13.5 for the tensor veli palatini followed by levator veli palatini, palatoglossus and palatopharyngeus at around E14.5 (Zhang et al., 1999). Next, they form myoblast fields and then differentiate into myocytes followed by the formation of muscle fibers. The morphology of the palatal muscles in mouse become evident by E15.5 and muscle fibers start to appear at E18.5 (Zhang et al., 1999). The development of muscle is controlled by the network of myogenic regulatory factors such as *MyoD* and *myogenin*, both are well known markers of myogenic lineage that promote differentiation (Arnold and Braun, 1996). Expression of these factors in the head muscles are controlled by specific combinations of transcription factors involving *capsulin*, *MyoR*, *Tbx1*, *Pitx2*, *Isl1*, and *Nkx2.5* in different craniofacial muscles (Tzahor, 2009), although the myogenic regulation specific to the soft palate muscle has not been investigated.

Figure 1.6 Schematic diagram of the soft palate muscle structures in human

In humans, five types of muscles (tensor veli palatini, levator veli palatini, palatopharyngeus, palatoglossus and uvula) are found within the soft palate, while the uvula is absent in mouse. Image is adopted from http://www.neuroanatomy.wisc.edu/virtualbrain/BrainStem/09NA.html. The figure is not shown due to copyright issues.

1.4 Orofacial clefting in humans

Orofacial clefts, particularly clefts of the lip and palate (Figure 1.7), are among the commonest birth defects with an incidence of about 1 in 700 births worldwide but with variability depending on geographic origin and ethnicity (Wyszynski et al., 1996; Vanderas, 1987). Cleft lip and palate are frequently described as multifactorial involving both genetic and environmental risk factors (Murray, 2002). Children born with clefts often suffer from difficulties with feeding, hearing and speech problems which require surgical intervention as well as issues with psychological development and social integration (Schutte and Murray, 1999; Stanier and Moore, 2004). The gold standard treatment for clefts of the lip and palate is plastic surgery, within the care of a multidisciplinary team consisting of surgeons, speech therapists, orthodontists, geneticists, specialist nurses and psychologists. It essentially involves repositioning of tissue and muscles in order to bring the lip muscle (orbicularis oris) into its correct anatomic orientation and rebuild the continuous palate (Millard, Jr. and Latham, 1990; Randall, 1965; Tollefson et al., 2008).

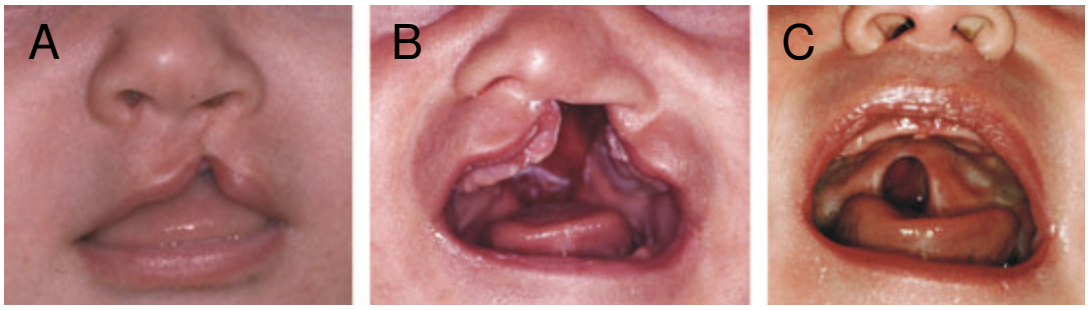

Figure 1.7 Clefts of the lip and palate
Unilateral cleft lip only (A), cleft lip with cleft palate (B), and isolated cleft palate (C) (Jugessur et al., 2009). Permission to reproduce this material has been granted by John Wiley & Sons.

1.4.1 Cleft lip and palate

Orofacial clefts including clefts of the lip and palate are a heterogeneous group of disorders. Clefts of the lip and palate are subdivided into clefts of the lip and/or cleft palate (CL/P) and clefts of the secondary palate only (CP). In addition, CL/P and CP can also be divided into either syndromic or non-syndromic forms depending on whether affected individuals exhibit other phenotypic anomalies. CP is thought to be more frequently associated with other congenital anomalies than CL/P (Mossey and Little, 2002). For CL/P, about 70% of cases are non-syndromic and the rest are associated with other anomalies (Calzolari et al., 2007). For CP, the ratio of non-syndromic to syndromic cases is about 1 to 1 (Calzolari et al., 2004). Some of the better known examples of human congenital syndromes that are associated with CL/P and CP are described in 1.4.3.

The prevalence for CL/P varies related to geographic origin and socioeconomic status (Murray et al., 1997; Vanderas, 1987), but overall, the frequency is about 1 in 700 births worldwide (Murray, 2002; Stanier and Moore, 2004). Geographically, the occurrence of CL/P has been found to be higher in parts of Asia and Latin America than in South Africa, Israel and southern Europe, whereas the rates of CP are higher in parts of northern Europe and Canada than in parts of Latin America and South Africa (Mossey et al., 2009). Ethnicity is clearly an important factor for the variable occurrence of clefts as shown by several studies where the prevalence of orofacial clefts in certain ethnic groups matches to the prevalence of their ethnic origins rather than that observed in the area they have migrated (Croen et al., 1998). Interestingly, CL/P is more frequent in males than in females and varies with different ethnic origins. In white populations for example, the ratio for CL/P is about 2 to 1 (male to female) (Mossey and Little, 2002). On the other hand, CP is slightly more common in females than in males and does not vary with ethnicity. In terms of etiology, CL/P and CP are generally considered to be distinct because families at high risk for CL/P are not at increased risk for CP and vice versa (Jugessur and Murray, 2005). However, the occurrence of both CL/P and CP within the same family are occasionally observed especially in syndromes such as Van der Woude syndrome caused by *IRF6* mutations (Kondo et al., 2002) and CL/P with hypodontia caused by *MSX1* mutations (van den Boogaard et al., 2000).

Anatomically, CL/P involves cleft of the upper lip and anterior part of the maxilla which is either unilateral (one sided) or bilateral (two sided), possibly accompanied by cleft of the secondary palate (Figure 1.8). In the case of CL/P, cleft of the secondary palate is thought to be secondary to disruption of the primary palate. The clinical phenotypes of CP are categorised as follows; complete cleft of the secondary palate in which both the hard and soft palate are affected, cleft of the soft palate in which only the soft palate is split, bifid uvula where the uvula at the posterior end of the soft palate is split, and submucous cleft palate.

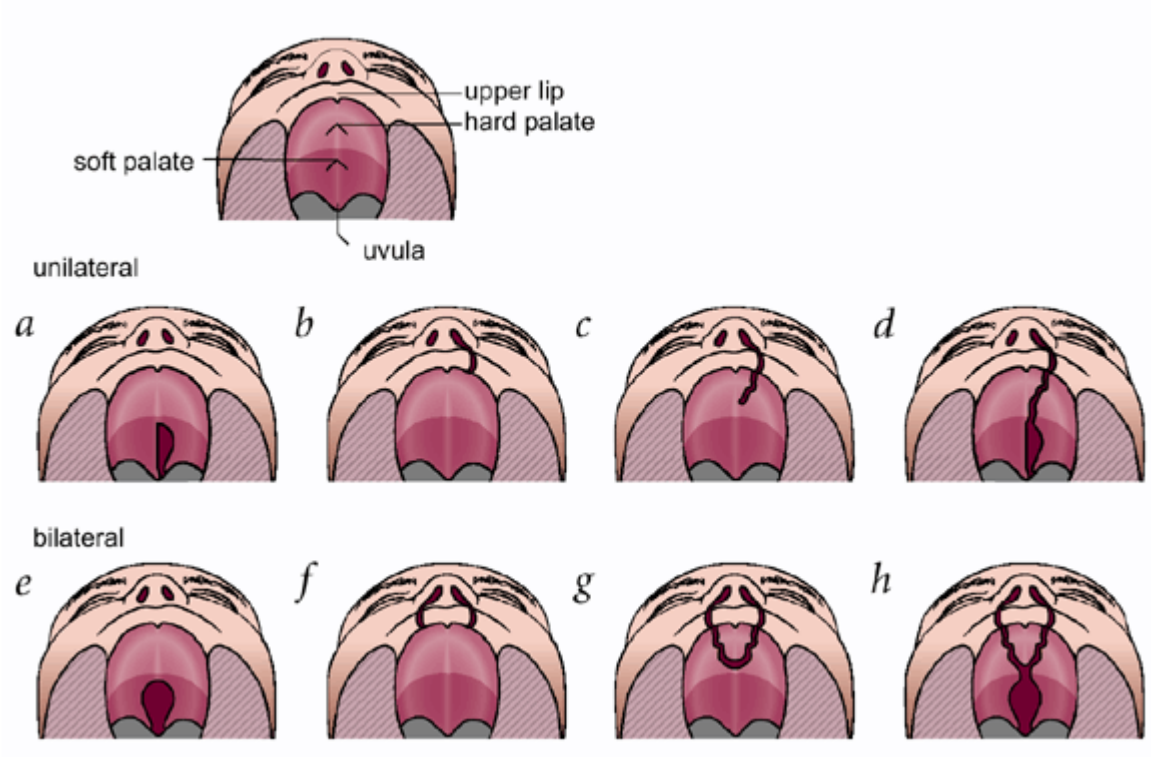

Figure 1.8 Cleft lip and/or palate phenotypes
Normal lip and palate (top panel). Unilateral cleft of the soft palate (a). Unilateral cleft lip (b). Unilateral cleft lip and palate involving the hard palate (c). Unilateral cleft lip and palate involving both the hard and soft palates (d). Bilateral cleft of the soft palate (e). Bilateral cleft lip (f). Bilateral cleft lip and palate involving the hard palate (g). Bilateral cleft lip and palate involving both the hard and soft palate (h) (Muenke, 2002). Permission to reproduce this material has been granted by Nature Publishing Group.

Submucous cleft palate is sometimes considered a clinical subcategory of cleft palate and is certainly part of the spectrum of developmental defects affecting the palate. It is also thought to be the most common type of cleft found in the posterior palate in human (Moss et al., 1988). It is called 'submucous' because the cleft is found within the mucous membrane which makes the diagnosis difficult because it is not as visually obvious as overt cleft palate. A submucous cleft palate can be further classified into a submucous cleft of the hard palate which is characterised by a bony defect within the hard palate, and a submucous cleft of the soft palate which is characterised by a lack of muscular tissue and abnormal positioning of the muscles within the soft palate. Classic submucous cleft palate, usually diagnosed during a thorough physical examination, is characterised by having a bifid uvula, palatal muscle diastasis, and a notch in the posterior surface of the hard palate (Figure 1.9), whereas occult submucous cleft palate lacks one or more of these overt anatomical findings with muscle malposition and hypernasal speech may be the only features (Stal and Hicks, 1998; Gosain et al., 1996). One of the functional findings found in classic submucous cleft palate and in some occult submucous cleft palate cases is velopharyngeal insufficiency (VPI) which is caused by an incorrect insertion of the palatine muscle onto the hard palate (Kaplan, 1975). VPI is associated with speech problems such as hypernasal resonance, feeding difficulties and otitis media (Gosain et al., 1996). There are few, if any, mouse models reported with classical features of submucous cleft palate apart from *Tbx22* null mouse featured in this thesis (Pauws et al., 2009a). Others include *Tgfβr2* (Xu et al., 2006) and *Tshz1* (core et al., 2007) mutant mice, although they feature cleft or premature truncation of the soft palate and could also be classified as partial clefts of the soft palate rather than a true submucous cleft. However, we strongly suspect that many cases of submucous clefts in mouse models may have gone unnoticed.

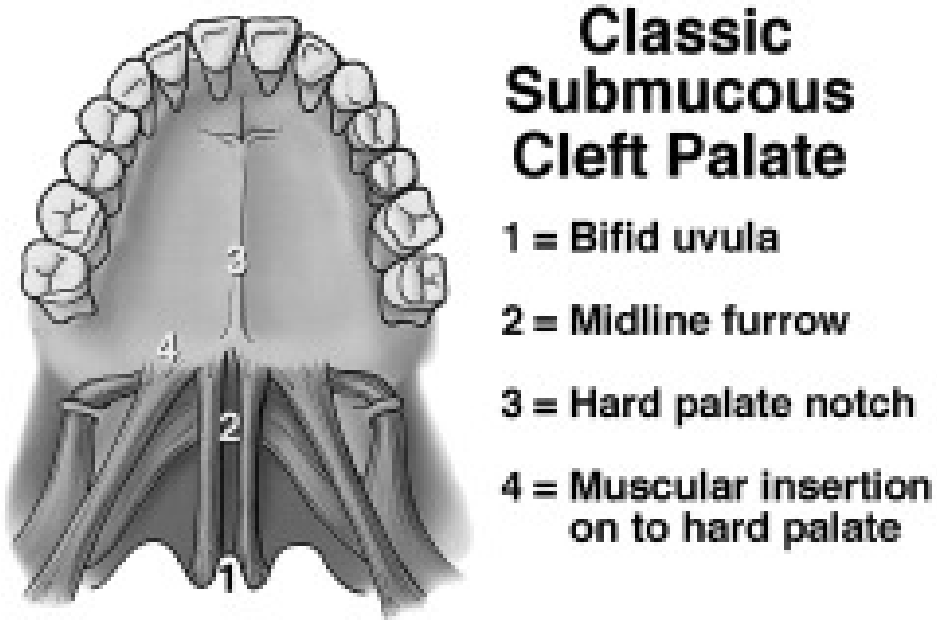

Figure 1.9 Physical features found in classic submucous cleft palate
Classic submucous cleft palate is characterised by a bifid uvula, palatal muscle diastasis, and a notch in the posterior surface of the hard palate (Stal and Hicks, 1998). Permission to reproduce this material has been granted by Allen Press Publishing Services.

1.4.2 Environmental factors

Cleft lip and palate are multifactorial disorders that involve environmental factors in the occurrence of cleft cases as well as genetic factors. Various studies have suggested environmental risk factors such as maternal smoking, alcohol consumption, poor diet, viral infection, drugs and teratogens, many of which have been associated with increased risks of orofacial clefts (Prescott et al., 2001). Other studies suggest that the occurrence of birth defects recur in families partly due to shared environment (Hayes, 2002).

Cigarette smoking during pregnancy has been almost uniformly associated with increased risks of both CL/P and CP possibly due to hypoxia, with the population attributable risk can be as high as 20% (Munger et al., 1996; Shaw and Lammer, 1999; Little et al., 2004; Honein et al., 2007). Alcohol consumption during pregnancy however, has been associated in some studies (Romitti et al., 1999; Chevrier et al., 2005) but not others (Meyer et al., 2003), making it uncertain. The risk increases when smoking or alcohol consumption are combined with certain allelic variants of cleft susceptible genes such as *TGFβ3* and *MSX1* (Romitti et al., 1999) indicating interaction or cumulative effects of environmental and genetic factors. In terms of nutrition, low intake of B-complex vitamins and deficient or excessive vitamin A are suggested to increase the risks of clefts (Finnell et al., 2004; Munger, 2002). In fact, supplementation of multivitamins in early pregnancy has been associated with a reduced prevalence of orofacial clefts (Krapels et al., 2004b; Krapels et al., 2004c). Similarly, folic acid antagonists are linked to the risk of orofacial clefts in human (Hernandez-Diaz et al., 2000). However, it has not been clearly established if folate supplementation reduces the risk of clefts. For instance, a reduced prevalence of orofacial clefts has been reported following folate fortification of grain in the U.S.A. (Yazdy et al., 2007) but this was not consistent in some other countries (Botto et al., 2006). Other nutrients such as zinc could also affect the occurrence of orofacial clefts (Krapels et al., 2004a; Tamura et al., 2005). The use of chemotherapeutic drugs during pregnancy is also associated with orofacial clefts. These include cholesterol-lowering drugs such as statins (Edison and Muenke, 2004) and a range of anti-epileptic drugs (Wide et al., 2004; Goldman, 1984). In terms of viral infection, having influenza during first couple of months of

pregnancy has been associated with a higher prevalence of CL/P (Acs et al., 2005). In this case, fever seemed to be blamed since the risk was reduced when antifever drugs were used. Still, it is interesting to note that genes such as *PVRL1* and *IRF6*, both involved in immune response, are associated with orofacial clefts in CLPED1 (Suzuki et al., 2000) and Van der Woude syndrome (Kondo et al., 2002) respectively (detailed in 1.4.3).

1.4.3 Genetic factors

The importance of genetic factors in the occurrence of human orofacial clefts has been illustrated in various ways from sibling and twin studies, to mapping of orofacial cleft susceptibility loci as well as identification of causative genes.

Familial clustering of orofacial clefts is well known and reflected in a high recurrence risk within families and between siblings (Lie et al., 1994; Wyszynski et al., 1998; Sivertsen et al., 2008). In twin studies, the concordance rate in monozygotic twins (40-60%) is much higher than that has been observed for dizygotic twins (3-5%), indicating a strong genetic involvement in orofacial clefts, but also implying a role of other factors such as environmental risks which are discussed above.

The identification of genetic loci and genes associated with CL/P has been an area of intense research. Linkage studies have suggested several loci susceptible to CL/P in regions on chromosomes 1, 2, 4, 6, 14, 17, 19 and X (Schliekelman and Slatkin, 2002; Prescott et al., 2000; Zeiger et al., 2003), although the number of loci suggested varies among studies. More recently, genome-wide association study, a powerful method to examine almost all the genes in individuals, has been used to identify a susceptibility locus on 8q24 for nonsysndromic CL/P (Birnbaum et al., 2009). The number of genes associated with human orofacial clefts is remarkably less than those identified in animal models for clefts but the list is expanding. These include *IRF6*, *TGFβ3*, *MSX1*, *MSX2*, *FGFR1*, *FGFR2*, *FGF8*, *FOXE1*, *p63*, *PDGFC*, *PVRL1*, *GABRB3*, *TBX10*, *TBX22*, *SATB2*, *GLI2*, *JAG2*, *SPRY2*, *LHX8*, *SK1*, *MTHFR* and *RARA* (reviewed in Jugessur et al., 2009). Those that have been identified in human are mostly the result of mapping and sequencing genes

responsible for monogenic and syndromic forms of clefts. In addition, exome sequencing has identified genes linked to Kabuki and Miller syndromes in which cleft palate is one of a clinical components (Ng et al., 2010b; Ng et al., 2010a). Exome sequencing is a relatively new technique to efficiently sequence the coding regions to discover novel genes. Powerful techniques such as this exome sequencing and whole-genome association studies are expected to play important roles in identification of genes for orofacial clefts in the future. Some of the most investigated cases in which genetic factors play an important role in human cleft phenotypes are detailed below.

1.4.3.1 Van der Woude syndrome (VDWS) and popliteal pterygium syndrome (PPS)

The two allelic autosomal dominant disorders VDWS (OMIM 119300) and PPS (OMIM 119500) are caused by mutations in the interferon regulatory factor 6 (*IRF6*) gene (Kondo et al., 2002). VDWS is a good model for isolated CL/P because the majority of patients exhibit only minor additional phenotypes such as lip pits and hypodontia while about 15% of patients do have isolated CL/P. PPS is clinically similar to VDWS but include additional phenotypes of popliteal pterygium, syngnathia, syndactyly, toe/nail abnormalities and genitor-urinary malformations. Mice deficient for *Irf6* have cleft palate along with abnormal skin and limb development (Kondo et al., 2002; Ingraham et al., 2006) which resemble clinical features of VDWS and PPS. It has been demonstrated that there is a genotype-phenotype correlation in that missense mutations that affect DNA binding cause PPS while the majority of missense mutations that do not affect DNA binding result in VDWS (Kondo et al., 2002). Later, the involvement of *IRF6* as a risk factor in the occurrence of isolated CL/P was demonstrated (Zucchero et al., 2004). More recently, a common SNP was identified in a highly conserved enhancer element of *IRF6* which essentially disrupted the binding site for AP-2α (Rahimov et al., 2008). AP-2α is known to be involved in craniofacial development (Schorle et al., 1996) and AP-2α chimeric mice show facial dysmorphology (Nottoli et al., 1998). Along with the finding that mutations in *TFAP2A*, a gene encodes for AP-2α, cause branchio-oculo-facial (BOF) syndrome in human which is a cleft palate-craniofacial disorder (Milunsky et al., 2008; Stoetzel et al., 2009), it is likely that

IRF6 and AP2-α are placed in the same pathway during craniofacial development in human as well as in mouse.

1.4.3.2 Malformation syndromes caused by mutations in p63

CL/P is a major feature in four of the five developmental disorders caused by mutations in the tumour protein P63 that are characterised by orofacial clefts, limb abnormalities and ectodermal dysplasia (van Bokhoven and Brunner, 2002). There is a clear genotype-phenotype correlation depending on the position of mutations (Celli et al., 1999; Celli et al., 1999; Rinne et al., 2007). In mice, *p63* is expressed in the branchial arch ectoderm and has a role in craniofacial and limb development (Yang et al., 1999). A heterozygous mutation in this gene has also been associated with non-syndromic CL/P (Leoyklang et al., 2006). Recently, P63 and IRF6 have been reported to cooperatively regulate epithelial proliferation and differentiation during palate development (Thomason et al., 2010; Moretti et al., 2010), linking the pathogenesis of syndromes caused by these two genes.

1.4.3.3 Orofacial clefting and tooth agenesis

MSX1 was found to be associated with orofacial clefting and tooth agenesis (OMIM 106600) in a family carrying a missense mutation following its original description in a null mouse with a similar phenotype (van den Boogaard et al., 2000; van den Boogaard, 2004; Satokata and Maas, 1994). Subsequently, a screen of 917 non-syndromic CL/P cases identified mutations in 2% of patients (Jezewski et al., 2003), although functional testing was not used to confirm that these were causative mutations. *Msx1* is known to be required for expression of *Bmp4*, *Bmp2* and *Shh*, which are all implicated in craniofacial development (Zhang et al., 2002) and suggest their genetic interaction in the craniofacial structure. *BMP4* has recently been associated with cleft lip as well as microform and subepithelial lip defects that are considered to be part of the CL/P spectrum (Suzuki et al., 2009). The mouse homolog of this gene appears to play important roles in lip and palate fusion also (Liu et al., 2005).

1.4.3.4 Kallman syndrome and Apert syndrome

A number of FGF signalling molecules and their receptors are expressed in the craniofacial region during development (Bachler and Neubuser, 2001) and are interesting candidates for orofacial clefts. A comprehensive sequencing study in individuals with non-syndromic CL/P involving members of the FGF signalling pathway identified a small number of nonsense and missense mutations in *FGFR1*, *FGFR2*, *FGFR3* and *FGF8* (Riley et al., 2007). Kallman syndrome (OMIM 147950) is an autosomal dominant disorder with hypogonadism and anosmia, caused by mutations in *FGFR1*. 5-10% of these patients have craniofacial malformations including CL/P (Dode et al., 2003). Apert syndrome (OMIM 101200) which is caused by mutations in *FGFR2*, includes about 75% of patients with CP or bifid uvula (Kreiborg and Cohen, Jr., 1992).

1.4.3.5 Cleft lip and palate-ectodermal dysplasia syndrome (CLPED1)

An autosomal recessive disorder CLPED1 (OMIM 225060) also known as Margarita Island syndrome is caused by homozygosity for a common mutation W185X in poliovirus receptor-related 1 (*PVRL1*) (Suzuki et al., 2000). It encodes a cell-cell adhesion molecule nectin-1 which is expressed in the medial edge epithelia of the palatal shelves as well as in the olfactory and skin surface epithelia and in the ectodermal component of tooth buds in mice (Suzuki et al., 2000). Heterozygosity for this common mutation and some other variants in *PVRL1* were later associated with isolated CL/P (Sozen et al., 2001; Avila et al., 2006), indicating a contribution of *PVRL1* in the occurrence of non-syndromic CL/P.

1.4.3.6 X-linked cleft palate and ankyloglossia (CPX)

The causative gene for CPX (OMIM 303400) was located in Xq21 region by linkage analyses in Icelandic, Native North American Indian and Manitoba Menonite kindreds (Gorski et al., 1992; Gorski et al., 1994; Stanier et al., 1993; Moore et al., 1987). Later, sequence analysis of CPX patients from the same families and two previously unreported Brazilian families identified *TBX22* as the causative gene (Braybrook et al., 2001). Patients were found to have frame shift, splice site, nonsense and missense mutations, which essentially result in a complete

loss of function of the gene in affected males (Braybrook et al., 2001; Braybrook et al., 2002). Mutations in TBX22 were also found to account for 4-8% of all non-syndromic cases of isolated cleft palate (Marcano et al., 2004).

The cleft phenotype varies between patients and even within family members ranging from a submucous cleft palate (50%), complete cleft of the secondary palate (20%), cleft of the soft palate, bifid uvula or absent tonsils, all frequently but not always accompanied by ankyloglossia (tongue-tie) (Figure 1.10) (Stanier and Moore, 2004). Family members who share an identical mutation can have either cleft palate or ankyloglossia, or both, indicating that these defects are caused independent of each other and partially penetrant. In males, cleft palate phenotype is highly penetrant and often present with ankyloglossia (78%) (Marcano et al., 2004). In addition to the males being affected, CPX is inherited in a semi-dominant manner where female carriers can also display a range of phenotypes from complete cleft of the secondary palate and ankyloglossia to unaffected (Bjornsson et al., 1989). Among one third of carrier females affected by CPX, 16% present with cleft palate regardless of ankyloglossia, while many carriers only have ankyloglossia without cleft palate (Marcano et al., 2004). The reason for the difference in penetrance between males and females are not known but may be due to variable non-random X-inactivation.

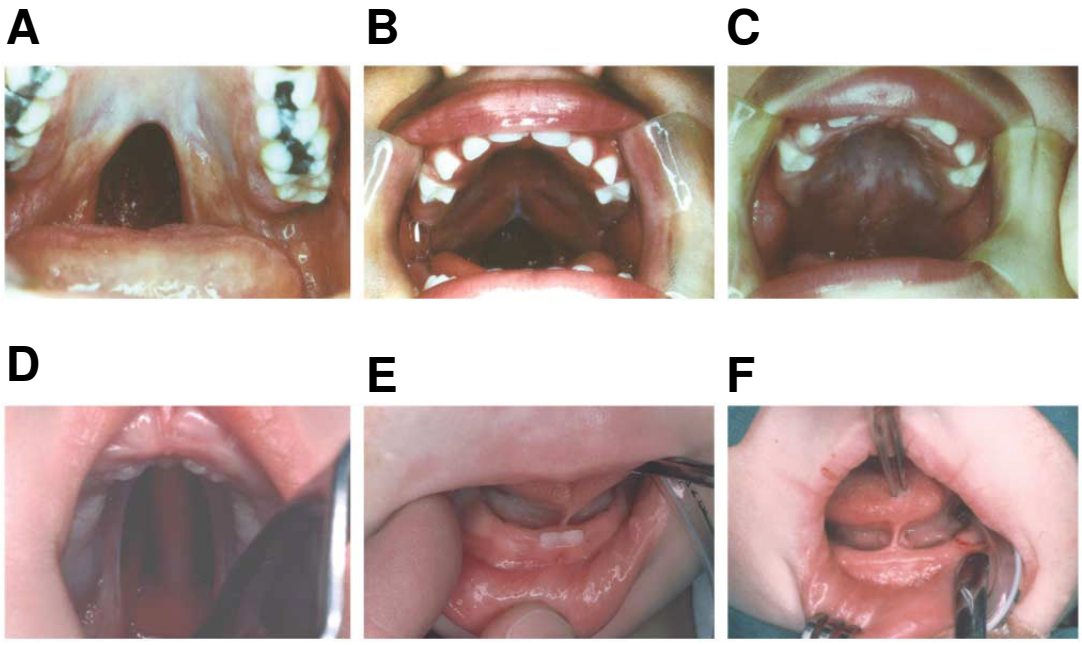

Figure 1.10 Physical features found in CPX patients
Isolated cleft palate (A), a less severe partial cleft with ankyloglossia (not shown) (B), a partial cleft in the process of repair (C), a complete cleft of the secondary palate (D), ankyloglossia (E), ankyloglossia in a patient with bifid uvula (not shown) (F) (Stanier and Moore, 2004). Permission to reproduce this material has been granted by Oxford University Press.

TBX22 is composed of eight coding exons and an alternative non-coding exon which is located about 10kb upstream of the first coding exon (Andreou et al., 2007). The gene encodes a 520 amino acid protein which contains a highly conserved T-box DNA binding domain of about 180 amino acids in its N-terminal half. *In vitro* experiments have demonstrated that the protein acts as a transcriptional repressor and is capable of autoregulation via the distal promoter P0 located immediately upstream of the non-coding exon (Andreou et al., 2007). Also, the protein was shown to undergo post-translational modification with the small ubiquitin-like modifier (SUMO-1) at the lysine 63 (K63) residue (Andreou et al., 2007). SUMO modification is known to have diverse effects on target protein activity but SUMOylation of transcriptional factors are often associated with inhibition of transcription (Gill, 2005). In this case, SUMOylation of TBX22 is required for its repressor activity (Andreou et al., 2007).

Previous data reporting the expression of *TBX22* indicated that it was found by *in situ* hybridisation in the tongue and mandible during the time of palatogenesis (eighth to twelfth weeks), as might be expected from the patient's phenotypes, and to a lesser extent also in brain, heart, limb, kidney, stomach, eye and intestine, as detected by RT-PCR (Braybrook et al., 2001). To date, no defects have been associated with these organs in CPX patients. Detailed temporal and spatial analyses of *TBX22*/*Tbx22*/*tbx22* expression in human, mouse, chick and zebrafish revealed a general agreement between species (Braybrook et al., 2002; Bush et al., 2002; Haenig et al., 2002; Herr et al., 2003; Jezewski et al., 2009). In the human embryo, the gene is expressed in the developing facial mesenchyme by the end of sixth week of development. The highest expression is observed in the palatal shelves, the nasal septum and at the base of the tongue prior to palatal shelf elevation (Figure 1.11) (Braybrook et al., 2002). The expression is stronger medially than laterally in the growing palatal shelves. It continues through to week eight but is significantly reduced by week nine at which time the palatal shelves have elevated, and made contact to fuse to form the palate (Braybrook et al., 2002). Similarly in mouse embryos, craniofacial *Tbx22* expression is detected anteriorly at the base of the tongue in the vicinity of the frenulum region, which corresponds to the ankyloglossia phenotype in CPX. It is also present in the medial and lateral nasal prominences and in the periocular mesenchyme around the eyes. Most

significantly, its expression is detected medially and posteriorly in the palatal shelves before palatal fusion at E13.5 (Braybrook et al., 2002; Bush et al., 2002; Herr et al., 2003). Mice deficient for *Tbx22* predominantly exhibit a closed but submucous cleft palate (94%) or more occasionally an overt cleft palate (6%). The mice also have a detectable ankyloglossia (100%) but with the additional feature of unilateral or bilateral choanal atresia (75%), which is not currently a recognised feature of CPX (Pauws et al., 2009a). Submucous cleft palate is very well known to the cleft surgeon but is less well documented in the literature, nevertheless it is a frequent and possibly predominant feature in CPX families, suggesting that *Tbx22* null mouse will be a good model to study mechanisms underlying the CPX phenotype.

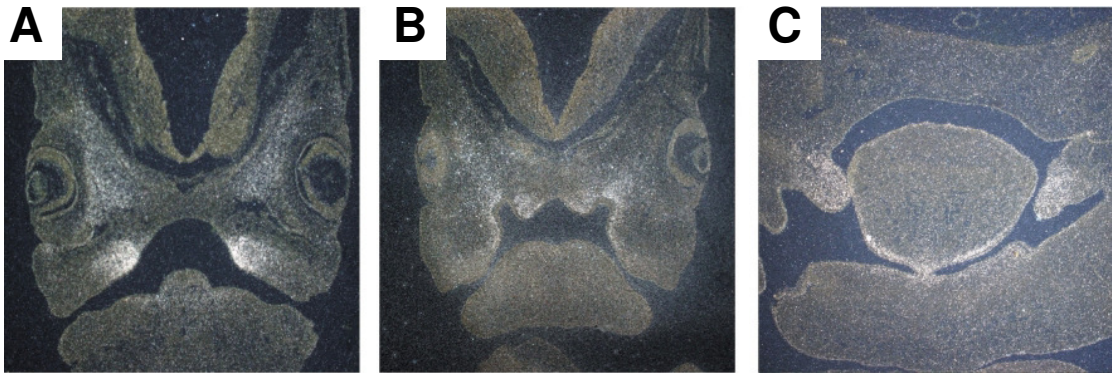

Figure 1.11 *TBX22* expression pattern in human embryo
TBX22 in situ hybridisation of Carnegie stage 19 (A and B) and Carnegie stage 20 (C) human embryo transverse sections (Braybrook et al., 2002). Strong expression is detected in the developing palatal shelves, the nasal septum/oronasal membrane and at the base of the tongue. Permission to reproduce this material has been granted by Oxford University Press.

1.5 Tongue development

In this section, development of the tongue with particular relevance to the ankyloglossia malformation associated with the CPX phenotype is discussed.

1.5.1 Embryonic development of the tongue

The tongue starts to develop as the *tuberculum impar* and the two lateral lingual swellings at around E11, followed by the elevation of the hypobranchial eminence. By E13, under normal circumstances, a selective degeneration occurs at the tip of the tongue which is facilitated by programmed cell death or apoptosis and resorption of the developing skeletal muscle in the anterior region of the tongue, leaving a thin lingual frenulum as the only attachment (Paulson et al., 1985; Morita et al., 2004). This effectively frees the distal end of the tongue from the mandible.

1.5.2 Ankyloglossia

Ankyloglossia, also known as tongue-tie, is a congenital anomaly caused by a short, thick lingual frenulum. The severity varies from a mild form with a slight impairment of tongue mobility, to a severe form where the tongue is closely attached to the floor of the mouth (Suter and Bornstein, 2009). The reported prevalence of ankyloglossia varies between 0.1% to 10.7 % and males in general are more affected than females but no ethnic predispositions have been found (Suter and Bornstein, 2009).

The pathogenesis of ankyloglossia is unclear. In most cases, ankyloglossia presents in isolation of other congenital anormalies. However, it is also found in several human syndromes including CPX (Bjornsson et al., 1989; Gorski et al., 1994; Braybrook et al., 2001), Van der Woude syndrome (Kantaputra et al., 2002; Burdick et al., 1987), Kindler syndrome (Hacham-Zadeh and Garfunkel, 1985) and Opitz syndrome (Brooks et al., 1992), suggesting an involvement of genetic components in its manifestation. Maternal cocaine use during pregnancy has been associated with higher occurrence (3.5 times increase) of ankyloglossia in neonates, indicating an involvement of environmental components (Harris et al., 1992).

Ankyloglossia can cause difficulties in feeding and speech as well as affecting mechanical aspects of oral hygiene. Surgical treatment like frenectomy is a routine for this condition which involves a division of the frenulum by cutting its thinnest portion. In some cases, an observation approach is taken as the frenulum recedes naturally while children grow during the first six months to six years of life (Ruffoli et al., 2005).

To date, only two mouse models have been described that exhibit ankyloglossia. One is the *Lgr5* null mice that exhibit aerophagia characterised by a gastrointestinal tract dilation with air and an absence of milk in the stomach, which are neonatal lethal (Morita et al., 2004). They revealed, by histological examination, that the null mice had a severe form of ankyloglossia where the tongue was fused to the floor of the oral cavity and concluded that this could account for the neonatal lethality (Morita et al., 2004). The other is *Tbx22* null mouse that shows a milder form of ankyloglossia compared to *Lgr5* null mice (Pauws et al., 2009a) and is further detailed in 1.8.2.

1.6 Choanae development

This section discusses specific development of the nasal choanae with particular relevance to the developmental disorder choanal atresia, present in *Tbx22* null mice (Pauws et al., 2009a).

1.6.1 Embryonic development of nasal cavity and choanae

In the mouse embryo, development of the nasal cavity starts at around E9.5. At this stage the frontonasal process develops at the rostral side of the stomodeum which consists largely of mesenchyme derived from fore and midbrain neural crest (Jiang et al., 2006). At around E10.0, the surface ectoderm on the ventrolateral part of the frontonasal process starts to thicken and gives rise to the nasal placodes, while the frontonasal process grows and bulges around them. As a result, the nasal placodes invaginate to form nasal pits surrounded by the swelling medial and lateral nasal processes (Hinrichsen, 1985). By E10.5, the shape of the nasal pits convert from round depressions into slits due to rapid growth of the medial nasal processes and the maxillary processes. The epithelial cells of medial and lateral nasal processes start to fuse at E10.5, followed by fusion between the medial nasal and maxillary processes, resulting in the formation of nasal fins. Posteriorly, the fins coalesce to form oronasal membranes that eventually degrade by E12.5 resulting in the formation of choanae, also called the posterior nasal aperture (Jiang et al., 2006; Dupe et al., 2003). The process of oronasal membrane degeneration during choanae development in mouse is depicted in Figure 1.12. Choanae is defined as the opening between the nasal cavity and the nasopharynx therefore permitting air flow between these structures. Though the choanae in human is located more posteriorly than the choanae in mouse, initial formation during embryonic development is similar between the two (Moore and Persaud, 2003). It was shown that the fusing epithelial cells between the medial and lateral nasal processes expressed activated Caspase-3 suggesting that apoptosis plays an important role at least in lip fusion process (Jiang et al., 2006).

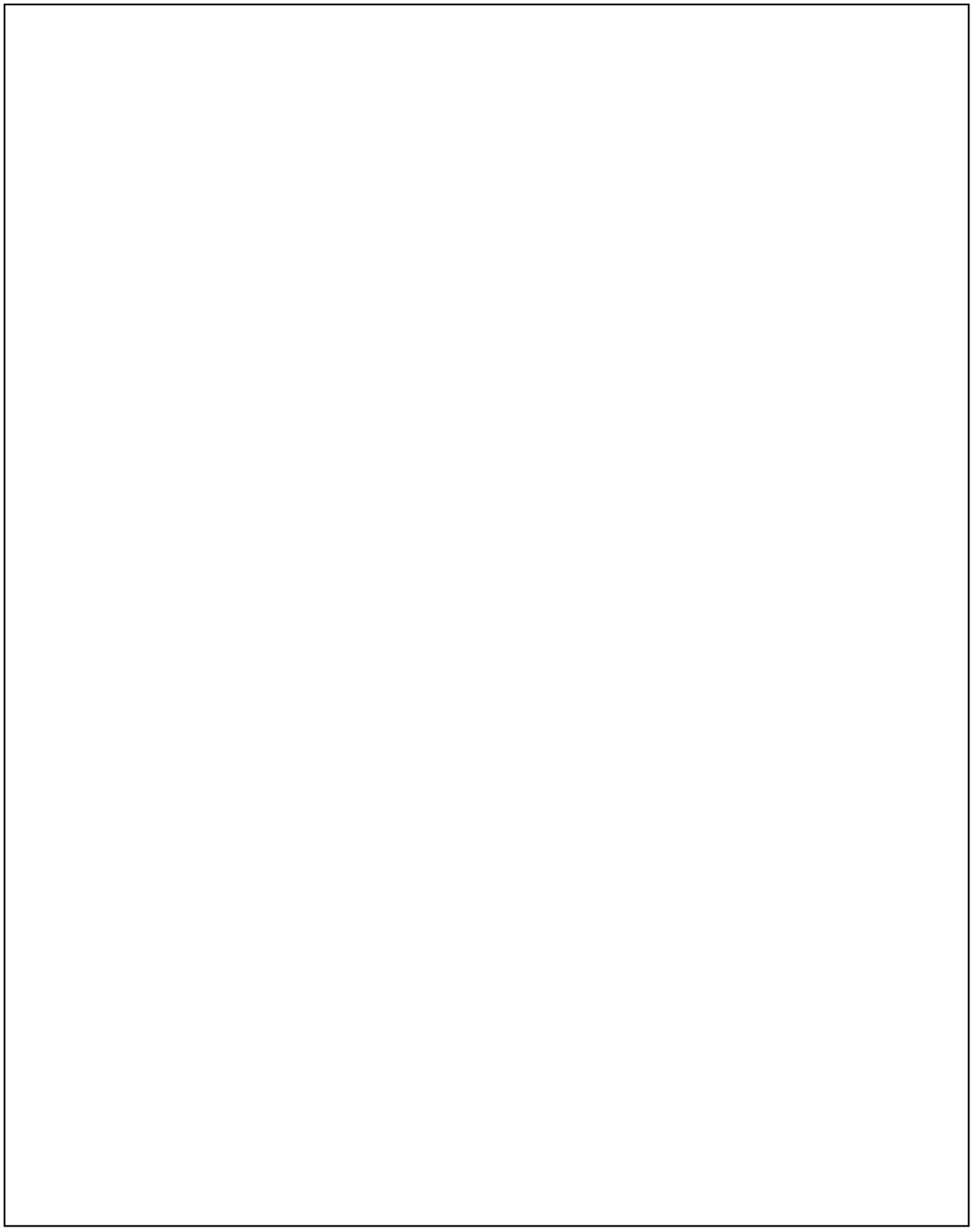

Figure 1.12 Development of the choanae in mouse
At E11.0, choanal pit is unperforated (A and B). At E11.5, interstitial gaps appear in the oronasal membrane (C and D) that enlarge and rupture by E12.5 (E and F). Complete opening of choanae is established by E13.5 (G and H). Arrows in A, C, G and H indicate choanae and rugae are numbered (H). Double arrows in E indicate oronasal grooves. l, lip; ln, lateral nasal process; md, mandibular process; mn, medial nasal process; mx, maxillary process; n, nasal canal; p, primary palate; r, roof of the stomodeum; s, secondary palate; tr, tectal ridge (Tamarin, 1982). The figure is not shown due to copyright issues.

1.6.2 Choanal atresia

Choanal atresia is a congenital craniofacial disorder characterised by narrowing or blockage of the posterior nasal aperture by bony or soft membranous tissue that can manifest unilaterally or bilaterally, which impairs or blocks air passage through the nasal cavity (Feuerstein et al., 1980; Rizzo et al., 1989; Ramsden et al., 2009). Computed tomography scan of the paranasal sinuses and skull base have demonstrated narrowing of posterior nasal cavity, an enlargement of the posterior portion of the vomer and occurrence of stenosis in the anterior nasal cavity associated with choanal atresia (Slovis et al., 1985; Cheung and Prince, 2001; Aslan et al., 2009). It affects one in 5,000-8,000 live births (Ramsden et al., 2009; Krespi et al., 1987; Nemechek and Amedee, 1994). Bilateral choanal atresia can be life threatening after birth because babies are obligate nasal breathers, requiring airway maintenance by oral airway or intubation. About half of the patients with choanal atresia also have associated anomalies (i.e. syndromic form) as in CHARGE syndrome (Coloboma, Heart defects, Atresia of the nasal choanae, Retardation of growth, Genital urinary abnormalities, Ear abnormalities and deafness) where mutations in *CHD7* gene account for most cases (Vissers et al., 2004; Hall, 1979), and craniosynostosis syndromes associated with *FGFR2* mutations including Crouzon, Apert, Pfeiffer, and Antley-Bixler syndromes (Freng, 1978; Burrow et al., 2009). Normally, the disorder is surgically treated by perforating the atresia to establish a nasopharyngeal passage.

The four classical theories that explain the etiology of choanal atresia are: persistence of the buccopharyngeal membrane from the foregut, abnormal persistence or location of mesoderm forming adhesions in the nasochoanal region, abnormal persistence of the nasobuccal membrane of Hochstetter, misdirection of neural crest cell migration and subsequent mesodermal flow (Flake and Ferguson, 1964; Hengerer and Strome, 1982). Although the pathogenesis remains largely unknown, recent molecular and genetic studies have advanced our understanding of the disorder as well as shed light to its pathogenesis. For example, the *Chd7* mutant mice are a good model for CHARGE syndrome (Bosman et al., 2005). Choanal atresia is found along with other congenital anomalies including inner ear malformations, eye and genital abnormalities, cardiovascular defects and cleft

palate that mimic the features of CHARGE syndrome. *Raldh3* null mice also develop choanal atresia (Dupe et al., 2003). Retinoic acid synthesis is suppressed in this mouse line but maternal administration of retinoic acid prevented the phenotype. They observed persistence of *Fgf8* expression in the nasal fins in the null mice which may have accounted for the occurrence of choanal atresia (Dupe et al., 2003). We have also observed choanal atresia in *Tbx22* null mice, which is morphologically very similar to that seen in *Chd7* and *Raldh3* null mice, and is further detailed in 1.8.2.

1.7 T-box family of transcription factors

Brachyury (or *T*, for short tail) mouse mutant was first described in 1927 (Dobrovolskaia-Zavadskaia, 1927). Homozygous mutant mice exhibited embryonic lethality while heterozygous had truncated tails. About 60 years later, the *T* gene was eventually cloned and found to encode a protein of 436 amino acids that was localised into the nucleus (Herrmann et al., 1990; Schulte-Merker et al., 1992). This was accompanied by the finding that the *T* gene was in fact expressed in early mesoderm which became restricted to the notochord, the tissues most affected by the *T* mutation in mice (Wilkinson et al., 1990). Since then, more than 50 members of the same protein family, that all share a highly conserved DNA binding domain called the T-box domain, have been identified throughout metazoan species. In mammals, 17 T-box genes are present, which can be categorised into 5 subfamilies; Brachyury/T, Tbx1, Tbx2, Tbx6 and T-brain 1 (Tbr1) (Figure 1.13) (Naiche et al., 2005). Genes in each subfamily are thought to have arisen as a result of chromosomal duplication and cluster dispersion of a common ancestral gene during evolution (Agulnik et al., 1996; Minguillon and Logan, 2003). For that reason, some genes are expressed in overlapping regions and in some cases they are functionally redundant. Recent advances in molecular biology techniques and the use of spontaneous and targeted mutations in model organisms have suggested important roles of T-box genes in early development, which is further underscored by the association of specific human disorders with most of the T-box genes as described in 1.7.2.

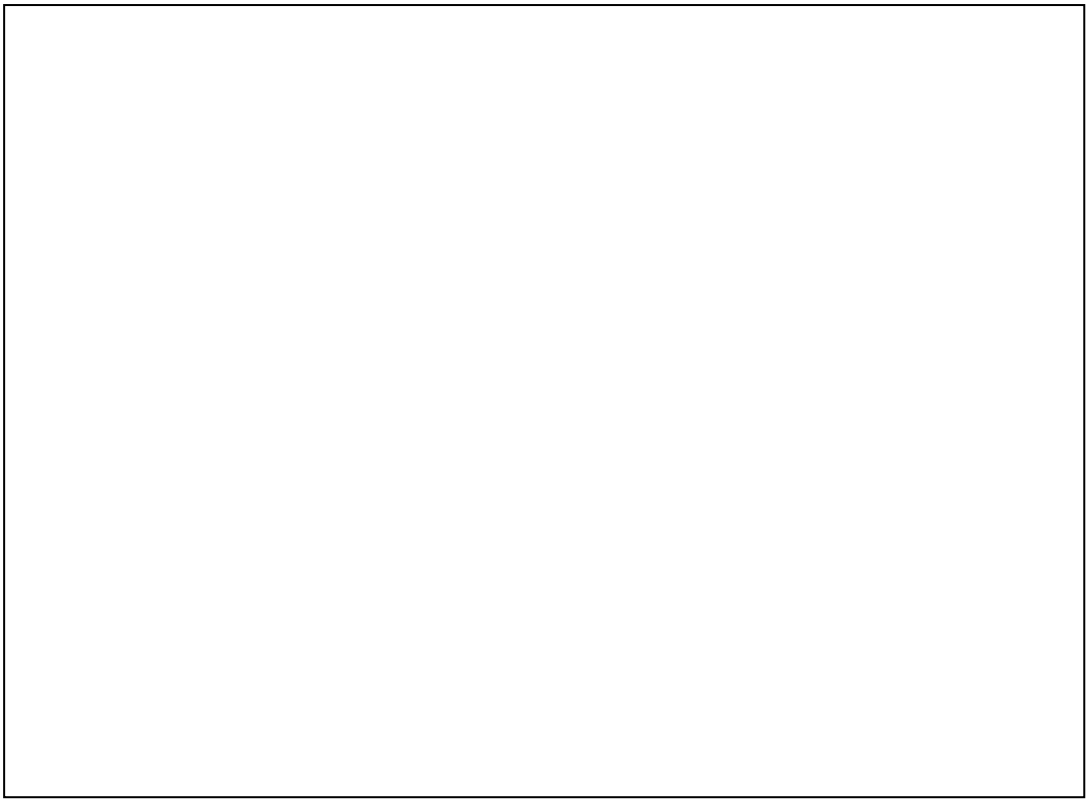

Figure 1.13 Phylogenetic tree of the T-box gene family of transcription factors
Schematic diagram showing a phylogenetic tree of the T-box family members found in vertebrates. All are present in mammals except the zebrafish *Drtbx6* and *Drtbx16* (Naiche et al., 2005). The figure is not shown due to copyright issues.

1.7.1 Properties of T-box transcription factors

1.7.1.1 T-box proteins and DNA binding specificity

T-box proteins are known to act as transcription factors, with the conserved ~180 amino acid T-box DNA binding domain being involved in DNA binding and dimerisation. The T-box binding element (TBE) to which they preferentially bind was first demonstrated by the high affinity of Brachyury to a 20 base pair palindromic sequence T(G/C)ACACCTAGGTGTGAAATT (Kispert and Herrmann, 1993). Brachyury binds as a dimer to this palindromic sequence, with each Brachyury monomer binding to a T-half site (5'-AGGTGTGAAATT-3') (Papapetrou et al., 1997). X-ray crystallography demonstrated an interaction between T-box domain and DNA where a dimer of T proteins appeared to bind to the T-palindrome (Muller and Herrmann, 1997). The T-box domain required for DNA binding is conserved in Brachyury homologues of other species such as *Xenopus* and zebrafish. All of the other T-box proteins are thought to be capable of binding to the T-palindrome with slightly different optimal DNA sequences or half of the sequence, the T-half site as monomers (Ghosh et al., 2001; Lingbeek et al., 2002; Tada and Smith, 2001). Sometimes the preference *in vivo* is for varying numbers of T-half sites arranged in different spacing and orientations (Conlon et al., 2001; Sinha et al., 2000).

1.7.1.2 Transcriptional regulation

Sequences in the N- and C-terminal domains flanking the T-box domain are more divergent among family members. The N-terminus may interact with cofactors and the C-terminus may act as transcriptional activator and/or repressor domain. For example, activation domains are found in C-terminal domains of some T-box proteins such as T and TBX5 (Zaragoza et al., 2004; Kispert et al., 1995). T has two activation and two repression domains in its C-terminal domain. Reporter gene expression experiments demonstrated that the protein worked as a transcriptional activator and the two activation domains acted additively (Kispert et al., 1995). TBX2 and TBX3 are known to repress transcription (Carreira et al., 1998; Habets et al., 2002; Lingbeek et al., 2002). However, depending on context, TBX2 is shown to be capable of both activating and repressing transcription (Paxton et al., 2002).

Some target genes are regulated by T-box proteins without cofactors (Kusch et al., 2002) but as with other transcription factors, many T-box proteins probably control transcriptional regulation in concert with other factors including homeodomain proteins (Bruneau et al., 2001; Hiroi et al., 2001; Lamolet et al., 2001), GATA zinc finger proteins (Stennard et al., 2003) and LIM domain proteins (Krause et al., 2004). For instance, T and TBX19 interact with the Pitx homeodomain proteins (Lamolet et al., 2001), and TBX5 has been shown to interact with the homeodomain protein NKX2-5 (Bruneau et al., 2001; Hiroi et al., 2001). TBX20 specifically and directly interacts with GATA4 and GATA5 in the developing heart (Stennard et al., 2003), and TBX4 and TBX5 interact with PDZ-LIM protein but they do so via different LIM domain repeat (Krause et al., 2004). As there is little sequence conservation outside the common T-box domain, interaction with these factors may define target gene promoter specificity, and whether activation or repression is induced.

1.7.2 T-box genes in development

Since the discovery of *Brachyury*, many other T-box family members have been cloned and their spatiotemporal expression patterns examined. T-box genes are expressed throughout embryonic development where they have biologically important roles in the specification of primary germ layers to the cell fate determination during organogenesis. Here, some of their functional roles in embryonic development and associated human disorders are detailed.

1.7.2.1 The role of T-box genes in extraembryonic tissue development and gastrulation

i) Some T-box genes are involved in extraembryonic tissue development as well as germ layer specification during early embryonic development. The role of T-box genes starts in trophectoderm which subsequently forms placental structures. In normal mouse trophoblast development, the expression of *Eomesodermin* is upregulated but the cells show defects in proliferation and uterine implantation in the absence of *Eomesodermin* (Russ et al., 2000). *Brachyury* and *Tbx4* are also known

to have roles in extraembryonic tissue development. *Brachyury* expression in the caudal primitive streak extends into an extraembryonic outgrowth, the future umbilical cord, whose growth is stunted by a deletion of *Brachyury*, although this may be a secondary effect to the defective mesodermal proliferation (Beddington et al., 1992). *Tbx4* is also required for extraembryonic mesodermal outgrowth, causing allantois defects such as disruption of vasculogenesis and failure to undergo morphological changes when mutated (Naiche and Papaioannou, 2003).

ii) During gastrulation, the primary germ layers are arranged through the gradual movement of presumptive mesoderm and endoderm cells. This creates a primitive streak from which mesodermal cells migrate and subsequently form structures such as notochord and somites (Beddington, 1982; Tam and Beddington, 1992). Many T-box genes are known to be involved in the process of mesoderm specification and patterning. *Brachyury* and *Eomesodermin* in mouse, *Xbra*, *Xeomesodermin* and *XvegT* in *Xenopus*, *no tail*, *spadetail*, *eomesodermin* and *Tbx6* in zebrafish are important in induction, formation and patterning of mesoderm (Reviewed in Showell et al., 2004). *Brachyury* homozygous mutant mice display loss of the posterior mesoderm (Gluecksohn-Schoenheimer, 1944; Gluecksohn-Schoenheimer, 1938). The importance of *Eomesodermin* in mesoderm patterning come from chimeric embryos whose extraembryonic tissues are predominantly wild type but embryo itself is composed of *Eomesodermin* mutant cells (Russ et al., 2000). These chimeric embryos thereby bypass embryonic death after implantation but die shortly after due to a failure in the formation of mesodermal layer (Russ et al., 2000). In terms of gene hierarchy, expression of *Eomesodemin* is known to precede that of *Brachyury*. *Tbx6* is required for somite formation as well as patterning as shown by the targeted disruption of the gene which resulted in a replacement of caudal somites with ectopic neural tubes (Chapman and Papaioannou, 1998).

1.7.2.2 The role of T-box genes in organogenesis and human disorders

The involvement of T-box genes in organogenesis is demonstrated by targeted mutagenesis in mice; *Tbx1*, *Tbx2*, *Tbx5* and *Tbx20* for cardiac development, *Tbx4* and *Tbx5* for limb development, *Tbx19/Tpit* for pituitary development and *Tbx1* and *Tbx22* for craniofacial development. In fact, some of the T-box genes are also linked to several human disorders including DiGeorge syndrome, Ulnar-mammary syndrome, Holt-Oram syndrome, ACTH deficiency, and orofacial clefts. Here, the role of T-box genes in organogenesis and the key features of human disorders caused by mutations in certain T-box genes are detailed.

i) In the developing heart, *Tbx1*, *Tbx2*, *Tbx3*, *Tbx5*, *Tbx18* and *Tbx20* are expressed in specific regions with some overlap (Papaioannou, 2001). Among these genes, null mutations in *Tbx1*, *Tbx2*, *Tbx5*, and *Tbx20* cause cardiac defects whereas mutations in *Tbx3* and *Tbx18* do not result in heart defects in mice. A role of *Tbx1* in cardiogenesis is suggested in proliferation of cardiac progenitor cells and the null mice have defects in anterior cardiac development (Jerome and Papaioannou, 2001; Lindsay et al., 2001). Homozygous mutant mice are neonatal lethal and also display craniofacial, glandular and vascular defects phenocopying virtually all features of the DiGeorge syndrome (OMIM 188400). The phenotype is less penetrant in the viable *Tbx1* heterozygous mice which display thymus and vascular abnormalities (Jerome and Papaioannou, 2001; Lindsay et al., 2001). In human, DiGeorge syndrome is associated with translocations and deletions of 22q11 region among which, *TBX1* is identified as a major contributor (Baldini, 2003). It affects about 1 in 4,000 live births and the phenotype can be highly variable between patients. The main clinical features include a congenital heart defect, hypoplastic or aplastic thymus and parathyroids, craniofacial defects including cleft palate, ear and mandible development, and in most cases learning difficulties and behavioural problems (Ryan et al., 1997; Wilson et al., 1993; Scambler, 2000). The penetrance may be affected by variation in genetic backgrounds including specific modifier genes along

with non-genetic effects mediated by environmental factors. *Tbx5* null mice show developmental defects in the posterior heart structure (Bruneau et al., 2001). Homozygous mutant mice are embryonic lethal due to severe heart malformations and heterozygotes also show heart abnormalities and forelimb defects with reduced viability (Bruneau et al., 1999; Bruneau et al., 2001). The human Holt-Oram syndrome (OMIM 142900) is caused by mutations in *TBX5* and is characterised by clinical features that include congenital heart and limb abnormalities (Basson et al., 1997; Li et al., 1997). It is a rare syndrome affecting about 1 in 100,000 live births. *TBX20* mutations are also associated with congenital heart disease (Kirk et al., 2007; Posch et al., 2010). Similarly, loss of *Tbx20* results in heart abnormalities in mice (Stennard et al., 2005). There are no known syndromes associated with *TBX2* in human although a microdeletion at 17q23.1q23.2, which includes *TBX2* and *TBX4* has been associated with individuals who have clinical features such as heart and limb abnormalities (Ballif et al., 2010). Recent association studies such as this, further underscore the importance of T-box genes in the pathology of human birth defects. It has also been demonstrated that mouse mutants for *Tbx2* develop heart abnormalities, implying biological importance of this gene in cardiogenesis (Harrelson et al., 2004; Stennard et al., 2005). Conversely, although both *Tbx3* and *Tbx18* are expressed in the mouse heart during development, mutations for either gene do not result in heart defects in mice. In fact, *Tbx3* null mice rather phenocopy human Ulnar-mammary syndrome (Davenport et al., 2003), and *Tbx18* null mice exhibit vertebral malformations (Bussen et al., 2004) but no human disorder has been linked to *TBX18*.

ii) *Tbx2*, *Tbx3*, *Tbx4*, *Tbx5* and *Tbx15* are all expressed during limb development (Agulnik et al., 1998; Gibson-Brown et al., 1996). *Tbx2* and *Tbx3* are expressed in the limb mesenchyme along the anterior and posterior margins of both developing forelimbs and hindlimbs. *Tbx4* and *Tbx5* are expressed in the mesenchyme of hindlimbs and forelimbs (Gibson-Brown et al., 1996). Homozygous mutant mice for *Tbx3* exhibit limb, mammary gland and yolk sac defects and embryonic lethal, and

heterozygous mice have hypoplastic mammary glands and abnormal external genitalia, phenocopying the Ulnar-mammary syndrome (OMIM 181450) (Davenport et al., 2003; Jerome-Majewska et al., 2005). Ulnar-mammary syndrome in human is caused by mutations in *TBX3* (Bamshad et al., 1997). The clinical features include limb abnormalities ranging from hypoplasia of the terminal phalanxof the fifth digit to the absence of forearm and hand, hypoplastic mammary glands and abnormal external genitalia (Bamshad et al., 1996). Mutations in *TBX4* cause small patella syndrome in human (OMIM 147891) (Bongers et al., 2004) and the null mice also exhibit hindlimb defects (Naiche and Papaioannou, 2003). Mutations in *TBX5* are linked to Holt-Oram syndrome which is characterised by heart and hand defects as mentioned above (Basson et al., 1997). The null mice exhibit lack of forelimb bud formation as well as heart defects (Agarwal et al., 2003). *Tbx15* null mice have defects in limb skeletal elements as well as the skeleton of the vertebral column and head due to reduced proliferation and smaller mesenchymal condensations (Singh et al., 2005). Recently, mutations in *TBX15* are identified in individuals with Cousin syndrome (OMIM 260660) which is a complex cranial, cervical, auricular and skeletal malformation syndrome with scapular and pelvic hypoplasia recapitulating the mouse dysmorphic phenotype (Lausch et al., 2008). Homozygous *Tbx2* null mice develop heart and limb defects (Harrelson et al., 2004) but no mutations have been reported for *TBX2* that cause human disorders other than a link to 17q23.1q23.2 microdeletion (Ballif et al., 2010) as mentioned above.

iii) In pituitary gland, *Tbx19/Tpit* is expressed in the corticotrophs and melanotrophs of the anterior and intermediate lobes which express pro-opiomelanocortin (POMC). It is required for the differentiation of corticotrophs and melanotrophs, and with the homeodomain protein Pitx1 it activates POMC expression (Lamolet et al., 2001). In human and mouse, loss of function mutations in *TPIT/Tpit* result in early onset of adrenocorticotrophic hormone (ACTH) deficiency (OMIM 201400) due to an absence of POMC (Pulichino et al., 2003).

iv) *Tbx1* is expressed in the anterior mesoderm and pharyngeal endoderm during craniofacial development (Chapman et al., 1996). *Tbx1* is known to regulate and be regulated by *Fgf8*, *Fgf10*, *Foxa2* and *Shh*, and both human and mouse lacking functional *TBX1*/*Tbx1* develop multiple craniofacial defects in addition to heart defects (Jerome and Papaioannou, 2001). Craniofacial defects caused by mutations in *TBX22*/*Tbx22* are detailed in 1.4.3.6 and 1.8.2.

1.8 The role of TBX22 in craniofacial development

1.8.1 Using mutant mice to model human disease

Model organisms are non-human animal species that are widely used in research to model human disease in order to better understand potential causes and treatments. Model organisms for biomedical research defined by National Institutes of Health (NIH) include several animal species of which genomic data are extensively studied. They are mouse (*Mus musculus*) and rat (*Rattus norvegicus*) for mammalian models as well as non-mammalian models such as zebrafish (*Danio rerio*), frog (*Xenopus laevi*) and chicken (*Gallus gallus*).

Among these, mouse has become an essential tool in medical and biological research. They are small in size; adult mice weigh 25-40g on average so that they can be housed efficiently. They have a short generation time; a gestation period of about 3 weeks, and they reach sexual maturity at 6-8 weeks. The litter size is relatively large; ranging from 6 to 12 or even more depending on strains. Also, pregnancy can be timed accurately by observing deposition of a copulatory plug upon mating.

Mouse and human diverged from a common ancestor about 65 million years ago, yet approximately 80% of mouse genes have at least one ortholog in the human genome, often with high degree of sequence similarity between them (Waterston et al., 2002; Lander et al., 2001). Most importantly, the technology of genetic manipulation is well established for mouse embryonic stem cells. This makes the mouse one of the most popular model organisms in terms of modelling human disease and studying human gene function *in vivo*.

1.8.2 *Tbx22* null mice

Mice deficient for *Tbx22* were recently generated using standard gene targeting techniques (Pauws et al., 2009a). The Cre-lox recombination system was employed in this study principally to avoid postnatal lethality, which usually occurs with the cleft palate phenotype. Constitutive knockout of a gene resulting in cleft palate may therefore not allow for future generation and maintenance of the transgenic line. Since the aim was to provide a model to allow a more detailed investigation of the pathogenesis that might underpin human CPX, a floxed line was first created by introducing loxP sites flanking the first three exons of *Tbx22*. By then breeding to a β-actin-Cre deleter strain (or other tissue specific Cre), the first three coding exons, which include the start codon, nuclear localisation signal and a part of the T-box domain, can be removed as desired. This essentially created a conditional *Tbx22* null allele. In the floxed *Tbx22* strain, the Neo cassette, which was used for selection in the ES cells, was located outside of the two LoxP sites. Therefore on recombination, it was still retained in the $Tbx22^{null}$ genome. In later studies, it was determined that many male null animals not only survived but were fertile and tended to be used for the majority of the breeding startegies. This allowed greater efficiency in numbers of embryos with the desired genotype.

Following birth, about half of all homozygous null mice die post-natally. Those that were found dying at P0 struggled to breathe and were unable to suckle milk, resulting in their stomach and intestine being filled with air (Pauws et al., 2009a). Although this is a classic symptom of cleft palate in mice, only a small proportion of null mice (6%) were found to have an overt cleft palate, while the majority of mutants had palatal shelves fused normally, along the entire length. A detailed examination of E18.5 embryos was performed by various methods including hematoxylin and eosin staining, skeletal preparations and computed tomography (CT) scanning (Figure 1.14). This revealed that palatine bone formation was severely reduced in the posterior hard palate of the null mice. In addition, the vomer, which supports the nasal cartilage and the secondary palate, was also reduced in size in the null mice. According to the computed tomography scan measurements, the palatine bone was reduced by 68% and the vomer by 74% in size. The under-developed palatal bone caused a semi translucent region in the mid palate region

which appeared as a notch, similar to that often described in human babies with submucous cleft palate. These mice therefore exhibit the entire spectrum of both the overt and submucous cleft palate phenotypes observed in human CPX patients.

Preliminary analysis of bone formation showed that alkaline phosphatase activity was lower in the null palate compared to the wild type at E15.5. This stage is after the completion of the fusion process and at the onset of ossification within the presumptive future hard palate. In the null palate, mesenchymal condensation was observed but osteoblast activity was reduced, indicating a significant delay in differentiation and/or maturation of osteoblasts leading to impaired intramembranous ossification in the absence of TBX22.

As described above, ankyloglossia is frequently observed in CPX patients. In the case of *Tbx22* null mice, the tongue was attached to the mandible more anteriorly but did not extend to the tip of the tongue, indicating a mild form of ankyloglossia (Figure 1.15). In addition, the null mice were found to have a persistent oronasal membrane at the site of the medial nasal prominence (Figure 1.15), which is equivalent to choanal atresia in humans. The oronasal membrane is a transient structure which disappears during development resulting in the formation of choanae. It was suggested that choanal atresia may have been the main cause of postnasal lethality because this phenotype was present in the null mice that died but absent in those that survived. This has not been reported as a feature of CPX but is well known in other syndromic conditions involving clefts such as CHARGE syndrome (Vissers et al., 2004).

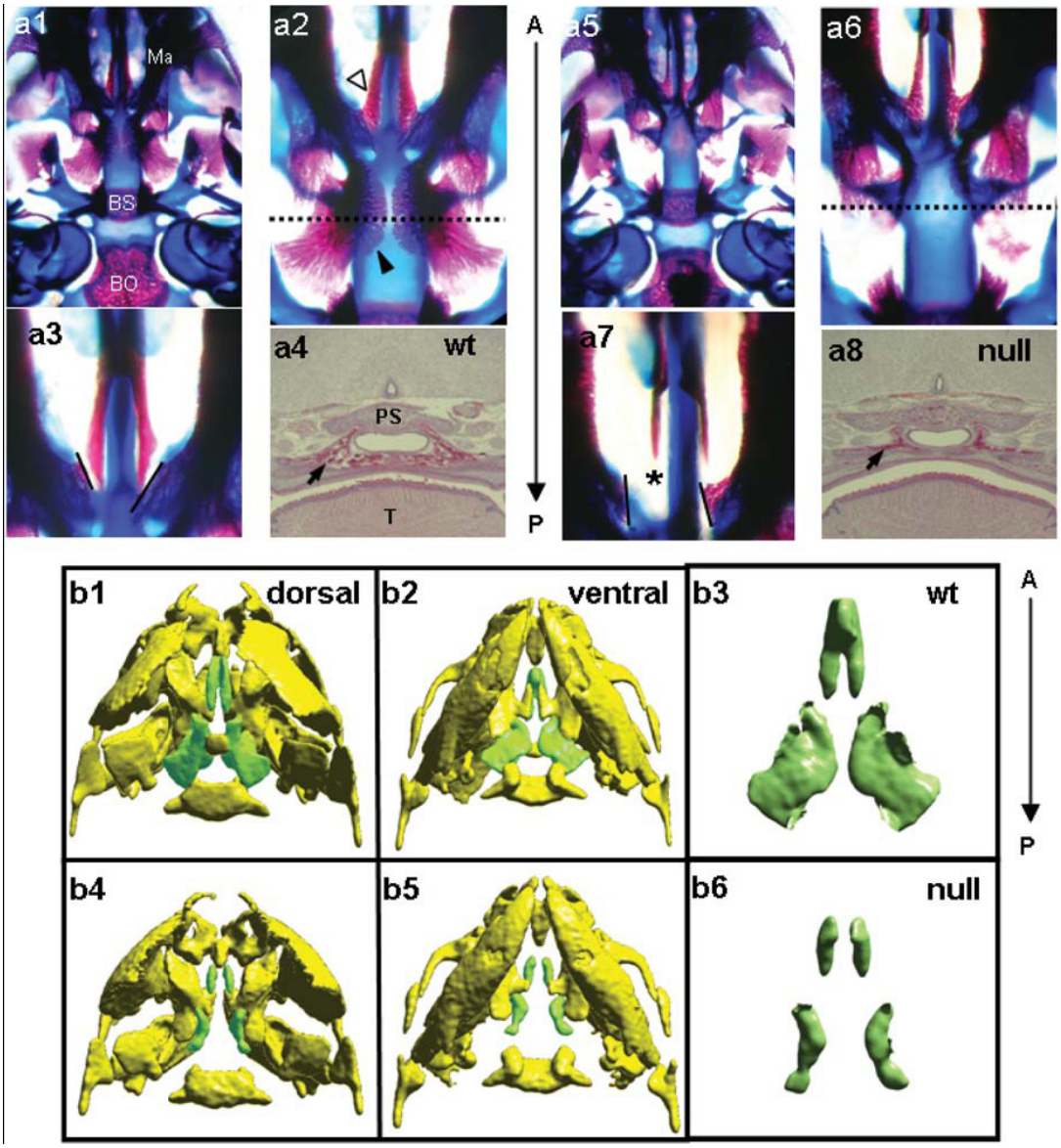

Figure 1.14 Posterior palatal bone is reduced in *Tbx22* null mice
Skeletal preparations with Alizarin Red (bone) and Alcian Blue (cartilage) (a1-3, a5-7) showed reduced palatine bones (brack arrowhead, a2) and the vomer (asterisk, a7) but not the maxillary palatal bones (white arrowhead, a2) in *Tbx22* null mice at E18.5. Reduced posterior palatal bones in the null mice compared to the wt were also detected by hematoxylin and eosin staining (arrows, a4 and a8) and computed tomography scan (b1-6). BS, basisphenoid; BO, basoccipital; Ma, mandible; PS, presphenoid; T, tongue; A, anterior; P, posterior (Pauws et al., 2009a).

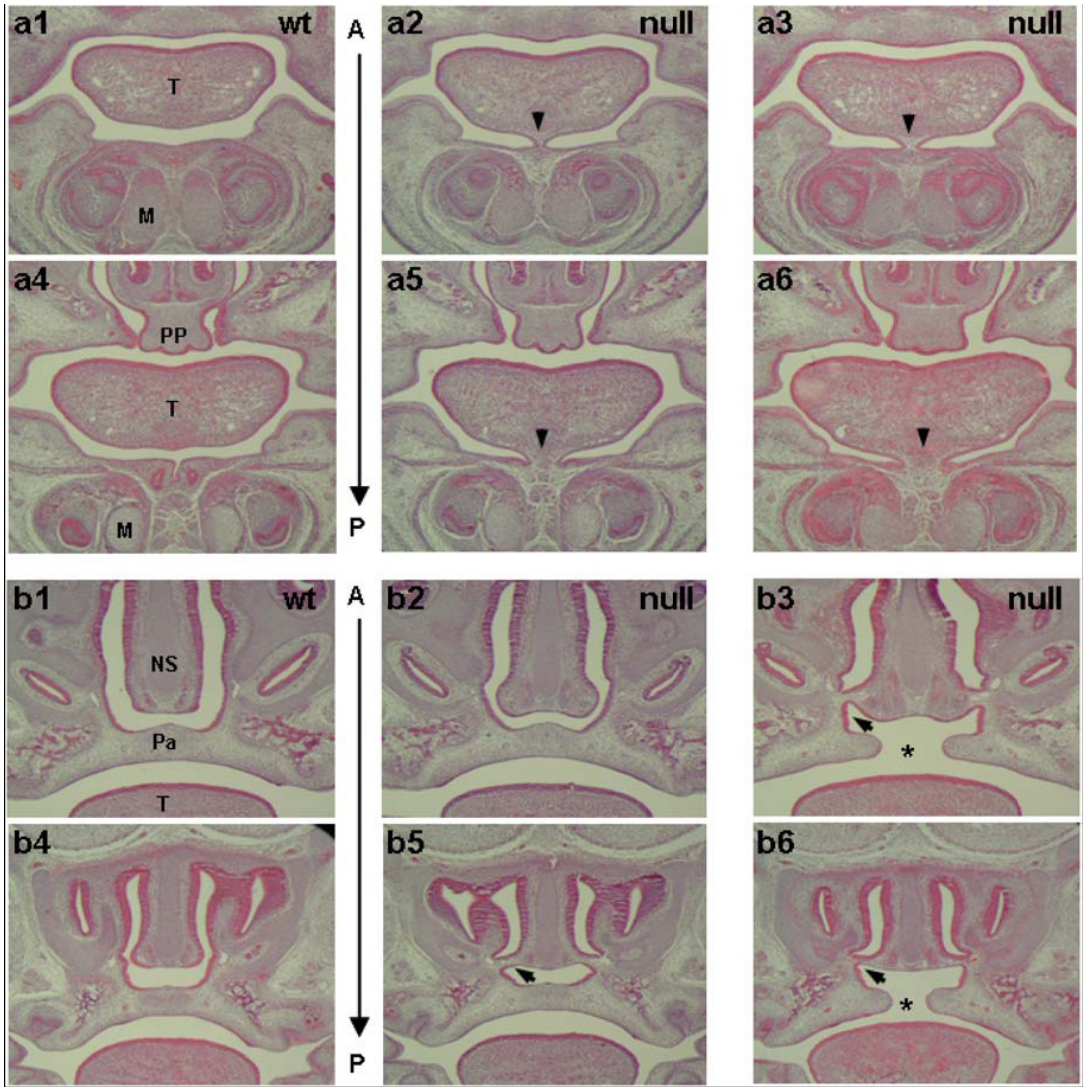

Figure 1.15 Ankyloglossia and choanal atresia in *Tbx22* null mice
In the null mice, the tongue is attached more anteriorly than in the wt indicating ankyloglossia (arrowheads, a2, a3, a5 and a6). The oronasal membrane persisted in the null mice indicating choanal atresia (arrows, b3, b5 and b6). Some had more severe atresia where the entire length of choanae was blocked by oronasal membrane (b3 and b6) at E15.5. Asterisks in b3 and b6 indicate overt cleft palate. M, Meckel's cartilage; NS, nasal septum; Pa, palate; PP, primary palate; T, tongue; A, anterior; P, posterior (Pauws et al., 2009a).

1.8.3 The role of TBX22 in craniofacial development

TBX22 was identified as a causative gene for CPX by positional cloning (Braybrook et al., 2001), a method which provides no insight into understanding of the regulation and function of the gene. Since its discovery, further clues have been revealed regarding its role in craniofacial development.

There are only a couple of studies reported in which the expression of *Tbx22* has been altered as a consequence of knocking down other craniofacial expressed genes in mice. In *36 Pub* mutant mouse palatal shelves, the expression of *Tbx22* was downregulated posteriorly at E14.5 (Welsh et al., 2007). The mutant mice essentially lacked the FGF signalling antagonist *Spry2* and as a consequence they developed overt cleft palate. This study indicates the importance of *Tbx22* expression for posterior palatal growth. The fact that its expression was reduced due to the lack of *Spry2* also implies that FGF signalling somehow affects the expression of *Tbx22*. However, it is not clear from this study if the reduced *Tbx22* expression was a direct consequence of an increased FGF signalling or if its expression was affected by elevated FGF responsive transcription factors such as *Etv5*, *Msx1*, *Barx1* and *Shh*.

Meningioma 1 (*Mn1*) null mice also develop cleft palate (Meester-Smoor et al., 2005) and are informative for *Tbx22* but for different reasons. *MN1* was originally identified as a gene disrupted in a benign brain tumor called meningioma (Lekanne Deprez et al., 1995). However, instead of having higher incidence of tumor formation, *Mn1* null mice develop severe defects of craniofacial bones including cleft palate (Meester-Smoor et al., 2005). Further investigation revealed no significant differences in cleft susceptible genes including *Fgf10*, *Fgfr2*, *Osr2*, *Shh*, *Ptch*, *Pax9*, *Shox2* and *Tgfβ3*, although a downregulation of *Tbx22* in the mutant E13.5 palatal shelves was noted (Liu et al., 2008). The regulation of *Tbx22* by Mn1 was then confirmed by an *in vitro* reporter assay. In the case of *Mn1* null mice, the cell proliferation rate was reduced in the growing palatal shelves, which is probably what caused the cleft phenotype at the cellular level. Interestingly, Mn1 is reported to have an important regulatory role in proliferation, differentiation and maturation of osteoblasts, both *in vitro* and *in vivo* (Zhang et al., 2009). These recent findings,

as well as a role in the bone differentiation and/or maturation defects observed in *Tbx22* null mice (Pauws et al., 2009a), strongly suggest that TBX22 is an essential component in the osteogenesis pathway in palatal shelves. However, this idea fails to explain other pathological phenotypes (i.e. ankyloglossia and choanal atresia) in *Tbx22* null mice since oronasal membrane and frenulum are not osteoblastic cells, making it difficult to speculate on other aspects of its function during development.

More recently, two independent groups reported the regulation of *Tbx22* by FGF and BMP signalling in chick (Higashihori et al., 2010; Fuchs et al., 2010) and mouse (Fuchs et al., 2010) embryos. Both groups used FGF and BMP soaked beads as well as the FGF antagonist SU5402 and the BMP anatagonist Noggin to investigate how expression of *Tbx22* is altered in the facial region. Higashihori et al. (2010) demonstrated that *Tbx22* failed to upregulate or was reduced in the chick frontonasal mass at stages 15 and 24 respectively, when injected with SU5402. Implantation of FGF2 and FGF8 soaked beads at stage 24 led to upregulation of *Tbx22*. They also showed that implantation of BMP4 and BMP7 soaked beads in the chick frontonasal mass at stage 24 repressed *Tbx22* while treatment with Noggin beads strongly induced its expression. In addition, overexpression of human *TBX22* using a viral expression construct resulted in reduced cell proliferation in the chick frontonasal mass and went on to induce a cleft of the lip. This suggested a potentially down-regulatory role for TBX22 in cell proliferation. As a consequence, the size of the frontonasal mass, maxillary and mandibular bones were all reduced with smaller ossification centres. Moreover, *Dlx5* and *Msx2* levels were reduced in the chick frontonasal mass following overexpression with human *TBX22*. This suggested that *TBX22* may act as a repressor of these genes. A very similar study was also reported by Fuchs et al. (2010). Here they extended the analysis of *Tbx22* regulation by FGF and BMP signalling in the facial mesenchyme by looking in mouse embryos as well as the chick. The results were remarkably similar to those reported by Higashihori et al. (2010). Interestingly, Fuchs et al. (2010) also showed that although expression of *Tbx22* was altered by addition of SU5402 or FGF8 in the chick and mouse maxillary explants at stage 23 and E10.5 respectively, its expression became independent of FGF signalling later at stage 26 and E12.5 in the palatal explants. Taken together, these studies demonstrated a positive regulation of

Tbx22 by FGF signalling during early facial development and a negative regulation by BMP signalling later on.

1.9 Aims of the study

It has previously been shown that mutations in *TBX22* are a frequent cause of X-linked cleft palate and ankyloglossia (CPX) (Braybrook et al., 2001; Braybrook et al., 2002; Chaabouni et al., 2005; Marcano et al., 2004). *In vitro* analysis has shown that TBX22 can function as a transcriptional repressor, which requires post-transcriptional modification by a small ubiquitin-like modifier (SUMO-1) for its action (Andreou et al., 2007). Thus far, little is known about the cellular and biochemical mechanisms involving TBX22 that lead to the disease phenotype. Identification of candidate genes that function in the same molecular pathway as *TBX22* will provide important insights into the occurrence of CPX as well as normal craniofacial development. Thus, this project aims to better understand the molecular and cellular role of TBX22 and the downstream effects of its loss of function.

As a starting point it is decided to perform whole mount and/or section *in situ* hybridisation for *Tbx22* on wt mouse embryos ranging between E9.5 to E15.5. Previously there has only been limited data covering the entire period of palatogenesis or craniofacial morphogenesis and this data would provide a comprehensive reference for the following experiments.

The next aim of this study is to identify genes that are differentially expressed in the presence and absence of *Tbx22*. This would help to elucidate the transcriptional events and regulatory networks involved, as well as reveal potential new candidate genes for cleft palate in humans. For this purpose, it was intended to perform a comparative gene expression analysis using a microarray between wild type and *Tbx22* null mice. *Tbx22* null mice display overt or submucous cleft palate and ankyloglossia with an additional feature of choanal atresia (Pauws et al., 2009a). These pathological phenotypes essentially recapitulate human CPX, thus they serve as a good model to investigate the effects caused by a loss of *Tbx22*. Based on the microarray results, genes of interest will be selected for independent verification by real-time PCR. These candidate gene(s) whose expression is altered due to a lack of *Tbx22* are considered to be downstream targets and will be further investigated by

functional analysis such as luciferase reporter assays and chromatin immunoprecipitation.

In addition, it is intended to investigate the molecular networks and mechanisms underlying pathogenic phenotypes and especially the submucous cleft palate observed in *Tbx22* null mice. In the developing palate of null animals, a deficiency or delay in palatine bone formation was observed. This was suggested to result from defective differentiation and/or maturation of osteoblasts. However, recent studies in different experimental systems have demonstrated a role for TBX22 in cell proliferation (Higashihori et al., 2010). In the null palate, although there is a bone deficiency, at least some osteoblasts do mature to become bone forming cells followed by mineralisation. Thus, it is possible that cell proliferation may also be down regulated in *Tbx22* null mice. In addition, the choanal atresia phenotype will be examined during early choanae development by histological staining and *in situ* hybridisation. These studies will contribute towards a better understanding of TBX22 function in craniofacial development.

CHAPTER 2: MATERIALS AND METHODS

2 MATERIALS AND METHODS

2.1 Materials

Chemicals and Solvents

Acetic anhydride	BDH
Agarose	Invitrogen
Ammonium persulphate	Sigma-Aldrich
Ampicillin	Sigma-Aldrich
BCIP	Roche Applied Science
Bovine serum albumin	Sigma-Aldrich
Bradford reagent	Sigma-Aldrich
Bromophenol blue	Sigma-Aldrich
Chloroform	BDH
Denhardt's solution 50× concentrate for molecular biology, liquid	Sigma-Aldrich
Deoxyribonucleic acid, low molecular weight, from salmon sperm	Sigma-Aldrich
Dextran sulfate Sodium salt from Leuconostoc spp.	Sigma-Aldrich
Dietylpyrocarbonate	Sigma-Aldrich
Dried skimmed milk	Marvel
DTT	Sigma-Aldrich
EDTA	Sigma-Aldrich
Ethanol	Hayman Ltd
Formaldehyde	Sigma-Aldrich
Formamide	Sigma-Aldrich
Glutaraldehyde	Sigma-Aldrich
Glycerol	BDH
Heparin	Sigma-Aldrich
Hydrochloric acid	Fisher Scientific
Hydrogen peroxide	Sigma-Aldrich
Isopropanol	BDH
LB Agar	Invitrogen
LB base	Invitrogen
Levamisole	Sigma-Aldrich
Magnesium chloride	Fisher Scientific
Methanol	Hayman Ltd
NBT	Roche Applied Science
Paraformaldehyde	Sigma-Aldrich
PBS tablets	Oxoid
Phenol chroloform isoamyl alcohol	Fisher Scientific

Polyvinyl alcohol	VWR
Potassium chloride	Sigma-Aldrich
RNaseA	Invitrogen
Sodium acetate	Sigma-Aldrich
Sodium bicarbonate	Sigma-Aldrich
Sodium chloride	Fisher Scientific
Sodium citrate	Sigma-Aldrich
Sodium deoxycholate	BDH
Sodium dodecyl sulfate	Sigma-Aldrich
TEMED	Sigma-Aldrich
TRI Reagent	Sigma-Aldrich
Triethanolamine	Sigma-Aldrich
Tris	Sigma-Aldrich
Triton X-100	Sigma-Aldrich
Tween-20	Sigma-Aldrich
β-mercaptoethanol	Sigma-Aldrich

Enzymes

Antarctic phosphatase	New England Biolabs
GoTaq® Hot Start Polymerase	Promega
M-MLV Reverse Transcriptase	Promega
Protease inhibitors	Roche Diagnostics
Proteinase K	Roche Diagnostics
Recombinant RNasin® Ribonuclease Inhibitor	Promega
Restriction endonucleases	Promega, New England Biolabs
RQ1 RNase-Free DNase	Promega
T4 DNA ligase	BIOLINE
TaqMan® Fast Universal Master Mix (2X), No AmpErase® UNG	Applied Biosystems

Bacterial strains

Fusion-Blue™ competent cells	Clontech
XL1-Blue supercompetent cells	Stratagene

Cell culture materials

Dimethyl sufoxide	Sigma-Aldrich

Dulbecco's Modified Eagle's Medium - high glucose	Sigma-Aldrich
Fetal bovine serum	Clontech
FuGENE 6 Transfection Reagent	Roche Applied Science
L-glutamine	Gibco
MEM Non Essential Amino Acids (100X), liquid	Gibco
Penicillin-Streptomycin, liquid	Gibco
Phosphate buffered saline	Gibco
Tissue culture plastic ware	Corning
Trypan blue	Sigma-Aldrich
Trypsin, 0.5% (10x) with EDTA 4Na, liquid	Gibco

Antibodies

Anti-digoxygenin, Fab fragments	Roche Applied Science
Anti-phospho-Histone H3 (Ser10)	Upstate
Anti-V5	Invitrogen
Cleaved caspase-3	Cell Signaling
Polyclonal goat anti-rabbit immunoglobulins biotinylated	DAKO
Rabbit anti-mouse HRP	DAKO
Streptavidin, Alexa Fluor® 555 conjugate	Invitrogen

Histology

Cover slips	BDH
Embedding molds	Thermo Scientific
Histoclear	National Diagnostics
Paraffin wax	Raymond A Lamb
SuperFrost Plus glass slides	VWR
Vectamount H-5000	Vector
VECTASHIELD mounting medium with DAPI	Vector Laboratories

Miscellaneous

30% Acrylamide/Bis solution	BIO-RAD
Amersham ECL Plus Western Blotting Detection System	GE Healthcare Life Sciences
BigDye® Terminator v3.1 Cycle Sequencing RR-100	Applied Biosystems
BioMax Light Film	Kodak
Bioruptor	Diagenode
CHROMA SPIN-100 DEPC-H_2O column	Clontech

Coelenterazin	Invitrogen
DIG RNA Labeling Kit (SP6/T7)	Roche Applied Science
dNTPs	Promega
GeneChip® Mouse Gene 1.0 ST Array	Affymetrix
Goat serum	Sigma-Aldrich
HiSpeed Plasmid Maxi Kit	QIAGEN
HiSpeed Plasmid Midi Kit	QIAGEN
HyperLadders	BIOLONE
PCR Nucleotide Mix	Promega
Precision Plus Protein Standards	BIO-RAD
Protein G	Thermo Fisher Scientific
PVDF membrane	Millipore
QIAprep Spin Miniprep Kit	QIAGEN
QIAquick Gel Extraction Kit	QIAGEN
QIAquick PCR Purification Kit	QIAGEN
QuikChange site-directed mutagenesis kit	Stratagene
Random primers	Promega
Ribonucleic acid, transfer from Baker's yeast (*S. cerevisiae*) buffered aqueous solution	Sigma-Aldrich
Sheep serum	Sigma-Aldrich
Steady Lite Plus	PerkinElmer
Trans-Blot SD Semi-Dry Transfer Cell	BIO-RAD

Plamids

pcDNA3.1.V5/His	Invitrogen
pcDNA3.1.TBX22.V5/His	A. Andreou, our laboratory
pcDNA3.1.TBX22(N264Y).V5/His	A. Andreou, our laboratory
pEGFP-N2	Clontech
pGEM®-T Easy	Promega
pGL3-Basic	Promega
pRL-CMV	Promega

In situ probes

Bmp4	B. Hogan, Duke University, USA
Msx1	P. Sharpe, University of Minnesota Duluth, USA
Msx2	P. Sharpe, University of Minnesota Duluth, USA
Pax9	A. Neubuser, University of Freiburg, Germany
Snail	M. Sefton and A. Nieto, Instituto Cajal, Spain

Tgfß3	R. Akhurst, University of California, San Francisco, USA
Osr1	A. Andreou, our laboratory
Tbx22	E. Pauws, our laboratory
Cyclin D2	R. Jiang, University of Rochester, USA
Fgf10	R. Jiang, University of Rochester, USA
Fgfr2	R. Jiang, University of Rochester, USA

TaqMan® Gene Expression Assays and TaqMan® Endogenous Controls	**Assay ID or Part Number**
Acta1	Mm00808218_g1
Casq2	Mm00486742_m1
Cdkn1a (p21)	Mm00432448_m1
Ctsk	Mm00484039_m1
Myf5	Mm00435125_m1
Myh3	Mm01332463_m1
MyoD	Mm00440387_m1
Myog	Mm00446194_m1
Osterix	Mm00504574_m1
Runx2	Mm01269515_mH
Eukaryotic 18S rRNA Endogenous Control	4352930E
Mouse GAPD (GAPDH) Endogenous Control	4352932E

Oligonucleotides	**Sequence 5' to 3'**
Tbx22_F	CAGCTTCCAAAACAGTGGAG
Tbx22_R	CTTCTAGGGACAGTCAACAG
Tbx22_R2	CAATAGCAGCCAGTCCCTTC
Smc_F	TGAAGCTTTTGGCTTTGAG
Smc_R	CCGCTGCCAAATTCTTTGG
MyoD_F_-683	ATTCTCGAGACCCGGAGTTTGAGCAGAAT
MyoD_R_+115	ATTCTCGAGACAAAGGTTCTGTGGGTTGG
FseqpGL3_RVprimer3	CTAGCAAAATAGGCTGTCCC
RseqpGL3_GLprimer2	CTTTATGTTTTTGGCGTCTTCCA
sMyoD_C-511A/C-509A	ATTTGTGCCAGGCTTGCTAA ACTAGACCTTCTGAGTCTC

asMyoD_C-511A/C-509A	GAGACTCAGAAGGTCTAGTT TAGCAAGCCTGGCACAAAT
MyoD_ChIP_F	ATTCTCGAGTCCGAGTTTGGAGAGATTGG
MyoD_ChIP_R	TGAGGAGTGAGACCGTGAAA
MyoD_insitu_F	AGCACGCACACTTCCCTACT
MyoD_insitu_R	AGGGCTCCAGAAAGTGACAA
Bmp2_insitu_F	AGGCTGCCACAAAAGACACT
Bmp2_insitu_R	GCCTGCGGTACAGATCTAGC
Bmp3_insitu_F	ACAGCAGGACTTCGCTATGG
Bmp3_insitu_R	GGGACCCTTTCCTCTGTTTC
Spry2_insitu_F	ACATCGCTGGAAGAAGAGGA
Spry2_insitu_R	CCTCTCACTGCAAACCACAA

Solutions

0.5 M EDTA	186.1 g EDTA dissolved in 800 ml H_2O, bring the pH to 8.0 with NaOH pellets, adjust the volume to 1 L with H_2O
0.5 M HEPES	119.2 g HEPES dissolved in 800 ml H_2O, adjust the pH to 7.8 with NaOH peletts, adjust the volume to 1 L with H_2O
1x PBS	10 PBS tablets dissolved in 1 L H_2O
1 M Tris-HCl	121.1 g Tris base dissolved in 800 ml H_2O, adjust to desired pH with HCl, adjust the volume to 1 L with H_2O
1x TAE	40 mM Tris, 20 mM acetic acid, 1 mM EDTA
20% SDS	200 g SDS dissolved in 800 ml H_2O, adjust the volume to 1 L with H_2O
20x SSC	175.3 g NaCl, 88.2 g sodium citrate in 800 ml H_2O, adjust the volume to 1 L with H_2O
4% paraformaldehyde in PBS	20 g PFA dissolved in 400 ml DEPC water and 50 ml 10X PBS at 60ºC, adjust the volume to 500 ml with

	DEPC water
DEPC treated water	1 ml diethylpyrocarbonate in 1 L H_2O, autoclaved
LB-agar	32 g LB agar dissolved in 1 L H_2O, autoclaved
LB-broth	25 g LB base dissolved in 1 L H_2O, autoclaved
Renilla buffer	5 ml 0.5 M HEPES pH 7.8, 400 µl 0.5 M EDTA
Renilla reagent	10 ng/µl coelenterazin in *Renilla* buffer
TE buffer	40 mM Tris-HCl pH 8.0, 1 mM EDTA pH 8.0

Water used in all experimental procedures was purified using a Millipore reverse osmosis and MilliQ system. Water used for RNA analysis was treated with DEPC.

2.2 Methods

2.2.1 General molecular biology techniques

2.2.1.1 Restriction digestion

DNA was digested with chosen restriction enzyme(s) and appropriate buffer at the recommended optimal temperature for 1-2 hours, typically in a total volume of 20 µl. 10X BSA was also added to the reaction to facilitate digestion.

2.2.1.2 Gel extraction of DNA

QIAquick Gel Extraction Kit (QIAGEN) was used to extract DNA from agarose gel slices according to the manufacturer's instruction. Briefly, DNA bands were excised under UV light following electrophoresis in a 0.8% agarose gel and dissolved in three volumes of Buffer QG at 50ºC for 10 min. The sample was mixed with one volume of isopropanol, applied to a QIAquick spin column and centrifuged for 1 min at 13,000 rpm followed by washing with Buffer PE. The DNA was eluted in 30 µl of Buffer EB and stored at -20ºC.

2.2.1.3 Ligation

Linearised vector and insert were combined at 1:1 to 3:1 molar ratio in a 10 µl reaction mixture containing ligase buffer and T4 DNA ligase (BIOLINE) and incubated overnight at 4ºC.

2.2.1.4 Transformation of chemically competent bacteria

Transformation by heat shock was performed using Fusion-Blue™ Competent Cells (Clontech) according to the manufacturer's instruction. 25 µl of cells were removed from -80ºC freezer and thawed on ice. 1 µl of DNA solution was added and incubated on ice for 5 min followed by heat shock for 30 sec at 42ºC, then immediately placed on ice for 2 min. 250 µl of LB medium was added and incubated at 37ºC for 1 hour while shaking at 180 rpm. Typically, 50-100 µl of

transformed cells was spread on an LB agar plate containing appropriate selective antibiotics (e.g. 100 µg/ml of Ampicillin) and incubated overnight at 37ºC. The next day, single colonies were picked and expanded in LB in the presence of selective antibiotics.

2.2.1.5 Mini, Midi and Maxiprep of DNA

Plasmid DNA from overnight cultures was purified using either QIAprep Spin Miniprep Kit, HiSpeed Plasmid Midi or Maxi kit (QIAGEN), depending on the amount of DNA required. The DNA purification procedure is based on alkaline lysis of bacterial cells followed by adsorption of DNA onto silica membrane. Briefly, appropriate amount of overnight cultures (1.5 ml for Mini, 50 ml for Midi or 150 ml for Maxi) were centrifuged, resuspended in Buffer P1 containing 1 mg/ml RNase A (250 µl for Mini, 6 ml for Midi or 10 ml for Maxi), lysed in Buffer P2 (250 µl for Mini, 6 ml for Midi or 10 ml for Maxi) and cell debris was precipitated by adding chilled Buffer P3 (350 µl for Mini, 6 ml for Midi or 10 ml for Maxi). Then for Miniprep, the supernatants were applied to the QIAprep spin column after centrifuging for 10 min at 13,000 rpm and the column was washed twice, first by adding 0.5 ml and then 0.75 ml of Buffer PB. The DNA was eluted in 50 µl Buffer EB and stored at -20ºC. For Midi and Maxi, the lysate was filtered through the QIAfilter Catridge and the supernatants were applied to the equilibrated HiSpeed Midi or HiSpeed Maxi Tip, washed with Buffer QC (20 ml for Midi or 60 ml for Maxi), and the DNA was eluted with Buffer QF (5 ml for Midi or 15 ml for Maxi). After precipitation with isopropanol (3.5 ml for Midi or 10.5 ml for Maxi), the DNA elute was filtered through QIAprecipitator Midi or Maxi Modules, washed with 2 ml of 70% ethanol, eluted in 0.5 ml of Buffer TE and stored at -20ºC.

2.2.1.6 Extraction of total RNA from cells and tissues

Total RNA was extracted from cells and tissues using TRI Reagent (Sigma-Aldrich). For cultured cells, semi-confluent cells in 6 well plates were harvested, homogenised in 1 ml of TRI Reagent. For tissues, a pair of palatal shelves dissected from individual mouse embryos was immediately homogenised in 0.5 ml of TRI Reagent. Samples were incubated for 5 min at room temperature to ensure complete

dissociation of nucleoprotein complexes. 0.2 ml of chloroform was added per ml of Tri Reagent used and samples were shaken vigorously for 15 sec which were left at room temperature for 10 min before centrifuging at 12,000 *g* for 15 min at 4ºC to separate the mixture into 3 phases. A colourless upper phase contained RNA, and a red organic phase and an interphase contained protein and DNA, respectively. For RNA extraction, a colourless upper phase was carefully transferred and was precipitated by adding 0.5 ml isopropanol per ml of TRI Reagent used, left for 5 min at room temperature and centrifuged at 12,000 *g* for 10 min at 4ºC. The RNA pellet was washed with 1 ml of 75% ethanol by inversion, centrifuged at 8,000 *g* for 5 min at 4ºC and air-dried before being dissolved in appropriate volume of DEPC treated water. RNA samples were then ethanol precipitated to remove residual phenol which may interfere with down stream applications.

2.2.1.7 Ethanol precipitation of DNA and RNA

Ethanol precipitation was carried out by adding a one tenth volume of 3M NaOAc pH 5.2 and three volumes of ice-cold 100% ethanol to DNA, or 5 µl of 3M NaOAc pH 5.2 and 450 µl of ice-cold 100% ethanol to ~50 µl of RNA. The samples were left overnight at -20ºC and centrifuged for 20 min at 14,000 rpm at 4ºC the following day. The pellet was washed with 1 ml of ice-cold 70% ethanol, centrifuged for 5 min at 14,000 rpm at 4ºC to remove supernatant and dissolved in appropriate amount of TE buffer or DEPC treated water. The DNA and RNA were stored at -20ºC and -80ºC, respectively.

2.2.1.8 Phenol chloroform extraction of DNA

Phenol chloroform extraction of DNA was carried out by adding an equal volume of pH 7.9 phenol chloroform isoamyl alcohol mixture. After centrifuging the sample for 2 min at 13,000 rpm, a top aqueous layer which contained DNA was collected and ethanol precipitated.

2.2.1.9 Determining nucleic acid concentration

Concentrations of DNA and RNA samples were determined spectrophotometrically using the NanoDrop ND-1000 (Themo Scientific). Typically, 1 µl of DNA or RNA was loaded onto the optical pedestal and absorbance at 260 nm was measured. The purity of nucleic acids was assessed by the absorbance ratio at 260/280 nm and 260/230 nm. A 260/280 ratio of ~1.8 for DNA and ~2.0 for RNA are considered to be pure and lower ratio indicates presence of substances such as proteins and phenol. A 260/230 ratio was used as a secondary measure. In this case, values between 2.0-2.2 are considered to be pure and lower ratio indicates presence of substances such as EDTA, carbohydrates and phenol which all absorb at around 230 nm.

2.2.1.10 DNA sequencing

DNA sequencing was performed by mixing 4 µl of miniprep plasmid DNA, 1.5 µl of BigDye® Terminator v3.1 Cycle Sequencing RR-100 (Applied Biosystems), 2.25 µl of BigDye® Terminator v1.1, v3.1 5x Sequencing Buffer (Applied Biosystems), 1 µl of sequencing primer (20ng/µl) and 0.75 µl of H_2O in 96 well plates and then subjected to the following thermal cycle conditions: 98ºC for 5 min followed by 30 cycles of 96ºC for 30 sec, 55ºC for 15 sec and 60ºC for 4 min using a DNA Engine Dyad Peltier Thermal Cycler (Bio-Rad Life Sciences). PCR sequencing products were ethanol precipitated and dissolved in 10 µl of deionised formamide to denature dsDNA. The sequencing plates were heated at 90ºC for 2 min before subjecting to capillary electrophoresis with a 3730xl DNA Analyzer (Applied Biosystems). The sequence outputs were analysed with Sequencher 4.8 (Gene Codes Corporation).

2.2.2 Cell culture

2.2.2.1 HEK 293T and C2C12 cell lines

HEK 293T cell line was originally derived from human embryonic kidney cells of a healthy aborted fetus. The transformation was brought by adenovirus that made the cells immortal (Graham et al., 1977; Louis et al., 1997). C2C12 is a mouse myoblast cell line, originally obtained through serial passage of myoblasts from the C3H mouse thigh muscle after a crush injury (Yaffe and Saxel, 1977). Both cell

lines were grown in Dulbecco's Modified Eagle's Medium - high glucose (Sigma-Aldrich) supplemented with 10% v/v FBS (Clontech), 2 mM L-glutamine (Gibco), 0.1 mM MEM Non Essential Amino Acids (100X), liquid (Gibco) and 50 units/ml Penicillin-Streptomycin, liquid (Gibco) in a humidified incubator at 37ºC with 5% CO_2. Cells were seeded at 1/10 dilutions and passaged every 3-4 days.

2.2.2.2 Trypsinising cells

Cells were trypsinised and passaged when semi-confluence was reached. For trypsinisation, the growth media was aspirated and cells were rinsed with 1X PBS (5 ml per 25 cm^3 flask area). Then Trypsin/EDTA solution (1 ml per 25 cm^3 flask area) was added to the cells and incubated in a 37ºC incubator until they detached from the flasks, normally within 5 min. A proportion of the trypsinised cells were seeded to a new flask.

2.2.2.3 Counting cells using a haemocytometer

For counting, cells were first trypsinised, centrifuged at 1000 rpm for 5 min and then resuspended in appropriate amount of media. 10 µl of the cell suspension was diluted in appropriate amount of 0.4% trypan blue (Sigma-Aldrich) and counted in eight squares (0.1 µl) of haemocytometer under the inverted microscope. The total number was averaged, multiplied by dilution factor and by 1 X 10^4 to determine the number of cells per ml. Those cells stained with trypan blue were dead and were excluded from counting.

2.2.2.4 Freezing cells for long term storage

The semi-confluent cells in a T-75 flask were trypsinised, centrifuged at 1000 rpm for 5 min and resuspended in 3 ml of complete growth media with 10% DMSO. 1 ml aliquots were transferred to cryogenic vials and stored at -80ºC overnight. Vials were placed in liquid nitrogen (-180ºC) the next day for long term storage.

2.2.2.5 Thawing cells for culture

Cells were taken from the liquid nitrogen tank and rapidly thawed in a 37ºC water bath and immediately diluted in 13 ml of complete growth media as DMSO is cytotoxic to cells. Then the cells were centrifuged at 1000 rpm for 5 min to remove DMSO containing media and plated to a T25 flask.

2.2.3 Western blot

2.2.3.1 Protein extraction

For western blot, HEK 293T cells in 6 well plate were transfected with 1 µg of mock (pcDNA3.1.V5/His), the full-length wild type TBX22 (pcDNA3.1.TBX22.V5/His) or the previously described N264Y pathogenic mutant (pcDNA3.1.TBX22(N264Y).V5/His) using FuGENE 6 according to the manufacturer's instruction. After 48 hours incubation, the cells were harvested and lysed in lysis buffer (150 mM NaCl, 25 mM Tris pH 7.5, 1% Triton X-100, 1% SDS, 0.5% sodium deoxycholate, 1x protease inhibitor) for 40 min at 4ºC with rotation. The lysate was centrifuged for 20 min at 3,000 *g* at 4ºC and the supernatant was collected and stored at -20ºC. Also, 10 µl of the supernatant was collected in a separate tube to estimate concentration using the Bradford assay.

2.2.3.2 Bradford assay to determine protein concentration

The Bradford reagent was gently mixed and brought to room temperature. Bovine serum albumin (BSA) protein standards were prepared at concentrations of 0 mg/ml, 0.125 mg/ml, 0.25 mg/ml, 0.5 mg/ml, 1 mg/ml in lysis buffer. 10 µl of the standards or 1:10 diluted samples were mixed with 250 µl of the Bradford reagent in 96 well plate and incubated for 5 min at room temperature before assayed on plate reader at 595 nm (DYNEX REVELATION 4.21). Each standard or sample was measured in triplicate. The read out from the BSA standards less the background was used to plot a standard curve (i.e. OD at 595 nm against BSA protein concentration) from which the concentration of the samples were calculated.

2.2.3.3 SDS-PAGE and immunoblotting

The protein samples were made up to a concentration of 20 µg/10 µl using lysis buffer and mixed with 5 µl of loading buffer (0.3 ml 0.5 M Tris pH 6.8, 2.5 ml glycerol, 2 ml 10% SDS, 0.1% bromophenol blue, 10% β-mercaptoethanol) and 1 µl of 0.5 M DTT, then boiled for 5 min at 95ºC. Samples and protein standards were loaded and gels (10% resolving gel: 2.5 ml 1.5 M Tris pH 8.8, 3.33 ml 30% acrylamide, 0.1 ml 10% SDS, 3.983 ml H_2O, 0.075 ml 10% APS, 0.012 ml TEMED; 5% stacking gel: 1.25 ml 1 M Tris pH 6.8, 0.66 ml 30% acrylamide, 0.05 ml 10% SDS, 3 ml H_2O, 0.05 ml 10% APS, 0.006 ml TEMED) were run at 150 V for 1 hour in 1X running buffer (3.02 g Tris, 14.4 g glycine, 0.1% SDS, H_2O to 1 L). Proteins were then immunoblotted onto PVDF membranes using Trans-Blot SD Semi-Dry Transfer Cell (BIO-RAD) in the following order; 3X filter papers, PVDF membrane, SDS-PAGE gel, 3X filter paper immersed in blot butter (1X running buffer, 20% methanol), and transferred at 400 mA for 30 min. The membranes were then incubated in blocking solution (5% milk in PBS-0.05% tween-20) overnight at 4ºC to reduce background. The next day, the membrane was incubated with primary antibody (anti-V5 antibody 1:5,000; anti-β-actin antibody 1:1,5000) in blocking solution for 1 hour at room temperature, washed three times in PBS-0.05% tween-20, incubated with secondary antibody (rabbit anti-mouse HRP 1:5,000) for 40 min at room temperature, washed three times in PBS-0.05% tween-20, followed by detection using ECL Plus Western Blotting Detection System (GE Healthcare Life Sciences). The membrane was incubated with 1 ml of 1:40 solution A:solution B for 5 min at room temperature and exposed to autoradiography film for different lengths of time.

2.2.4 Luciferase assay

2.2.4.1 PCR amplification of the *MyoD* putative promoter

Primers to amplify the *MyoD* putative promoter region contained *Xho*I site at 5' ends. For PCR reaction, 4 µl of mouse genomic DNA template was mixed with 20 µl of 5X Green GoTaq® Flexi Buffer, 4 µl of 10 mM dNTPs, 20 µl of 25 mM $MgCl_2$, 20 µl of 5 M Betaine, 0.8 µl of GoTaq® Hot Start Polymerase (Promega),

3.2 µl of MyoD_F_-683 and 3.2 µl of MyoD_R_+115 primers. The total reaction volume was made up to 100 µl with H_2O. PCR reactions were performed in 96 well plates using DNA Engine Dyad Peltier Thermal Cycler (Bio-Rad Life Sciences) with the following thermal cycle conditions: 94ºC for 5 min followed by 35 cycles of 94ºC for 30 sec, 65ºC for 1 min 30 sec and 74ºC for 1 min 30 sec. The PCR products were visualised on a 1% agarose gel under UV light.

2.2.4.2 Cloning the *MyoD* putative promoter into pGL3-Basic vector

The PCR products were first ligated into 50 ng of pGEM®-T Easy at 1:1 to 1:3 vector:insert molar ratios using T4 DNA ligase in a 10 µl reaction volume. After transformation of competent cells by heat shock, the PCR products were released from the pGEM®-T Easy vector by *Xho*I digestion and gel extracted using QIAquick Gel Extraction Kit (QIAGEN). 1 µg of the pGL3-Basic vector was also digested with *Xho*I, treated with 1 µl of 5 u/µl Antarctic phosphatase (NEB) for 15 min at 37ºC and gel extracted using QIAquick Gel Extraction Kit (QIAGEN). Concentrations of the insert and vector were estimated on a gel and the insert was ligated into 50 ng of the pGL3-Basic vector at 1:1 to 1:3 vector:insert molar ratios using T4 DNA ligase in a 10 µl reaction volume. After transformation of competent cells by heat shock, plasmid DNA was purified from isolated colonies and analysed by restriction digestion. For pGL3-MyoD-683/+115, *Sma*I digest of positive clones with correct orientation produced bands at 5112 bp and 636 bp.

2.2.4.3 Site-directed mutagenesis

The QuikChange site-directed mutagenesis kit (Stratagene) was used to substitute two bases in the TBE of pGL3-MyoD. Predicted TBE sequence in the *MyoD* promoter region was TGCTCACCTAG that was located between -515 bp to -505 bp relative to the transcription start site (TSS). Two complimentary oligonucleotides containing the mutations that resulted in substitutions of a base C to a base A at -511 bp relative to TSS and a base C to a base A at -509 bp relative to TSS, flanked by unmodified nucleotides were synthesized (Sense: 5'ATTTGTGCCAGGCTTGCTAAACTAGACCTTCTGAGTCTC3'; antisense: 5'-GAGACTCAGAAGGTCTAGTTTAGCAAGCCTGGCACAAAT-3'). 2 µl (10 ng)

of pGL3-MyoD was mixed with 5 µl of 10X reaction buffer, 1.25 µl (125 ng) of sense and antisense oligonucleotide primers, 1 µl of 10 mM dNTPs and 1 µl of *PfuTurbo* DNA polymerase (2.5 U/µl). The total reaction volume was made up to 5 µl with H_2O. Then, thermal cycling reaction was performed using DNA Engine Dyad Peltier Thermal Cycler (Bio-Rad Life Sciences) with the following thermal cycle conditions: 95ºC for 30sec followed by 16 cycles of 95ºC for 30 sec, 55ºC for 1 min and 68ºC for 6 min. The reaction was cooled on ice for 2 min, and then incubated with 1 µl of *Dpn* I restriction enzyme (10 U/µl) at 37ºC for 1 hour to digest the parental non-mutated dsDNA. After digestion, 1 µl of the *Dpn* I-treated DNA was added to 50 µl of XL1-Blue supercompetent cells, incubated on ice for 30 min followed by heat shock for 45 sec at 42ºC, then immediately placed on ice for 2 min. 0.5 ml of LB medium was added and incubated at 37ºC for 1 hour while shaking at 180 rpm. Transformed cells was spread on LB agar plate containing 100 µg/ml of ampicillin and incubated overnight at 37ºC. The next day, isolated colonies were picked and expanded accordingly in LB in the presence of 100 µg/ml of ampicillin, and the base substitutions in the insert was verified by DNA sequencing.

2.2.4.4 Measuring luciferase activity in cells transfected with pGL3-MyoD promoter

HEK 293T cells, which lack endogenous *TBX22* expression, were used in luciferase assay. One day before transfection, 1.2 x 10^4 cells/well were seeded in a 96 well plate. The following day, sub-confluent cells were transiently co-transfected with 0.15 µl of FuGENE 6 (Roche) containing 50 ng of luciferase reporter construct (pGL3-MyoD), 2.5 ng or 10 ng of wtTBX22 or N264Y and 5 ng of *Renilla* luciferase construct (pRL-CMV) and left incubated for 48 hours. Luciferase activity was measured as follows. 50 µl of medium was removed and 50 µl of Steady Lite Plus (Perkin Elmer) in reconstitution buffer was added to each well. Cells were left at room temperature for 10 min, transferred to a 96 well MICROLITE plate (Dynex) and read by FLUOstar OPTIMA (BMG LABTECH). Then 25 µl of coelenterazin (10 ng/µl) in *Renilla* buffer was added to the same samples, incubated for 10 min and *Renilla* luciferase activity was read. Firefly luciferase reading was

normalised to *Renilla* luciferase reading. Each set of experiment was done in quadruplicate wells and repeated three times.

2.2.5 Chromatin immunoprecipitation

The direct interaction of TBX22 with the *MyoD* promoter was analysed by chromatin immunoprecipitation in transfected HEK 293T cells. One day before transfection, 3.84 x 10^5 cells were seeded in a 6 well plate. The following day, subconfluent cells were transiently transfected with 3 µl of FuGENE 6 containing 1 µg of mock, wtTBX22 or N264Y. After incubating for 48 hours, the cells were cross linked with 0.8% formaldehyde at room temperature for 10 min, and stopped by addition of glycine to a final concentration of 0.125 M, followed by 5 min incubation at room temperature. The fixed cells were washed twice with PBS and harvested by scraping. Then, the cells were pelleted by centrifugation for 3 min at 1,000 rpm and resuspended in lysis buffer (150 mM NaCl, 25 mM Tris pH 7.5, 1% Triton X-100, 1% SDS, 2 mM EDTA, 0.5% sodium deoxycholate, protease inhibitors) at a concentration of 1.5 x 10^6 cells/300 µl. Followed by 5 min incubation on ice, 1.5 x 10^6 cells were sonicated for 15 min at high power setting (320 W) with a 30 sec on 30 sec off cycle by water-based sonicator Bioruptor (Diagenode) to fragment the DNA to a size of 100-500 bp. After sonication, cell debris was pelleted by centrifugation for 30 sec at 8,000 *g* and supernatant was transferred to a new tube. 50 µl of sonicated sample was removed as the total input which served as a control in the PCR. For immunoprecipitation, 150 µl of sonicated chromatin preparation was diluted 1:10 with RIPA buffer (0.01% SDS. 1.1% Triton X-100, 1.2 mM EDTA, 16.7 mM Tris pH 7.5, 167 mM NaCl, protease inhibitors) and incubated overnight with rotation at 4Cº with 1 µg of anti-V5 antibody (invitrogen) and 20 µl of protein G agarose beads (Pierce) which was preadsorbed with 75 ng/µl salmon sperm DNA and 0.1 µg/µl BSA. The next day, the protein G agarose beads were washed three times with 1 ml wash buffer (0.1% SDS, 1% Triton X-100, 2 mM EDTA pH 8.0, 150 mM NaCl, 20 mM Tris pH 8.0) followed by a wash with 1 ml final wash buffer (0.1% SDS, 1% Triton X-100, 2 mM EDTA pH 8.0, 500 mM NaCl, 20 mM Tris pH 8.0) for 15 min at room temperature. Then, bound DNA was eluted by adding 120 µl of elution buffer (1% SDS, 100 mM $NaHCO_3$) and rotated for 15 min at room temperature. 100 µl of the sample was

incubated with 2 µl of RNaseA (20 mg/ml) and 140 µl of elution buffer at 65Cº overnight to reverse cross link. For input samples, 1 µl of RNaseA (20 mg/ml) and 70 µl of elution buffer were added. The DNA was purified using the QIAquick PCR purification kit (QIAGEN) according to the manufacturer's instruction before subjected to PCR amplification. Primer pairs used for PCR amplification were MyoD_ChIP_F and MyoD_ChIP_R which produced a 310 bp fragment.

2.2.6 Mouse techniques

2.2.6.1 Animal husbandry

Mice were treated in accordance with the UK Animals (Scientific Procedures) Act, 1986 and all procedures were approved by the British Home Office Inspectorate. The original *Tbx22* null mouse strain was generated by Dr. Erwin Pauws. Briefly, exon 1 and exon 3 of *Tbx22* were flanked by *lox*P sites and then removed by crossing with a β-actin-Cre deleter strain (Pauws et al., 2009a).

2.2.6.2 Embryo collection

Mice were kept on a 12 hour light-dark cycle. Male null ($Tbx22^{Neo/Y}$) and female heterozygote ($Tbx22^{+/Neo}$) pairs were set up in a breeding cage to obtain four possible genotype embryos $Tbx22^{+/Y}$, $Tbx22^{Neo/Y}$, $Tbx22^{+/Neo}$ and $Tbx22^{Neo/Neo}$. On the following day, female mice were examined for a copulatory plug. Noon of the day a plug was observed was referred to as embryonic day 0.5 (E0.5), assuming mating took place around midnight. Pregnant female mice were sacrificed by cervical dislocation at different embryonic time points and embryos were dissected from the uterus in cold PBS, then either fixed overnight at 4ºC in 4% paraformaldehyde in PBS, or homogenised in TRI Reagent (Sigma-Aldrich) and stored at -80ºC.

2.2.6.3 Genotyping

To obtain embryo specific DNA for genotyping, the yolk sac was collected and digested overnight at 55ºC in 100 µl PBS with 2 µl of proteinase K (10 mg/ml), and

boiled for 5 min before being subjected to PCR. 0.2 µl of proteinase K digested DNA template was mixed with 1 µl of 5X Green GoTaq® Flexi Buffer, 0.2 µl of 10 mM dNTPs, 1 µl of 25 mM $MgCl_2$, 1 µl of 5 M Betaine, 0.04 µl of GoTaq® Hot Start Polymerase (Promega), and 0.16 µl of 10 µM Tbx22_F, Tbx22_R and Tbx22_R2 primers for genotyping PCR or 0.16 µl of 10 µM Smc_F and Smc_R primes for sexing PCR. The total reaction volume was made up to 5 µl with H_2O. PCR reactions were performed in 96 well plates using DNA Engine Dyad Peltier Thermal Cycler (Bio-Rad Life Sciences) with the following thermal cycle conditions: 94ºC for 5 min followed by 35 cycles of 94ºC for 30 sec, 65ºC for 1 min 30 sec and 74ºC for 1 min 30 sec. The PCR products were visualised on a 1% agarose gel under UV light.

2.2.7 Expression microarray analysis

2.2.7.1 Extraction of total RNA from tissues

Mouse embryos were dissected from the uterus and pairs of palatal shelves were cut out under a dissecting microscope. Tissue samples were immediately homogenised in TRI Reagent (Sigma-Aldrich) and total RNA was extracted. The samples were then ethanol precipitated.

2.2.7.2 Microarray hybridisation

Quality control of the RNA samples and microarray analysis were performed by the ICH Microarray Centre which is now part of UCL Genomics. The yield and quality of the RNA samples were determined by spectrophotometry measurements using a NanoDrop (Thermo Scientific), and RNA integrity was checked by ribosomal 18S/28S ratio using the Agilent 2100 Bioanalyzer (Agilent Technologies).
RNA samples collected from *Tbx22*$^{+/Y}$ and *Tbx22*$^{Neo/Y}$ were appropriately processed and hybridised to GeneChip® Mouse Gene 1.0 ST Array (Affymetrix). Briefly, double-stranded cDNA was synthesised form 100 ng of total RNA with random hexamers tagged with a T7 promoter sequence which was subsequently amplified by T7 RNA polymerase to produce antisense cRNA. Then the cRNA was reverse transcribed with random hexamers to produce single-stranded cDNA which was

fragmented and labelled with Affymetrix® proprietary DNA Labeling Reagent. The labelled cDNA was hybridised to the array, washed and stained using the GeneChip® Hybridization, Wash and Stain Kit. The array was then scanned by the GeneChip® Scanner 3000 7G.

2.2.8 Quantitative real-time PCR

2.2.8.1 Extraction of total RNA

Total RNA was extracted from cells and tissues using TRI Reagent (Sigma-Aldrich) and samples were ethanol precipitated.

2.2.8.2 First strand cDNA synthesis

500 ng of total RNA was treated with 1 µl of RQ1 RNase-Free DNase (1 u/1 µl) (Promega) for 30 min at 37ºC to remove possible genomic DNA contamination. The reaction was terminated by incubating with 1 µl of RQ1 DNase Stop Solution (Promega) for 10 min at 65ºC. Prior to first strand cDNA synthesis, 9 µl of the DNase treated RNA sample was mixed with 1 µl of random primers (Promega) and incubated for 10 min at 70ºC, followed by cooling on ice for 5 min. First strand cDNA synthesis was performed by adding 4 µl of M-MLV 5X Reaction Buffer (Promega), 2 µl of 10 mM dNTPs, 0.5 µl of Recombinant RNasin® Ribonuclease Inhibitor (Promega), 1 µl of M-MLV Reverse Transcriptase (Promega) and 2.5 µl of DEPC treated water. The reaction mixture was incubated at 37ºC for 1 hour followed by incubation at 95ºC for 10 min to denature M-MLV Reverse Transcriptase.

2.2.8.3 Taqman quantitative real-time PCR

Quantitative real-time PCR technique enables either absolute or relative quantification of target DNA samples based on the fact that there is a quantitative relationship between the starting amount of DNA and the amount of PCR product made. In this study, TaqMan® Gene Expression Assays (Applied Biosystems) were used to perform relative quantification of gene expression. Its chemistry is based on

the 5' exonuclease activity of AmpliTaq Gold® DNA polymerase which cleaves and releases a fluorescent reporter dye (6-FAM™ dye) linked to the TaqMan® probes resulting in an increase in fluorescence during PCR amplification. Real-time PCR reaction mixture was composed of 1 µl of cDNA, 5 µl of TaqMan® Fast Universal Master Mix (2X), No AmpErase® UNG (Applied Biosystems), 0.5 µl of TaqMan® Gene Expression Assay or Endogenous Control (20X) (Applied Biosystems) and 3.5 µl of DEPC treated water. The fluorescent signals were detected with 7500 FAST Real-Time PCR system (Applied Biosystems) using the following thermal cycle conditions: 95ºC for 20 sec followed by 40 cycles of 95ºC for 3 sec, 60ºC for 30 sec. All samples were tested in triplicate wells for both target and endogenous control genes and repeated at least three times. For data analysis, comparative CT method for relative quantification was carried out using SDS 3.1 (Applied Biosystems).

2.2.9 Section *in situ* hybridisation

2.2.9.1 Embryo fixation, dehydration and wax embedding

Mouse embryos were dissected at different embryonic time points, washed twice with PBS for 2 min and fixed overnight in 4% paraformaldehyde in PBS at 4ºC with rocking. The next day, embryos were washed twice in PBS for 30 min and dehydrated through graded ethanol series (25%, 50%, 70%, 85% and 95%) for 1 hour each, then 100% overnight. Dehydrated embryos were processed for wax embedding starting with tissue clearing in Histoclear twice for 40 min at room temperature, 1:1 = histoclear:wax for 30 min at 60ºC followed by three times in wax for 40 min at 60ºC. Then embryos were transferred to embedding moulds and left at 60ºC for further 30 min, then appropriately orientated. Blocks were left to cool at room temperature until they solidified.

2.2.9.2 Non-radioactive riboprobe synthesis

Typically, 10 µg of plasmid DNA which contained *in situ* riboprobe insert was digested with 50 units of restriction enzymes in a 200 µl reaction volume for 3 hours. Digested DNA was incubated with 2 µl of 0.5 M EDTA, 10 µl of 20% SDS

and 4 µl of proteinase K (10 mg/ml) for 30 min at 37ºC, and purified by phenol chloroform extraction. *In vitro* transcription was performed using DIG RNA Labelling Kit (SP6/T7) (Roche Applied Science) with the following components: 1 µg of digested DNA, 2 µl of 10X DIG RNA labelling mix, 2 µl of 10X transcription buffer, 0.5 µl of Recombinant RNasin® Ribonuclease Inhibitor (Promega), 1 µl of SP6 or T7 RNA polymerase and appropriate volume of DEPC treated water to a total volume of 20 µl. Reaction mixture was incubated for 3 hours at 37ºC for T7 and 40ºC for SP6. Efficiency of transcription was determined by analysing the riboprobe on a 1% agarose gel and visualising under UV. Good probes usually showed a 10 fold brighter band than the plasmid DNA band. Finally, the riboprobe was cleaned by passing through a CHROMA SPIN-100 DEPC-H_2O column (Clontech) according to the manufacturer's instruction.

2.2.9.3 Section *in situ* hybridisation

Wax embedded embryos were sectioned at 8 µm thickness using microtome, mounted onto glass slides and dried in a 37ºC oven overnight. Non-radioactive RNA *in situ* hybridisation was performed as previously described (Wilkinson, 1998) with some modifications. The process can be divided into pre-hybridisation treatment, post-hybridisation washing and antibody detection.

Pre-hybridisation treatment; wax sections were deparaffinised by placing into Histoclear twice for 10 min, rehydrated through graded ethanol series (100% twice for 1 min, 70% for 1 min, 50% for 1 min, 25% for 1 min), then placed into 1X PBS for 2 min, 4% paraformaldehyde in 1X PBS for 20 min, 1X PBS twice for 2 min, proteinase K (20 µg/ml) in 1X PBS for 8 min, 4% paraformaldehyde in 1X PBS for 5 min, 1X PBS twice for 2 min, 0.1 M triethanolamine with 1 ml acetic anhydride for 10 min, 1X PBS twice for 2 min and then dehydrated through graded ethanol series (25% for 1 min, 50% for 1 min, 70% for 1 min, 100% twice for 1 min). After the slides were air dried, 100 µl of hybridisation mixture was added and cover slipped. The mixture contained riboprobe at 1:100 dilution, 1 µl/ml of RNase inhibitor and 0.5 mg/ml of tRNA in Hybmix (50% formamide, 0.3 M sodium chloride, 20 mM Tris-HCl, 5 mM EDTA, 10% dextran sulphate and 1X Denhardt's). The slides were incubated at 65ºC overnight.

Post hybridisation washing; All washes were performed at hybridisation temperature in a glass staining trough in a water bath. The slides were washed in 2X SSC twice for 30 min, formamide (50% formamide, 10% 20X SSC, 40% H_2O) twice for 30 min, 2X SSC twice for 30 min and 0.2X SSC twice for 30 min. After the last wash the slides were removed from water bath and allowed to cool to room temperature.

Antibody detection; the slides were washed in buffer 1 (0.1 M Tris-HCl pH 7.6, 0.15 M sodium chloride) for 2 min at room temperature, then blocked with 10% foetal calf serum (FCS) in buffer 1 for 1 hour. The slides were incubated with 0.5 ml of antibody solution containing anti-digoxygenin, Fab fragments (1:1000) (Roche Applied Science) in buffer 1 with 2% FCS at 4ºC overnight. The next day, slides were washed in buffer 1 three times for 5 min, twice in buffer 2 (0.1 M Tris-HCl pH 9.5, 0.1 M sodium chloride, 0.05 M magnesium chloride) for 5 min and developed with 0.5 ml of NBT/BCIP solution (4.5 µl/ml of NBT and 3.5 µl/ml BCIP in 1:1 = 2X buffer 2:10% PVA) at room temperature. When developed sufficiently, slides were washed in running tap water for 10 min, dried and mounted with Vectamount H-5000 (Vector).

2.2.10 Whole mount *in situ* hybridisation

2.2.10.1 Embryo preparation

Mouse embryos were dissected at different embryonic time points, washed twice with PBS for 2 min and fixed overnight in 4% paraformaldehyde in PBS at 4ºC with rocking. The next day, embryos were washed twice in PBT (PBS, 0.1% Tween-20) for 30 min at 4ºC and dehydrated through graded methanol series (25%, 50% and 75%) for 1 hour each, followed by two washes in 100% methanol. Dehydrated embryos were stored in 100% methanol at -20ºC.

2.2.10.2 Whole mount *in situ* hybridisation

All washes were performed at room temperature for 10 min unless otherwise stated. Embryos were rehydrated by washes in 75%, 50% and 25% methanol in PBT followed by two washes in PBT. Then the embryos were bleached in 6% hydrogen

peroxide in PBT for 1 hour, washed three times in PBT, and treated with 10 µg/ml proteinase K for 10 min to 30 min depending on embryonic stage. The reaction was stopped by washing in 2 mg/ml glycine in PBT followed by two washes in PBT. Next, embryos were refixed in 0.2% glutaraldehyde in 4% paraformaldehyde for 20 min and washed twice in PBT which was then replaced by 2 ml of prehybridisation mix (50% formamide, 5x SSC pH 4.5, 50 µg/ml yeast RNA, 1% SDS, 50 µg/ml heparin). Once the embryos had sunk, the prehybridisation mix was replaced with 5 ml of fresh mix and incubated for 3 hours at 70ºC. Then, the embryos were incubated in fresh 1 ml prehybridisation mix containing 10 µl of digoxigenin-labelled probe at 70ºC overnight. The next day, the hybridisation mix was removed and embryos were washed in solution 1 (50% formamide, 5x SSC pH 4.5, 1% SDS) for 15 min, followed by two more washes in solution 1 for 30 min at 70ºC, and then two washes in solution 2 (50% formamide, 2x SSC pH 4.5, 1% SDS) for 30 min at 65ºC. Then embryos were washed three times in TBST (8 mg/ml NaCl, 0.2 mg/ml KCl, 25 mM Tris pH 7.5, 1% Tween-20, 0.48 mg/ml levamisole) before preblocked for 90 min in TBST containing 10% sheep serum. The 10% sheep serum was then replaced with 2 ml of antibody solution containing anti-digoxygenin, Fab fragments (1:2000) (Roche Applied Science) in TBST with 1% sheep serum and incubated overnight at 4ºC with rocking. The next day, antibody solution was removed and embryos were washed three times in TBST for 5 min and the washes in TBST were repeated hourly for six times at room temperature and overnight at 4ºC. The next day, embryos were washed three times in NTMT (100 mM NaCl, 100 mM Tris pH 9.5, 50 mM $MgCl_2$, 0.1% Tween-20) and developed in 1 ml NTMT containing 4.5 µl NBT and 3.5 µl BCIP with rocking until the colour developed, and stopped by washing in PBT and stored in PBT at 4ºC.

2.2.11 Immunohistochemistry

For immunohistochemistry, wax sections were deparaffinised by placing into Histoclear twice for 10 min, rehydrated through graded ethanol series (100% for 2 min, 95% for 2 min, 75% for 2 min), then washed three times in PBS-0.1% Triton X-100 for 10 min each. The slides were blocked in blocking buffer (5% goat serum in PBS-0.1% Triton X-100, 0.15% glycine, 2 mg/ml BSA) for 30 min at room temperature, and incubated with primary antibody (phospho-Histone H3 (1:200);

cleaved caspase-3 (1:200)) in blocking buffer overnight at 4ºC. The next day the slides were washed three times in PBS-0.1% Triton X-100, and incubated with polyclonal goat anti-rabbit immunoglobulins biotinylated (1:250) in blocking buffer for 1 hour at room temperature. After three time washes in PBS-0.1% Triton X-100, the slides were incubated with streptavidin, Alexa Fluor® 555 conjugate (1:300) in PBS-0.1% Triton X-100 for 2 hours at room temperature, washed three times in PBS-0.1% Triton X-100, and mounted in VECTASHIELD mounting medium with DAPI.

CHAPTER 3: RESULTS

3 RESULTS

3.1 Expression pattern of *Tbx22* in mice

Loss of function mutations in TBX22 have been shown to be the molecular basis of X-linked cleft palate with or without ankyloglossia, in both human (Braybrook et al., 2001; Braybrook et al., 2002; Chaabouni et al., 2005; Marcano et al., 2004) and mouse (Pauws et al., 2009a). The phenotype has been shown to be closely allied to the spatiotemporal expression pattern that is conserved in several different species including mouse, chick and zebrafish (Braybrook et al., 2002; Bush et al., 2002; Haenig et al., 2002; Herr et al., 2003; Jezewski et al., 2009). Though several groups have shown *Tbx22* expression using both section and whole mount *in situ* hybridisation especially at around E13.5 prior to palatal shelf elevation, it was decided to perform whole mount and/or section *in situ* hybridisation from E9.5 to E15.5 to provide a reference for the experimental data presented in the rest of this thesis.

3.1.1 Expression of *Tbx22* from E9.5 to E15.5

In order to investigate the expression of *Tbx22* in the early stages of lip and palate morphogenesis, it was decided to start with E9.5 mouse embryos (Figure 3.1, A and B). At this developmental stage, the mandibular processes of the first branchial arch were already visible while the maxillary processes were not established until about a day later. Although expression of the gene was observed at this stage by RT-PCR (Braybrook et al., 2002), no obvious expression was detected in the first branchial arch from which the future maxillary processes arise, or in fact any other parts of the embryos by the whole mount *in situ* hybridisation method used. It is possible that at this stage, the gene may be expressed at a very low level that it was under the detection limit by whole mount *in situ* hybridisation method used, whereas it was detectable by RT-PCR which in theory is sensitive enough to detect very low copy numbers of mRNA.

By E10.5, the first branchial arch was divided into maxillary and mandibular processes. As shown in Figure 3.1 (C-F), expression of *Tbx22* was observed in the maxillary and mandibular processes, in the medial nasal processes and also in the nasal fin area where the medial and lateral nasal processes meet. At this stage, expression was especially strong in the top half of the mandibular prominences that were fusing to form the mandible, and around the nasal fins, which in the wt gradually degrade by the end of E11.5 to E12.0. This could indicate that TBX22 may be having an important role in these tissues at or around this developmental time point. In addition, the expression was also detected in the somites and otic vesicles (Figure 3.1, C and D).

The swelling of palatal shelves were first observed from the maxillary prominences at around E11.5. The frontal view of whole mount *in situ* hybridisation showed a defined and specific expression of *Tbx22* in the anterior tip of the mandible indicated by an arrow in Figure 3.1, H. The tongue extends from the *tuberculum impar*, which appears on the lower edge of the mandible and further two swellings called the lateral lingual prominences that extend to form the anterior two thirds of the tongue. Expression at the anterior tip observed at this stage is of particular interest because this anterior region corresponds to the future frenulum region which in the null mice attached more anteriorly to the mandible than wt (ankyloglossia phenotype) (Pauws et al., 2009a). By removing the mandible, expression was also visible in almost the entire swelling of the palatal shelves as well as around the fused medial and lateral nasal processes (Figure 3.1, I and J). Expression was also noted in the otic vesicles as well as in the periocular mesenchyme around the eyes which was not detectable at earlier stages (Figure 3.1, K and L).

By E12.5, the growing palatal shelves started to become more apparent. A specific expression of *Tbx22* was observed in the middle region of the palatal shelves, and in the medial and lateral nasal mesenchyme (Figure3.1, M and N). Also, section *in situ* hybridisation showed expression of the gene at the base of the tongue anteriorly around the frenulum, in the medial and lateral nasal mesenchyme where there were nasal fins up until E11.5 in the wt, and in the periocular mesenchyme around the eyes (Figure 3.2, A and C). Higher magnification of the palatal shelf indicated its

expression in the mesenchyme but not in the epithelium (Figure 3.2, E). These observations are in agreement with previous studies (Braybrook et al., 2002; Bush et al., 2002; Herr et al., 2003).

The embryos became generally bigger in size at E13.5. The expression pattern of *Tbx22* was similar to that seen at E12.5 while the expression in the growing palatal shelves was slightly shifted posteriorly compared to E12.5 embryos (Figure 3.1, O-R). However, this was somewhat variable between embryos where some had stronger expression in the middle region and others had more intense staining in posterior regions. Again, section *in situ* hybridisation showed expression at the base of the tongue anteriorly around the frenulum, in the medial and lateral nasal mesenchyme and in the periocular mesenchyme around the eyes (Figure 3.2, B and D). Also, the expression was more prominent in the palatal mesenchyme but not in the epithelium, although less obvious than at E12.5 (Figure 3.2, F).

The elevation of downward growing palatal shelves to the horizontal position seemed to occur in a rather short time window between E14.0-E15.0. Therefore dissecting embryos at E14.5 often resulted in harvesting morphologically mixed samples as far as the palatal shelves were concerned. These included embryos in which the palatal shelves had still not elevated to the horizontal position, palatal shelves in the middle of the elevation process and even those that were already elevated and beginning to fuse in the middle region of the horizontally oriented shelves (Figure 3.1, S-V). Expression of *Tbx22* at this stage seemed shifted further towards more posterior parts of the palatal shelves. Interestingly, there was no expression detected around the middle region of the fusing palatal shelves, whereas expression persisted in the posterior region while the palatal shelves extended towards each other in a horizontal direction. This may suggest a specific role for TBX22 in posterior palatal shelf growth at around this developmental stage.

Craniofacial expression of *Tbx22* was detected up until E16.5 by RT-PCR (Braybrook et al., 2002). However, no obvious expression was observed in the palate post-fusion at E15.5 using the whole mount *in situ* hybridisation method (Figure 3.1, W and X). Again, it is possible that at this stage the gene may not have

been expressed strongly enough to be detected by this method, with RT-PCR being considerably more sensitive.

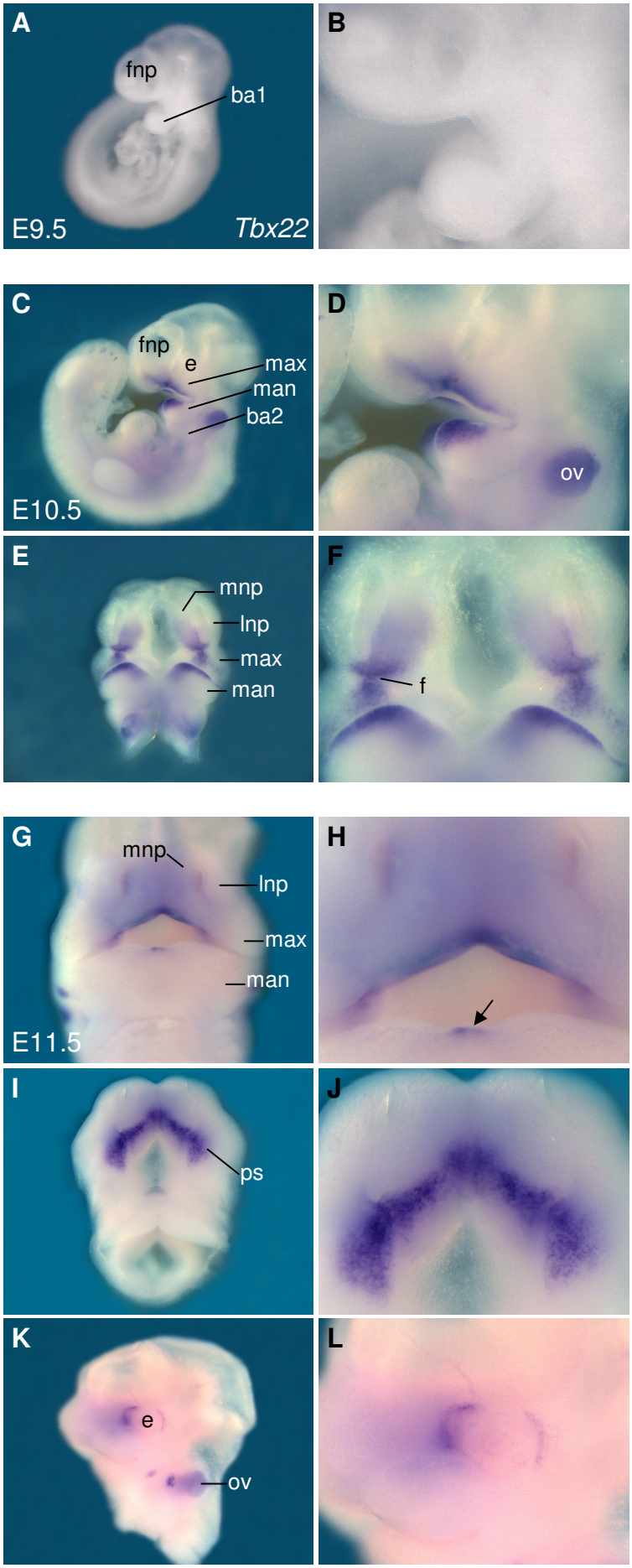
A
fnp
ba1
E9.5
Tbx22
B
C
fnp
e
max
man
ba2
E10.5
D
ov
E
mnp
lnp
max
man
F
f
G
mnp
lnp
max
man
E11.5
H
I
ps
J
K
e
ov
L

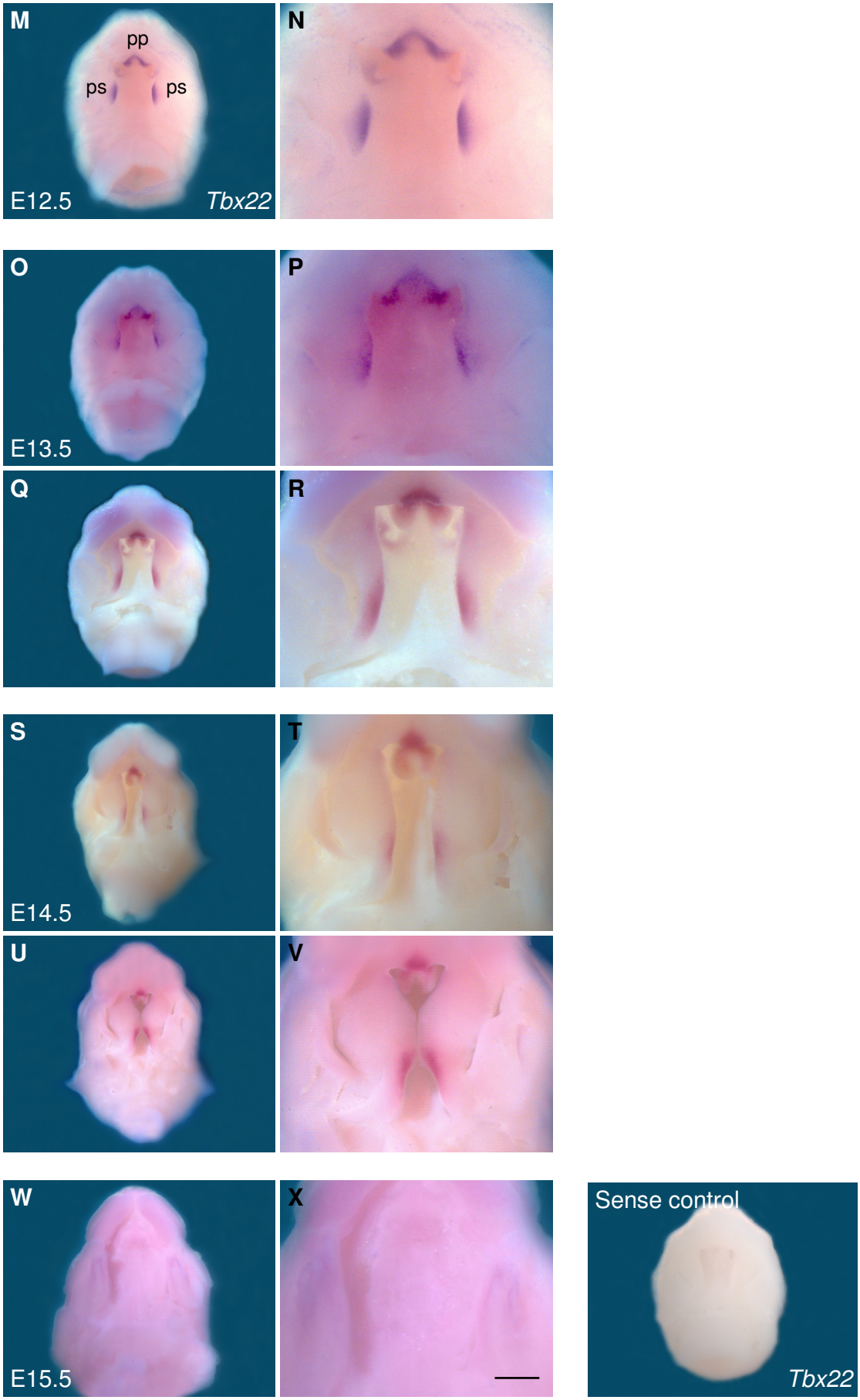
M
pp
ps
ps
E12.5
Tbx22
N
O
E13.5
P
Q
R
S
E14.5
T
U
V
W
E15.5
X
Sense control
Tbx22

Figure 3.1 Expression pattern of *Tbx22* from E11.5 to E15.5
Expression pattern of *Tbx22* was detected by whole mount *in situ* hybridisation from E9.5 to E15.5 using *Tbx22* antisense probe (A-X). The sense probe control did not give signals. Arrow in H indicates the anterior tip of mandible. ba1, first branchial arch; ba2, second branchial arch; e, eye; f, nasal fin; lnp, lateral nasal process; man, mandibular process; max, maxillary process; mnp, medial nasal process; ov, otic vesicle; p, palate; pp, primary palate; ps, palatal shelf. Scale bar = 250 µm (A, E and I), 320 µm (C, K and M), 100 µm (B, F and J), 128 µm (D, L and N), 200 µm (G, T, V and X), 80 µm (H), 400 µm (O and Q), 160 µm (P and R), 500 µm (S, U and W).

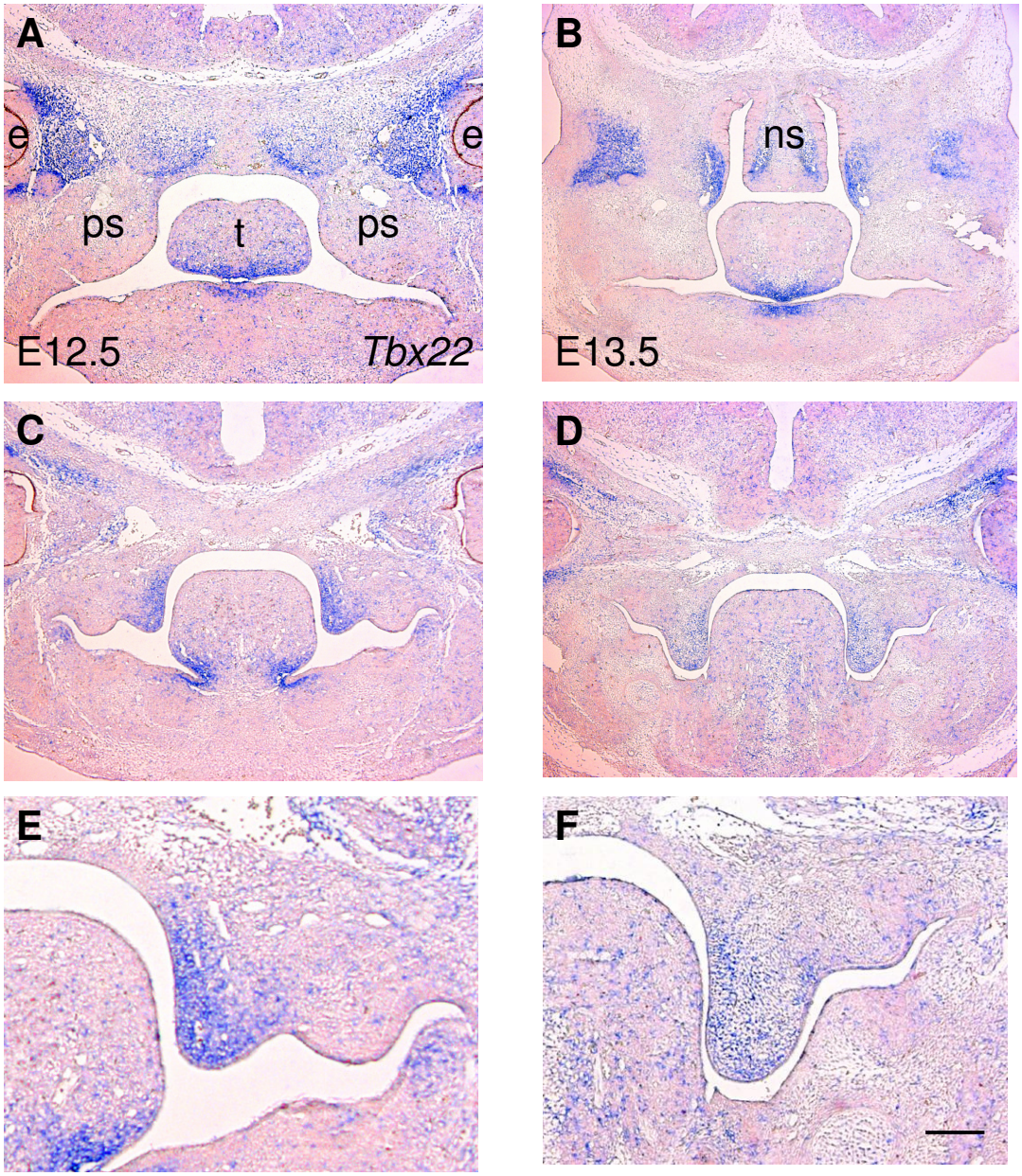

Figure 3.2 Expression pattern of *Tbx22* at E12.5 and E13.5
Expression pattern of *Tbx22* was detected by section *in situ* hybridisation at E12.5 and E13.5 using *Tbx22* antisense probe (A-F). High magnification views of the palatal shelves show that *Tbx22* expression is most intense in the mesenchyme but undetectable in the epithelium (E and F). e, eye; ns, nasal septum; ps, palatal shelf; t, tongue. Scale bar = 125µm (A-D), 50µm (E and F).

3.1.2 Summary

Using whole mount and section *in situ* hybridisation, the spatial and temporal expression patterns of *Tbx22* between E9.5 to E15.5 were determined. The gene was expressed at easily detectable levels from E10.5 to E14.5. In the maxillary processes and palatal shelves, expression was first observed at E10.5 and persisted throughout the period of palatogenesis until E14.5. The expression was rather broad at E10.5 and E11.5 in the maxillary processes, becoming restricted to the middle portion of the palatal shelves at E12.5, then shifting towards more posterior regions of the palatal shelves at E13.5 and E14.5. Expression in the periocular mesenchyme around the eyes appeared at around E11.5 and persisted into later stages. Expression around the nasal fins where the medial and lateral nasal processes first meet became evident at E10.5 and then persisted in the medial and lateral nasal mesenchyme at least up until E13.5. Similarly, expression in the mandibular processes started at around E10.5, at which time the processes were not yet fused. It persisted after the mandibular processes were fused to form the intact mandible at around E11.5, and continued to be expressed at the anterior base of the tongue around the site of the future frenulum. Staining in the otic vesicles at E10.5 and E11.5 has not been reported previously. This could be purely due to trapping of the probe in the vesicle or might be a true staining which requires further analysis. At this point, no ear defects have been demonstrated in *Tbx22* null mice. Expression patterns observed at E13.5, prior to shelf elevation, were in good agreement with other previously published studies (Braybrook et al., 2002; Bush et al., 2002; Herr et al., 2003). Overall, a good match with the tissues affected by pathological phenotypes in *Tbx22* null mice was observed. These include expression in the middle to posterior palatal shelves at the site of submucous cleft palate, while expression in the medial and lateral mesenchyme as well as the frenulum correlate with the appearance of choanal atresia and ankyloglossia respectively (Pauws et al., 2009a). No obvious eye phenotype in *Tbx22* null mice has been observed and no eye-related defects have been reported in human CPX patients either.

3.2 Microarray and real-time PCR analyses show increased expression of muscle genes in *Tbx22* null mice

Tbx22 null mice were developed using the conditional LoxP/Cre method, and were recently reported by our group (Pauws et al., 2009a). In this mouse line, the first three exons were removed by crossing floxed animals with *β-actin*-Cre deleter mice. The neo^R cassette was retained on the $Tbx22^{null}$ allele and also in all the relevant embryos described in this thesis. In other experiments not described here, removal of the neo^R cassette did not change the phenotype.

Tbx22 null mouse phenotype was investigated by a number of methods including visual inspection, histology, skeletal preparation and microCT analysis. The next objective was to investigate the mechanism behind the phenotype, first by looking at a number of key genes that are expressed in the craniofacial region known to be required for normal palate development. These included *Pax9*, *Snail*, *Msx1*, *Msx2*, *Bmp4*, *Osr1* and *Tgfβ3* (Peters et al., 1998; Proetzel et al., 1995; Satokata and Maas, 1994; Murray et al., 2007; Winograd et al., 1997; Zhang et al., 2002; Lu et al., 2000; Nie, 2005). Cleft palate has not been observed in *Osr1* homozygous mutant mice because they die with severe cardiac and urogenital defects before palate development is complete (Wang et al., 2005), but an *Osr1* knockin has been shown to rescue the developmental defects of the *Osr2* mutant mouse including cleft palate (Gao et al., 2009; Lan et al., 2004). In addition, previous observation by luciferase reporter assays suggested an interaction between TBX22 and the *OSR1* putative promoter, making *OSR1* a candidate target gene for TBX22 (Dr. A. Andreou unpublished observation). Expression of these genes was investigated by comparing wild type and null mice at E13.5 (or E14.5 for *Tgfβ3*), using section *in situ* hybridisation (Figure 3.3). In general, no specific differences were detected, except for a modest increase in *Msx2* in the posterior tongue (Figure 3.3, D) and *Pax9* which appeared to be upregulated in the mesenchyme at the base of the nasal septum through the oronasal membranes in the null embyros, at the site of rupture in the wild type (Figure 3.3, A). The latter could reflect a primary role of the gene in cell survival (Robson et al., 2006), but this seemed to be more of a secondary to the persistence of the oronasal membranes. Although a small proportion of *Tbx22*

null mice exhibit an overt cleft palate at later stages (>E15.5), no differences to the gross morphology of the palatal shelves was noted at E13.5 and the expression pattern of these genes did not differ significantly (Pauws et al., 2009a).

A

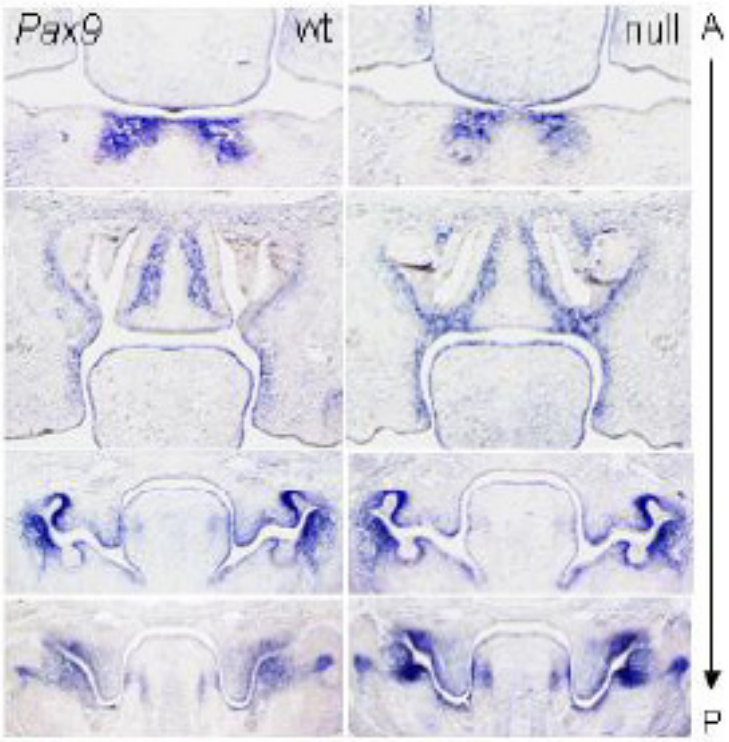

B

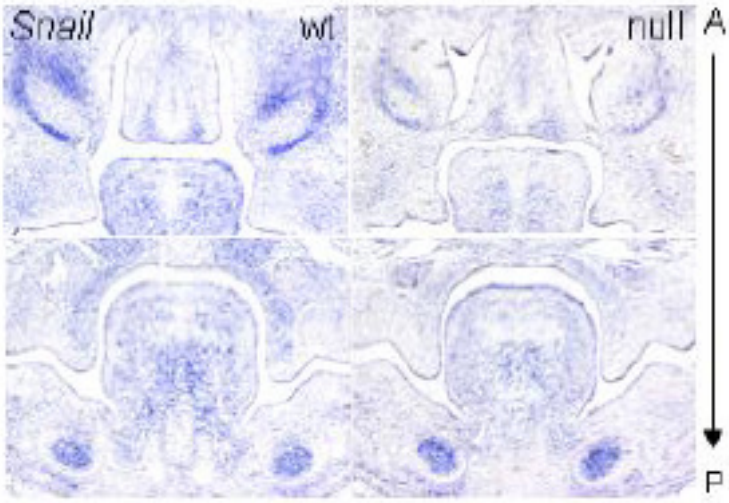

C

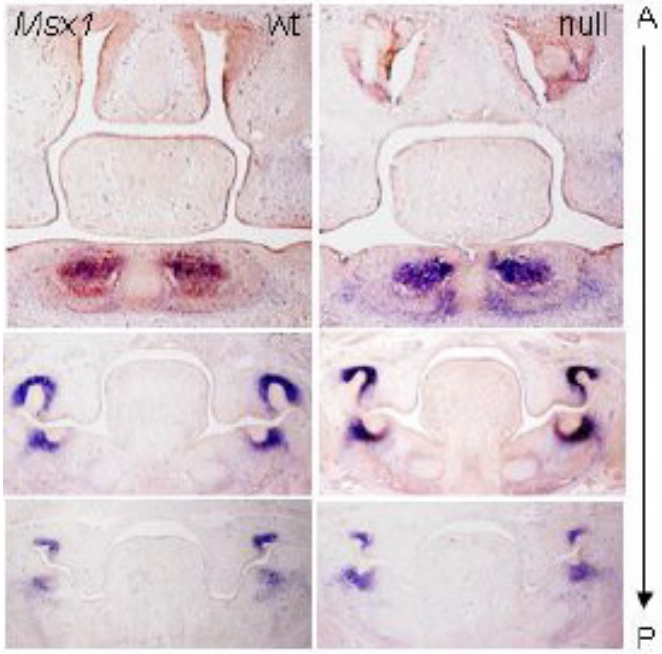

D

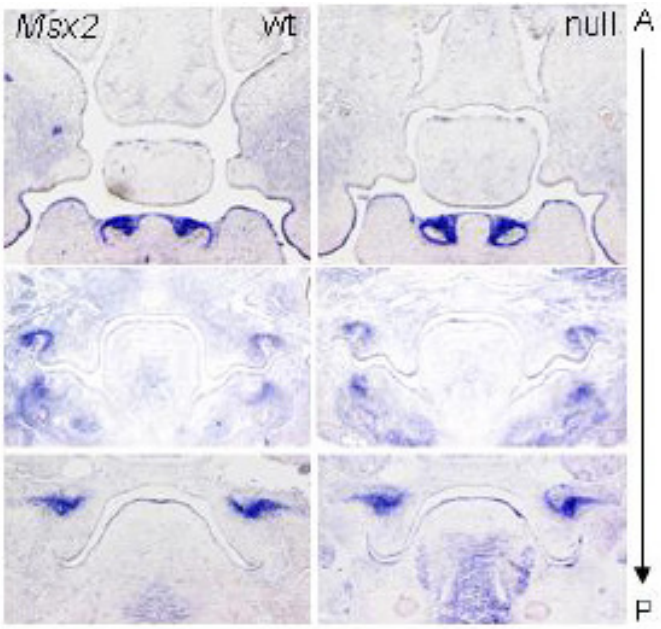

E

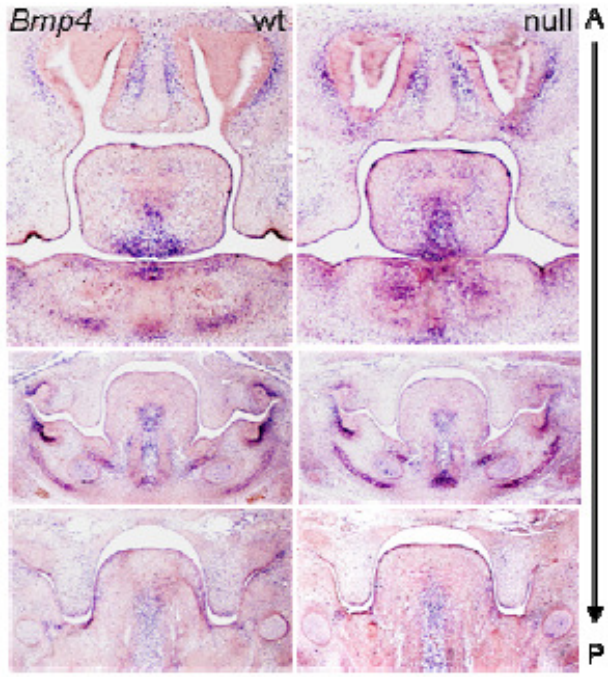

F

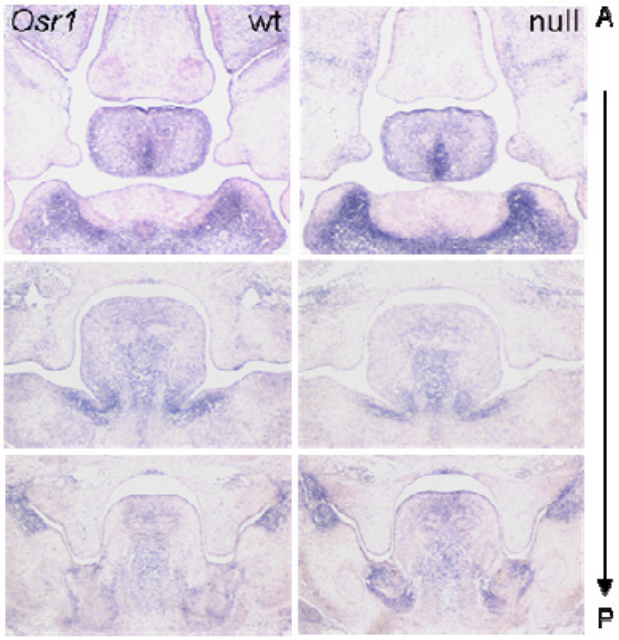

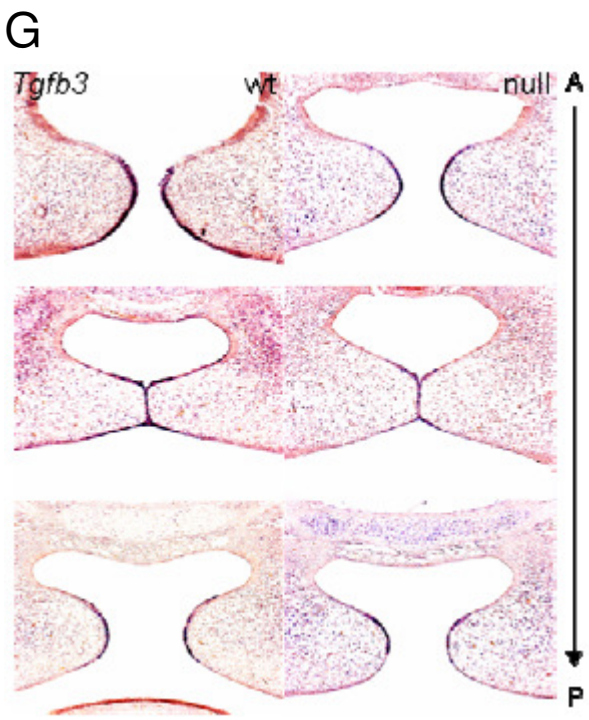

Figure 3.3 Expression patterns of *Pax9*, *Snail*, *Msx1*, *Msx2*, *Bmp4*, *Osr1* and *Tgfβ3*
Expression patterns of *Pax9* (A), *Snail* (B), *Msx1* (C), *Msx2* (D), *Bmp4* (E), *Osr1* (F) and *Tgfβ3* (G) were examined by *in situ* hybridision at E13.5 (E14.5 for *Tgfβ3*). A, anterior; P, posterior (Pauws et al., 2009a).

Since TBX22 is a transcription factor, and likely to be a transcriptional repressor (Andreou et al., 2007) it was expected that its loss would result in significant expression changes to one or more of the known or unknown genes active in the developing palate. It was therefore decided to perform a global comparative expression analysis using a method that does not introduce biases based on preconception. One of the most powerful tools for this is microarray analysis, which can be used to compare the expression of thousands of genes between samples. The array consists of spots of oligonucleotides, each corresponding to a short section of a specific gene to which target cDNA or cRNA can be hybridised. The abundance of each transcript in the target sample is normally detected by fluorophore labelling. In the experiments described below, comparative gene expression profiles were generated for developing palatal shelves at E13.5 in the presence and absence of functional *Tbx22*. E13.5 embryos were used because the gross morphology of the wt and null palatal shelves was similar and *Tbx22* was detected specifically in the palatal shelves at this stage (Figure 3.1, O-R). RNA samples were collected from the dissected palatal shelves of three wt and three null littermates and converted into cDNA. Integrity and concentration of these samples were determined according to standard methods before hybridisation to Affymetrix GeneChip® Mouse Gene 1.0 ST Arrays (which contained probes representing for ~29,000 genes) was performed by Dr Tony Brooks in the UCL Genomics facility. The quality control of the array data was also carried out by Dr Tony Brooks and indicated a good reproducibility of biological replicates and detected no outliers (Appendix Figure 1.1). Thus all six arrays performed were included in the data analysis.

3.2.1 Dysregulated gene expression in *Tbx22* null mice

The resulting array data was then returned for analysis with GeneSpring GX 10 (Agilent) software. The programme processes raw array data through background correction and normalisation between samples (or arrays) to allow identification of differentially expressed genes. A user can set parameters for selection criteria. For example, the programme will display genes (or probes, in more precise term, as some of the probes spotted on array chips do not encode or correlate to known genes) that changed above the fold change threshold set by a user. In this study, a threshold of 1.2 fold was chosen in order to incorporate a modest number of

differentially expressed genes (Figure 3.4 and Table 3.1). The majority of the genes fall within the blank area between the black lines, while those plotted outside the lines represent genes that were up or downregulated by 1.2 fold or more (Figure 3.4). Similarly, a statistical test can also be carried out to generate p-values for each gene.

The MicroArray Quality Control (MAQC) consortium and other groups have suggested that differentially expressed genes are better identified and results are more reproducible when selected by fold change rather than statistical t-tests, pointing out that the impact of normalisation and background correction become minimal when the fold change is used instead of p-values (Shi et al., 2005; Guo et al., 2006; Shi et al., 2006). Therefore, initial selection of differentially expressed genes was made on this basis. Commonly used thresholds are in the region of 2 to 3 fold (Mariani et al., 2003). However, due to the small number of genes that changed more than 2 fold, the threshold was arbitrarily set to 1.2 fold in order to include a manageable number of genes for initial target discovary (Table 3.1). Probes that represented for either predicted or hypothetical proteins for which no gene information was available, were excluded from the study hereafter (the number of total probes before removing unknown genes is shown in brackets in Table 3.1). In the palatal shelves of E13.5 *Tbx22* null mice, 85 genes were changed (apart from *Tbx22* itself) at FC >1.2. Of those, 43 genes showed an increase in the null palatal shelves compared to the wt palatal shelves, while 42 showed a decrease in the null palatal shelves compared to the wt palatal shelves. The number of genes that were up and downregulated at this threshold level did not greatly reflect the idea that *Tbx22* mainly acts as a transcriptional repressor (Andreou et al., 2007). However, it is difficult to judge at this stage, as the biological significance of the 1.2 fold threshold has not yet been investigated. It may reflect the fact that TBX22 acts only on a small number of target genes or because of the heterogeneous nature of the dissected tissue samples used and that only a limited number of the total cell population from the middle to posterior regions may be *Tbx22* positive cells.

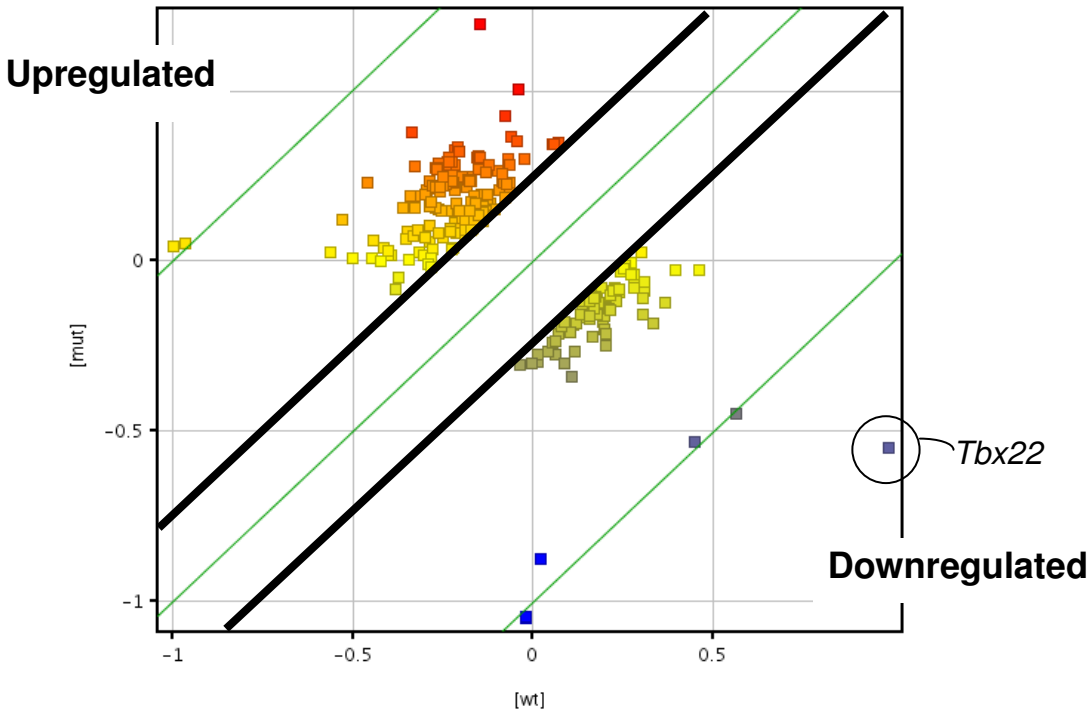

Figure 3.4 Scatter plot graph generated by GeneSpring showing genes that are changed more than 1.2 fold
The majority of the genes fall in the blank area between the black lines, while the dots plotted above and below the black lines represent genes that were up or downregulated by 1.2 fold or more in the *Tbx22* null palatal shelves compared to the wt palatal shelves, respectively.

FC	Up	Down
> 2.0	0 (2)	1 (8)
> 1.9	0 (2)	1 (9)
> 1.8	1 (3)	1 (10)
> 1.7	1 (3)	1 (10)
> 1.6	2 (5)	1 (10)
> 1.5	5 (8)	1 (10)
> 1.4	9 (40)	2 (11)
> 1.3	19 (85)	9 (24)
> 1.2	43 (154)	42 (90)
> 1.1	(888)	(1076)

Table 3.1 Fold change and the number of genes up and down regulated in the *Tbx22* null palatal shelves compared to the wt palatal shelves
The number of genes that changed more than the given thresholds is tabulated. The number of total probes before removing those represented for predicted genes and hypothetical proteins where no gene information was available is shown in brackets. For FC >1.1, the probes that encode known genes were not manually screened for but is also expected to be lower than the number shown in brackets.

Next, the genes that increased or decreased more than 1.2 fold were tabulated with the Affymetrix Transcripts Cluster ID, gene symbol, gene description, gene function, fold change and p-value (Table 3.2 and 3.3). The fold change values in general were modest and the p-values for the majority of genes were above 0.05. The fold change for *Tbx22* itself was 2.88 (p=0.0087).

Those that had FC >1.2 and p<0.05 in the upregulated list included carbonic anhydrase 10 (FC=1.39 p=0.025), troponin T3, skeletal, fast (FC=1.32, p=0.027), myosin, heavy polypeptide 7, cardiac muscle, beta (FC=1.25, p=0.022), cholinergic receptor, nicotinic, beta polypeptide 1 (muscle) (FC=1.22, p=0.0068), DENN/MADD domain containing 4A (FC=1.22, p=0.032), X-linked lymphocyte-regulated 5B | 5C | 5A (FC=1.21, p=0.028), alkaline phosphatase 3, intestine, not Mn requiring (FC=1.21, p=0.00048) and collectin sub-family member 10 (FC=1.21, p=0.0084).

Those that had FC >1.2 and p<0.05 in the downregulated list included cytochrome c oxidase subunit VIIb (FC=2.01, p=0.0047), magnesium transporter 1 (FC=1.33, p=0.0019), zinc finger protein 294 (FC=1.28, p=0.026), gamma-aminobutyric acid (GABA-A) receptor, subunit beta 2 (FC=1.24, p=0.000024), multiple inositol polyphosphate histidine phosphatase 1 (FC=1.23, p=0.030), coiled-coil domain containing 46 (FC=1.23, p=0.0031), angiotensin II, type I receptor-associated protein (FC=1.22, p=0.025) and a disintegrin-like and metallopeptidase with thrombospondin type 1 motif, 17 (FC=1.20, p=0.028).

However, none of these were obvious candidate genes known to be important for normal palate development, with the possible exception of gamma-aminobutyric acid (GABA-A) receptor, subunit beta 2 (*Gabrb2*). Downregulation of *Gabrb2* as well as gamma-aminobutyric acid (GABA-A) receptor, subunit alpha 1 (*Gabra1*) (FC=1.22, p=0.15) and glutamate receptor, ionotropic AMPA4 (alpha 4) (*Gria4*) (FC=1.21, p=0.13) is potentially interesting considering the importance of GABAergic inhibitory neurotransmission in normal palate development. This is demonstrated by cleft palate mice that lack gamma-aminobutyric acid (GABA-A) receptor, beta 3 subunit (*Gabrb3*) (Hagiwara et al., 2003; Homanics et al., 1997) or

the glutamic acid decarboxylase (*Gad1* also known as *Gad67*) that synthesise GABA from glutamate (Asada et al., 1997; Condie et al., 1997).

Next, the up or downregulated genes above FC >1.2 were looked at regardless of their p-values. The array data showed an increase in Keratin 5 (*Krt5*) in the null palatal shelves (FC=1.27, p=0.097). It is known that the palatal epithelium is orthokeratinised following fusion of the palatal shelves (Gibbs and Ponec, 2000). Upregulation of *loricrin* which encodes for a predominant protein Loricrin found in keratinocytes, as well as type I and II *keratin* are reported to be increased between E14.5 and E15.5 (Brown et al., 2003). However, it is not straightforward to put this into the biological context of *Tbx22* null mice as there is no obvious defect found in the palatal epithelium or palatal fusion. Paired box gene 3 (*Pax3*) was downregulated in the null palatal shelves (FC=1.21, p=0.40). This is potentially interesting since persistent expression of *Pax3* in the neural crest is known to cause cleft palate (Wu et al., 2008). Alcohol dehydrogenase 1 (*Adh1*) was also downregulated (FC=1.27, p=0.27). Dehydrogenase enzymes are required in retinoid metabolism, and cleft palate can be induced by retinoic acid in mice (Padmanabhan and Ahmed, 1997; Degitz et al., 1998). Therefore this could also be interesting to follow up in the future.

Despite the fact that we observed an ossification defect in the null mice at later stages, other than cathepsin K (*Ctsk*) which increased by 1.62 fold (p=0.074), no obvious gene markers of osteogenesis were detected at FC >1.2 at the stage examined. Some of the cleft palate candidate genes and genes related to ossification described in the Introduction were then individually checked for their FC, but the values for many of those were between 1.0 to 1.1 (Appendix Table 1.1). There is a possibility that expression of these genes might be slightly altered, in which case it is unlikely to be detected especially because the palatal shelves contained both *Tbx22* expressing and non-expressing cells.

Interestingly, there was a noticeable general increase in muscle related genes in the null palatal shelves compared to the wt palatal shelves. There were 20 muscle related genes in the upregulated list at FC >1.2, including members of the myosin, actin, actinin, titin, troponin, tropomyosin and calsequestrin gene families

(highlighted in yellow in Table 3.2). In contrast, no muscle genes were represented in the downregulated list. This prompted an investigation of some of these muscle genes for validation by real-time PCR since *Tbx22* mainly acts as a transcriptional repressor (Andreou et al., 2007) and thus the potential downstream target genes were expected to be upregulated. Of those upregulated, myosin, heavy polypeptide 3, skeletal muscle, embryonic (*Myh3*) (FC=1.57, p=0.061), actin, alpha 1, skeletal muscle (*Acta1*) (FC=1.35, p=0.12) and calsequestrin 2 (*Casq2*) (FC=1.30, p=0.21) were initially chosen as representatives to be examined by real-time PCR.

ID	Gene symbol	Gene description	Gene function	FC	p-value
10566205	*Dub2a*	Deubiquitinating enzyme 2a	Metabolism	1.81	0.11
10494262	*Ctsk*	Cathepsin K	Bone resorption, peptidolysis	1.62	0.074
10377018	*Myh3*	Myosin, heavy polypeptide 3, skeletal muscle, embryonic	Metabolism, muscle contraction	1.57	0.061
10345016	*Tcfap2b*	Transcription factor AP-2 beta	Transcription factor	1.53	0.33
10485982	*Actc1*	Actin, alpha, cardiac	Skeletal muscle filament assembly	1.51	0.12
10413012	*Fut11*	Fucosyltransferase 11	Protein amino acid glycosylation	1.46	0.16
10429048	*Oc90*	Otoconin 90	Metabolism	1.46	0.34
10414802	*Trav16d/dv11*	T cell receptor alpha variable 16D/DV11	Unknown	1.42	0.11
10355259	*Myl1*	Myosin, light polypeptide 1	Metabolism, muscle contraction	1.42	0.27
10380303	*Car10*	Carbonic anhydrase 10	Unknown	1.39	0.025
10483871	*Ttn*	Titin	Skeletal muscle filament assembly, muscle contraction	1.37	0.25
10377148	*Myh8*	Myosin, heavy polypeptide 8, skeletal muscle, perinatal	Skeletal muscle filament assembly, muscle contraction	1.37	0.13
10407792	*Gpr137b-ps*	G protein-coupled receptor 137B, pseudogene	Unknown	1.36	0.35
10582592	*Acta1*	Actin, alpha 1, skeletal muscle	Skeletal muscle filament assembly and development	1.35	0.12
10407742	*Actn2*	Actinin alpha 2	Muscle contraction	1.34	0.19
10413726	*Tnnc1*	Troponin C, cardiac/slow skeletal	Muscle contraction	1.34	0.14
10350149	*Tnni1*	Troponin I, skeletal, slow 1	Muscle contraction	1.34	0.18
10559221	*Tnnt3*	Troponin T3, skeletal, fast	Muscle contraction	1.32	0.027
10496822	*Gng5*	Guanine nucleotide binding protein, gamma 5	Hormone mediated signalling	1.32	0.31
10358515	*Hmcn1*	Hemicentin 1	Protein amino acid phosphorylation	1.30	0.15
10494804	*Casq2*	Calsequestrin 2	Muscle contraction	1.30	0.21
10482528	*Neb*	Nebulin	Sarcomere organisation	1.28	0.15
10346250	*Mstn*	Myostatin	Muscle differentiation and growth	1.27	0.43

10350173	*Tnnt2*	Troponin T2, cardiac	Muscle contraction	1.27	0.17
10432785	*Krt5*	Keratin 5	Hemidesmosome assembly	1.27	0.097
10608567	*Srsy*	Serine-rich, secreted, Y-linked	Unknown	1.26	0.69
10472562	*Kbtbd10*	Kelch repeat and BTB (POZ) domain containing 10	Regulation of lateral pseudopodium formation	1.25	0.11
10449644	*Glo1*	Glyoxalase 1	Metabolism	1.25	0.35
10467124	*Acta2*	Actin, alpha 2, smooth muscle, aorta	Muscle contraction	1.25	0.33
10419934	*Myh7*	Myosin, heavy polypeptide 7, cardiac muscle, beta	Metabolism, muscle contraction	1.25	0.022
10489545	*Tnnc2*	Troponin C2, fast	Muscle contraction	1.24	0.11
10598236	*Nudt11| 10*	Nudix-type motif 11 | motif 10	Metabolism	1.24	0.10
10445293	*Pla2g7*	Phospholipase A2, group VII	Metabolism	1.24	0.29
10471675	*Glo1*	Glyoxalase 1	Metabolism	1.24	0.38
10457669	*Dsc3*	Desmocollin 3	Cell adhesion	1.24	0.52
10557575	*Mylpf*	Myosin light chain, phosphorylatable, fast skeletal muscle	Metabolism, skeletal muscle development	1.23	0.27
10387625	*Chrnb1*	Cholinergic receptor, nicotinic, beta polypeptide 1 (muscle)	Transmembrane transport, muscle contraction	1.22	0.0068
10586252	*Dennd4a*	DENN/MADD domain containing 4A	Unknown	1.22	0.032
10605044	*Xlr5b|5c|5a*	X-linked lymphocyte-regulated 5B | 5C | 5A	Unknown	1.21	0.028
10348131	*Akp3*	Alkaline phosphatase 3, intestine, not Mn requiring	Metabolism	1.21	0.00048
10424105	*Colec10*	Collectin sub-family member 10	Immunity, embryo development, cell-cell adhesion	1.21	0.0084
10512499	*Tpm2*	Tropomyosin 2, beta	Muscle contraction	1.20	0.17
10496091	*Lef1*	Lymphoid enhancer binding factor 1	Immunity	1.20	0.31

Table 3.2 Upregulated genes in the *Tbx22* null palatal shelves at 1.2 fold change threshold
The genes that increased more than 1.2 fold in the *Tbx22* null palatal shelves at E13.5 compared to the wt palatal shelves were tabulated with the Affymetrix Transcripts Cluster ID, gene symbol, gene description, gene function, FC and p-values. Muscle related genes are highlighted in yellow.

ID	Gene symbol	Gene description	Gene function	FC	p-value
10601433	*Tbx22*	T-box 22	Transcription factor	2.88	0.0087
10358709	*Cox7b*	Cytochrome c oxidase subunit VIIb	Metabolism, transmembrane transport	2.01	0.0047
10536405	*Nxph1*	Neurexophilin 1	Receptor binding	1.42	0.092
10560481	*Fosb*	FBJ osteosarcoma oncogene B	Transcription factor	1.40	0.27
10491773	*Slc25a31*	Solute carrier family 25, member 31	Transmembrane transport	1.40	0.43
10605954	*Tex11*	Testis expressed gene 11	Testis development	1.34	0.38
10606301	*Magt1*	Magnesium transporter 1	Cell redox homeostasis	1.33	0.0019
10415472	*Rnf17*	Ring finger protein 17	Metabolism, differentiation, spermatogenesis	1.31	0.16
10579607	*B3gnt3|Cnot8*	UDP-GlcNAc:betaGal beta-1,3-N-acetylglucosaminyltransferase 3 | CCR4-NOT transcription complex, subunit 8	Protein glycosylation, regulation of transcription	1.30	0.27
10592355	*Panx3*	Pannexin 3	Cell-cell signalling	1.30	0.17
10440566	*Zfp294*	Zinc finger protein 294	Metabolism	1.28	0.026
10496438	*Adh1*	Alcohol dehydrogenase 1 (class I)	Metabolism	1.27	0.27
10476628	*Otor*	Otoraplin	Cartilage condensation	1.25	0.15
10563112	*Snord33*	Small nucleolar RNA, C/D box 33	Unknown	1.24	0.35
10538222	*Stk31*	Serine threonine kinase 31	Protein phosphorylation	1.24	0.28
10375261	*Gabrb2*	Gamma-aminobutyric acid (GABA-A) receptor, subunit beta 2	Transmembrane transport	1.24	0.000024
10355312	*Ikzf2*	IKAROS family zinc finger 2	Regulation of transcription	1.24	0.076
10516211	*Ndufs5*	NADH dehydrogenase Fe-S protein 5	Electron transport chain	1.24	0.33
10549546	*Ndufa3*	NADH dehydrogenase 1 alpha subcomplex, 3	Electron transport chain	1.24	0.24
10561187	*Mia1*	Melanoma inhibitory activity 1	Extracellular matrix organisation	1.23	0.26
10462504	*Minpp1*	Multiple inositol polyphosphate histidine phosphatase 1	Metabolism, dephosphorylation	1.23	0.030
10397346	*Fos*	FBJ osteosarcoma oncogene	Regulation of transcription	1.23	0.070
10382200	*Ccdc46*	Coiled-coil domain containing 46	Unknown	1.23	0.0031

10404061	*Hist1h2bb*	Histone cluster 1, H2bb	Nucleosome assembly	1.23	0.34
10490818	*Stmn2*	Stathmin-like 2	Regulation of neuron projection	1.22	0.63
10385297	*Gabra1*	Gamma-aminobutyric acid (GABA-A) receptor, subunit alpha 1	Transmembrane transport	1.22	0.15
10382321	*Kcnj2*	Potassium inwardly-rectifying channel, subfamily J, member 2	Transmembrane transport	1.22	0.14
10353632	*Bai3*	Brain-specific angiogenesis inhibitor 3	Signal transduction	1.22	0.088
10518455	*Agtrap*	Angiotensin II, type I receptor-associated protein	Signal transduction	1.22	0.025
10464583	*Gstp1*	Glutathione S-transferase, pi 1	Metabolism	1.22	0.46
10423742	*Polr2k*	Polymerase (RNA) II (DNA directed) polypeptide K	Cellular transcription	1.21	0.25
10583021	*Pdgfd*	Platelet-derived growth factor, D polypeptide	Regulation of cell division	1.21	0.081
10412155	*Ddx4*	DEAD (Asp-Glu-Ala-Asp) box polypeptide 4	Metabolism	1.21	0.49
10349138	*Serpinb11*	Serine (or cysteine) peptidase inhibitor, clade B, member 11	Regulation of peptidase activity	1.21	0.45
1.206607	*Gria4*	Glutamate receptor, ionotropic, AMPA4 (alpha 4)	Transmembrane transport	1.21	0.13
10466624	*Aldh1a7*	Aldehyde dehydrogenase family 1, subfamily A7	Metabolism	1.21	0.47
10359801	*Mael*	Maelstrom homolog (Drosophila)	Regulation of gene expression, spermatogenesis	1.21	0.40
10355916	*Pax3*	Paired box gene 3	Transcription factor	1.21	0.40
10554045	*Adamts17*	A disintegrin-like and metallopeptidase with thrombospondin type 1 motif, 17	Metabolism	1.20	0.028
10380059	*Rnu3b1/ 4/ 3*	U3B small nuclear RNA 1 | 4 | 3	Unknown	1.20	0.27
10591208	*Uba52*	Ubiquitin A-52 residue ribosomal protein fusion product 1	Regulation of ubiquitin activity	1.20	0.22
10599187	*Zcchc12*	Zinc finger, CCHC domain containing 12	Regulation of transcription	1.20	0.19
10402020	*Eml5*	Echinoderm microtubule associated protein like 5	Microtubule associated	1.20	0.51

Table 3.3 Downregulated genes in the *Tbx22* null palatal shelves at 1.2 fold change threshold
The genes that decreased more than 1.2 fold in the *Tbx22* null palatal shelves at E13.5 compared to the wt palatal shelves were tabulated with the Affymetrix Transcripts Cluster ID, gene symbol, gene description, gene function, FC and p-values.

3.2.2 Validation of results

Since the results obtained from microarray studies can contain false positives, several upregulated genes of interest were investigated by the commonly used validation procedure of real-time PCR. Initially, gene expression of *Ctsk* and three different muscle genes *Myh3*, *Acta1* and *Casq2* were compared between the wt and null mice at E13.5. At least three biological triplicates (littermates of the same genotype but from a different litter to the original microarray analysed samples) were performed for each gene and both *Gapdh* and 18S rRNA (data not shown for 18S rRNA since no significant differences between the two housekeeping genes were detected) were used as endogenous controls.

Ctsk encodes for a lysosomal cysteine protease expressed in osteoclasts that are involved in bone resorption. Despite the fact that the obvious phenotype in the null palate is a defective ossification which becomes apparent from E15.5, this was the only gene related to osteogenesis at E13.5. The microarray data showed that *Ctsk* was upregulated in the null palatal shelves compared to those from the wt (FC=1.62, p=0.074). However, expression of *Ctsk* examined by real-time PCR showed only a slight increase by 1.13 fold which was not significantly different (p=0.54) (Figure 3.5) and thus was not investigated further. *Runx2* and *Osterix*, key osteogenic markers, were also examined by real-time PCR, but no differences were detected at this stage (Figure 3.5). Since the microarray data indicated a general upregulation of muscle related transcripts in the null palatal shelves, several of these genes were investigated by real-time PCR. For this purpose, *Myh3*, *Acta1* and *Casq2* were chosen as representatives from different muscle gene families. *Myh3* encodes for heavy chain of myosin which is a major muscle contractile protein. *Acta1* encodes for alpha actin which is also a major constituent of the muscle contractile protein found in skeletal muscle. *Casq2* encodes for a cardiac calsequestrin which is a calcium binding protein found in the sarcoplasmic reticulum. Though it is termed 'cardiac' and its expression is exclusively found in the heart primordium during early development (E8-E9), later it is known to be highly expressed in the fetal skeletal muscles including those of the soft palate (Park et al., 1998). Using real-time PCR, expression of these muscle related genes, *Myh3*, *Acta1* and *Casq2*, were increased by 2.44 (p=0.030), 2.16 (p=0.030) and 2.32 (p=0.035) fold respectively in

the palatal shelves of the null compared to the wt (Figure 3.5). Though the fold change values calculated by real-time PCR were higher than those from the microarray data, the two assays indicated consistent trends of upregulation for these three muscle genes. Thus far, the microarray results for other genes have not been validated by real-time PCR.

3.2.3 Myogenic regulatory factors

In the microarray analysis, the threshold was arbitrarily set to 1.2 fold change so that the list included a manageable number of genes for initial screening. Although no obvious early muscle markers or markers of muscle differentiation were detected above the 1.2 fold threshold, it was decided to investigate several such genes to try to explain the global upregulation of late structural muscle genes such as myosin and muscle actin. Myogenesis is the formation of muscular tissue, involving the determination of mesodermal precursor cells, myoblast proliferation, fusion and differentiation into myotubes. These steps are regulated by the MyoD family of bHLH transcription factors including MyoD, Myf5, myogenin and Mrf4. Of these, MyoD and Myf5 are known to have a role in initiation of myogenic differentiation while myogenin is critical for terminal differentiation of myoblasts (Hasty et al., 1993; Nabeshima et al., 1993). Interestingly Mrf4 does not direct skeletal muscle identity in the developing head (Kassar-Duchossoy et al., 2004), suggesting that the myogenesis pathway operates differently in the head and trunk. This may be due to the fact that the majority of craniofacial muscles, except the tongue and laryngeal muscles, arise from anterior paraxial and prechordal mesoderm whereas skeletal muscles in the trunk are derived from somitic mesoderm.

The fold changes for the myogenic regulatory factors were individually examined as none of them appeared in the list at FC >1.2. The microarray data indicated a general trend towards increased expression for *MyoD* (FC=1.17, p=0.27), *myogenin* (FC=1.09, p=0.70) and *Myf5* (FC=1.19, p=0.13) as well as *p21* (FC=1.09, p=0.53), a known target of MyoD (Table 3.4). Next, the array data was confirmed by real-time PCR. Expressions of *MyoD* (FC=1.73, p=0.017), *myogenin* (FC=1.69, p=0.038) and *p21* (FC=1.62, p=0.031) were increased in the null palatal shelves compared to the wt (Figure 3.5). *Myf5* also showed a tendency towards increased

expression but did not achieve a statistical significance (FC=1.75, p=0.10) (Figure 3.5).

ID	Gene symbol	Gene description	Regulation	FC	p-value
10553256	*MyoD*	Myogenic differentiation 1	up	1.17	0.27
10349993	*Myog*	Myogenin	up	1.09	0.70
10372226	*Myf5*	Myogenic factor 5	up	1.19	0.13
10443463	*Cdkn1a* (*p21*)	Cyclin-dependent kinase inhibitor 1A (P21)	up	1.09	0.53

Table 3.4 The microarray data show a trend towards increased expression of MRFs and *p21* in the *Tbx22* null palatal shelves
Microarray data for *MyoD*, *Myf5*, *myogenin* and *p21* comparing between the wt and *Tbx22* null palatal shelves at E13.5 are tabulated with the Affymetrix Transcripts Cluster ID, gene symbol, gene description, regulation, fold change and p-values.

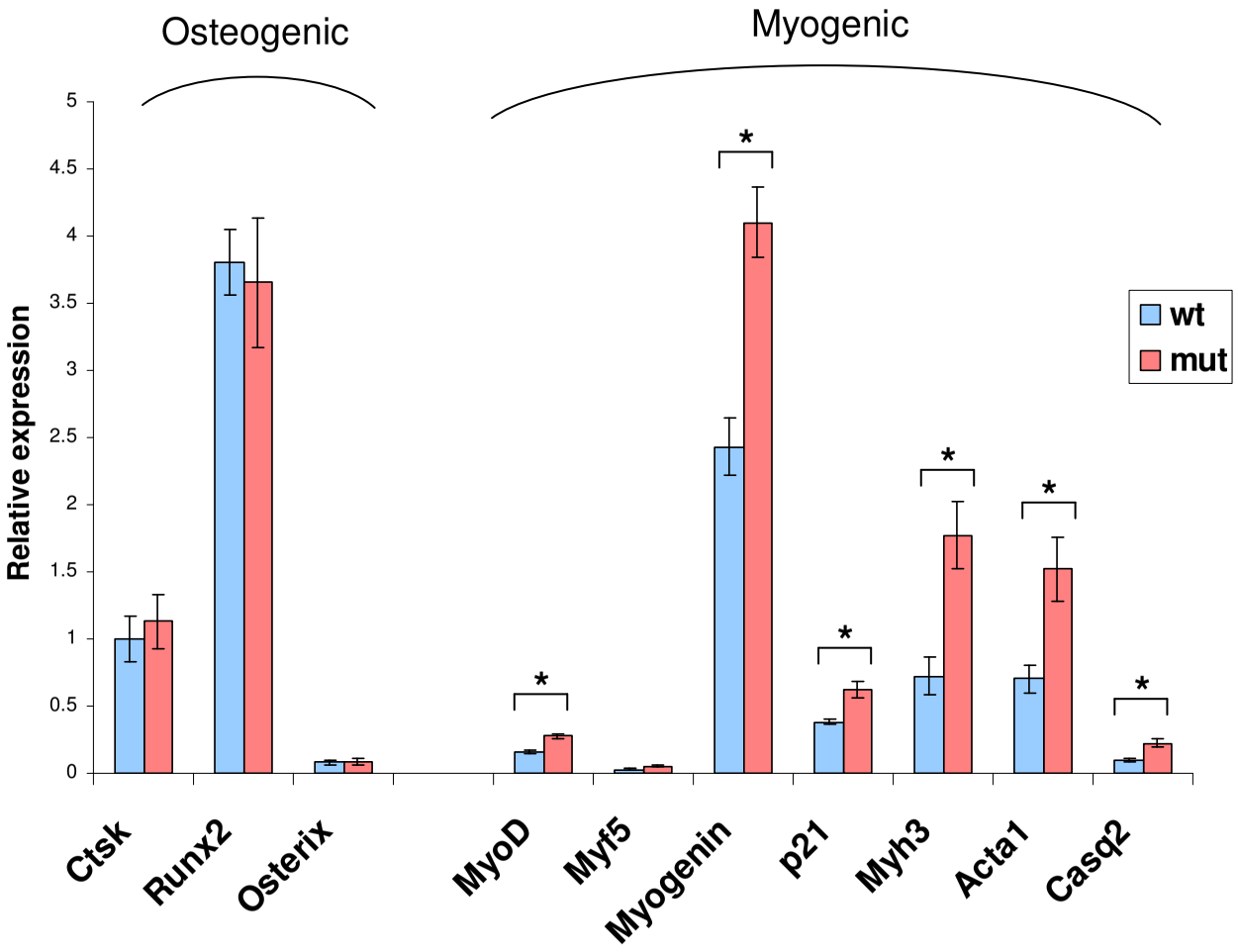
Osteogenic
Myogenic
Relative expression
5
4.5
4
3.5
3
2.5
2
1.5
1
0.5
0
wt
mut
*
Ctsk
Runx2
Osterix
MyoD
Myf5
Myogenin
p21
Myh3
Acta1
Casq2

Figure 3.5 Expression of muscle genes are increased in the null palatal shelves
Expression of *Ctsk*, *Runx2*, *Osterix*, *MyoD*, *Myf5*, *myogenin*, *p21*, *Myh3*, *Acta1* and *Casq2* in the wt and *Tbx22* null palatal shelves were determined by real-time PCR using comparative CT method for relative quantification and were normalised to *Gapdh*. Relative expression of *Ctsk* from the wt was arbitrarily set at 1. The error bars represent standard deviation. At least three biological samples from the wt and null were tested for both target and endogenous control genes. *$p<0.05$, paired Student's t test.

3.2.4 Summary

Initially, several well-known cleft palate candidate genes (*Pax9*, *Snail*, *Msx1*, *Msx2*, *Bmp4*, *Osr1* and *Tgfβ3*) were investigated for their expression pattern in wt and *Tbx22* null mice. However, no obvious or significant differences were detected. Therefore, in order to obtain a global picture of differentially expressed genes in the absence of *Tbx22*, we performed a microarray on E13.5 palatal shelves. Though the fold changes were generally modest, possibly due to the heterogeneous nature of the samples, the assay data revealed several interesting genes above the set threshold. These include *Gabrb2*, *Gabra1*, *Gria4*, *Adh1* and *Pax3* that were all downregulated. These were not followed up in this particular project because the primary aim was to look at upregulated genes, based on the hypothesis that TBX22 mainly acts as a transcriptional repressor. In the list of upregulated genes, many genes relating to muscle development were identified. This was unlikely to have been a random occurrence especially because no similar genes were present in the downregulated list. Increased expression of some of these genes including the key myogenic regulatory factors *MyoD* and *myogenin* were confirmed by real-time PCR. There were no obvious changes in several osteogenic genes tested in the *Tbx22* null palatal shelves at E13.5.

3.3 TBX22 is capable of regulating *MyoD in vitro*

3.3.1 Putative promoters of MRFs contain TBEs

As *Tbx22* has been shown to preferentially interact with a conserved T-box binding element (TBE) (Andreou et al., 2007), genomic sequences up to 2 kb upstream of the transcription start site to the first exon of several genes were scanned for the presence of possible TBEs using the JASPAR database (http://jaspar.cgb.ki.se/) (Table 3.5). Of those analysed, the putative promoters for *MyoD*, *myogenin*, *Myf5* and *Acta1* all contained one or more TBE. The presence of a TBE in the putative promoter suggested that *Tbx22* could potentially bind or indeed regulate the expression of this gene *in vivo*. However, this was a very inexact determination and required testing by functional assays. For this analysis, *Myf5* was excluded because it was not significantly changed in the *Tbx22* null palatal sheves as measured by real-time PCR. *Myogenin* and muscle specific genes including myosin and actin are known to be regulated by MyoD (Asakura et al., 1993; Deato et al., 2008; Sartorelli and Caretti, 2005; Shklover et al., 2007; Wheeler et al., 1999). In addition, No tail, a zebrafish ortholog of Brachyury, has previously been shown to interact with the upstream region of the *MyoD* gene (Morley et al., 2009). Therefore it was decided to follow up the potential interaction between TBX22 and *MyoD*.

Gene	Position relative to TSS	Strand	Predicted site sequence
MyoD	-515 bp to -505 bp	-1	5'-TGCTCACCTAG-3' 3'-ACGAGTGGATC-5'
Myf5	-699 bp to -689 bp	1	5'-CTAGGTCTGAT-3' 3'-GATCCAGACTA-5'
"	-1316 bp to -1306 bp	1	5'-CCAAGTGTGAA-3' 3'GGTTCACACTT-5'
myogenin	-813 bp to -803 bp	1	5'-CTAGGGGAGAA-3' 3'-GATCCCCTCTT-5'
"	-1810 bp to -1800 bp	-1	5'-CTAGGTGTGAT-3' 3'-GATCCACACTA-5'
Myh3	-	-	-
Acta1	-938 bp to -928 bp	-1	5'-CTGGGTCTGAA-3' 3'-GACCCAGACTT-5'
Casq2	-	-	-
p21	-	-	-

Table 3.5 MRF putative promoters contain one or more TBEs
Genomic sequences extending 2 kb upstream of the transcription start site to the first exon were scanned for the presence of putative TBEs. For each gene, predicted site sequence and its position relative to the transcription start site is shown. Strand 1 and strand -1 refer to positive and negative strands, respectively.

3.3.2 TBX22 is expressed in HEK 293T cells

Initially, it was decided to investigate whether TBX22 can regulate or interact with the *MyoD* promoter using *in vitro* reporter assays and chromatin immunoprecipitation in HEK 293T cells. These experiments used V5-tagged human TBX22 constructs, including the wt sequence (pcDNA3.1.TBX22.V5/His) and a mutant containing a missense asparagine to a tyrosine substitution at position 264 (pcDNA3.1.TBX22(N264Y).V5/His). This N264Y mutation was identified in one of the classic CPX families (Marcano et al., 2004), and has previously been shown to abolish TBX22 function, as assessed by DNA binding and repression of the TBX22 P0 promoter (Andreou et al., 2007). Therefore the mutant N264Y was used as a control alongside the wtTBX22 sequence in the following experiments. It was first necessary to confirm that both constructs were correctly expressed following transfection. Figure 3.6 shows that the wtTBX22 and N264Y proteins were successfully detected, while no band was observed in the mock (pcDNA3.1.V5/His) transfected lane. β-actin was used as a loading control, which showed a similar level of expression in all samples.

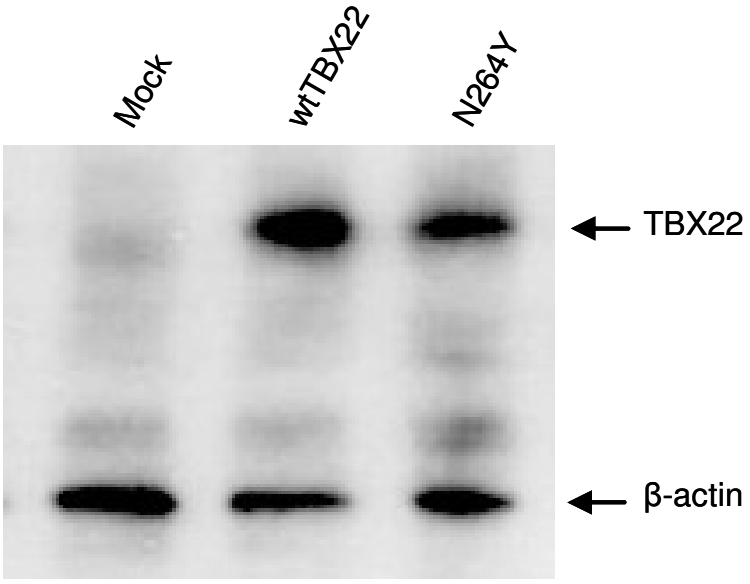

Figure 3.6 Immunoblot analysis of HEK 293T cells transfected with mock, wtTBX22 or N264Y
HEK 293T cells were transfected with mock, wtTBX22 or N264Y, and subjected to immunoblot analysis using anti-V5 antibody. β-actin was used as a loading control.

3.3.3 TBX22 can repress the *MyoD* promoter activity *in vitro*

In silico analysis revealed a TBE upstream of *MyoD* transcription start site (-515 bp/-505 bp). To assess the transcriptional activity of TBX22 on the *MyoD* putative promoter, HEK 293T cells were transfected with *MyoD* promoter-luciferase construct (pGL3-MyoD) which included the TBE (Figure 3.7, A) and vectors constitutively expressing either the wtTBX22 or the mutant N264Y. Luciferase is an enzyme that produces light upon oxidising its substrate luciferin and is commonly used as a reporter gene to assess the transcriptional activity of a gene of interest on a putative promoter. pGL3-Basic vector contains firefly luciferase gene (*luc*+) but lacks eukaryotic promoter or enhancer sequences. Thus successful expression of luciferase depends on a functional promoter being placed upstream from the *luc* gene. The basal promoter activity of pGL3-MyoD in HEK 293T cells was 23.7 fold higher than that of empty pGL3 (p=0.00010) (Figure 3.7, B). A dose-dependent repression of *MyoD* promoter activity down to 46.2% was observed with addition of wtTBX22 (down to 67.0% by 2.5 ng wtTBX22 (p=0.0060) and 46.2% by 10 ng wt TBX22 (p=0.0015)) but not by the addition of a control construct expressing GFP (Figure 3.7, B). This effect was largely abrogated in the N264Y mutant. The data presented is a representative of three independent experimental repeats and the average values were calculated based on four replicates.

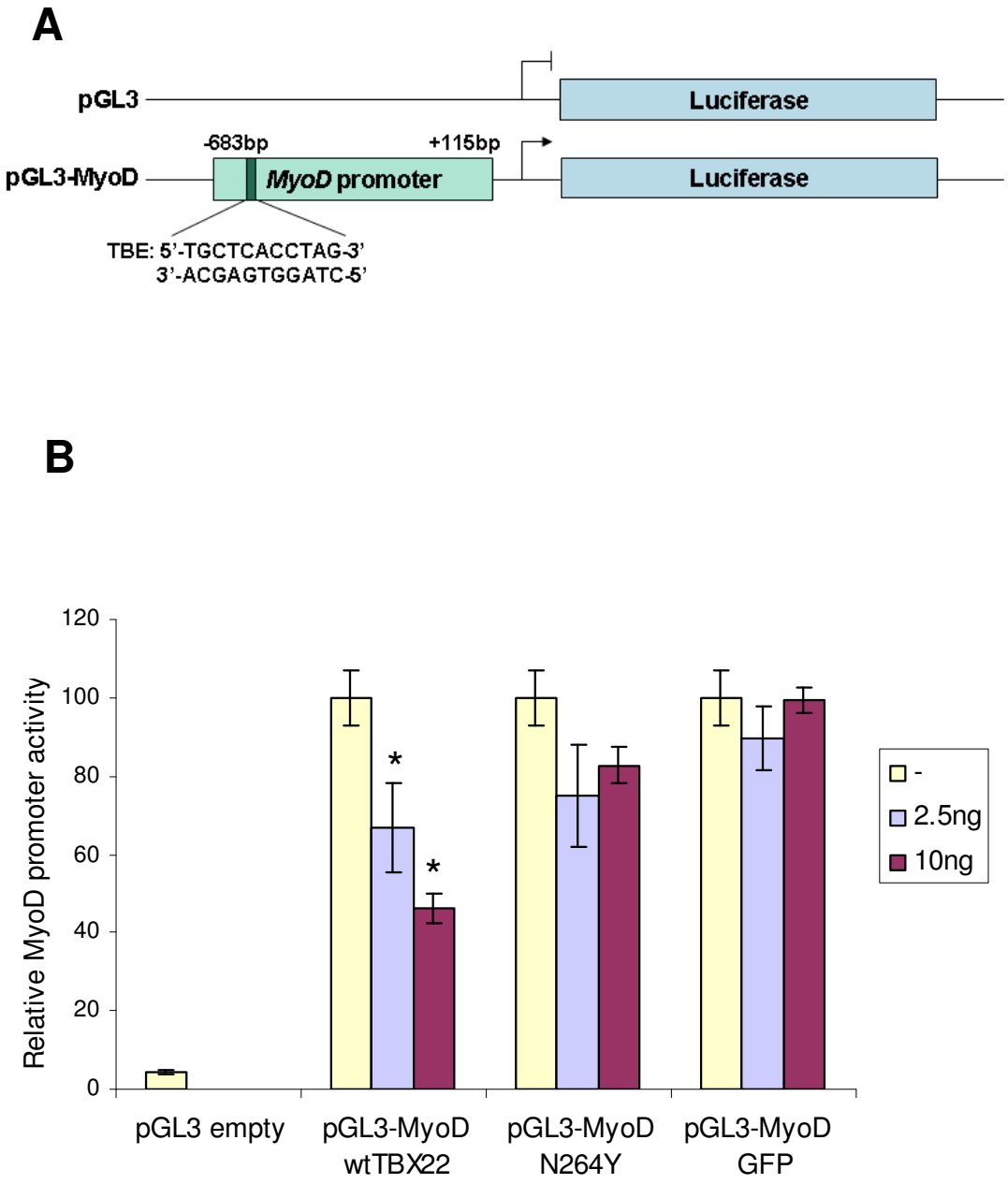

Figure 3.7 TBX22 represses the *MyoD* promoter activity
Schematic showing pGL3 and pGL3-MyoD constructs (A). TBX22 repressed the *MyoD* promoter activity in luciferase assay (B). 50 ng of pGL3 vector containing the *MyoD* putative promoter region (-683 bp/+115 bp) was cotransfected with 10 ng of pcDNA3.1 empty vector, 2.5 and 10 ng of wtTBX22, N264Y or GFP in HEK 293T cells. Bars represent relative promoter activity after normalising firefly luciferase light unit to *Renilla* luciferase light unit. Relative promoter activity of pGL3-MyoD cotransfected with 10 ng of pcDNA3.1 empty vector was arbitrarily set at 100. The graph is a representative of three independent experimental repeats and the values shown are the average of four replicates. The error bars represent standard deviation. *p<0.05, paired Student's t test.

3.3.4 Abolition of the putative TBE sequence in the *MyoD* promoter does not affect TBX22 dependant repression

To investigate a direct effect of TBX22 on the putative *MyoD* TBE, two invariant bases of the consensus sequence (TGCTCACCTAG) were substituted using *in vitro* mutagenesis. This resulted in substitutions of the C to A at -511 bp relative to TSS and C to A at -509 bp relative to TSS (TGCTAAACTAG), known as pGL3-mut MyoD hereafter. Using pGL3-mut MyoD, the transcriptional activity of TBX22 on the mutated *MyoD* putative promoter in HEK 293T cells was assessed. Cells were transfected with pGL3-mut MyoD which included the mutated TBE, and expression vector that constitutively expressed the wtTBX22. The basal promoter activity of pGL3-mut MyoD in HEK 293T cells was 24.6 fold higher than that of pGL3 (p=0.00027) (Figure 3.8). Similarly to the results obtained from pGL3-MyoD, a dose-dependent repression of the mutated *MyoD* promoter activity down to 36.8% was observed with the wtTBX22 (down to 65.6% by 2.5 ng wtTBX22 (p=0.0045) and 36.8% by 10 ng wt TBX22 (p=0.00037)) but not by the addition of a GFP control construct (Figure 3.8). The data presented is a representative of three independent experimental repeats and the average values were calculated based on four replicates. This experiment indicates that the inhibition detected does not occur through specific interaction with the predicted TBE.

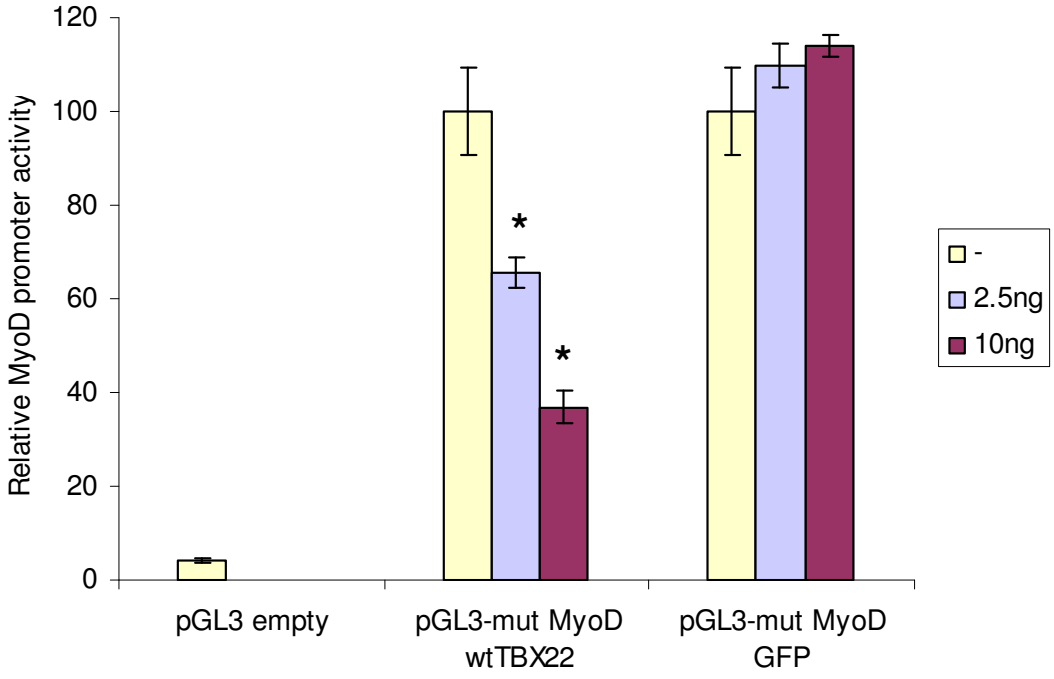

Figure 3.8 Change in the putative TBE sequence in *MyoD* promoter region does not alter repressive effect of TBX22
50 ng of pGL3 vector containing the mutated *MyoD* putative promoter region (-683 bp/+115 bp) was cotransfected with 10 ng of pcDNA3.1 empty vector, 2.5 and 10 ng of wtTBX22, or GFP in HEK 293T cells. Bars represent relative promoter activity after normalising firefly luciferase light unit to *Renilla* luciferase light unit. Relative promoter activity of pGL3-MyoD cotransfected with 10 ng of pcDNA3.1 empty vector was arbitrarily set at 100. The graph is a representative of three independent experimental repeats and the values shown are the average of four replicates. The error bars represent standard deviation. *p<0.05, paired Student's t test.

3.3.5 TBX22 can interact with *MyoD* promoter region

Although TBX22 had a specific repressive effect on the *MyoD* promoter *in vitro*, it appeared to be independent of the putative TBE. In order to investigate if a physical interaction exists between TBX22 and the *MyoD* promoter region, the technique of chromatin immunoprecipitation was used. The assay however, does not distinguish if the interaction is direct or indirect (i.e. via co-factors or other accessory proteins that may exist). As above, the expression vectors used were V5-tagged so that they could be immunoprecipitated with anti-V5 antibody and protein G. Following transient transfection into HEK 293T cells, the *MyoD* promoter region was detected by PCR amplification from total inputs as expected, and from the wtTBX22 immunoprecipitated with anti-V5 antibody but not from the N264Y mutant (Figure 3.9). This suggested either direct or indirect interaction did specifically occurred between the wtTBX22 and the *MyoD* promoter region but was abolished by the N264Y mutation. No amplification was observed from mock transfected samples, or samples immunoprecipitated without anti-V5 antibody (Data published in Kantaputra et al., J. Dent. Res. 2011 – in press).

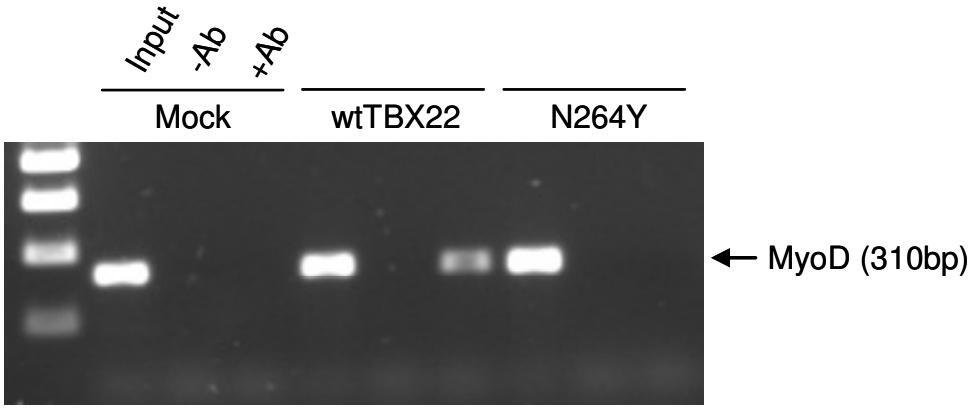

Figure 3.9 ChIP-PCR MyoD
HEK 293T cells were transfected with mock, wtTBX22 and N264 expression vectors prior to chromatin immunoprecipitation. PCR amplification of the *MyoD* promoter region was detected from total inputs as expected, and from the wtTBX22 immunoprecipitated with anti-V5 antibody but not from N264Y. No amplification was observed from mock transfected samples, or samples immunoprecipitated without anti-V5 antibody.

3.3.6 Endogenous *MyoD* is not repressed by overexpression of *TBX22* in C2C12 cells

Next, C2C12 cells were used to examine if overexpression of *TBX22* has any effect on the endogenous level of *MyoD* expression. C2C12 is a mouse myoblast cell line which was originally obtained by Yaffe and Saxel (1977) through selective serial passage of myoblasts cultured from the thigh muscle of C3H mice 70 hours after a crush injury (Yaffe and Saxel, 1977), and have been shown to express muscle proteins including MyoD. The C2C12 cells differentiate when they become confluent, forming myotubes. This eventually depletes the myoblastic population. In the experiment, the undifferentiated cells were transfected with mock, wtTBX22, N264Y or GFP. 1 µg of each DNA plasmid was used for cells in 6 well plate. Then mRNA was collected from the transfected cells after 48 hours of incubation, and subjected to real-time PCR for quantitative assay. A high transfection efficiency was reflected in the huge increase in *Tbx22* expression (Figure 3.10). However, overexpression of the wtTBX22 did not alter the level of endogenous *MyoD* expression in C2C12 cells (Figure 3.10). The endogenous *MyoD* expression level in cells transfected with N264Y and GFP constructs were also similar to that of the mock transfected cells.

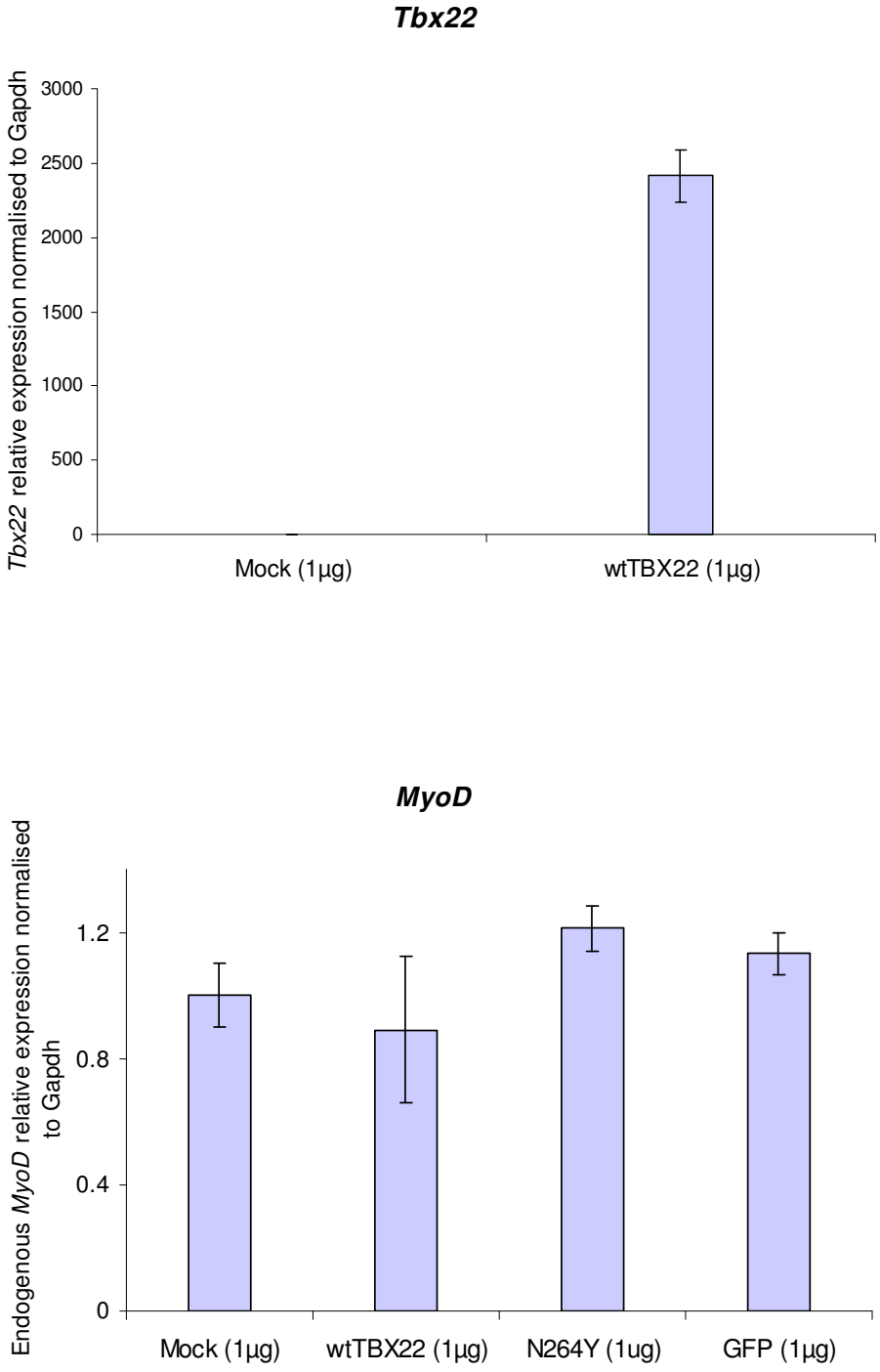

Figure 3.10 Overexpression of TBX22 does not alter endogenous *MyoD* expression in C2C12 cells

Effect of *Tbx22* overexpression on endogenous *MyoD* in C2C12 cells was quantified by real-time PCR and normalised against *Gapdh*. Relative expression of mock transfected sample was arbitrarily set at 1. The error bars represent standard deviation. The graph is a representative of four independent experimental repeats. *$p<0.05$, paired Student's t test.

3.3.7 Summary

Real-time PCR revealed increased expression of *MyoD* and *myogenin* in the palatal shelves of *Tbx22* null mice. Another key transcription factor of myogenesis *Myf5* also showed a trend towards increased expression in the null palatal shelves but failed to achieve a statistical significance. These MRFs form heterodimers with ubiquitously expressed E proteins which bind to a specific DNA sequence called E-box (consensus sequence CANNTG) found in many muscle gene promoters to activate gene expression (Lassar et al., 1991). It is possible that a number of late muscle structural genes were found upregulated in microarray analysis as a consequence of increased MRFs. Luciferase assay showed TBX22 can regulate *MyoD* promoter activity in HEK 293T cells which provides a link between lack of functional TBX22 and increased *MyoD* expression followed by increased late muscle markers in *Tbx22* null mice. Substitution of two bases in the TBE sequence in *MyoD* promoter region, however, did not affect TBX22 dependent repression. This suggests possibilities that the protein may act on sequence other than the TBE or involves co-factors (Pauws et al., 2009b). ChIP-PCR demonstrated that TBX22 is capable of interacting with the *MyoD* promoter region in HEK293T cells. Taken together, these assays indicate TBX22 can regulate *MyoD* expression *in vitro*. However, endogenous *MyoD* was not repressed by overexpression of TBX22. This was performed in C2C12 cell line because HEK 293T cells do not express endogenous *MyoD*. Thus, this could be due to context differences between these cell lines, where C2C12 cells may not express, for example, the necessary co-factors or other accessory proteins.

3.4 Molecular mechanisms underlying the submucous cleft palate phenotype in *Tbx22* null mice

Concurrent with the efforts to identify downstream target genes of TBX22, an important focus of this project was also to elucidate a possible molecular mechanism underlying the pathology of the submucous cleft palate phenotype observed in *Tbx22* null mice.

In *Tbx22* null mice, the majority of null animals exhibit submucous cleft palate rather than a complete cleft of the secondary palate. It is estimated that ossification of the palatine bone in the secondary palate is severely reduced by 68% compared to the wt (Pauws et al., 2009a). Detailed analysis of the null palate at E15.5 revealed a lack of mineralized bone and reduced osteoblastic activity measured by alkaline phosphatase, an osteoblast marker, in the null palatine bone. In addition, the area of *Runx2* expression was smaller in the null posterior palate, indicating a reduced number of osteoblasts (Pauws et al., 2009a). However, it was not entirely clear if the severe palatine bone reduction in the null posterior palate was primarily caused by a reduction in osteoblast proliferation or delayed differentiation and/or maturation, or another mechanism.

Unlike overt cleft palate, only a couple of animal models of submucous cleft palate have been described including *Tshz1* and *Tgfbr2* deficient mice (Core et al., 2007; Xu et al., 2006). These, however, exhibit a cleft or premature truncation of the soft palate and might be considered a partial overt cleft rather than a true submucous cleft. There are several mouse models with overt cleft palate where *Tbx22* expression analyses have been performed, including *Mn1*$^{-/-}$ mutant mice (Liu et al., 2008; Meester-Smoor et al., 2005) and *36Pub* mutant mice deficient for *Spry2* (Welsh et al., 2007). Meningioma 1 (*MN1*) was first described as the gene disrupted by balanced chromosomal translocation in meningioma (Lekanne Deprez et al., 1995), although mice with a targeted deletion in *Mn1* did not lead to increased incidence of tumour formation but instead they developed severe craniofacial bone defects including cleft palate (Meester-Smoor et al., 2005). This mouse model is of particular interest because a recent study which used these mice showed that the

transcription factor acts upstream of *Tbx22* by demonstrating a downregulated expression of the gene in the null palatal shelves at E13.5. They also noted a reduced expression of *Cyclin D2* accompanied by reductions in cell proliferation in the middle and posterior regions of the null palatal shelves at E13.5 (Liu et al., 2008). More recently, another group showed an essential role of MN1 in osteoblast proliferation, differentiation and maturation (Zhang et al., 2009). The altered expression of *Tbx22* was also shown in the *36Pub* mutant mice that essentially lacked the FGF signalling antagonist *Spry2* which resulted in palate and facial clefting due to excessive cell proliferation, revealing importance of growth signal dosage (Welsh et al., 2007). In these mice, expression of *Tbx22* did not expand to the posterior end of the palatal shelves as it did in the wt at E14.5.

These studies prompted the investigation of cell proliferation rates in *Tbx22* null mice, since an altered cell cycle rate could also explain the submucous cleft palate phenotype, possibly in combination with defects in osteoblast differentiation and/or maturation. In addition to cell proliferation, cellular apoptosis in the *Tbx22* null palatal shelves was also examined although there are only a couple of animal models where altered apoptosis is thought to be responsible for a cleft palate phenotype (Dudas et al., 2006; Rice et al., 2004).

3.4.1 Cell proliferation measured by phospho-Histone H3 in the palatal shelves at E13.5

It was decided to investigate E13.5 embryos as *Tbx22* is expressed specifically and at relatively high levels in the growing palatal shelves at this time. This is also the developmental stage just prior to palatal shelf elevation when some other mouse models with cleft palate such as *Osr2*, *Msx1*, *Fgf10* and *Fgfr2*b mutant mice exhibit defects in cell proliferation (Ito et al., 2003; Lan et al., 2004; Rice et al., 2004; Satokata and Maas, 1994).

Cell proliferation was measured by immunohistochemical assay using phospho-Histone H3 (Ser10) as a primary antibody. Histone H3 is specifically phosphorylated on serine 10 during late S or G2 cell cycle phases and is a convenient way to assess the mitotic index. For analysis, the palatal shelves were

categorised into the anterior, middle and posterior regions. The number of cells stained with DAPI and the number of phospho-Histone H3 positive cells on six serial sections per region from four wt and four null littermates were then counted in the palatal epithelium and mesenchyme.

In the palatal epithelium at E13.5, the percentage of the phospho-Histone H3 positive cells in the anterior (2.47±1.34% in the wt, 2.69±0.89% in the null, p=0.84), middle (3.34±0.57% in the wt, 3.30±1.09% in the null, p=0.95) or posterior (2.55±0.67% in the wt, 2.78±1.10% in the null, p=0.77) regions did not differ significantly between the wt and null mice (Figure 3.11, A-F, G). In the palatal mesenchyme, the percentage of phospho-Histone H3 positive cells was significantly reduced by 53.9% in the middle region of the null palatal shelves compared to the wt (4.25±1.15% in the wt, 1.96±0.19% in the null, p=0.03) (Figure 3.11, B, E and H). In the posterior region, a 42.7% reduction was observed in the null palatal mesenchyme on average but was not statistically significant (2.93±1.25% in the wt, 1.68±0.27% in the null, p=0.20) (Figure 3.11, C, F and H), whereas no alteration in cell proliferation was detected in the anterior palatal mesenchyme where there is no expression of *Tbx22* (2.03±0.20% in the wt, 1.94±0.27% in the null, p=0.41) (Figure 3.11, A, D and H).

The results suggest that loss of *Tbx22* leads to reduced cell proliferation rates especially in the middle to posterior palatal mesenchyme where the gene is expressed (Figure 3.2), but not in the anterior region at E13.5. There was no significant difference in the proliferation rate in the palatal epithelium along the anterior to posterior regions. This was expected as *Tbx22* is known to be expressed almost exclusively in the palatal mesenchyme but not in the epithelium (Braybrook et al., 2002; Bush et al., 2002). Therefore, it seems like TBX22 has a role in cell proliferation in the palatal mesenchyme at E13.5, in addition to previously suggested roles in osteoblast differentiation and maturation at later stages. It could also be that, in the growing palatal shelves, those cells actively proliferating more in the wt might be the ones that become osteoblasts later in palate development.

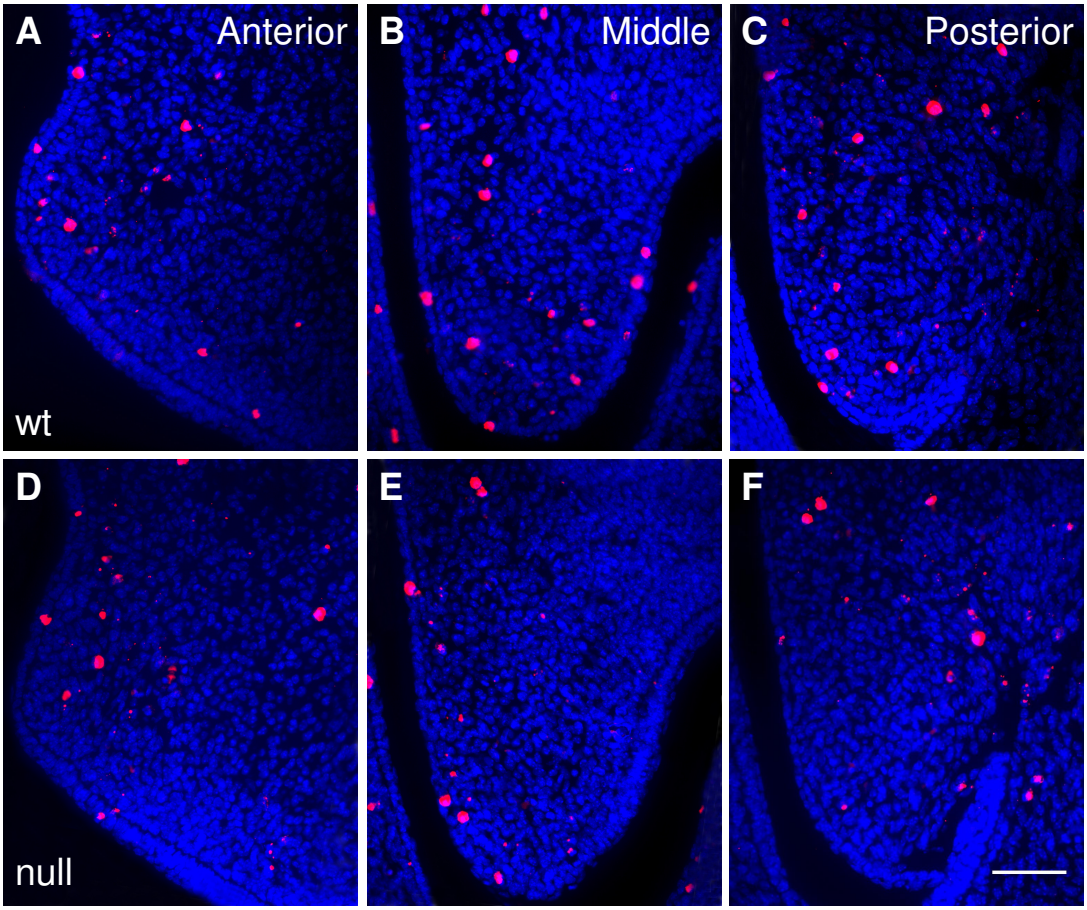
A
Anterior
B
Middle
C
Posterior
wt
D
E
F
null

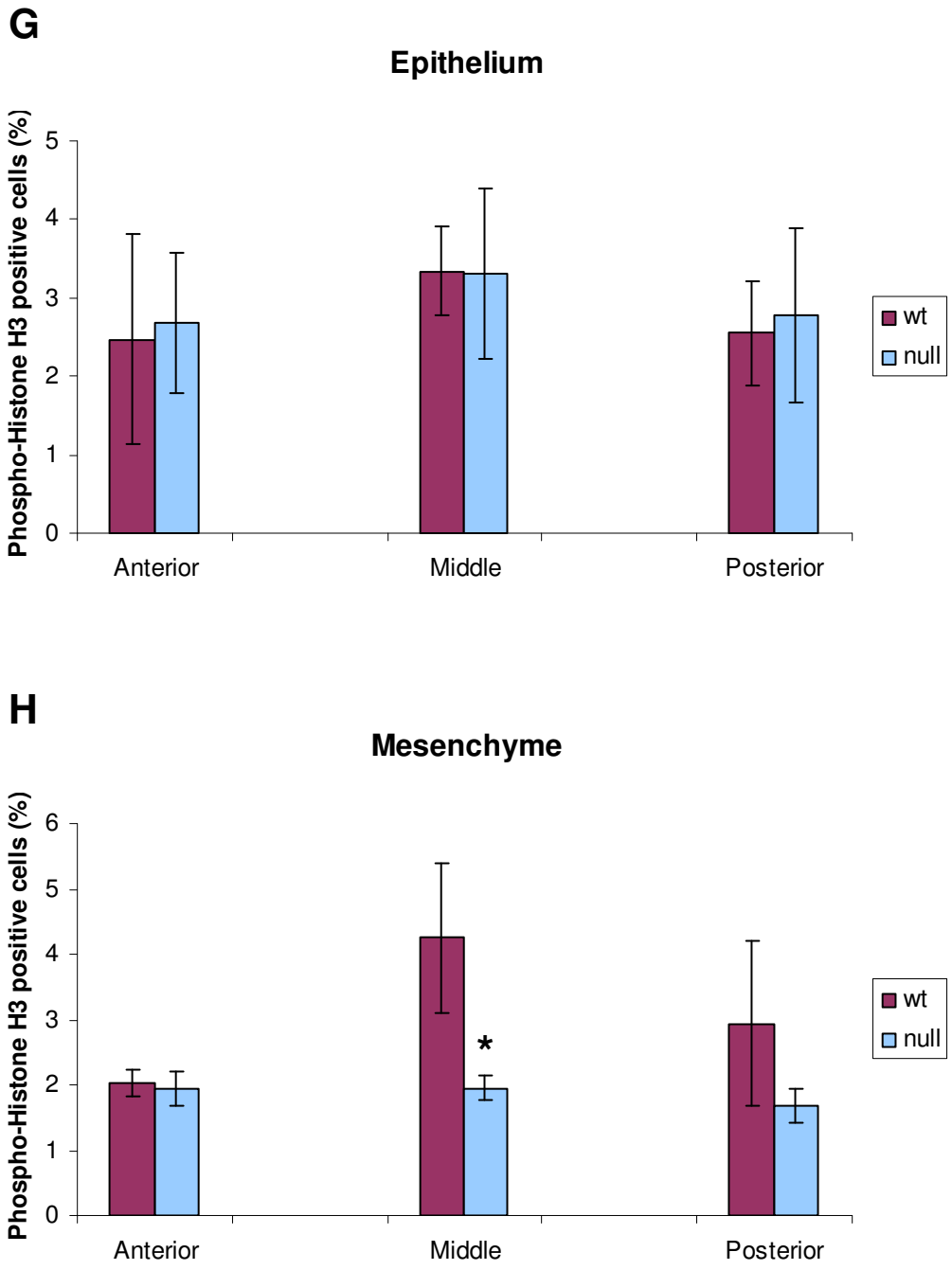

Figure 3.11 Analysis of cell proliferation in the wt and *Tbx22* null mouse palatal shelves at E13.5

Cell proliferation in the palatal shelves at E13.5 was measured by immunohistochemical assay using phospho-Histone H3 antibody. For analysis, the palatal shelves were categorised into the anterior (A and D), middle (B and E) and posterior (C and F) regions. The area of tissue counted for positive cells was restricted to the approximate area of each palatal shelf as shown in panels A-H. The percentage of phospho-Histone H3 positive cells was seperately analysed for the epithelium (G) and mesenchyme (H) in each region. In comparison with the wt, the number of phospho-Histone H3 positive cells in the null palatal mesenchyme was significantly reduced in the middle region (H). The error bars represent standard deviation. *p<0.05, paired Student's t test. Scale bar = 50 µm.

3.4.2 Apoptosis measured by cleaved Caspase-3 in the palatal shelves at E13.5

Apoptosis was measured by immunohistochemical assay using cleaved Caspase-3 as a primary antibody. Inactive full length Caspase-3 zymogen is activated during apoptosis, by cleavage into p17 and p12 fragments. The p17 fragment is then recognised by the primary antibody. For analysis, the palatal shelves were categorised into the anterior, middle and posterior regions as described above. The total number of cells stained with DAPI and the number of Caspase-3 positive cells on six serial sections from four wt and four null littermates were then counted.

At E13.5, only very few cells were positive for cleaved Caspase-3 in the palatal shelves (Figure 3.12, A-F), and no significant difference in terms of percentage of cleaved Caspase-3 positive cells was detected in the anterior (0.05±0.02% in the wt, 0.04±0.01% in the null, p=0.23), middle (0.11±0.04% in the wt, 0.09±0.04% in the null, p=0.49) or posterior (0.08±0.02% in the wt, 0.08±0.01% in the null, p=0.97) regions of the wt and null palatal shelves (Figure 3.12, G). The results suggest that *Tbx22* does not seem to have an obvious role in apoptosis in the growing palatal shelves at this developmental stage.

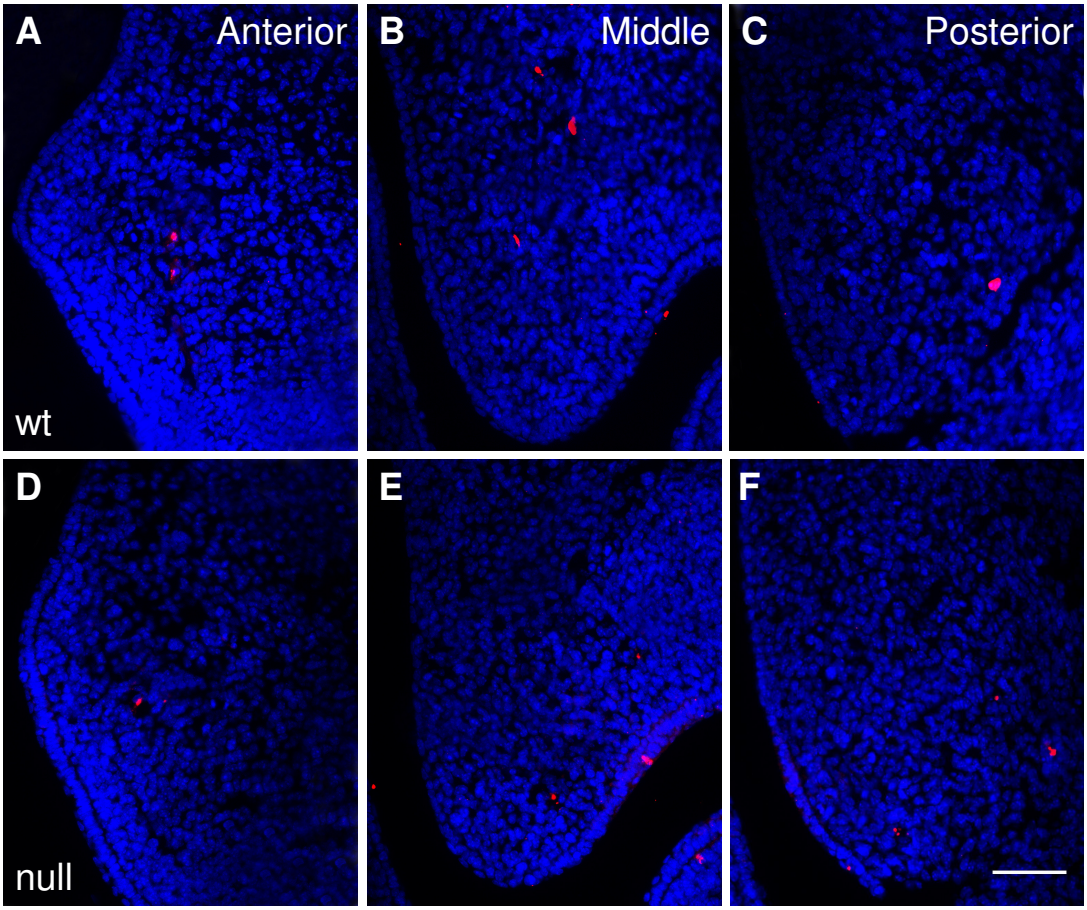
A
Anterior
B
Middle
C
Posterior
wt
D
E
F
null

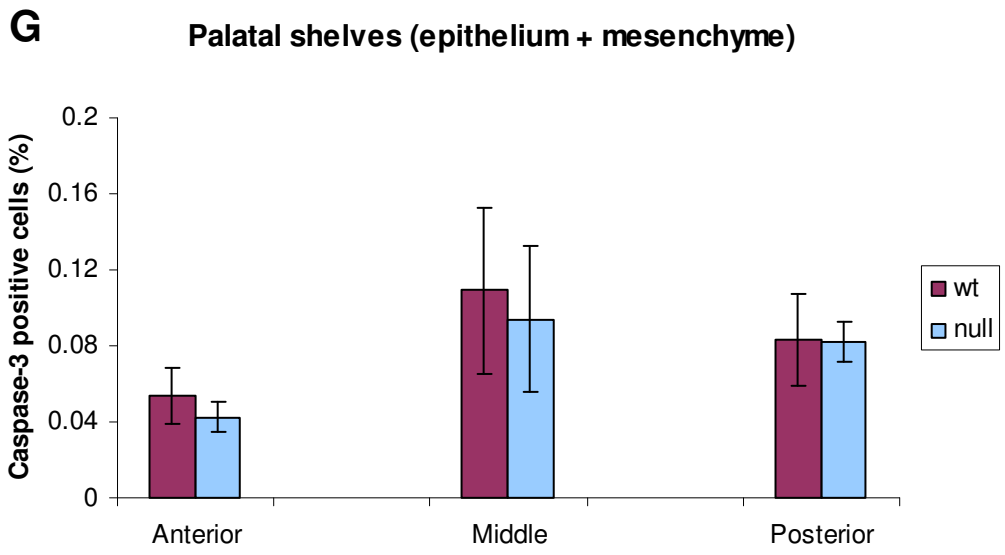

Figure 3.12 Analysis of cell apoptosis in the wt and *Tbx22* null mouse palatal shelves at E13.5

Cell apoptosis in the palatal shelves at E13.5 was measured by immunohistochemical assay using cleaved Caspase-3 antibody. For analysis, the palatal shelves were categorised into the anterior (A and D), middle (B and E) and posterior (C and F) regions, and the percentage of Caspase-3 positive cells were analysed (G) in each region. The area of tissue counted for positive cells was restricted to the approximate area of each palatal shelf as shown in panels A-H. The number of cleaved Caspase-3 positive cells did not differ significantly between the wt and null palatal shelves (G). The error bars represent standard deviation. *$p<0.05$, paired Student's t test. Scale bar = 50 µm.

3.4.3 Reduced cell proliferation in the null palatal shelves is accompanied by a decreased *Cyclin D2* expression

The process of cell cycle regulation is mainly controlled by two key factors, cyclins and cyclin-dependent kinases (CDKs) that are well conserved among all eukaryotes. Of these, CDKs are expressed constitutively whereas cyclins are produced in response to various signals. Of particular note, Cyclin D is the first to be synthesised in response to growth factors stimulating the cell cycle.

It was interesting to note that the expression level of *Cyclin D2* was shown to be reduced in *Mn1*$^{-/-}$ mice where cell proliferation was also decreased (Liu et al., 2008). Moreover, it was also reported that the expression level of *Tbx22* in *Mn1*$^{-/-}$ mice was dramatically reduced in the palatal shelves at E13.5. Therefore, to examine if the reduced cell proliferation in *Tbx22* null mice is accompanied by a decreased *Cyclin D2* expression, expression levels of this gene were examined by whole mount *in situ* hybridisation.

Although *Cyclin D2* was expressed globally, expression in the anterior to middle regions of the growing palatal shelves in the null compared to the wt at E12.5 and E13.5 was specifically downregulated (Figure 3.13). *Tbx22* expression in the palatal shelves partially overlapped with *Cyclin D2* expression. However this seemed ambiguous especially at E13.5 because *Tbx22* expression in some embryos was found in the middle regions but in other embryos it was detected in more posterior regions of the palatal shelves. It is therefore possible that TBX22 plays a role in regulating cell proliferation rates, which may or may not be via modulating the level of *Cyclin D2* expression in the palatal shelves at these developmental stages.

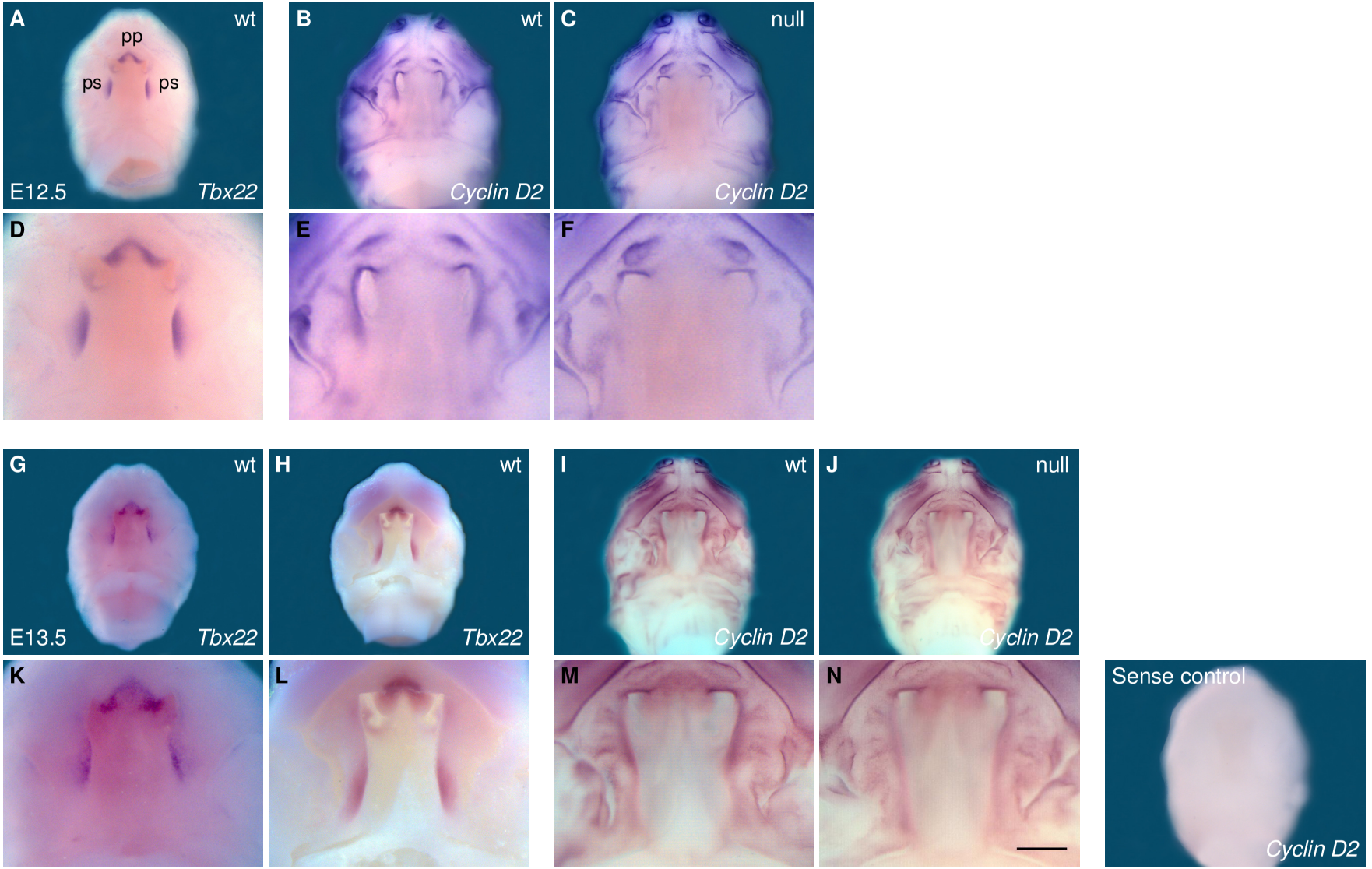
A
wt
pp
ps
ps
E12.5
Tbx22
B
wt
Cyclin D2
C
null
Cyclin D2
D
E
F
G
wt
E13.5
Tbx22
H
wt
Tbx22
I
wt
Cyclin D2
J
null
Cyclin D2
K
L
M
N
Sense control
Cyclin D2

Figure 3.13 Expression pattern of *Cyclin D2* at E13.5
Expression pattern of *Cyclin D2* was detected by whole mount *in situ* hybridisation at E13.5 using *Cyclin D2* antisense probe. In comparison with the wt, the expression was specifically reduced in the middle regions of the growing palatal shelves at E12.5 (B, C, E and F) and E13.5 (I, J, M and N). pp, primary palate; ps, palatal shelf. Scale bar = 375 µm (A, I and J), 586 µm (B and C), 150 µm (D, M and N), 234 µm (E and F), 469 µm (G, and H), 375 µm (I and J), 188 µm (K and L).

3.4.4 Summary

To summarise, cell proliferation seemed to have been compromised in the middle regions of the palatal shelves in *Tbx22* null mice compared to the wt littermates, whereas no obvious difference in apoptosis was observed at E13.5. The reduced proliferation in the *Tbx22* null palatal shelves was specific to the palatal mesenchyme. *Tbx22* is almost exclusively expressed in the mesenchyme but not in the epithelium, suggesting a cell autonomous effect in the regulation of cell proliferation. Examination of *Cyclin D2* expression revealed a reduction in the null palatal shelves at E12.5 and E13.5 which may help to explain the reduced cell proliferation although *Tbx22* and *Cyclin D2* only partially overlapped. *Cyclin D2* expression in the anterior region seemed to have decreased but cell proliferation rate was unaffected anteriorly. This aspect needs more careful examination by techniques such as section *in situ* hybridisation, nevertheless *Tbx22* seems to regulate cell proliferation whether it is through *cyclin D2* expression or not.

3.5 Expression analyses of growth factor genes in wt and *Tbx22* null mouse palatal shelves

The most common cause of cleft palate found in mouse models is defective palatal shelf growth often caused by altered cell proliferation. This has been the case for *Tbx22* null mice that also display delayed ossification of the posterior hard palate (Pauws et al., 2009a). Palatal growth is a complex process and many factors are involved throughout. These include transcription factors such as *Msx1*, *Osr2* and *Shox2* as well as signalling molecules and growth factors such as *Shh*, *Tgfβs*, *Bmps* and *Fgfs* (Gritli-Linde, 2007; Wilkie and Morriss-Kay, 2001). These are potentially worth investigating in *Tbx22* null mice in relation to the cell proliferation defects observed. In particular, the level of Cyclins is essentially determined by extracellular growth factors (Sherr, 1995) and it would be interesting to investigate if expression of these are altered in the *Tbx22* null palatal shelves. In the scope of this project, it was intended to examine some of the BMP and FGF signalling components.

3.5.1 Expression of growth factor genes is not significantly altered in *Tbx22* null mice

Expression analyses of *Bmp2*, *Bmp3*, *Bmp4*, *Fgf10*, *Fgfr2b* and *Spry2* genes which are all implicated in palatal shelf growth were examined by whole mount *in situ* hybridisation. The experiments were carried out on E13.5 embryos in order to investigate if any of these growth factors were responsible for the reduced cell proliferation in *Tbx22* null mice detected at this developmental stage.

In the developing palate, expression of *Bmps* is regulated in a spatiotemporal manner. Before shelf elevation, at E13.0, *Bmp4* is reported to be expressed in both epithelial and mesenchymal cells, whereas *Bmp2* expression only appears in mesenchymal cells (Lu et al., 2000). In this study, *Bmp2* was expressed anteriorly but absent in the posterior region of the palatal shelves at E13.5 both in the wt and null palatal shelves (Figure 3.14, B, C, E and F). *Bmp4* expression, albeit very weak, was detected in the posterior end of the shelves both in the wt and null mice (Figure

3.14, I, J, M and N). The pattern and intensity of expression of *Bmp2* and *Bmp4* are reported to be dynamic, and both become more intensely expressed in the condensed mesenchyme as the palate develops from E13.0 to E16.0, indicating their roles for palatal bone formation as well as mesenchymal proliferation before fusion (Liu et al., 2005). Though *Bmp3* was almost negative throughout the course of palatogenesis in one study (Lu et al., 2000), its expression has been reported in the posterior palate during palatal fusion in another study (Nie, 2005). Here, a specific and intense expression of *Bmp3* was observed in the posterior palatal shelves before fusion at E13.5, although the expression pattern was similar between wt and null mice (Figure 3.14, G, H, K and L). It has been reported that BMP3 acts as a negative regulator of osteogenesis by antagonising osteogenic BMPs such as BMP2 (Daluiski et al., 2001). In fact, *Bmp2* and *Bmp3* display a reciprocal expression pattern along the anterior to posterior palatal shelves. These findings suggest that posterior expression of *Bmp3* may contribute to the development of soft palate to some extent by suppressing the *Bmp2* which can act as a potent inducer of osteoblast differentiation (Lian et al., 2006; Ryoo et al., 2006).

Expression of *Fgf10* during palatogenesis has been detected in the palatal mesenchyme from E11.5 to E13.5 (Alappat et al., 2005). The expression was reported in the anterior to middle shelves throughout this period although expression within the mesenchyme was shifted from close apposition to the palatal epithelium to more ventrolaterally away from the MEE as shelf growth progressed. In agreement with the previous study, *Fgf10* was expressed in the anterior to middle regions of the palatal shelves but posteriorly it was undetectable (Figure 3.15, B, C, E and F). The pattern of expression in the wt and null palatal shelves was similar. For *Fgfr2b*, expression has been reported in the developing oral epithelium particularly in the palatal epithelium from E12 to E14, as well as in the palatal mesenchyme of the nasal side at E13 (Rice et al., 2004). Here, expression of *Fgfr2b* was found in the anterior to middle regions of the palatal shelves that overlapped with *Fgf10* expression (Figure 3.15, G, H, K and L), which was expected considering that FGFR2b is a receptor for FGF10. However, no significant difference was detected between the wt and null palatal shelves. *Spry2* expression is reported in the epithelium and mesenchyme of anterior palatal shelves at E12.5 which becomes more restricted to the epithelium of the middle shelves by E14.5

(Welsh et al., 2007). Similarly in this study, expression was detected in the anterior to middle shelves which was particulary intense in the growing tip of palatal shelves and in the developing rugae at E13.5 (Figure 3.15, I, J, M and N). This expression pattern was similar in both the wt and null palatal shelves. Submucous cleft palate in *Tbx22* null mice is translated into an aberrant pattern of the rugae in the posterior half of the hard palate (Pauws et al., 2009a), but the rugae irregularity was not apparent at E13.5. This may not be surprising since palatal bone formation starts from E15.0 onwards and probably aberrant rugae in the null mice may be a reflection of having poorly developed palatine bones.

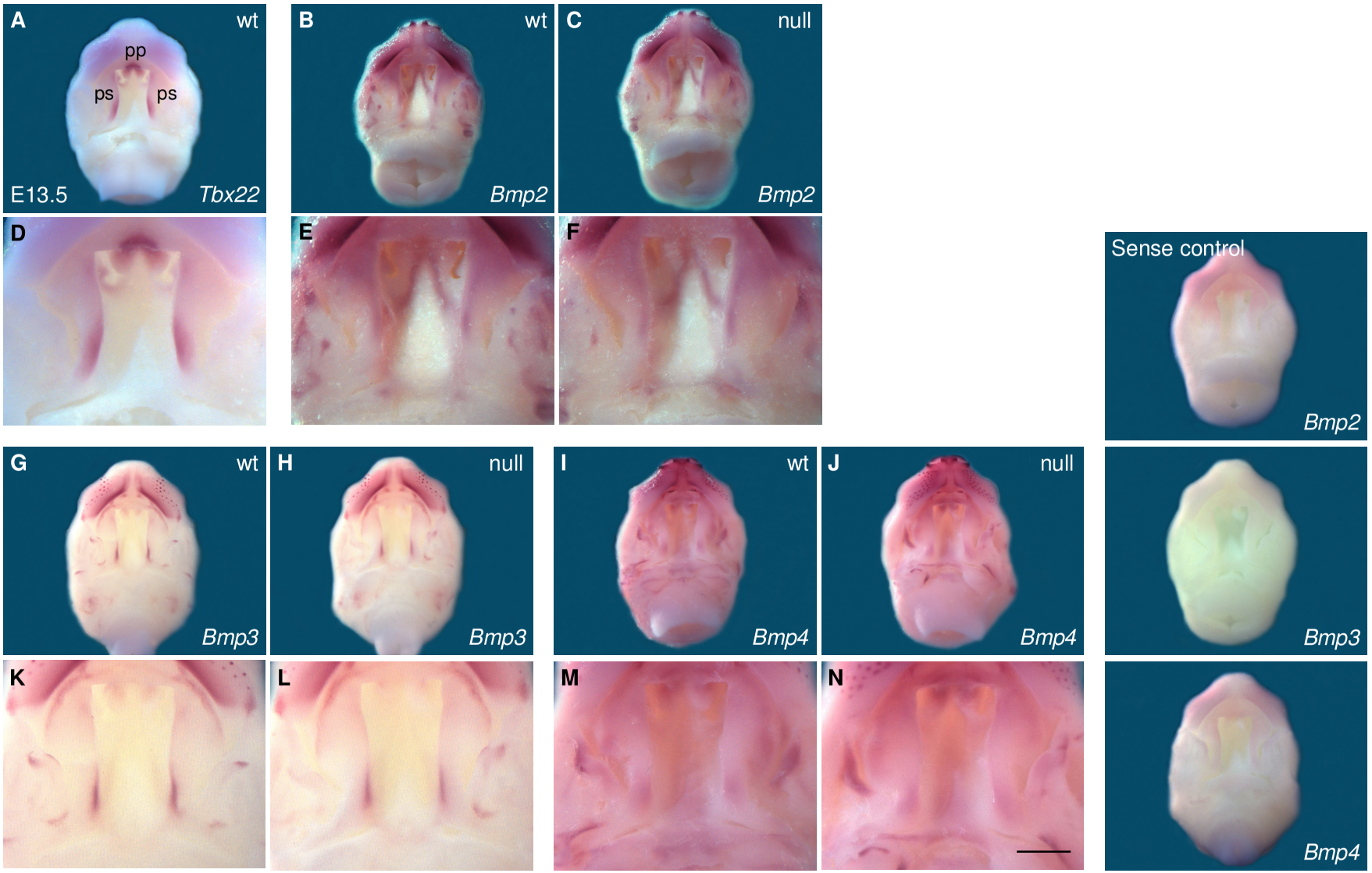
A
wt
pp
ps
ps
E13.5
Tbx22
B
wt
Bmp2
C
null
Bmp2
D
E
F
Sense control
Bmp2
G
wt
Bmp3
H
null
Bmp3
I
wt
Bmp4
J
null
Bmp4
Bmp3
K
L
M
N
Bmp4

Figure 3.14 Expression patterns of *Bmp2*, *Bmp3* and *Bmp4*
Expression patterns of *Bmp2*, *Bmp3* amd *Bmp4*were detected by whole mount *in situ* hybridisation at E13.5 using antisense riboprobes. *Bmp2* was expressed anteriorly but absent in the posterior region of the palatal shelves both in the wt (B and E) and null palatal shelves (C and F). *Bmp3* was similarly detected in the posterior palatal shelves of the wt (G and K) and null mice (H and L). Weak *Bmp4* expression was detected in the anterior region and in the very posterior end of the shelves both in the wt (I and M) and null mice (J and N). pp, primary palate; ps, palatal shelf. Scale bars = 500 µm (A-C and G-J), 200 µm (D-F and K-N).

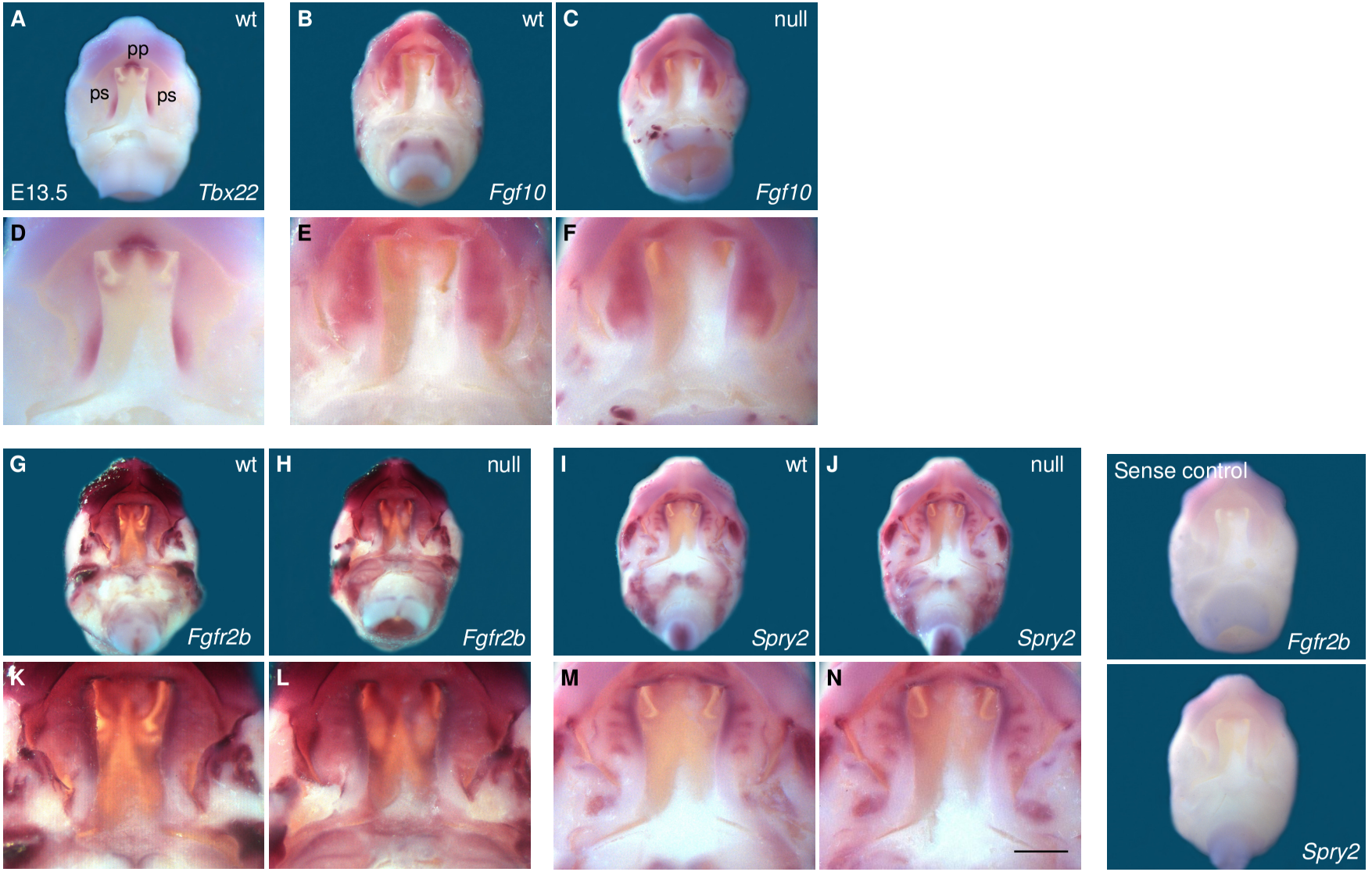
A
wt
pp
ps
ps
E13.5
Tbx22
B
wt
Fgf10
C
null
Fgf10
D
E
F
G
wt
Fgfr2b
H
null
Fgfr2b
I
wt
Spry2
J
null
Spry2
Sense control
Fgfr2b
K
L
M
N
Spry2

Figure 3.15 Expression patterns of *Fgf10*, *Fgfr2b* and *Spry2*
Expression patterns of *Fgf10*, *Fgfr2b* and *Spry2* were detected by whole mount *in situ* hybridisation at E13.5 using antisense riboprobes. *Fgf10* was similarly expressed in the anterior to middle regions of the palatal shelves in both the wt (B and E) and null palatal shelves (C and F). Expression of *Fgfr2b* was found in the anterior to middle regions of the palatal shelves that were similar between the wt (G and K) and null palatal shelves (H and L). *Spry2* was expressed in the anterior half of the palatal shelves, with specific expression found in the developing rugae both in the wt (I and M) and null palatal shelves (J and N). pp, primary palate; ps, palatal shelf. Scale bars = 500 µm (A-C and G-J), 200 µm (D-F and K-N).

3.5.2 Summary

Although *Tbx22* seems to be involved in the regulation of cell proliferation, none of the growth signalling components tested by whole mount *in situ* hybridisation were altered in the palatal shelves of *Tbx22* null mice at E13.5. However, more precise comparisons of expression patterns within the palatal shelves can be made by section *in situ* hybridisation. In terms of a regulatory relationship, there is now mounting evidence that *Tbx22* may be downstream of FGF and BMP signalling pathways. For instance, FGFs were found to positively regulate *Tbx22* in early facial morphogenesis whereas BMPs could repress expression of the gene at later stage in the chick and mouse frontonasal mass (Higashihori et al., 2010; Fuchs et al., 2010). The results presented here indicate that there may be no feedback from TBX22 to BMP or FGF signalling components investigated, in the palatal shelves at E13.5.

3.6 Characterisation of ankyloglossia and choanal atresia

In addition to submucous cleft palate, *Tbx22* null mice display ankyloglossia and choanal atresia (Pauws et al., 2009a). Ankyloglossia, also called tongue-tie, is defined as having a shortened frenulum attachment near the tip of the tongue which can restrict movement of the tongue. In the null mice, the tongue attaches more anteriorly to the floor of the mouth (Figure 1.15). This resembles ankyloglossia frequently seen in human CPX patients.

Another defect found in the null mice was choanal atresia, which is characterised by a persistent oronasal membrane in the choanae (Figure 1.15). The severity of atresia varies from mild cases where only the posterior part of the choanae is obstructed to more severe cases where the entire length of choanae are blocked from anterior to posterior. Also, it can manifest as unilateral or bilateral. This phenotype, rather than submucous cleft palate or ankyloglossia, is suggested to be the main cause of the post-natal lethality because it was absent in the surviving pups but present in pups that died after birth. Unlike submucous or overt cleft palate and ankyloglossia, this has not until now been a feature synonymous with CPX.

3.6.1 Morphological analysis of facial regions in early development

Previously, the detailed analysis of craniofacial structures revealed that ankyloglossia and choanal atresia phenotypes in *Tbx22* null mice were evident at E15.5 (Pauws et al., 2009a). At this developmental time point, the tongue in the null mice is attached as anteriorly as the incisive foramen while it is free at this position in the wt mice. Similarly at this stage, oronasal membranes persist with variable severity in the null mice whereas they are already disappeared in the wt. In order to examine the morphology of relevant tissues at earlier developmental stages, H&E staining was carried out on embryos at E12.5 and E11.5. H&E staining allows easy visualisation of histological sections whereby nuclei are stained dark blue by hematoxylin and cytoplasm is stained pink by eosin.

With regard to the ankyloglossia phenotype, the coronal sections of wt at E12.5 indicated that the anterior tip of the tongue was freed from the floor of the mouth

and the frenulum was beginning to be established (Figure 3.16, A and C). In contrast, in the null mice the tip of the tongue was still attached to the floor of the mouth and no obvious frenulum was detected (Figure 3.16, B and D). This suggests that formation of the frenulum in the null mice occurs later than in the wt, starting at or after this time point. Eventually, the frenulum in the null mice becomes visible by E15.5 although located more anteriorly compared to the wt (Figure 1.15).

The developing choanae can be observed in coronal sections of wt embryos at E12.5, which showed the appropriate degradation of the oronasal membranes (Figure 3.16, A and C). In contrast, oronasal membranes in the null mice persisted in the choanae between the oral and nasal cavities (Figure 3.16, B and D). This particular embryo displayed bilateral choanal atresia although we have also observed unilateral atresia while in a small percentage of null mice the phenotype was completely absent (Pauws et al., 2009a). Since the various facial prominences undergo complex fusion events between E10.5 to E12.5, the general facial structure at E11.5 differs dramatically to that of E12.5. At E11.5, the posterior nasal fins seemed to have degenerated in the wt choanae, leaving what looked like a disappearing oronasal membrane behind (Figure 3.17, A). This is consistent with the findings that, in the wt, the posterior nasal fins persist until E11.0, which usually undergo degeneration by E11.5 (Dupe et al., 2003; Tamarin, 1982). This leaves oronasal membranes in the choanae that disappear by E12.5 in the wt. In contrast, the nasal fins failed to undergo cleavage and the fins persisted in many of the null choanae at the equivalent stage (Figure 3.17, C). On occasions, the choanae from null mice resembled those of the wt whereby the nasal fins did degenerate (Figure 3.17, B). In this case, the morphology was very similar to that of the wt where there were still oronasal membranes in the choanae at this stage, but they were likely to disappear soon after. This finding was most likely because some null mice have unilateral atresia or do not display the phenotype (Pauws et al., 2009a).

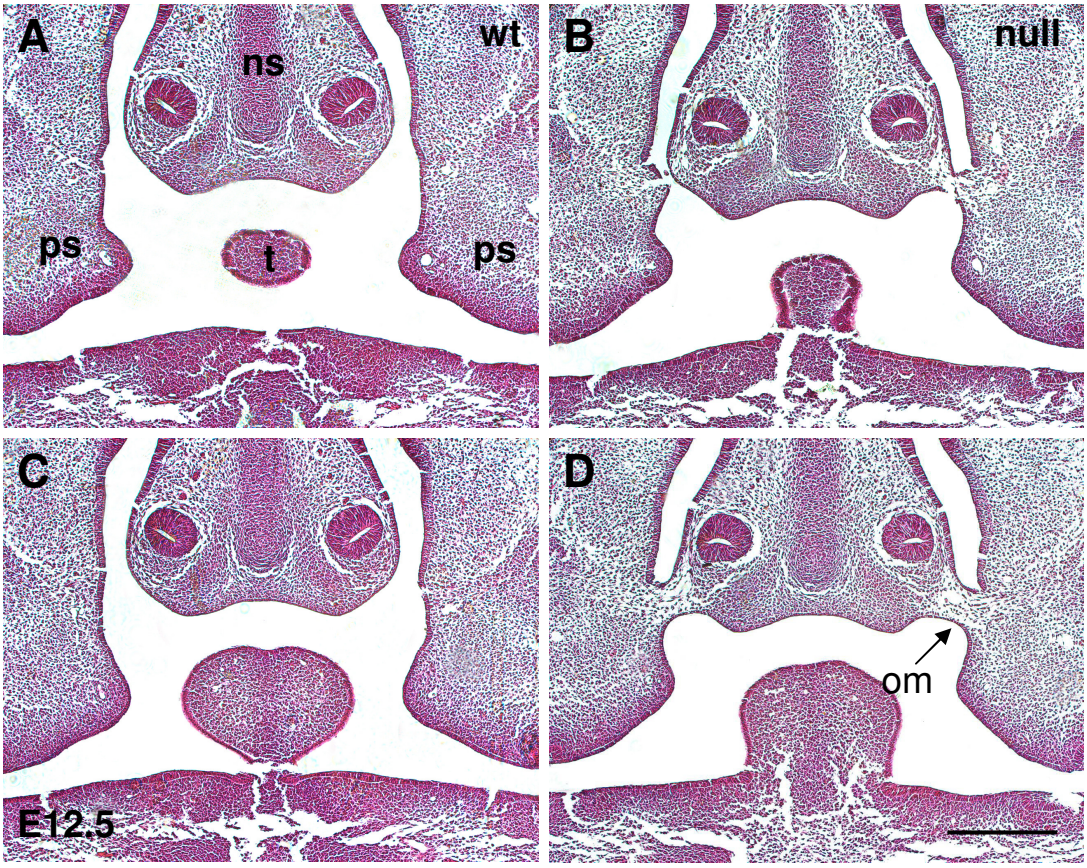

Figure 3.16 Histological analyses of *Tbx22* null mouse craniofacial regions at E12.5

H&E staining was carried out on embryos at E12.5. At this developmental stage, the anterior tip of the tongue was freed from the floor of the mouth and oronasal membrane had disappeared in the wt (A and C). In the null mice, the tip of the tongue was attached to the floor of the mouth and oronasal membranes persisted in the choanae (B and D). ns, nasal septum; om, oronasal membrane; ps, palatal shelves; t, tongue. Scale bar = 250 µm.

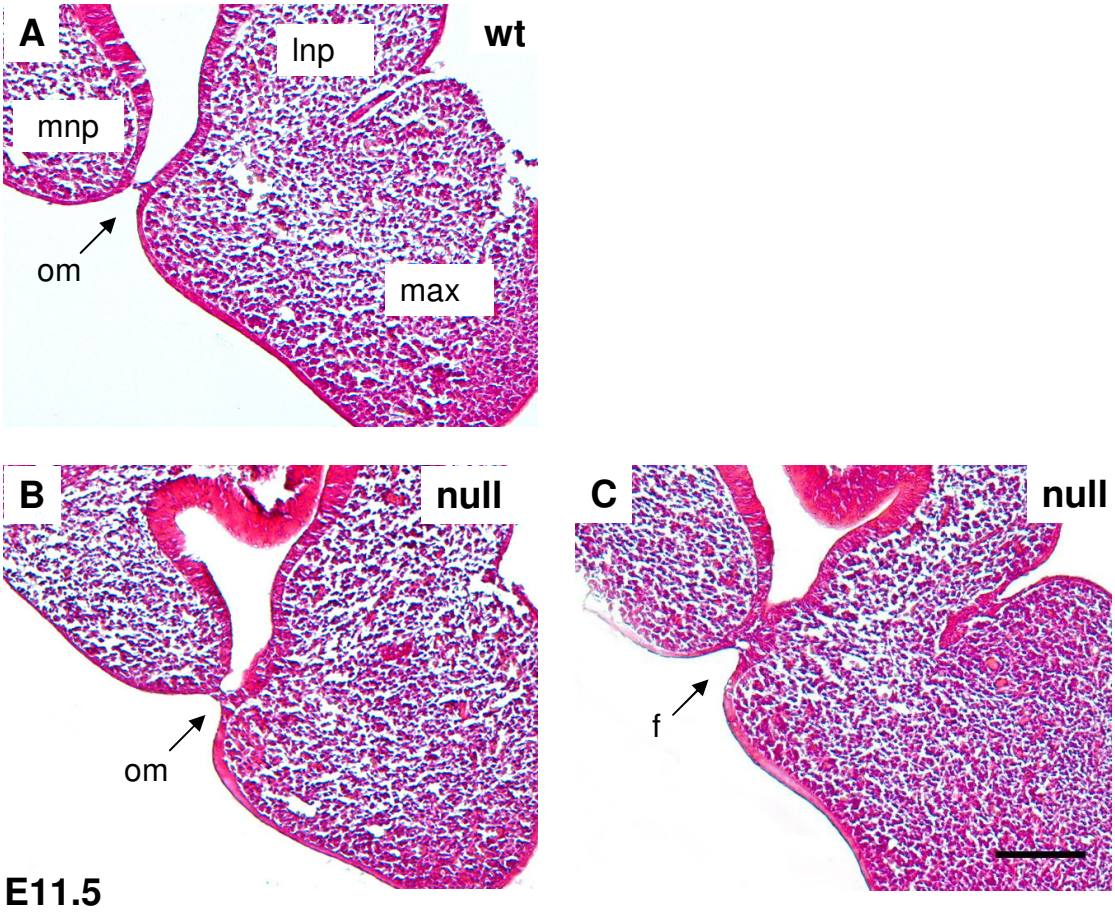

Figure 3.17 Histological analyses of *Tbx22* null mouse choanal regions at E11.5
H&E staining of coronal sections of E11.5 wt and null mice through the posterior portions of nasal fins. The nasal fins degenerated in the wt, leaving oronasal membrane behind (A). The nasal fins persisted in many of the choanae in the null mice (C). On occasions, the nasal fin did degenerate in the null mice giving rise to the oronasal membrane (B). f, nasal fin; lnp, lateral nasal process; max, maxillary process; mnp, medial nasal process; om, oronasal membrane. Scale bar = 50 µm.

3.6.2 Expression pattern of *Fgf8* during degeneration of the nasal fins is not significantly altered in *Tbx22* null mice

Genetic pathways underlying the development of choanae have not been subjected to intense research in the past. This is probably because the occurrence of choanal atresia is relatively rare in the human, and as a consequence there are only a limited number of animal models available to study the phenotype. Nevertheless, as described above, *Raldh3* null mice provide an interesting insight into the occurrence of choanal atresia. In the absence of *Raldh3*, *Fgf8* expression persists in the nasal fins at E11.0, suggesting that expression of *Fgf8* needs to be inhibited for normal choanae development. Therefore, we next investigated *Fgf8* expression in the nasal fins in the wt and *Tbx22* null mice at E10.5 and E11.0 at which time the nasal fins are still present in the wt (Dupe et al., 2003).

The medial and lateral nasal processes are formed by the mesenchyme surrounding the nasal placodes by E10.5. This defines the nasal pits. At this stage, *Tbx22* was expressed in the medial nasal processes as well as around the presumptive nasal fins where medial and lateral nasal processes merge that were found ventrally to the nasal pits (Figure 3.18, A and D). The expression was also detected in the maxillary and mandibular processes. At the same stage, in the wt, *Fgf8* was expressed in the medial and lateral nasal processes forming a horseshoe pattern around the nasal pits which extended ventrally in nascent fins (Figure 3.18, B and E). The expression was also detected at the oral edge of the medial nasal process. In addition, the expression was observed in the maxillary processes and in the mandibular processes as well as in the medial anterior forebrain between the two medial nasal processes. In the null mice, the pattern of *Fgf8* expression and intensity appeared very similar to the wt (Figure 3.18, C and F).

At E11.0, *Tbx22* expression was not detected in the nasal fins anteriorly as shown by the frontal view (Figure 3.18, G and J). However, its expression was evident around the fused medial and lateral nasal processes on the stomodeum side around the posterior end of nasal fins between the future primary and secondary palate which corresponded to where the choanae would form (Figure 3.18, M and P). At the equivalent stage, *Fgf8* continued to be strongly expressed in the epithelium of

the nasal processes surrounding the nasal pits both in the wt and null mice (Figure 3.18, H, I, K and L). Expression was also visible at the posterior end of the nasal fins partially overlapping with *Tbx22* expression and in the maxillary processes. This was similar between the wt and null mice (Figure 3.18, N, O, Q and R). Thus, a lack of *Tbx22* does not seem to affect *Fgf8* expression in the craniofacial regions at E10.5 and E11.0.

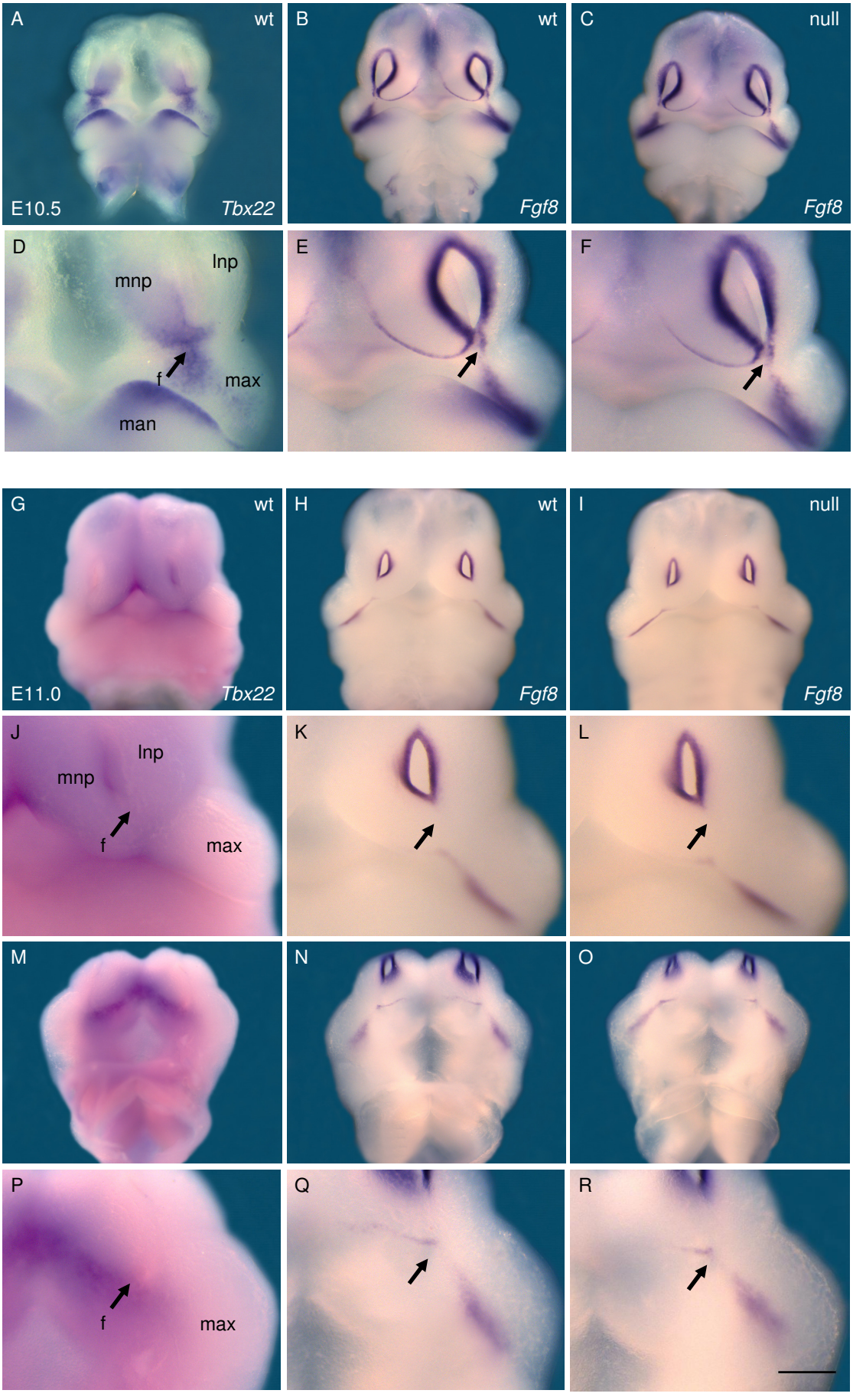
A
wt
E10.5
Tbx22
B
wt
Fgf8
C
null
Fgf8
D
lnp
mnp
f
max
man
E
F
G
wt
E11.0
Tbx22
H
wt
Fgf8
I
null
Fgf8
J
lnp
mnp
f
max
K
L
M
N
O
P
f
max
Q
R

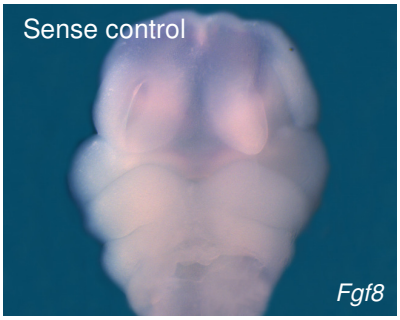

Figure 3.18 Expression pattern of *Fgf8* at E10.5 and E11.0
Expression pattern of *Tbx22* and *Fgf8* was detected by whole mount *in situ* hybridisation at E10.5 (A-F) and E11.0 (G-R). The arrows indicate nasal fins. f, nasal fin; lnp, lateral nasal process; man, mandibular process; max, maxillary process; mnp, medial nasal process. Scale bar = 250 µm (A-C, G-I and M-O), 100 µm (D-F, J-L and P-R).

3.6.3 Summary

H&E staining showed that the ankyloglossia phenotype in *Tbx22* null mice was visible at the base of the tongue at E12.5. At this stage, the frenulum was not established in the null mice but it was formed in the wt. Choanal atresia was also evident in the null mice at E12.5 characterised by the persisted oronasal membranes in the choanae. Slightly earlier at E11.5, nasal fins almost disappeared in the wt choanae, leaving oronasal membranes that were going to rupture soon after. In the null choanae, the nasal fins persisted at the equivalent stage. As *Fgf8* is one of only a few genes known to be important for the choana development, its expression pattern was examined at E10.5 and E11.0 before the choanal atresia defect becomes apparent in the null mice. However, the expression pattern was very similar between the wt and null mice, suggesting *Tbx22* does not regulate *Fgf8* during nasal development.

CHAPTER 4: DISCUSSION

4 DISCUSSION

Clefts of the lip and palate are a heterogeneous group of disorders that rank among the commonest birth defects known, affecting 1 in 700 births worldwide (Murray, 2002; Vanderas, 1987; Wyszynski et al., 1996). The underlying cause is poorly understood, with a complex interaction of genes and environmental factors being implicated. Nevertheless, several important genetic factors have been identified, including mutations in the T-box transcription factor *TBX22* that cause X-linked cleft palate and ankyloglossia (CPX) (Braybrook et al., 2001). CPX is characterised by cleft palate phenotypes ranging from a complete cleft of the secondary palate, submucous cleft palate, cleft of the soft palate, bifid uvula or absent tonsils, which are all frequently but not exclusively associated with ankyloglossia (Stanier and Moore, 2004). The expression of *TBX22*/*Tbx22* is detected in both human and mouse developing palatal shelves as well as at the base of the tongue, medial and lateral nasal prominences and periocular mesenchyme correlating well with the various CPX phenotypes (Braybrook et al., 2002; Bush et al., 2002; Herr et al., 2003). Similar expression in the facial mesenchyme is also observed in other species including chick and zebrafish (Haenig et al., 2002; Jezewski et al., 2009), indicating a conserved role for TBX22 in craniofacial development. Recent studies have shed light on the regulation of *Tbx22* by BMP and FGF signalling during mouse and chick frontonasal morphogenesis (Fuchs et al., 2010; Higashihori et al., 2010), although little is known about molecular pathways that lead to the disease phenotype in CPX. Thus, this project aimed to better understand the functional role of TBX22 by characterising and investigating the recently described *Tbx22* null mouse (Pauws et al., 2009a).

4.1 *Tbx22* expression during craniofacial development

The pathogenic phenotypes found in CPX patients include cleft palate with a varying spectrum from submucous to overt cleft palate which are frequently associated with ankyloglossia (Braybrook et al., 2001; Stanier and Moore, 2004). A detailed spatial analysis of *Tbx22* expression has been described, especially at around E13.5 prior to palatal shelf elevation. Not surprisingly, expression of *TBX22* has been reported in the developing palatal shelves, at the base of the tongue and around the nasal septum (Braybrook et al., 2002). This pattern of expression in craniofacial region is generally conserved in other species including mouse, chick and zebrafish (Braybrook et al., 2002; Bush et al., 2002; Haenig et al., 2002; Herr et al., 2003; Jezewski et al., 2009).

At E9.5, no significant *Tbx22* expression was detected. Some of the previous studies have reported *Tbx22* expression at E9.5, especially using RT-PCR (Braybrook et al., 2002) but also in the somite and craniofacial regions (Farin et al., 2008). Meanwhile, other studies concentrating on the craniofacial region reported no expression at this stage with transcripts becoming detectable from E10.5 onwards (Bush et al., 2002; Fuchs et al., 2010). This suggests that expression first appears between E9.5 and E10.5 in facial region. Differences between studies might reflect the specific probes used, the different mouse strains employed, or difference in timing or staging of embryos, even within litters. For this latter point, it is known that mouse staging based on copulatory plug for E9.5 can range from E9.0 to E10.25. This range in embryonic days converts to 21 to 29 somite stages, and therefore more accurate and consistent observation would be achieved by matching embryos by the number of somites at early stages. *Tbx22* expression in the maxillary and mandibular processes only became detectable at E10.5 along with expression in the medial nasal processes and in the nasal fins found in between the fusing medial and lateral nasal processes. Expression in the medial nasal processes ceased by E11.5 but persisted around the presumptive choanae where the maxillary, the medial and lateral nasal processes merge in between the future primary and secondary palates. Expression was also noted at the anterior tip of the mandible. This would probably correspond to the expression domain observed later at the anterior base of the tongue, around the frenulum which becomes obvious from

E12.5 onwards. From E12.5 onwards, expression has been well described in several studies (Braybrook et al., 2002; Bush et al., 2002; Herr et al., 2003) continuing up until shelf fusion, where *Tbx22* expression becomes undetectable or at least significantly reduced in the palate.

Although the expression pattern of *Tbx22* generally correlates well with where the clinical features of CPX are found (Stanier and Moore, 2004), the choanal atresia phenotype in *Tbx22* null mice is novel (Pauws et al., 2009a). This has not been a recognised feature in human CPX patients, which may be due to a selection bias, where patients with choanal atresia are simply not screened for mutations in *TBX22*. Similarly, although there is significant *Tbx22* expression in the somites, neither human CPX patients nor the null mice show any obvious somitic defect. However, a combined loss of *Tbx18* and *Tbx22*, that are expressed in an overlapping manner in the early somites, has been suggested to lead to posteriorisation of the somites (Farin et al., 2008 and Andreas Kispert personal communication). This suggests that these closely related T-box genes may be functionally redundant in the somites. Overall, it can be seen that *Tbx22* expression is detected in a very temporal and tissue specific pattern between E9.5 and E15.5 in the craniofacial region, which explains its requirement in normal craniofacial development. *Tbx22* null mouse should therefore provide a good model to study the CPX phenotypes.

4.2 Microarray analysis of the wt and *Tbx22* null palatal shelves

Earlier data for T-box genes in general and TBX22 in particular (Andreou et al., 2007) show that their major cellular function is in transcriptional regulation. Therefore, one of the principle aims of this project was to identify putative downstream targets under the transcriptional control of TBX22. For this purpose, it was decided to employ a global approach of microarray expression analysis. Comparative gene expression profiling is a powerful technique with the potential to reveal the gene networks that TBX22 is involved in during normal palatogenesis and provide tools for the further study of cleft palate. For the microarray analysis, the palatal shelves from the transgenic mouse model which lacked functional *Tbx22* (Pauws et al., 2009a) were appropriate to use because they recapitulated the cleft palate phenotypes observed in human CPX patients, namely an overt cleft of the secondary palate and submucous cleft palate characterised by delayed ossification of the palatine bone.

Affymetrix GeneChip® Mouse Gene 1.0 ST Arrays were used to compare the expression of ~29,000 gene transcripts in the presence and absence of *Tbx22*. To do this, expression profiles of dissected E13.5 palatal shelves from three wt and null littermates were examined. This time point was chosen because maximal and specific *Tbx22* expression is observed in the palatal shelves just prior to elevation (Braybrook et al., 2002; Bush et al., 2002; Herr et al., 2003). Also, it seemed reasonable to compare the wt and null palatal shelves when they are most similar in their gross morphology and just prior to developing phenotypic differences. At the slightly later stage of E14.5, the palatal shelves are in any case quite variable in shape between normal littermates, due to variability in the timing of elevation. Later still (>E15.5), when the ossification defects become obvious, expression differences could easily be attributed as secondary effects to the more severe morphological differences, while *Tbx22* expression is by now greatly reduced (This thesis and Braybrook et al., 2002).

There are several methods that exist for the identification of differentially expressed genes between samples in the microarray data analysis (Allison et al., 2006). GeneSpring GX 10 programme, for instance, provides an array of statistical tools that can be applied to the dataset. Two of the most commonly employed methods to identify such genes are fold change and the t-statistic, owing to their relative simplicity and interpretability. Here, we used two experimental groups (the wt and *Tbx22* null palatal shelves) with three biological replicates each, and then looked at fold change and p-values based on unpaired t-test. Since it has been suggested that differentially expressed genes are best identified and more reproducible using fold change rather than t-statistic (Guo et al., 2006; Shi et al., 2005; Shi et al., 2006), we decided to rank the differentially expressed genes according to their fold changes and then calculate p-values alongside. In such a situation, it would be ideal to follow up genes with large fold change and low p-value. Setting a threshold at 2 to 3 fold is generally considered to be a good starting point for identification of significantly changed genes. However, none of the probes encoding for known genes, apart from *Tbx22* and *Cox7b*, had a fold change above 2. In this experiment, whole palatal shelves were used for the analysis, which in wt contained cells positive and negative for *Tbx22*. This could well have diluted or contributed to the relatively low fold changes generally. This includes those found for *Tbx22* itself because the expression of *Tbx22* is specifically restricted to the middle and posterior regions of the palatal shelves but not in other areas. For that reason, it seemed sensible to set a threshold at level that would include a modest number of genes that could be validated by other methods. Ideally, it may have been more appropriate to perform analysis that involved some sort of cell-type specific selection before the microarray. For instance, isolation of specific cell population in targeted gene knockout mice by fluorescence-activated cell sorting for GFP positive cells has been coupled with microarrays to circumvent this problem (Bouchard et al., 2005).

Tbx22 itself had a fold change of only 2.88 (p=0.0087). This may seem very low considering that the knockout gene is theoretically absent from the null mice. For example, in a different study of wild type mice at different developmental stages, a fold change of 43 was described for *loricrin* in the developing palate simply between E14.5 and E15.5 (Brown et al., 2003). However, this might at least in part

be explained by the mutant cells containing a low level of non-protein coding RNA from the *Tbx22* null allele that does not involve the first three exons (Dr. E. Pauws unpublished observation). Although the relative level of gene expression between samples would also be optimised if the samples were specifically sorted for *Tbx22* expressing cells, it was not practical to achieve this at the time when the experiments were carried out.

Under the 1.2 fold threshold model, 43 genes were upregulated while 42 genes were downregulated in the E13.5 palatal shelves of *Tbx22* null mice compared to the wt. However, of these, only 8 genes each in the up and downregulated lists had p-values less than 0.05. Moreover, most of these did not seem to be of obvious relevance to palate development. In general, the recommended number of replicates for microarray analysis to obtain reliable estimates of true differences between conditions is six (i.e. twelve for 2 conditions). An increased number of replicates would therefore have been very likely to improve the p-values for many of the genes listed. However, since the current study was aimed at finding a small number of important differences between conditions, it was decided to validate selected candidates by other methods such as quantitative real-time PCR and functional analysis rather than repeat expression arrays that already showed relatively few major differences.

4.2.1 Downregulated genes

Though the downregulated genes were not followed up in this project, a selection of genes that may be related to cleft palate are discussed below.

The importance of GABAergic inhibitory neurotransmission in the normal palate development is demonstrated by mice with cleft palate that lack *Gabrb3* or *Gad1* (Asada et al., 1997; Condie et al., 1997; Hagiwara et al., 2003; Homanics et al., 1997). In humans, associations between non-syndromic CL/P and *GABRB3* (Inoue et al., 2008; Scapoli et al., 2002) and *GAD1* (Kanno et al., 2004) have been reported. The fold changes for *Gabrb3* (FC=+1.04, p=0.54) and *Gad1* (FC=+1.03, p=0.48) in the *Tbx22* null palatal shelves were close to 1.0 (Appendix Table 1.1). Still, downregulation of *Gabrb2* by 1.24 fold (p=0.000024) may be worth noting. In

addition, the microarray data showed a downregulation of another subunit for GABA type A receptor (*Gabra1*) (FC=1.22, *p*=0.15) as well as glutamate receptor alpha 4 (*Gria4*) (FC=1.21, *p*=0.13) although they were not significant in terms of p-values. There are two types of GABA receptors, type A and B, and both *Gabrb2* and *Gabrb3* encode for a beta subunit of type A receptor. Besides their expression in the central and peripheral nervous system, GABRB3, GAD1 and GABA are all detected in the developing palatal shelves implying a potential role of GABA neurotransmission for normal palate development (Brown et al., 2003). In fact, various neurotransmitters including GABA are thought to be involved in the shelf reorientation process (Babiarz et al., 1979; Zimmerman, 1985). In this particular respect however, GABAergic neurotransmission could be less relevant to *Tbx22* null mice since the elevation process proceed normally in the vast majority of null mice. These genes may not be directly regulated by TBX22 considering the finding that it mainly acts as a transcriptional repressor (Andreou et al., 2007), but the possible decrease in expression in the null palatal shelves is potentially interesting to follow up in the future.

Pax3 is normally expressed in the neural crest precursors and is required for development of neural crest cell lineages. Its expression, however, is generally much reduced after migration of the cells from the neural tube and this downregulation is crucial for differentiation to proceed. In the wt palatal shelves, endogenous expression of *Pax3* is detected medially at E12.5 and E13.5 which is abated at birth, and the mice develop cleft palate when the expression persists (Wu et al., 2008). In contrast, palatal morphology is unaffected by reduced *Pax3* expression level (Zhou et al., 2008). Therefore, downregulation of *Pax3* (FC=1.21, *p*=0.40) in the null palatal shelves may not be directly related to the pathlogical phenotype in *Tbx22* null mice. It is also possible that the fluctuation indicated by the microarray data could be a false positive and thus this aspect requires further investigation.

Retinoic acid (RA) has been associated with the development of cleft palate. RA is synthesised from retinol (vitamin A) via retinal as the intermediate (Duester, 2000). The first step involves oxidation of retinol to retinal and the second step involves oxidation of retinal to RA. The first enzymatic reaction can be catalysed by several

alcohol dehydrogenases, one of which is alcohol dehydrogenase of class I (ADH1). *In vivo* gene disruption of *Adh1* in mice leads to a reduction in retinoid metabolism (Deltour et al., 1999), and the physiological role of ADH1 has been suggested in minimising retinol toxicity (Molotkov et al., 2002). The next step of oxidation from retinal to RA is carried out by retinaldehyde dehydrogenases (Raldh) 1 to 3 whose enzymatic activities in retinoid metabolism have been demonstrated by *in vivo* studies (Duester, 2001). The microarray data revealed a reduced expression of *Adh1* (FC=1.27, p=0.27) in the *Tbx22* null palatal shelves. This could be interesting to follow up in the future considering the importance of dehydrogenase enzymes implicated in retinoid metabolism as has been shown by cleft palate induced by retinoic acid in mice (Padmanabhan and Ahmed, 1997; Degitz et al., 1998). *Aldh1a7* is shown not to be involved in the biosynthesis of retinoic acid although it is closely related to *Aldh1* (*Raldh1*) (Hsu et al., 1999). Thus, its downregulation (FC=1.21, p=0.47) may be less relevant with regard to the cleft phenotype in *Tbx22* null mice.

4.2.2 Upregulated genes

Since TBX22 has been shown to act as a transcriptional repressor *in vitro* (Andreou et al., 2007), we focused on genes that were upregulated in the absence of *Tbx22* and decided to follow up some of them by real-time PCR. Verification of microarray results by an alternative method is necessary because of their inherent problems with inconsistent quantification and false positive results (Chagovetz and Blair, 2009). Real-time PCR is the most commonly used method for this purpose.

At the 1.2 fold change threshold, *Ctsk* (FC=1.62, p=0.074) was the only known gene related to osteogenesis. It is involved in bone resorption and is expressed exclusively in osteoclasts during mouse embryonic development (Dodds et al., 1998). In the normal mouse palatal shelves, genes involved in ossification process are generally increased as the palatal bone forms. For instance, the *Ctsk* precursor expression is increased between E13.5 to E14.5, and osteopontin, one of the organic components of bone, is also upregulated between E14.5 to E15.5 (Brown et al., 2003). However, the microarray data for *Ctsk* was not verified by real-time PCR, suggesting that it was a false positive. Several other genes related to osteogenesis or

ossification including *Runx2*, *Osterix*, *Osteopontin*, *Alkaline phosphatase*, *type I collagen* and others were checked for their fold changes in the array data but those were in the range of 1.0 to 1.1 fold increase or decrease. Taken together, the results indicated that there was no obvious change in bone markers between the wt and null palatal shelves at E13.5. In fact, this stage probably is slightly too early to look for any major changes in bone markers considering the fact that palatal bone formation does not start until around E15.5, after the palatal shelves have fused. Thus, with regard to the ossification defect, it would be more interesting to carry out experiments just before the defect in the null palate becomes obvious, which would be around E15.0.

Interestingly, there was a general upregulation of muscle related genes in the *Tbx22* null palatal shelves. In fact, 20 out of 43 upregulated genes were muscle related while no such genes came up in the downregulated list at 1.2 fold change threshold. The upregulated muscle genes belong to members of the myosin, actin, actinin, titin, troponin and calsequestrin gene families. Their main functions include muscle metabolism, contraction and filament assembly. Of those upregulated in the microarray data, three muscle genes *Myh3*, *Acta1*, *Casq2* were chosen as representatives from different gene families to examine by real-time PCR while the other muscle genes were not investigated by this technology. The microarray data showed increased expression of *Myh3* (FC=1.57, p=0.061), *Acta1* (FC=1.35, p=0.12) and *Casq2* (FC=1.30, p=0.21). The real-time PCR results also indicated upregulation for *Myh3* (FC=2.44, p=0.030), *Acta1* (FC=2.16, p=0.030) and *Casq2* (FC=2.32, p=0.035) confirming the direction of the change in gene expression detected by microarrays. However, the magnitude of fold change was larger in real-time PCR. This is largely down to the fact that real-time PCR detects the amount of product as the reaction progresses so that it allows quantitative measurements in a wider dynamic range relative to microarrays. Similarly, p-values were improved in real-time PCR probably because of the larger difference in the average fold change.

4.3 Myogenic regulatory factors

The global upregulation of muscle genes suggested an increase in muscle differentiation or myogenesis, perhaps triggered through deregulation of some of the key myogenic regulatory factors. Myogenesis refers to the formation of muscles during embryonic development in particular. The initial process involves the determination of mesodermal cells to myoblasts that are embryonic progenitor cells of myocytes. These myoblasts proliferate in the presence of growth factors such as FGF2 (Kelvin et al., 1989). Eventually, the mononucleated myoblasts align and fuse with each other to form multinucleated myotubes or skeletal muscles. These steps are largely controlled by four myogenic regulatory factors, *MyoD*, *Myf5*, *myogenin* and *Mrf4* (Arnold and Braun, 1996). The functional roles for each of these factors have been defined by targeting inactivation studies of single or multiple genes in mice. Surprisingly, null mutation for *MyoD* in mice results in normal muscle development (Rudnicki et al., 1992). In these mice, expression of *Myf5* is upregulated instead. Similarly, skeletal muscle morphology is normal in *Myf5* mutant mice (Braun et al., 1992). These results have indicated that individually, neither gene is critical for normal myogenesis. However, the mice that are double mutant for *MyoD* and *Myf5* are devoid of skeletal muscles and myoblasts (Rudnicki et al., 1993), suggesting that they compensate for each other and are functionally redundant. The double null mutant mice develop cleft palate but it has not been determined if the defect is intrinsic to the palate or caused as a secondary effect by a lack of mechanical help from the facial musculature (Rot-Nikcevic et al., 2006). In terms of hierarchical relationships, *MyoD* is genetically downstream of *Myf5* because its expression is delayed in *Myf5* null mice (Tajbakhsh et al., 1997). Similarly, *Mrf4* acts upstream of *MyoD* as has been demonstrated by delayed *MyoD* expression when *Mrf4* is inactivated (Kassar-Duchossoy et al., 2004). Mouse mutants for *myogenin* show reduced skeletal muscle mass but normal myoblasts, indicating its role in terminal differentiation (Hasty et al., 1993; Nabeshima et al., 1993). It is also known that *MyoD* activates *myogenin* (Deato et al., 2008). As myogenesis proceeds, other muscle specific marker genes for differentiated cells such as myosin heavy chain and actin start to be expressed (Arnold and Braun, 1996). Therefore, it was reasonable to assume that expression of the myogenic regulatory factors might also have been affected in the *Tbx22* null palatal shelves.

Of the four myogenic regulatory factors described, *MyoD*, *Myf5* and *myogenin* were further investigated while *Mrf4* was not followed up as it was suggested not to be involved in the developmpent of head muscles (Kassar-Duchossoy et al., 2004). However, none of these were detected above the 1.2 fold threshold in microarray analysis although there was a general trend towards upregulation for *MyoD* (FC=1.17, p=0.27), *myogenin* (FC=1.09, p=0.70) and *Myf5* (FC=1.19, p=0.13) in the *Tbx22* null palatal shelves. Nevertheless, a statistically significant increase in the palatal shelves of *Tbx22* null mice was detected by real-time PCR for both *MyoD* (FC=1.73, p=0.017) and *myogenin* (FC=1.69, p=0.038). In addition, *p21*, the known target of *MyoD*, was also increased as measured by real-time PCR (FC=1.62, p=0.031). Again, the magnitude of fold change was larger when expression was examined by real-time PCR compared to the microarray. *Myf5* expression detected by real-time PCR was also increased on average although it was not statistically significant (FC=1.75, p=0.10). Therefore, the results indicate that upregulation of some of the myogenic regulatory factors may explain, at least in part, the global upregulation of muscle specific genes detected by microarray analysis.

It has not yet been determined whether the upregulation of muscle specific genes reflect an increased number of myoblasts within the null palatal shelves or result from a specific increase of expression within each cell. To address this, it is necessary to understand the normal pattern of expression for these muscle genes during normal palate development. In the presumptive mouse soft palate in the posterior region, muscles first emerge as mesenchymal condensation at around E13.5 (Zhang et al., 1999). At this stage, both MyoD and myogenin are detected in the condensed mesenchyme using immunohistochemistry. Moreover, the myofilaments start to appear in the condensed mesenchymal cells or myoblasts, indicating muscle differentiation. These myoblastic cells follow myogenic differentiation and muscle fibers begin to appear by E18.5. Accordingly, a general rise in muscle markers such as myosin heavy and light chains and actin have been reported throughout palate development from E13.5 to E15.5, which may be important for shelf reorientation (Brown et al., 2003).

To answer the question as to where the differential expression of muscle genes originate in the *Tbx22* null palatal shelves, we attempted to localise the *MyoD*

mRNA by *in situ* hybridisation in the wt and null palatal shelves. However, no obvious staining was visible within the palatal shelves (data not shown). This could be due to its relatively low expression level compared to some other genes (Figure 3.5). In order to locate the origin of differential expression, the experiment may need optimisation (e.g. by using alternative *in situ* probes) or alternatively immunohistochemistry should be performed since the method has been shown to work efficiently to mark MyoD and myogenin (Zhang et al., 1999).

It is also possible that the fluctuations of muscle gene expression are secondary to what is happening in non-myoblastic cells and irrelevant to soft palate muscles. In relation to this issue, what is still not clear is whether *Tbx22* is expressed in palatal mesenchymal cells of mesodermal origin. The role of TBX22 in cranial paraxial mesoderm in particular has not been reported, but studies have shown that *Tbx22* is expressed in the cranial paraxial mesoderm at primitive streak stages which lasts at least until E3 in chick embryos (approximately equivalent to E11.5 in mouse) (Haenig et al., 2002). However, whether it is expressed in palatal mesenchymal cells specifically of mesodermal origin at E13.5 has not been examined although we know that the vast majority of palatal mesenchyme is of CNC origin (Ito et al., 2003) and some of which is *Tbx22* positive. For those reasons, it is difficult at the moment to speculate precisely where the differential *MyoD* expression as well as other muscle related gene expression come from. Nevertheless, it is a reasonable assumption that the difference in *MyoD* expression would have been mainly contributed by CNC-derived palatal mesenchyme, based on the fact that the majority of mesenchymal cells originate from the CNC (Ito et al., 2003).

4.4 *MyoD* is regulated by TBX22 *in vitro*

T-box binding element (TBE) consists of one or more copies of the minimal AGGTGTGA sequence (Naiche et al., 2005). It was first demonstrated by the high affinity of Brachyury to a 20 base pair palindromic sequence T(G/C)ACACCTAGGTGTGAAATT (Kispert and Herrmann, 1993). Later, it was shown that not only Brachyury but other T-box proteins were capable of binding to the TBE or half of the sequence called a T-half site which is thought to be mediated via the highly conserved T-box DNA binding domain (Ghosh et al., 2001; Lingbeek et al., 2002; Tada and Smith, 2001). TBX22 itself has been demonstrated to have the potential to autoregulate its own P0 promoter which contains several putative TBEs (Andreou et al., 2007). Therefore, it was next intended to search the promoter regions of muscle related genes for a putative TBE *in silico*.

Scanning the genomic sequences spanning 2 kb upstream of the transcription start site found TBEs in some of the genes. Among the muscle specific genes, *MyoD* and *Acta1* had one TBE each whereas *Myf5* and *myogenin* had two TBEs. *Myh3* and *Casq2* did not have any TBE. Apart from muscle specific genes, *p21* whose expression was significantly altered was also examined but no TBE was detected within the region scanned. Though *in silico* analysis can give an indication that a gene could be regulated by TBX22 or perhaps another T-box protein, a demonstration of relevance using alternative functional assays is necessary. *Myf5* was excluded because the gene was not confirmed as differentially expressed by real-time PCR. *Myogenin* is known to be activated by MyoD via binding to its E-box in the promoter region (Sartorelli and Caretti, 2005; Deato et al., 2008). This may suggest that *myogenin* expression in the null palatal shelves may have been increased due to the higher level of *MyoD* rather than itself being a direct target of TBX22. Similarly, MyoD is capable of regulating expression of muscle specific genes such as myosin and actin (Asakura et al., 1993; Shklover et al., 2007; Wheeler et al., 1999), which could explain the global upregulation of those genes. Likewise, *p21* is also a well known target of MyoD (Guo et al., 1995; Halevy et al., 1995; Peschiaroli et al., 2002).

Some key evidence that links T-box genes to *MyoD* regulation has been reported recently by Morley et al (2009). These authors combined chromatin immunoprecipitation with zebrafish genomic microarrays (called ChIP-chip) to investigate the binding capacity to promoter sequences of No tail (Ntl), a transcription factor, which is a zebrafish ortholog of Brachyury. An interaction between Ntl and the upstream region of the zebrafish *myod* was among those identified in this study (Morley et al., 2009). Tbx6 has been shown to be involved in regulation of *MyoD* expression and is able to bind to the T half-site found in its promoter (Fang et al., 2004; Goering et al., 2003). Another example is the regulation of branchiomeric myogenesis by *Tbx1* (Kelly et al., 2004). In the absence of *Tbx1*, both *Myod* and *Myf5* failed to be activated in the pharyngeal mesoderm, suggesting a direct or indirect role of *Tbx1* in the regulation of these myogenic factors (Kelly et al., 2004). Thus, it may be possible that other T-box family members could have a similar role in myogenesis. The microarray data and a finding that *MyoD* contained a predicted TBE in its proximal promoter region prompted a more detailed investigation of the effect of TBX22 on *MyoD* promoter activity *in vitro*.

Luciferase reporter assay and chromatin immunoprecipitation were both used to follow up on the possibility that TBX22 may have a regulatory role in *MyoD* expression in the palatal shelves. Using luciferase reporter assay, overexpression of *TBX22* in HEK 293T cells were found to result in a dose-dependent repression of *MyoD* promoter activity, down to ~50%, whereas the *TBX22* N264 mutant was ineffective in its ability to repress. However, contradicting the original premise, base substitutions in the TBE within the *MyoD* promoter did not affect repressor activity. It could be that there are other sequences in the *MyoD* proximal promoter region that can interact with TBX22, other than the putative TBE described, that are yet to be determined. It is also possible that some interaction between TBX22 and its target genes may involve co-factors rather than direct DNA binding. As described in the Introduction, some T-box proteins are known to regulate transcription cooperatively with other factors including homeodomain, GATA zinc finger and LIM domain proteins that may mediate their selectivity for target genes rather than by DNA sequence recognition alone (Bruneau et al., 2001; Hiroi et al., 2001; Krause et al., 2004; Lamolet et al., 2001; Stennard et al., 2003). This is also

true for other transcription factors such as homeobox proteins that display DNA binding specificity (Laughon, 1991; Scott et al., 1989).

Chromatin immunoprecipitation was performed to investigate if there was any physical interaction between TBX22 protein and the *MyoD* promoter region. The positive results of this assay suggested that there is a specific interaction since not only did TBX22 pull down the *MyoD* promoter sequence, but this interaction was abolished for the TBX22 N264Y mutant. However, this assay does not distinguish direct or indirect interaction between TBX22 and the *MyoD* promoter region tested because the technique involves cross-linking or fixation with formaldehyde which inevitably cross-links both DNA-protein and protein-protein interactions in live cells.

Finally, in order to try to investigate the effect of TBX22 on *MyoD* in a more *in vivo* fashion, levels of endogenous *MyoD* in C2C12 myoblastic cells were measured in the presence and absence of overexpressed *TBX22*. In this experiment, *MyoD* levels were not found to be repressed in the presence of *TBX22*. At face value, these results are contradictory and confusing. It could simply be due to cellular context differences where C2C12 cells used may not have expressed the relevant co-factors or accessory proteins that were present in HEK 293T cells. HEK 293T cells do not express *MyoD* at a detectable level and hence was not suitable to look at effects on endogenous expression levels. We anticipate that further investigation of *MyoD* regulation by TBX22 will be performed in the future studies, initially analysing different cell lines that express endogenous *MyoD*.

4.5 TBX22 and myogenesis

Thus far, our studies have failed to confirm a direct role for TBX22 in myogenesis. Nevertheless, it is interesting to note that in addition to its prominent expression in the craniofacial region, it also has a distinct, transient expression profile in the developing somites and myotome, detected between E9.5 and E11.5 (Farin et al., 2008; Andreas Kispert personal communication). In the early somites, *Tbx22* and its closely related paralog *Tbx18* are co-expressed with both proteins being shown to interact with PAX3, which at this stage is associated with myogenic cell specification. These factors are suggested to act cooperatively in maintaining anterior-posterior somite polarity, indicating their roles in the somitic paraxial mesoderm (Farin et al., 2008 and Andreas Kispert personal communication). *Tbx18* is expressed in the craniofacial region including otic mesenchyme and smooth muscle cells surroung vessels in the head (Haenig and Kispert, 2004; Trowe et al., 2008) but so far not implicated in the occurrence of cleft palate. In addition, *Pax3* is not expressed in the muscle primordium of the branchial arch (Horst et al., 2006). Thus, it seems unlikely that these three factors act in a similar cooperative manner in the cranial region as they do in the somites with regard to myogenesis.

Research concerning structural abnormalities of the palatal muscles during embryonic development is scarce, although a few studies have suggested prenatal abnormal muscle morphology in clefts of the soft palate. In prenatal periods, palatal muscles emerge from condensed mesenchyme within the soft palate during the sixth to ninth weeks in human. In terms of sequence of appearance, the tensor veli palatini muscle appears first followed by the levator veli palatini, palatopharyngeus, palatoglossus and the uvula last which is absent in mice (Cohen et al., 1993). Comparison of soft palate morphogenesis between fetuses with cleft palate and control specimens demonstrated a similar muscular morphology of the tensor veli palatini, levator veli palatini, palatopharyngeus and palatoglossus in both experimental groups (Cohen et al., 1994). However, muscle fiber directions were found to be disoriented and disorganised in fetuses with cleft palate especially near the medial edge epithelia. Despite the small number of samples, this study has to some extent demonstrated abnormal myogenesis in cleft palate.

The importance of normal muscle function is clear, especially in patients with submucous cleft of the soft palate which features muscle defects as described in the Introduction. In fact, this remains one of the more complicated challenges to repair for cleft palate surgeons who aim to close off the oral from nasal passages to improve speech and other side effects of a submucous cleft. In terms of a developmental model, it is still not clear if the lack of functional *Tbx22* in the mouse leads to an intrinsic defect of muscle development or if this is secondary to the bone defect. It is possible that a general increase in muscle gene expression might be a common feature in other models of cleft palate. However, studies using model organisms that feature an involvement of muscles in the occurrence of clefts are also limited. One example where soft palate morphologies have been investigated in cleft-induced and normal A/Jax mice, indicated no discernible differences of the soft palate muscles between the cleft and non-cleft mice (Trotman et al., 1995). However, mice that are double mutant for *Myf5* and *MyoD* completely lack striated muscle and display a cleft of the seconday palate as well as a cleft between the primary and secondary palates (Rot-Nikcevic et al., 2006). In this case, the authors suggested that the clefts seemed to be caused by an absence of any mechanical help from the facial musculature during palate development as well as by micrognathia, an undersized mandible rather than by intrinsic defects in the palate. To date, only a cursory examination of palatal muscles in *Tbx22* null mice has been undertaken and no muscle defects have been found by dissection and visual inspection under light microscope (unpublished data). This work requires a more detailed study starting with histological examination at different stages and may be aided by more accurate measures such as MRI scanning. It is hoped that this type of study will be of great benefit to bring about future improvements of patient treatment, particularly in the more complicated but esoteric submucous clefts.

4.6 The role of TBX22 in palate development

Concurrent with the efforts to identify downstream target genes of TBX22, an important focus of this project was also to investigate the molecular network and mechanisms underlying pathogenic phenotypes observed in *Tbx22* null mice. Thus far, an obvious and clearly demonstratable defect in the *Tbx22* null palate is the delayed ossification of the palatine bone which is classified as submucous cleft palate (Pauws et al., 2009a). In the wt palate, mineralisation of the palatine bone becomes visible by E15.5. In contrast, it is almost completely absent in the null palate although the mesenchymal condensation is observed. Interestingly, only a few days later at E18.5, mineralisation becomes detectable in the null palate but is severely reduced in size compared to the wt palate of equivalent stage. It is interesting that there is very little or any *Tbx22* expression in the post fusion palate (Braybrook et al., 2002; Bush et al., 2002) yet the ossification defect in the hard palate becomes obvious from around this stage onwards. Further analysis of bone maturation using alkaline phosphatase histochemistry at E15.5 detected strong staining in the condensed osteoblasts surrounding the mineralised bone matrix, whereas it was much weaker in the condensed mesenchyme of the null palate (Pauws et al., 2009a). Alkaline phosphatase activity and mineralised bone matrix indicated that mature bone forming osteoblasts were produced by E15.5 in wt. However in the null palate it seemed that the mineralisation defect resulted as a consequence of defective osteoblastogenesis either through a lack of osteoblast differentiation and/or maturation. However, it was not yet clear how, or which steps of osteogenesis were affected by a lack of functional *Tbx22*.

Osteogenesis is a multi-step process. Initially, the palatal mesenchymal cells are undifferentiated that proliferate and eventually form mesenchymal condensation. Then they start to differentiate into osteoprogenitor cells marked by expression of *Runx2* (Ducy et al., 1997; Ducy et al., 2000; Komori et al., 1997). These immature progenitor cells further differentiate into mature bone forming osteoblasts, aided by key transcription factors of osteogenesis including *Runx2* and *Osterix* (Nakashima et al., 2002) as well as various growth factors such as BMP2 in particular (Ryoo et al., 2006). *Runx2* is a key regulator of osteoblast differentiation and a lack of *Runx2* blocks maturation of osteoblast progenitor cells into mature osteoblasts leading to a

complete lack of both intramembranous and endochondral ossification in mouse (Komori et al., 1997). Therefore, we initially investigated *Runx2* expression, which was detected in the condensed mesenchyme in the null palate at a similar level to that observed in the osteoblasts in the wt palate, although the area was smaller indicating a reduced number of differentiated osteoblasts (Pauws et al., 2009a). In *Tbx22* null mice, ossification of the palatine bone was not completely lost but took place instead to a much lesser extent. This was interpreted as there being a delay in the ossification process, since at least some osteoblast progenitors did mature to become bone forming osteoblasts. Taken together, it seemed that the differentiation and/or maturation process was partially but not completely blocked and the ossification defect was independent of *Runx2*. It is a possibility that other key osteogenic factors such as *Osterix* may have been affected but this still remains to be tested.

4.6.1 Cell proliferation and apoptosis analysis in the wt and *Tbx22* null palatal shelves

Next, it was intended to investigate other possible functions or indeed consequences of a lack of TBX22, apart from its putative roles in myogenesis or osteoblast differentiation and/or maturation. Cell proliferation is a key process in normal palatal growth. In particular, a decrease in cell proliferation in the palatal shelves is one of the most common features found in mice with cleft palate. For instance, mice mutant for *Msx1*, *Fgf10*, *Fgfr2b*, *Tgfβr2*, *Shox2* and *Osr2* all display reduced cell proliferation (Alappat et al., 2005; Ito et al., 2003; Lan et al., 2004; Rice et al., 2004; Satokata and Maas, 1994; Yu et al., 2005). Among these, *Fgf10* and *Shox2* mutant mice also show increased apoptosis. In contrast, Wnt1-Cre mediated removal of *Tgfβr1* (*Alk5*) in mice results in an increased cell proliferation and apoptosis in the palatal shelves (Dudas et al., 2006). With regard to *Tbx22*, differential changes in the cell proliferation rate in $Mn1^{-/-}$ mice (MN1 acts upstream of *Tbx22*) (Liu et al., 2008) as well as in chick with overexpressed human *TBX22* (Higashihori et al., 2010) have been reported. In addition, *in vitro* experiments have suggested an important role for MN1 in osteoblast proliferation and maturation (Zhang et al., 2009). These studies implicate a possible role for TBX22 in cell proliferation as well as differentiation and maturation of osteoblasts in *Tbx22* null

mouse during palatal shelf growth. Therefore, analyses of cell proliferation and apoptosis were measured using standard techniques involving phospho-Histone H3 and cleaved Caspase-3, respectively.

There were only a few cells positive for Caspase-3 in the E13.5 wt and null palatal shelves with no significant difference found between them in the anterior, middle or posterior regions. The cell counting for Caspase-3 was not done separately for the palatal epithelium or mesenchyme since there were so few positive cells. This suggested that apoptosis was a relatively rare event in the rapidly growing shelves. Though increased apoptosis may contribute toward the occurrence of cleft palate in mice mutant for *Fgf10* (Alappat et al., 2005; Rice et al., 2004), *Shox2* (Yu et al., 2005) or *Alk5* (Dudas et al., 2006), it seemed unlikely that *Tbx22* has a major role in this process at E13.5. This may agree with the finding that apoptosis rate in *Mn1* null mice at the equivalent stage was not affected either (Liu et al., 2008). However, in this mouse model, apoptosis was increased in the palatal mesenchyme later at E15.5. Therefore, it is still possible that the process might be affected in *Tbx22* null mice at different stages.

For cell proliferation analysis, the cells positive for phospho-Histone H3 were counted separately in the palatal mesenchyme and epithelium since *Tbx22* is known to be expressed in the palatal mesenchyme but not in the epithelium (Braybrook et al., 2002; Bush et al., 2002). In the palatal mesenchyme at E13.5, no reduction was detected in the anterior region of the null palatal shelves compared to those of wt while a statistically significant 53.9% reduction was found in the null palatal shelves in the middle region (p=0.03). In the posterior region, the percentage of positive cells was reduced by 42.7% on average in the null palatal shelves but this was not statistically significant (p=0.20). Overall, the reduction in proliferation coincided with the region normally expressing *Tbx22*. In the palatal epithelium at the same stage, no significant difference was detected in the anterior, middle or posterior regions between the wt and *Tbx22* null palatal shelves. The results therefore indicate that *Tbx22* regulates cell proliferation in a cell autonomous manner whereby the differential rate is only detected in the palatal mesenchyme but not in the epithelium. In *Mn1* null mice, cell proliferation is reduced in both middle and posterior palatal mesenchyme and epithelium where *Mn1* is expressed (Liu et

al., 2008). These observations imply that cell proliferation in the palatal mesenchyme may be regulated, at least in part, through the MN1-TBX22 pathway but MN1 acts independent of TBX22 in the palatal epithelium in the regulation of cell proliferation.

4.6.2 *Cyclin D2* is reduced in the *Tbx22* null palatal shelves

We next tested *Cyclin D2* expression in the wt and *Tbx22* null mice since downregulation of the gene has been reported in *Mn1*$^{-/-}$ mice, which probably explained the reduced cell proliferation in the null palatal shelves (Liu et al., 2008). Regulation of cell proliferation through the level of cyclins has also been demonstrated by other genes such as *Gli2* during embryonic lung development (Rutter et al., 2010). *Cyclin D2* and other members of the cyclin family have characteristic periodicity in abundance through the cell cycle. *Cyclin D2* functions as a regulator of cyclin-dependent kinases (CDK) 4 and 6 that are required for progression through G1 to S phase. In the murine and human embryonic palatal mesenchymal cells, the blockage of G1 to S phase by mycotoxin secalonic acid D (SAD) leads to inhibition of cell proliferation (Hanumegowda et al., 2002; Dhulipala et al., 2004). This outcome is explained by the reduced levels of CDKs and cyclins D, E and A as well as an increased level of p21 in the palatal mesenchymal cells *in vitro* and murine embryonic palates *in vivo* (Dhulipala et al., 2005). These studies clearly demonstrate the importance of an appropriate level of cell-cycle related proteins for normal cell proliferation during palatal growth. In the *Tbx22* null palatal shelves, decreased *Cyclin D2* expression was observed compared to the wt in the anterior to middle regions of the palatal shelves at E12.5 and E13.5. However, *Cyclin D2* expression only partially overlapped with that of *Tbx22* in both the E12.5 and E13.5 wt palatal shelves, which at these stages shifts from the middle to more posterior regions as detected by whole mount *in situ* hybridisation. Therefore it may be necessary to perform a more detailed study using sections to better correlate the expression of *Tbx22* and *Cyclin D2* with the proliferation index along the anterior to posterior axis within each region. Nevertheless, *Tbx22* is likely to play a role in the regulation of palatal mesenchymal cell proliferation, whether it is through *Cyclin D2* expression or not. On a similar note, the increased expression of *p21* in the *Tbx22* null palatal shelves detected by real-time PCR may also explain

the reduced cell proliferation as its main role is to inhibit the activity of cyclin-CDK2 and 4 in the G1 phase. It is well known that the expression of *p21* is tightly controlled by the tumor suppressor protein P53 but can also be induced by factors such as MyoD in a P53 independent manner during differentiation (Guo et al., 1995). Currently, it still remains to be answered if the upregulation of *p21* was primarily caused by increased *MyoD* or by other factors.

4.6.3 Regulation of cell proliferation by *Tbx22*/*TBX22*

A recent study has shown that overexpression of human *TBX22* resulted in decreased cell proliferation in the frontonasal mass in chick leading to cleft beak (Higashihori et al., 2010). In this case it is not clear if the human TBX22 is equivalent to the chick TBX22, so it is not known whether it is acting by simple overexpression or instead downregulating by competing out the endogenous protein. If the former is the case, this implies a negative role of TBX22 in cell proliferation. However, it is not known if the same mechanism operates later during development of palate, which in any case differs between chick and mammals. It appears that the chick study contradicts the results obtained in this study in terms of the direction of cell proliferation rate controlled by TBX22. In the case of *Tbx1*, gene dosage is known to be critical in the manifestation of cleft palate, as well as other pathogenic phenotypes implicated in DiGeorge syndrome which is caused by haploinsufficiency in humans. This is clearly illustrated by the occurrence of cleft palate in both *Tbx1*$^{-/-}$ mice and transgenic mice overexpressing *TBX1* (Liao et al., 2004). Therefore either too little or too much expression of the gene caused the same cleft phenotype, underscoring the importance of appropriate expression level for normal palate development. This could also be the case for *Tbx22* because a complete lack of functional *Tbx22* in mouse (Pauws et al., 2009a) and overexpression of *TBX22* in chick (Higashihori et al., 2010) both result in a cleft phenotype in the form of overt or submucous cleft palate and cleft lip, respectively. Indeed, a gene dosage probably is important for TBX22 as it is thought to be capable of autoregulating its own promoter, suggesting a negative feedback loop to fine tune the level of expression (Andreou et al., 2007). Still, direct comparison between species in these experiments has to be tempered by the apparent

differences in the facial structures between the two species (i.e. chick not only has a beak but also has a natural cleft palate).

4.6.4 Expression pattern of BMP and FGF signalling components

Defective cell proliferation is a common cause of cleft palate in mice and there have been many genetic factors implicated for normal palatal growth. These include transcription factors such as *Msx1*, *Osr2* and *Shox2* as well as signalling molecules and growth factors such as *Shh*, *Tgfβs*, *Bmps* and *Fgfs* (Gritli-Linde, 2007; Wilkie and Morriss-Kay, 2001). In the scope of this project, it was intended to examine some of the BMP and FGF signalling components in relation to the cell proliferation defect observed in the *Tbx22* null palatal shelves.

The importance of BMP signalling in lip and palate development has been implied in human and mouse. In human, mutations in *BMP4* have been associated with subepithelial, microform and over cleft lip (Suzuki et al., 2009). Mutations in the BMP target gene *MSX1* are also associated with cleft lip and palate (Jezewski et al., 2003; van den Boogaard et al., 2000). In line with this, *Msx1* deletion in mice leads to a cleft of the secondary palate (Satokata and Maas, 1994). Convincing evidence regarding the role of BMP signalling is provided by several mouse studies. *Bmp2*, *Bmp3*, *Bmp4* and *Bmp5* are all expressed in the palatal shelves prior to, during and after fusion (Lu et al., 2000; Nie, 2005). Among these, expression of *Bmp2*, *Bmp4* and *Bmp5* are decreased when cleft palate is induced by retinoic acid, suggesting that they are required during normal palatogenesis (Lu et al., 2000). Conditional inactivation of the type 1 Bmp receptor *Alk2* in neural crest cells, that contribute to various craniofacial structures including palate, leads to multiple craniofacial defects including cleft palate (Dudas et al., 2004). Similarly, conditional inactivation of the type 1 Bmp receptor *Bmpr1a* (*Alk3*) in the facial primordia results in reduced cell proliferation in the maxillary process and palatal cleft (Liu et al., 2005). Though with some contradictory results, several studies have shown the regulatory role of BMP signalling in facial mesenchymal cell proliferation. One study reported that application of BMP2 soaked beads to the chick maxillary primordia resulted in elevated proliferation (Barlow and Francis-West, 1997). Another study found that implantation of BMP2 beads in chick frontonasal mass

did not affect cell proliferation although Noggin (a BMP antagonist) treatment resulted in reduced proliferation of the maxillary prominences and frontonasal mass ultimately leading to the deletion of the maxillary and palatine bones (Ashique et al., 2002). These studies clearly indicate the importance of BMP signalling for palatal growth. Using whole mount *in situ* hybridisation, expression patterns of *Bmp2*, *Bmp3* and *Bmp4* were determined. As described in the results, these genes were expressed in specific domains along the anterior to posterior axis of the developing shelves. However, little difference was determined between the wt and *Tbx22* null mice at E13.5. Recent studies indicate BMP signalling pathway in the regulation of *Tbx22* expression in stage and tissue specific manner in chick and mouse facial mesenchyme (Fuchs et al., 2010; Higashihori et al., 2010). In palatal shelf explants taken from chick (HH26) and mouse (E12.5), BMP4 repressed *Tbx22* (Fuchs et al., 2010). Given the findings of Fuchs et al. (2010) and Higashihori et al. (2010), it is reasonable to assume that TBX22 is likely to be placed downstream of BMP signalling but there may be no feedback from TBX22 to BMPs investigated in this thesis.

Fgf signalling is another key factor during palatogenesis, and it has been reported that up to 5% of non-syndromic cleft lip and palate in human could be caused by mutations in FGF components including *FGFR1*, *FGFR2* and *FGF8* (Pauws and Stanier, 2007; Riley et al., 2007). In the developing palate, *Fgfr2b* and *Fgf10* mediate epithelial-mesenchymal signalling to regulate cellular functions such as cell proliferation and cell survival. The importance of FGF signalling in palate development is highlighted with *Fgf10* and *Fgfr2b* null mice that develop cleft palate (Rice et al., 2004; Alappat et al., 2005). In the *Fgfr2b* null mice, cell proliferation was found to be decreased in both the palatal epithelium and in the mesenchyme which probably explains the cleft phenotype. In contrast, cell proliferation was not altered in *Fgf10* null mice but apoptosis within the anterior MEE was significantly increased, leading to cleft secondary palate. Interestingly, recent findings indicated that a gain-of-function mutation in FGFR2 resembled loss of FGF function in palatal mesenchymes (Snyder-Warwick et al., 2010). It was shown that mesenchymal cell proliferation was increased at E13.5 but decreased significantly by E14.5 leading to the cleft palate phenotype. Also, the *36Pub* mice which lacked *Spry2*, an antagonist of FGF signalling, showed increased cell

proliferation at E14.5 which resulted in cleft palate phenotype (Welsh et al., 2007). In this mouse model, *Tbx22* expression was unchanged at E13.5 but reduced at the posterior end of palatal sheves at E14.5. These findings indicate that both augmentation and inhibition of FGF-FGFR signalling could result in the identical cleft phenotype due to increased or decreased cell proliferation, suggesting that an adequate dose is essential for normal palatogenesis. These studies imply the importance of FGF signalling pathway for palatal growth, particularly in cell proliferation. However, expression of *Fgf10*, *Fgfr2* and *Spry2* detected by whole mount *in situ* hybridisation did not differ significantly between the wt and *Tbx22* null mice at E13.5. Both studies by Fuchs et al. (2010) and Higashihori et al. (2010) suggested that FGF signalling is necessary for the induction of *Tbx22* expression in early facial mesenchyme. However, *Tbx22* expression became independent of FGF signalling at later stages in palatal shelf explants taken from chick (HH26) and mouse (E12.5) (Fuchs et al., 2010). These results suggest that in the palatal shelves, FGF and TBX22 may operate independently and there is no feedback between these two pathways. However, regulation of *Tbx22* by FGF signalling in the developing palatal shelves may be stage specific since its expression is altered in the *36Pub* mice which lacked *Spry2* at E14.5 but not at E13.5 (Welsh et al., 2007).

Overall, one might speculate that in the null palatal shelves, muscle related genes (expressed normally in the palatal mesenchyme) have increased as a consequence of there being fewer osteoblastic cells. This is probably a more reasonable assumption than *Tbx22* having a direct effect on soft palate muscle development, especially as no obvious muscle defects have been observed so far. There are few links between myogenic and osteogenic markers. For instance, C2C12 cells normally follow myogenic differentiation but BMP2 is capable of suppressing the expression of *MyoD* and *myogenin* to induce osteoblastic differentiation (Katagiri et al., 1994). This suggests that the level or balance between myogenic and osteogenic marker expression can determine cell fate. *Tbx22* is likely to be downstream of BMP and FGF pathways. Thus, it could be that BMP or FGF signallings may be affected by a lack of *Tbx22* and the myogenic markers appeared altered as a consequence. Interestingly, MyoD has recently been shown to be able to stimulate the *Osterix* promoter in C3H/10T1/2 mesenchymal cells and C2C12 cells (Hewitt et al., 2008). Osterix is one of the key factors for bone development as has been shown by lack of

mineralisation in null mouse (Nakashima et al., 2002). This may seem counterintuitive considering the general role of MyoD in myogenesis, but the authors have shown that suppression of *MyoD* in C2C12 cells led to reduction of *Osterix* expression and also prevented the expected rise in alkaline phosphatase stimulated by BMP2. However, the level of *Osterix* expression was not altered by the increased *MyoD* in the *Tbx22* null palatal shelves. In fact, it would be surprising if *Osterix* was increased in the null palatal shelves. These clearly indicate that observations made by *in vitro* manipulations do not always reflect *in vivo* situations. Nevertheless, the relationship between these factors and how they regulate each other during palate development are areas of considerable interest. Alternatively, it is also possible that the defective osteogenesis and altered myogenic genes are entirely independent of each other.

4.6.5 The regulation and regulatory role of *Tbx22*

The regulation and regulatory role of *Tbx22* based on previous studies and this study are summarised in Figure 4.1. In early face, *Tbx22* is regulated by FGF and BMP signalling (Fuchs et al., 2010; Higashihori et al., 2010). Implantation of FGF2 and FGF8 soaked beads upregulated its expression while BMP4 and BMP7 downregulated the expression. Also, antagonists of FGF and BMP signalling resulted in downregulation and upregulation of *Tbx22*, respectively. *Msx2* and *Dlx5* were suggested to be downstream of *Tbx22* as their expression was repressed by *TBX22* overexpression (Higashihori et al., 2010). In the palatal shelf, *Tbx22* expression was unaltered by FGF signalling but was repressed by addition of BMP4 soaked beads (Fuchs et al., 2010). A lack of *Mn1* (Liu et al., 2008) or *Spry2* (Welsh et al., 2007) in mice resulted in downregulation of *Tbx22* in the palatal shelves, placing these genes upstream of *Tbx22*. This study has demonstrated a downregulation of *MyoD* in the *Tbx22* null palatal shelves and the functional assays have shown that it can be regulated by TBX22 *in vitro*. In addition, *Cyclin D2* was reduced in the *Tbx22* null palatal shelves. Cell proliferation assay performed in this study suggested a role of TBX22 in proliferation in addition to the previously reported role in differentiation and maturation of osteoblasts during palate development.

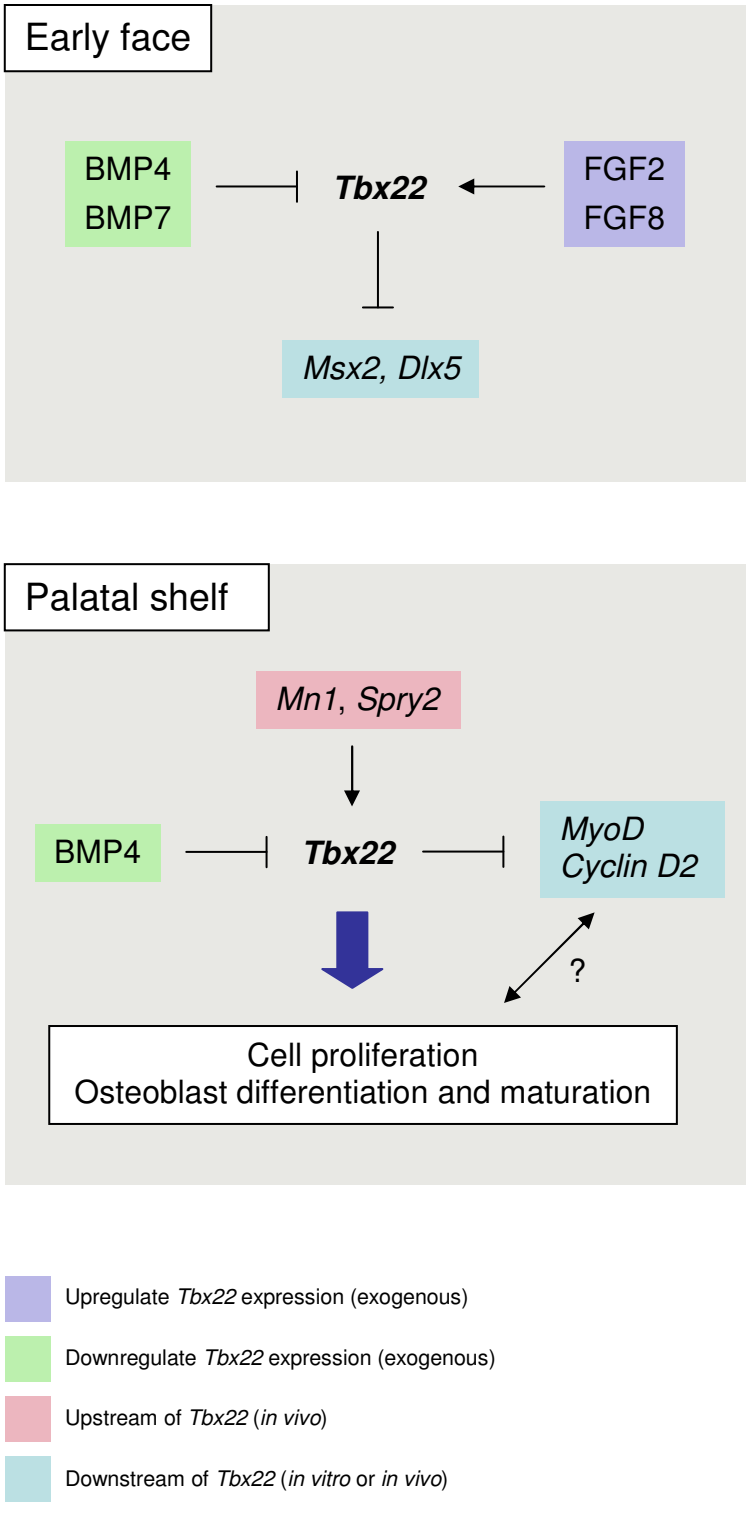

Figure 4.1 The regulation and role of *Tbx22* in the early face and palatal shelf
In the early facial mesenchyme, *Tbx22* can be upregulated by the addition of exogenous FGF2 and FGF8, but downregulated by BMP4 and BMP7. In addition, *Msx2* and *Dlx5* are reduced by overexpression of *TBX22*. In the palatal shelf, *Mn1* and *Spry2* are both upstream of *Tbx22* whereas *MyoD* and *Cyclin D2* are downstream. Exogenous BMP4 is capable of downregulating *Tbx22* in the shelf. TBX22 is involved in cell proliferation, osteoblast differentiation and maturation.

4.7 Characterisation of other craniofacial anomalies in *Tbx22* null mice

Tbx22 null mice show ankyloglossia and choanal atresia phenotypes in addition to the submucous and overt cleft palate. These pathogenic phenotypes have been well characterised at E15.5 but less is known at earlier stages. In this part of the project, it was intended to investigate the morphology of relevant tissues by H&E staining, and in particular the involvement of *Fgf8* in choanae formation at E10.5 and E11.0 by whole mount *in situ* hybridisation.

4.7.1 Ankyloglossia

Under normal circumstances, a selective degeneration occurs at the tip of the tongue by E13 due to cellular apoptosis and resorption process, leaving a frenulum as the only attachment (Paulson et al., 1985; Morita et al., 2004). Although the exact pathogenesis of ankyloglossia is not clear (Klockars, 2007), the failure of cellular degeneration is suggested to lead to a much longer anchor between the anterior tongue and the floor of the mouth (Morowati et al., 2010). The histological sections of wt showed that the formation of frenulum was evident at E12.5. This freed the anterior tip of the tongue from the floor of the mouth. In contrast, the frenulum was not visible in *Tbx22* null mice at the equivalent stage. In the null mice, it clearly seemed that there were excess tissues at the anterior base of the tongue. Interestingly, the difference between the wt and null mice seems more obvious at earlier stages compared to E15.5 at which time the phenotype is considered to be mild. In human, the frenulum recedes naturally in some ankyloglossia cases while children grow (Ruffoli et al., 2005). This might as well be the case for mice. At this time, it is not clear if the ankyloglossia phenotype in *Tbx22* null mice results from a lack of cell death, excess proliferation, a combination of both or other mechanisms. A recent study has suggested a negative role of TBX22 in cell proliferation in early facial mesenchyme (Higashihori et al., 2010). If this was the case at the anterior base of the tongue, the lack of *Tbx22* would increase proliferation. However, the present study suggests that a lack of *Tbx22* results in decreased cell proliferation at least in the palatal shelves. In either way, this needs further testing in the relevant tissue to understand molecular basis of the defect.

4.7.2 Choanal atresia

The choanae are the passageways at the back of the nose between the nasal cavity and the pharynx that originates at the junction between the primordia of the primary and secondary palates. In normal choanae development, epithelial cells of medial and lateral nasal processes initially merge to form nasal fins at E10.5 (Tamarin, 1982; Diewert and Wang, 1992). By late E11, the fins undergo cleavage which results in the formation of oronasal membranes, and they begin to involute with the formation of interstitial gaps that enlarge and eventually rupture so that complete opening between nasal and oral cavities is achieved by E13. Apoptosis plays an important role in degeneration of nasal fins anteriorly upon lip fusion (Jiang et al., 2006), but the exact molecular mechanism for choanae formation is not known. The H&E staining of the wt showed that the posterior nasal fins underwent cleavage process by E11.5 but the oronasal membranes were still existed in the choanae. By E12.5, the choanae were open, indicating that the oronasal membranes in the wt rupture between E11.5 and E12.5. This is consistent with the previous findings. In contrast, the nasal fins persisted in many of the null mice at E11.5 and the oronasal membranes were evident at E12.5 (if not ruptured by this stage, are likely to persist into later embryonic stages).

Apart from *Tbx22* null mice, choanal atresia is also seen in the mutant mouse models of *Chd7* (Bosman et al., 2005) and *Raldh3* (Dupe et al., 2003). *Chd7* mutant mice closely resemble human CHARGE syndrome which is predominantly caused by mutations in *CHD7* (Vissers et al., 2004). The mutant mice develop a range of defects such as eye and genital abnormalities and cardiac defects as well as cleft palate and choanal atresia. To the latter point, oronasal membranes in some mutant mice persist which could explain the postnatal lethality. However, to date, the cause of choanal atresia in *Chd7* mutant mice has not been defined. *Raldh3* knockout in mice impairs retinoic acid synthesis during nasal development, leading to choanal atresia. In this case, the phenotype is believed to result from persistence of *Fgf8* expression in the mutant nasal fins at E11.0. FGF signalling is considered essential in the midfacial development and a range of *Fgfs* including *Fgf8* and their receptors are expressed in spatially restricted manners in the early facial prominences (Bachler and Neubuser, 2001). In this study, whole mount *in situ* hybridisation

indicated similar *Fgf8* expression in the wt and *Tbx22* null mice in the epithelial layers of the medial and lateral nasal processes around the nasal pits as well as in the nascent fins at E10.5. At E11.0, *Fgf8* was not detected in the nasal fins anteriorly in both the wt and *Tbx22* null mice, whereas the expression was evident at the posterior end of the nasal fins. However, this was similar between the wt and null mice suggesting that *Fgf8* is not altered in *Tbx22* null mice during choanae development. Recent findings indicate that FGF signalling regulates *Tbx22* expression in early facial mesenchyme (Fuchs et al., 2010; Higashihori et al., 2010), but the results presented here suggest no negative feedback loop in the nasal regions.

4.8 Future studies

As a consequence of this project, there are a number of interesting lines of investigation that may be followed up. It is hoped that these will continue in the lab to provide a better understanding of the role of TBX22 in craniofacial development.

4.8.1 Verification of microarray data

The expression microarray experiments provided a list of differentially expressed genes in the absence of *Tbx22* in the palatal shelves. In the scope of this project, only selected upregulated genes were further investigated and downregulated genes were not followed up. However, there were few interesting genes including *Gabrb2*, *Gabra1*, *Gria4*, *Adh1* and *Pax3*. Microarray is a useful tool to obtain a global view of differentially expressed genes but it can easily contain false positives. These genes in particular will first need verification by another method such as real-time PCR. Although they may not be directly regulated by TBX22, it would be of considerable interest if their differential expressions are confirmed because of the potential implication in the occurrence of cleft palate.

Importantly, *Tbx22* positive cells around the nasal septum and at the base of the tongue were not included in the microarray experiments and expression profiles from these tissues would be somewhat different from the data obtained from E13.5 palatal shelves. Thus, it would also be interesting to examine gene expression profiles of these tissues.

4.8.2 Further testing of the effect of *Tbx22* overexpression

Functional analysis including luciferase reporter assays and chromatin immunoprecipitation indicated the regulation of *MyoD* by TBX22 in HEK 293T cells. However, the overexpression study has failed to show the effect of TBX22 on the level of endogenous *MyoD* expression in C2C12 cells. This could be due to the difference in cellular contexts, and will be investigated further. Though it is known to be difficult to achieve high transfection efficiency in murine or human embryonic palatal mesenchymal cells, it would be interesting to look for endogenous *MyoD*

expression because these cells are more likely to accurately reflect the *in vivo* situation.

4.8.3 Determining the origin of differentially expressed muscle genes

The study indicated the global upregulation of muscle related genes in the *Tbx22* null palatal shelves. However, where the differences come from in the palatal shelves is not clear. This needs more examination at both mRNA and protein levels. It is not known which cells are specifically affected by the lack of *Tbx22* because of the heterogeneous nature of palatal mesenchyme. One way in which this issue could be resolved would be to perform double labelling experiments on palatal mesenchymal cells using antibodies specific for TBX22 as well as a marker for CNC-derived cells or mesoderm derived cells. Another useful experiment would be to cross the floxed *Tbx22* mice to Wnt1-Cre/R26R (Chai et al., 2000) or Mesp1-Cre/R26R (Yoshida et al., 2008) in order to indelibly mark the progeny of the CNC or mesoderm, respectively, during embryogenesis. This will allow a specific knockdown of *Tbx22* in CNC-derived or paraxial mesoderm derived cell lineages, and would clarify specific phenotypic effects that *Tbx22* has on each cell type.

4.8.4 Further investingation of the ankyloglossia and choanal atresia phenotypes

In this project, there was insufficient time to adequately analyse the ankyloglossia and choanal atresia phenotypes in *Tbx22* null mice. Firstly, a more comprehensive histological analysis from E10.5 to E12.5 is required to better understand the relevant morphology during early tongue and choanae development. At a developmental level, there is still very little known about the precise origins and occurrence of these features. Apoptosis and/or cell proliferation may be of particular interest because persistence of the oronasal membrane and having excess tissue at the base of the tongue could well be caused by a failure in one or a combination of these mechanisms.

REFERENCES

Acs,N., Banhidy,F., Puho,E., and Czeizel,A.E. (2005). Maternal influenza during pregnancy and risk of congenital abnormalities in offspring. Birth Defects Res. A Clin. Mol. Teratol. *73*, 989-996.

Agarwal,P., Wylie,J.N., Galceran,J., Arkhitko,O., Li,C., Deng,C., Grosschedl,R., and Bruneau,B.G. (2003). Tbx5 is essential for forelimb bud initiation following patterning of the limb field in the mouse embryo. Development *130*, 623-633.

Agata,H., Asahina,I., Yamazaki,Y., Uchida,M., Shinohara,Y., Honda,M.J., Kagami,H., and Ueda,M. (2007). Effective bone engineering with periosteum-derived cells. J. Dent. Res. *86*, 79-83.

Agulnik,S.I., Garvey,N., Hancock,S., Ruvinsky,I., Chapman,D.L., Agulnik,I., Bollag,R., Papaioannou,V., and Silver,L.M. (1996). Evolution of mouse T-box genes by tandem duplication and cluster dispersion. Genetics *144*, 249-254.

Agulnik,S.I., Papaioannou,V.E., and Silver,L.M. (1998). Cloning, mapping, and expression analysis of TBX15, a new member of the T-Box gene family. Genomics *51*, 68-75.

Alappat,S.R., Zhang,Z., Suzuki,K., Zhang,X., Liu,H., Jiang,R., Yamada,G., and Chen,Y. (2005). The cellular and molecular etiology of the cleft secondary palate in Fgf10 mutant mice. Dev. Biol. *277*, 102-113.

Allison,D.B., Cui,X., Page,G.P., and Sabripour,M. (2006). Microarray data analysis: from disarray to consolidation and consensus. Nat. Rev. Genet. *7*, 55-65.

Andreou,A.M., Pauws,E., Jones,M.C., Singh,M.K., Bussen,M., Doudney,K., Moore,G.E., Kispert,A., Brosens,J.J., and Stanier,P. (2007). TBX22 missense mutations found in patients with X-linked cleft palate affect DNA binding, sumoylation, and transcriptional repression. Am. J. Hum. Genet. *81*, 700-712.

Arnold,H.H. and Braun,T. (1996). Targeted inactivation of myogenic factor genes reveals their role during mouse myogenesis: a review. Int. J. Dev. Biol. *40*, 345-353.

Asada,H., Kawamura,Y., Maruyama,K., Kume,H., Ding,R.G., Kanbara,N., Kuzume,H., Sanbo,M., Yagi,T., and Obata,K. (1997). Cleft palate and decreased brain gamma-aminobutyric acid in mice lacking the 67-kDa isoform of glutamic acid decarboxylase. Proc. Natl. Acad. Sci. U. S. A *94*, 6496-6499.

Asakura,A., Fujisawa-Sehara,A., Komiya,T., Nabeshima,Y., and Nabeshima,Y. (1993). MyoD and myogenin act on the chicken myosin light-chain 1 gene as distinct transcriptional factors. Mol. Cell Biol. *13*, 7153-7162.

Ashique,A.M., Fu,K., and Richman,J.M. (2002). Endogenous bone morphogenetic proteins regulate outgrowth and epithelial survival during avian lip fusion. Development *129*, 4647-4660.

Aslan,S., Yilmazer,C., Yildirim,T., Akkuzu,B., and Yilmaz,I. (2009). Comparison of nasal region dimensions in bilateral choanal atresia patients and normal controls: a computed tomographic analysis with clinical implications. Int. J. Pediatr. Otorhinolaryngol. *73*, 329-335.

Avila,J.R., Jezewski,P.A., Vieira,A.R., Orioli,I.M., Castilla,E.E., Christensen,K., Daack-Hirsch,S., Romitti,P.A., and Murray,J.C. (2006). PVRL1 variants contribute to non-syndromic cleft lip and palate in multiple populations. Am. J. Med. Genet. A *140*, 2562-2570.

Babiarz,B.S., Wee,E.L., and Zimmerman,E.F. (1979). Palate morphogenesis. III. Changes in cell shape and orientation during shelf elevation. Teratology *20*, 249-278.

Bachler,M. and Neubuser,A. (2001). Expression of members of the Fgf family and their receptors during midfacial development. Mech. Dev. *100*, 313-316.

Baldini,A. (2003). DiGeorge's syndrome: a gene at last. Lancet *362*, 1342-1343.

Ballif,B.C., Theisen,A., Rosenfeld,J.A., Traylor,R.N., Gastier-Foster,J., Thrush,D.L., Astbury,C., Bartholomew,D., McBride,K.L., Pyatt,R.E., Shane,K., Smith,W.E., Banks,V., Gallentine,W.B., Brock,P., Rudd,M.K., Adam,M.P., Keene,J.A., Phillips,J.A., III, Pfotenhauer,J.P., Gowans,G.C., Stankiewicz,P., Bejjani,B.A., and Shaffer,L.G. (2010). Identification of a recurrent microdeletion at 17q23.1q23.2 flanked by segmental duplications associated with heart defects and limb abnormalities. Am. J. Hum. Genet. *86*, 454-461.

Bamshad,M., Lin,R.C., Law,D.J., Watkins,W.C., Krakowiak,P.A., Moore,M.E., Franceschini,P., Lala,R., Holmes,L.B., Gebuhr,T.C., Bruneau,B.G., Schinzel,A., Seidman,J.G., Seidman,C.E., and Jorde,L.B. (1997). Mutations in human TBX3 alter limb, apocrine and genital development in ulnar-mammary syndrome. Nat. Genet. *16*, 311-315.

Bamshad,M., Root,S., and Carey,J.C. (1996). Clinical analysis of a large kindred with the Pallister ulnar-mammary syndrome. Am. J. Med. Genet. *65*, 325-331.

Barlow,A.J. and Francis-West,P.H. (1997). Ectopic application of recombinant BMP-2 and BMP-4 can change patterning of developing chick facial primordia. Development *124*, 391-398.

Barrow,J.R. and Capecchi,M.R. (1999). Compensatory defects associated with mutations in Hoxa1 restore normal palatogenesis to Hoxa2 mutants. Development *126*, 5011-5026.

Basson,C.T., Bachinsky,D.R., Lin,R.C., Levi,T., Elkins,J.A., Soults,J., Grayzel,D., Kroumpouzou,E., Traill,T.A., Leblanc-Straceski,J., Renault,B., Kucherlapati,R.,

Seidman,J.G., and Seidman,C.E. (1997). Mutations in human TBX5 [corrected] cause limb and cardiac malformation in Holt-Oram syndrome. Nat. Genet. *15*, 30-35.

Beddington,R.S. (1982). An autoradiographic analysis of tissue potency in different regions of the embryonic ectoderm during gastrulation in the mouse. J. Embryol. Exp. Morphol. *69*, 265-285.

Beddington,R.S., Rashbass,P., and Wilson,V. (1992). Brachyury--a gene affecting mouse gastrulation and early organogenesis. Dev. Suppl 157-165.

Biddle,F.G. (1980). Palate development in the mouse: a quantitative method that permits the estimation of time and rate of palate closure. Teratology *22*, 239-246.

Birnbaum,S., Ludwig,K.U., Reutter,H., Herms,S., Steffens,M., Rubini,M., Baluardo,C., Ferrian,M., meida de,A.N., Alblas,M.A., Barth,S., Freudenberg,J., Lauster,C., Schmidt,G., Scheer,M., Braumann,B., Berge,S.J., Reich,R.H., Schiefke,F., Hemprich,A., Potzsch,S., Steegers-Theunissen,R.P., Potzsch,B., Moebus,S., Horsthemke,B., Kramer,F.J., Wienker,T.F., Mossey,P.A., Propping,P., Cichon,S., Hoffmann,P., Knapp,M., Nothen,M.M., and Mangold,E. (2009). Key susceptibility locus for nonsyndromic cleft lip with or without cleft palate on chromosome 8q24. Nat. Genet. *41*, 473-477.

Bjornsson,A., Arnason,A., and Tippet,P. (1989). X-linked cleft palate and ankyloglossia in an Icelandic family. Cleft Palate J. *26*, 3-8.

Bongers,E.M., Duijf,P.H., van Beersum,S.E., Schoots,J., Van Kampen,A., Burckhardt,A., Hamel,B.C., Losan,F., Hoefsloot,L.H., Yntema,H.G., Knoers,N.V., and van Bokhoven,H. (2004). Mutations in the human TBX4 gene cause small patella syndrome. Am. J. Hum. Genet. *74*, 1239-1248.

Bosman,E.A., Penn,A.C., Ambrose,J.C., Kettleborough,R., Stemple,D.L., and Steel,K.P. (2005). Multiple mutations in mouse Chd7 provide models for CHARGE syndrome. Hum. Mol. Genet. *14*, 3463-3476.

Botto,L.D., Lisi,A., Bower,C., Canfield,M.A., Dattani,N., De,V.C., De,W.H., Erickson,D.J., Halliday,J., Irgens,L.M., Lowry,R.B., McDonnell,R., Metneki,J., Poetzsch,S., Ritvanen,A., Robert-Gnansia,E., Siffel,C., Stoll,C., and Mastroiacovo,P. (2006). Trends of selected malformations in relation to folic acid recommendations and fortification: an international assessment. Birth Defects Res. A Clin. Mol. Teratol. *76*, 693-705.

Bouchard,M., Grote,D., Craven,S.E., Sun,Q., Steinlein,P., and Busslinger,M. (2005). Identification of Pax2-regulated genes by expression profiling of the mid-hindbrain organizer region. Development *132*, 2633-2643.

Braun,T., Rudnicki,M.A., Arnold,H.H., and Jaenisch,R. (1992). Targeted inactivation of the muscle regulatory gene Myf-5 results in abnormal rib development and perinatal death. Cell *71*, 369-382.

Braybrook,C., Doudney,K., Marcano,A.C., Arnason,A., Bjornsson,A., Patton,M.A., Goodfellow,P.J., Moore,G.E., and Stanier,P. (2001). The T-box transcription factor gene TBX22 is mutated in X-linked cleft palate and ankyloglossia. Nat. Genet. *29*, 179-183.

Braybrook,C., Lisgo,S., Doudney,K., Henderson,D., Marcano,A.C., Strachan,T., Patton,M.A., Villard,L., Moore,G.E., Stanier,P., and Lindsay,S. (2002). Craniofacial expression of human and murine TBX22 correlates with the cleft palate and ankyloglossia phenotype observed in CPX patients. Hum. Mol. Genet. *11*, 2793-2804.

Brinkley,L.L. and Morris-Wiman,J. (1984). The role of extracellular matrices in palatal shelf closure. Curr. Top. Dev. Biol. *19*, 17-36.

Brinkley,L.L. and Vickerman,M.M. (1982). The effects of chlorcyclizine-induced alterations of glycosaminoglycans on mouse palatal shelf elevation in vivo and in vitro. J. Embryol. Exp. Morphol. *69*, 193-213.

Brooks,J.K., Leonard,C.O., and Coccaro,P.J., Jr. (1992). Opitz (BBB/G) syndrome: oral manifestations. Am. J. Med. Genet. *43*, 595-601.

Brown,N.L., Knott,L., Halligan,E., Yarram,S.J., Mansell,J.P., and Sandy,J.R. (2003). Microarray analysis of murine palatogenesis: temporal expression of genes during normal palate development. Dev. Growth Differ. *45*, 153-165.

Bruneau,B.G., Logan,M., Davis,N., Levi,T., Tabin,C.J., Seidman,J.G., and Seidman,C.E. (1999). Chamber-specific cardiac expression of Tbx5 and heart defects in Holt-Oram syndrome. Dev. Biol. *211*, 100-108.

Bruneau,B.G., Nemer,G., Schmitt,J.P., Charron,F., Robitaille,L., Caron,S., Conner,D.A., Gessler,M., Nemer,M., Seidman,C.E., and Seidman,J.G. (2001). A murine model of Holt-Oram syndrome defines roles of the T-box transcription factor Tbx5 in cardiogenesis and disease. Cell *106*, 709-721.

Burdick,A.B., Ma,L.A., Dai,Z.H., and Gao,N.N. (1987). van der Woude syndrome in two families in China. J. Craniofac. Genet. Dev. Biol. *7*, 413-418.

Burrow,T.A., Saal,H.M., de,A.A., Martin,L.J., Cotton,R.T., and Hopkin,R.J. (2009). Characterization of congenital anomalies in individuals with choanal atresia. Arch. Otolaryngol. Head Neck Surg. *135*, 543-547.

Bush,J.O., Lan,Y., Maltby,K.M., and Jiang,R. (2002). Isolation and developmental expression analysis of Tbx22, the mouse homolog of the human X-linked cleft palate gene. Dev. Dyn. *225*, 322-326.

Bussen,M., Petry,M., Schuster-Gossler,K., Leitges,M., Gossler,A., and Kispert,A. (2004). The T-box transcription factor Tbx18 maintains the separation of anterior and posterior somite compartments. Genes Dev. *18*, 1209-1221.

Calzolari,E., Bianchi,F., Rubini,M., Ritvanen,A., and Neville,A.J. (2004). Epidemiology of cleft palate in Europe: implications for genetic research. Cleft Palate Craniofac. J. *41*, 244-249.

Calzolari,E., Pierini,A., Astolfi,G., Bianchi,F., Neville,A.J., and Rivieri,F. (2007). Associated anomalies in multi-malformed infants with cleft lip and palate: An epidemiologic study of nearly 6 million births in 23 EUROCAT registries. Am. J. Med. Genet. A *143*, 528-537.

Carette,M.J. and Ferguson,M.W. (1992). The fate of medial edge epithelial cells during palatal fusion in vitro: an analysis by DiI labelling and confocal microscopy. Development *114*, 379-388.

Carreira,S., Dexter,T.J., Yavuzer,U., Easty,D.J., and Goding,C.R. (1998). Brachyury-related transcription factor Tbx2 and repression of the melanocyte-specific TRP-1 promoter. Mol. Cell Biol. *18*, 5099-5108.

Celli,J., Duijf,P., Hamel,B.C., Bamshad,M., Kramer,B., Smits,A.P., Newbury-Ecob,R., Hennekam,R.C., Van Buggenhout,G., van Haeringen,A., Woods,C.G., van Essen,A.J., de Waal,R., Vriend,G., Haber,D.A., Yang,A., McKeon,F., Brunner,H.G., and van Bokhoven,H. (1999). Heterozygous germline mutations in the p53 homolog p63 are the cause of EEC syndrome. Cell *99*, 143-153.

Chaabouni,M., Smaoui,N., Benneji,N., M'rad,R., Jemaa,L.B., Hachicha,S., and Chaabouni,H. (2005). Mutation analysis of TBX22 reveals new mutation in Tunisian CPX family. Clin. Dysmorphol. *14*, 23-25.

Chagovetz,A. and Blair,S. (2009). Real-time DNA microarrays: reality check. Biochem. Soc. Trans. *37*, 471-475.

Chai,Y., Jiang,X., Ito,Y., Bringas,P., Jr., Han,J., Rowitch,D.H., Soriano,P., McMahon,A.P., and Sucov,H.M. (2000). Fate of the mammalian cranial neural crest during tooth and mandibular morphogenesis. Development *127*, 1671-1679.

Chapman,D.L., Garvey,N., Hancock,S., Alexiou,M., Agulnik,S.I., Gibson-Brown,J.J., Cebra-Thomas,J., Bollag,R.J., Silver,L.M., and Papaioannou,V.E. (1996). Expression of the T-box family genes, Tbx1-Tbx5, during early mouse development. Dev. Dyn. *206*, 379-390.

Chapman,D.L. and Papaioannou,V.E. (1998). Three neural tubes in mouse embryos with mutations in the T-box gene Tbx6. Nature *391*, 695-697.

Chen,D., Zhao,M., and Mundy,G.R. (2004). Bone morphogenetic proteins. Growth Factors *22*, 233-241.

Cheung,R. and Prince,M. (2001). Comparison of craniofacial skeletal characteristics of infants with bilateral choanal atresia and an age-matched normative population: computed tomography analysis. J. Otolaryngol. *30*, 173-178.

Chevrier,C., Perret,C., Bahuau,M., Nelva,A., Herman,C., Francannet,C., Robert-Gnansia,E., and Cordier,S. (2005). Interaction between the ADH1C polymorphism and maternal alcohol intake in the risk of nonsyndromic oral clefts: an evaluation of the contribution of child and maternal genotypes. Birth Defects Res. A Clin. Mol. Teratol. *73*, 114-122.

Cohen,S.R., Chen,L., Trotman,C.A., and Burdi,A.R. (1993). Soft-palate myogenesis: a developmental field paradigm. Cleft Palate Craniofac. J. *30*, 441-446.

Cohen,S.R., Chen,L.L., Burdi,A.R., and Trotman,C.A. (1994). Patterns of abnormal myogenesis in human cleft palates. Cleft Palate Craniofac. J. *31*, 345-350.

Condie,B.G., Bain,G., Gottlieb,D.I., and Capecchi,M.R. (1997). Cleft palate in mice with a targeted mutation in the gamma-aminobutyric acid-producing enzyme glutamic acid decarboxylase 67. Proc. Natl. Acad. Sci. U. S. A *94*, 11451-11455.

Conlon,F.L., Fairclough,L., Price,B.M., Casey,E.S., and Smith,J.C. (2001). Determinants of T box protein specificity. Development *128*, 3749-3758.

Core,N., Caubit,X., Metchat,A., Boned,A., Djabali,M., and Fasano,L. (2007). Tshz1 is required for axial skeleton, soft palate and middle ear development in mice. Dev. Biol. *308*, 407-420.

Croen,L.A., Shaw,G.M., Wasserman,C.R., and Tolarova,M.M. (1998). Racial and ethnic variations in the prevalence of orofacial clefts in California, 1983-1992. Am. J. Med. Genet. *79*, 42-47.

Cuervo,R. and Covarrubias,L. (2004). Death is the major fate of medial edge epithelial cells and the cause of basal lamina degradation during palatogenesis. Development *131*, 15-24.

Cui,X.M., Chai,Y., Chen,J., Yamamoto,T., Ito,Y., Bringas,P., and Shuler,C.F. (2003). TGF-beta3-dependent SMAD2 phosphorylation and inhibition of MEE proliferation during palatal fusion. Dev. Dyn. *227*, 387-394.

Daluiski,A., Engstrand,T., Bahamonde,M.E., Gamer,L.W., Agius,E., Stevenson,S.L., Cox,K., Rosen,V., and Lyons,K.M. (2001). Bone morphogenetic protein-3 is a negative regulator of bone density. Nat. Genet. *27*, 84-88.

Davenport,T.G., Jerome-Majewska,L.A., and Papaioannou,V.E. (2003). Mammary gland, limb and yolk sac defects in mice lacking Tbx3, the gene mutated in human ulnar mammary syndrome. Development *130*, 2263-2273.

Deato,M.D., Marr,M.T., Sottero,T., Inouye,C., Hu,P., and Tjian,R. (2008). MyoD targets TAF3/TRF3 to activate myogenin transcription. Mol. Cell *32*, 96-105.

Degitz,S.J., Francis,B.M., and Foley,G.L. (1998). Mesenchymal changes associated with retinoic acid induced cleft palate in CD-1 mice. J. Craniofac. Genet. Dev. Biol. *18*, 88-99.

Deltour,L., Foglio,M.H., and Duester,G. (1999). Metabolic deficiencies in alcohol dehydrogenase Adh1, Adh3, and Adh4 null mutant mice. Overlapping roles of Adh1 and Adh4 in ethanol clearance and metabolism of retinol to retinoic acid. J. Biol. Chem. *274*, 16796-16801.

Depew,M.J., Simpson,C.A., Morasso,M., and Rubenstein,J.L. (2005). Reassessing the Dlx code: the genetic regulation of branchial arch skeletal pattern and development. J. Anat. *207*, 501-561.

Dhulipala,V.C., Maddali,K.K., Welshons,W.V., and Reddy,C.S. (2005). Secalonic acid D blocks embryonic palatal mesenchymal cell-cycle by altering the activity of CDK2 and the expression of p21 and cyclin E. Birth Defects Res. B Dev. Reprod. Toxicol. *74*, 233-242.

Dhulipala,V.C., Welshons,W.V., and Reddy,C.S. (2004). Inhibition of human embryonic palatal mesenchymal cell cycle by secalonic acid D: a probable mechanism of its cleft palate induction. Orthod. Craniofac. Res. *7*, 227-236.

Diewert,V.M. and Wang,K.Y. (1992). Recent advances in primary palate and midface morphogenesis research. Crit Rev. Oral Biol. Med. *4*, 111-130.

Ding,H., Wu,X., Bostrom,H., Kim,I., Wong,N., Tsoi,B., O'Rourke,M., Koh,G.Y., Soriano,P., Betsholtz,C., Hart,T.C., Marazita,M.L., Field,L.L., Tam,P.P., and Nagy,A. (2004). A specific requirement for PDGF-C in palate formation and PDGFR-alpha signaling. Nat. Genet. *36*, 1111-1116.

Dixon,J., Jones,N.C., Sandell,L.L., Jayasinghe,S.M., Crane,J., Rey,J.P., Dixon,M.J., and Trainor,P.A. (2006). Tcof1/Treacle is required for neural crest cell formation and proliferation deficiencies that cause craniofacial abnormalities. Proc. Natl. Acad. Sci. U. S. A *103*, 13403-13408.

Dobrovolskaia-Zavadskaia,N. (1927). Sur la mortification sponta-nee de la queue chez la souris nouveau-nee et sur l'existence d'un caractere hereditaire "non-viable". C. R. Acad. Sci. Biol. *97*, 114-116.

Dodds,R.A., Connor,J.R., Drake,F., Feild,J., and Gowen,M. (1998). Cathepsin K mRNA detection is restricted to osteoclasts during fetal mouse development. J. Bone Miner. Res. *13*, 673-682.

Dode,C., Levilliers,J., Dupont,J.M., De,P.A., Le,D.N., Soussi-Yanicostas,N., Coimbra,R.S., Delmaghani,S., Compain-Nouaille,S., Baverel,F., Pecheux,C., Le,T.D., Cruaud,C., Delpech,M., Speleman,F., Vermeulen,S., Amalfitano,A., Bachelot,Y., Bouchard,P., Cabrol,S., Carel,J.C., Delemarre-van de Waal,H., Goulet-Salmon,B., Kottler,M.L., Richard,O., Sanchez-Franco,F., Saura,R., Young,J., Petit,C., and Hardelin,J.P. (2003). Loss-of-function mutations in FGFR1 cause autosomal dominant Kallmann syndrome. Nat. Genet. *33*, 463-465.

Ducy,P. and Karsenty,G. (1995). Two distinct osteoblast-specific cis-acting elements control expression of a mouse osteocalcin gene. Mol. Cell Biol. *15*, 1858-1869.

Ducy,P., Schinke,T., and Karsenty,G. (2000). The osteoblast: a sophisticated fibroblast under central surveillance. Science *289*, 1501-1504.

Ducy,P., Zhang,R., Geoffroy,V., Ridall,A.L., and Karsenty,G. (1997). Osf2/Cbfa1: a transcriptional activator of osteoblast differentiation. Cell *89*, 747-754.

Dudas,M., Kim,J., Li,W.Y., Nagy,A., Larsson,J., Karlsson,S., Chai,Y., and Kaartinen,V. (2006). Epithelial and ectomesenchymal role of the type I TGF-beta receptor ALK5 during facial morphogenesis and palatal fusion. Dev. Biol. *296*, 298-314.

Dudas,M., Sridurongrit,S., Nagy,A., Okazaki,K., and Kaartinen,V. (2004). Craniofacial defects in mice lacking BMP type I receptor Alk2 in neural crest cells. Mech. Dev. *121*, 173-182.

Duester,G. (2000). Families of retinoid dehydrogenases regulating vitamin A function: production of visual pigment and retinoic acid. Eur. J. Biochem. *267*, 4315-4324.

Duester,G. (2001). Genetic dissection of retinoid dehydrogenases. Chem. Biol. Interact. *130-132*, 469-480.

Dupe,V., Matt,N., Garnier,J.M., Chambon,P., Mark,M., and Ghyselinck,N.B. (2003). A newborn lethal defect due to inactivation of retinaldehyde dehydrogenase type 3 is prevented by maternal retinoic acid treatment. Proc. Natl. Acad. Sci. U. S. A *100*, 14036-14041.

Eberhart,J.K., He,X., Swartz,M.E., Yan,Y.L., Song,H., Boling,T.C., Kunerth,A.K., Walker,M.B., Kimmel,C.B., and Postlethwait,J.H. (2008). MicroRNA Mirn140 modulates Pdgf signaling during palatogenesis. Nat. Genet. *40*, 290-298.

Edison,R.J. and Muenke,M. (2004). Mechanistic and epidemiologic considerations in the evaluation of adverse birth outcomes following gestational exposure to statins. Am. J. Med. Genet. A *131*, 287-298.

Fakhry,A., Ratisoontorn,C., Vedhachalam,C., Salhab,I., Koyama,E., Leboy,P., Pacifici,M., Kirschner,R.E., and Nah,H.D. (2005). Effects of FGF-2/-9 in calvarial bone cell cultures: differentiation stage-dependent mitogenic effect, inverse regulation of BMP-2 and noggin, and enhancement of osteogenic potential. Bone *36*, 254-266.

Fang,P.F., Hu,R.Y., He,X.Y., and Ding,X.Y. (2004). Multiple signaling pathways control Tbx6 expression during Xenopus myogenesis. Acta Biochim. Biophys. Sin. (Shanghai) *36*, 390-396.

Farin,H.F., Mansouri,A., Petry,M., and Kispert,A. (2008). T-box protein Tbx18 interacts with the paired box protein Pax3 in the development of the paraxial mesoderm. J. Biol. Chem. *283*, 25372-25380.

Ferguson,M.W. (1988). Palate development. Development *103 Suppl*, 41-60.

Feuerstein,S.S., Krespi,Y.P., and Sachdev,R.K. (1980). Transnasal correction of choanal atresia. Head Neck Surg. *3*, 97-104.

Finnell,R.H., Shaw,G.M., Lammer,E.J., Brandl,K.L., Carmichael,S.L., and Rosenquist,T.H. (2004). Gene-nutrient interactions: importance of folates and retinoids during early embryogenesis. Toxicol. Appl. Pharmacol. *198*, 75-85.

Fitchett,J.E. and Hay,E.D. (1989). Medial edge epithelium transforms to mesenchyme after embryonic palatal shelves fuse. Dev. Biol. *131*, 455-474.

Flake,C.G. and Ferguson,C.F. (1964). Congenital choanal atresia in infants and children. Ann. Otol. Rhinol. Laryngol. *73*, 458-473.

Freng,A. (1978). Congenital choanal atresia. Etiology, morphology and diagnosis in 82 cases. Scand. J. Plast. Reconstr. Surg. *12*, 261-265.

Fuchs,A., Inthal,A., Herrmann,D., Cheng,S., Nakatomi,M., Peters,H., and Neubuser,A. (2010). Regulation of Tbx22 during facial and palatal development. Dev. Dyn. *239*, 2860-2874.

Gao,Y., Lan,Y., Ovitt,C.E., and Jiang,R. (2009). Functional equivalence of the zinc finger transcription factors Osr1 and Osr2 in mouse development. Dev. Biol. *328*, 200-209.

Ghosh,T.K., Packham,E.A., Bonser,A.J., Robinson,T.E., Cross,S.J., and Brook,J.D. (2001). Characterization of the TBX5 binding site and analysis of mutations that cause Holt-Oram syndrome. Hum. Mol. Genet. *10*, 1983-1994.

Gibbs,S. and Ponec,M. (2000). Intrinsic regulation of differentiation markers in human epidermis, hard palate and buccal mucosa. Arch. Oral Biol. *45*, 149-158.

Gibson-Brown,J.J., Agulnik,S.I., Chapman,D.L., Alexiou,M., Garvey,N., Silver,L.M., and Papaioannou,V.E. (1996). Evidence of a role for T-box genes in the evolution of limb morphogenesis and the specification of forelimb/hindlimb identity. Mech. Dev. *56*, 93-101.

Gill,G. (2005). Something about SUMO inhibits transcription. Curr. Opin. Genet. Dev. *15*, 536-541.

Gluecksohn-Schoenheimer,S. (1938). The development of two tailless mutants in the house mouse. Genetics *23*, 573-584.

Gluecksohn-Schoenheimer,S. (1944). The development of normal and homozygous Brachy (T/T) mouse embryos in the extraembryonic coelom of the chick. Proc. Natl. Acad. Sci. U. S. A *30*, 134-140.

Goering,L.M., Hoshijima,K., Hug,B., Bisgrove,B., Kispert,A., and Grunwald,D.J. (2003). An interacting network of T-box genes directs gene expression and fate in the zebrafish mesoderm. Proc. Natl. Acad. Sci. U. S. A *100*, 9410-9415.

Goldman,A.S. (1984). Biochemical mechanism of glucocorticoid-and phenytoin-induced cleft palate. Curr. Top. Dev. Biol. *19*, 217-239.

Gorski,S.M., Adams,K.J., Birch,P.H., Chodirker,B.N., Greenberg,C.R., and Goodfellow,P.J. (1994). Linkage analysis of X-linked cleft palate and ankyloglossia in Manitoba Mennonite and British Columbia Native kindreds. Hum. Genet. *94*, 141-148.

Gorski,S.M., Adams,K.J., Birch,P.H., Friedman,J.M., and Goodfellow,P.J. (1992). The gene responsible for X-linked cleft palate (CPX) in a British Columbia native kindred is localized between PGK1 and DXYS1. Am. J. Hum. Genet. *50*, 1129-1136.

Gosain,A.K., Conley,S.F., Marks,S., and Larson,D.L. (1996). Submucous cleft palate: diagnostic methods and outcomes of surgical treatment. Plast. Reconstr. Surg. *97*, 1497-1509.

Graham,F.L., Smiley,J., Russell,W.C., and Nairn,R. (1977). Characteristics of a human cell line transformed by DNA from human adenovirus type 5. J. Gen. Virol. *36*, 59-74.

Greene,R.M. and Pisano,M.M. (2010). Palate morphogenesis: Current understanding and future directions. Birth Defects Res. C. Embryo. Today *90*, 133-154.

Greene,R.M. and Pratt,R.M. (1976). Developmental aspects of secondary palate formation. J. Embryol. Exp. Morphol. *36*, 225-245.

Griffith,C.M. and Hay,E.D. (1992). Epithelial-mesenchymal transformation during palatal fusion: carboxyfluorescein traces cells at light and electron microscopic levels. Development *116*, 1087-1099.

Gritli-Linde,A. (2007). Molecular control of secondary palate development. Dev. Biol. *301*, 309-326.

Guo,K., Wang,J., Andres,V., Smith,R.C., and Walsh,K. (1995). MyoD-induced expression of p21 inhibits cyclin-dependent kinase activity upon myocyte terminal differentiation. Mol. Cell Biol. *15*, 3823-3829.

Guo,L., Lobenhofer,E.K., Wang,C., Shippy,R., Harris,S.C., Zhang,L., Mei,N., Chen,T., Herman,D., Goodsaid,F.M., Hurban,P., Phillips,K.L., Xu,J., Deng,X., Sun,Y.A., Tong,W., Dragan,Y.P., and Shi,L. (2006). Rat toxicogenomic study reveals analytical consistency across microarray platforms. Nat. Biotechnol. *24*, 1162-1169.

Habets,P.E., Moorman,A.F., Clout,D.E., van Roon,M.A., Lingbeek,M., van Lohuizen,M., Campione,M., and Christoffels,V.M. (2002). Cooperative action of Tbx2 and Nkx2.5 inhibits ANF expression in the atrioventricular canal: implications for cardiac chamber formation. Genes Dev. *16*, 1234-1246.

Hacham-Zadeh,S. and Garfunkel,A.A. (1985). Kindler syndrome in two related Kurdish families. Am. J. Med. Genet. *20*, 43-48.

Haenig,B. and Kispert,A. (2004). Analysis of TBX18 expression in chick embryos. Dev. Genes Evol. *214*, 407-411.

Haenig,B., Schmidt,C., Kraus,F., Pfordt,M., and Kispert,A. (2002). Cloning and expression analysis of the chick ortholog of TBX22, the gene mutated in X-linked cleft palate and ankyloglossia. Mech. Dev. *117*, 321-325.

Hagiwara,N., Katarova,Z., Siracusa,L.D., and Brilliant,M.H. (2003). Nonneuronal expression of the GABA(A) beta3 subunit gene is required for normal palate development in mice. Dev. Biol. *254*, 93-101.

Halevy,O., Novitch,B.G., Spicer,D.B., Skapek,S.X., Rhee,J., Hannon,G.J., Beach,D., and Lassar,A.B. (1995). Correlation of terminal cell cycle arrest of skeletal muscle with induction of p21 by MyoD. Science *267*, 1018-1021.

Hall,B.D. (1979). Choanal atresia and associated multiple anomalies. J. Pediatr. *95*, 395-398.

Hall,B.K. (1999). The neural crest in development and evolution. New York: Springer-Verlag.

Hanumegowda,U.M., Judy,B.M., Welshons,W.V., and Reddy,C.S. (2002). Selective inhibition of murine palatal mesenchymal cell proliferation in vitro by secalonic acid D. Toxicol. Sci. *66*, 159-165.

Harrelson,Z., Kelly,R.G., Goldin,S.N., Gibson-Brown,J.J., Bollag,R.J., Silver,L.M., and Papaioannou,V.E. (2004). Tbx2 is essential for patterning the atrioventricular canal and for morphogenesis of the outflow tract during heart development. Development *131*, 5041-5052.

Harris,E.F., Friend,G.W., and Tolley,E.A. (1992). Enhanced prevalence of ankyloglossia with maternal cocaine use. Cleft Palate Craniofac. J. *29*, 72-76.

Hasty,P., Bradley,A., Morris,J.H., Edmondson,D.G., Venuti,J.M., Olson,E.N., and Klein,W.H. (1993). Muscle deficiency and neonatal death in mice with a targeted mutation in the myogenin gene. Nature *364*, 501-506.

Hayes,C. (2002). Environmental risk factors and oral clefts. Cleft lip and palate: from origin to treatment. Wyszynski,D.F. ed. Oxford University press, pp. 159-169.

Hengerer,A.S. and Strome,M. (1982). Choanal atresia: a new embryologic theory and its influence on surgical management. Laryngoscope *92*, 913-921.

Hernandez-Diaz,S., Werler,M.M., Walker,A.M., and Mitchell,A.A. (2000). Folic acid antagonists during pregnancy and the risk of birth defects. N. Engl. J. Med. *343*, 1608-1614.

Herr,A., Meunier,D., Muller,I., Rump,A., Fundele,R., Ropers,H.H., and Nuber,U.A. (2003). Expression of mouse Tbx22 supports its role in palatogenesis and glossogenesis. Dev. Dyn. *226*, 579-586.

Herrmann,B.G., Labeit,S., Poustka,A., King,T.R., and Lehrach,H. (1990). Cloning of the T gene required in mesoderm formation in the mouse. Nature *343*, 617-622.

Hewitt,J., Lu,X., Gilbert,L., and Nanes,M.S. (2008). The muscle transcription factor MyoD promotes osteoblast differentiation by stimulation of the Osterix promoter. Endocrinology *149*, 3698-3707.

Higashihori,N., Buchtova,M., and Richman,J.M. (2010). The function and regulation of TBX22 in avian frontonasal morphogenesis. Dev. Dyn. *239*, 458-473.

Hinrichsen,K. (1985). The early development of morphology and patterns of the face in the human embryo. Adv. Anat. Embryol. Cell Biol. *98*, 1-79.

Hiroi,Y., Kudoh,S., Monzen,K., Ikeda,Y., Yazaki,Y., Nagai,R., and Komuro,I. (2001). Tbx5 associates with Nkx2-5 and synergistically promotes cardiomyocyte differentiation. Nat. Genet. *28*, 276-280.

Homanics,G.E., DeLorey,T.M., Firestone,L.L., Quinlan,J.J., Handforth,A., Harrison,N.L., Krasowski,M.D., Rick,C.E., Korpi,E.R., Makela,R., Brilliant,M.H., Hagiwara,N., Ferguson,C., Snyder,K., and Olsen,R.W. (1997). Mice devoid of gamma-aminobutyrate type A receptor beta3 subunit have epilepsy, cleft palate, and hypersensitive behavior. Proc. Natl. Acad. Sci. U. S. A *94*, 4143-4148.

Honein,M.A., Rasmussen,S.A., Reefhuis,J., Romitti,P.A., Lammer,E.J., Sun,L., and Correa,A. (2007). Maternal smoking and environmental tobacco smoke exposure and the risk of orofacial clefts. Epidemiology *18*, 226-233.

Horst,D., Ustanina,S., Sergi,C., Mikuz,G., Juergens,H., Braun,T., and Vorobyov,E. (2006). Comparative expression analysis of Pax3 and Pax7 during mouse myogenesis. Int. J. Dev. Biol. *50*, 47-54.

Hsu,L.C., Chang,W.C., Hoffmann,I., and Duester,G. (1999). Molecular analysis of two closely related mouse aldehyde dehydrogenase genes: identification of a role for Aldh1, but not Aldh-pb, in the biosynthesis of retinoic acid. Biochem. J. *339 (Pt 2)*, 387-395.

Hunt,P., Gulisano,M., Cook,M., Sham,M.H., Faiella,A., Wilkinson,D., Boncinelli,E., and Krumlauf,R. (1991). A distinct Hox code for the branchial region of the vertebrate head. Nature *353*, 861-864.

Ingraham,C.R., Kinoshita,A., Kondo,S., Yang,B., Sajan,S., Trout,K.J., Malik,M.I., Dunnwald,M., Goudy,S.L., Lovett,M., Murray,J.C., and Schutte,B.C. (2006). Abnormal skin, limb and craniofacial morphogenesis in mice deficient for interferon regulatory factor 6 (Irf6). Nat. Genet. *38*, 1335-1340.

Inoue,H., Kayano,S., Aoki,Y., Kure,S., Yamada,A., Hata,A., Matsubara,Y., and Suzuki,Y. (2008). Association of the GABRB3 gene with nonsyndromic oral clefts. Cleft Palate Craniofac. J. *45*, 261-266.

Ito,Y., Yeo,J.Y., Chytil,A., Han,J., Bringas,P., Jr., Nakajima,A., Shuler,C.F., Moses,H.L., and Chai,Y. (2003). Conditional inactivation of Tgfbr2 in cranial neural crest causes cleft palate and calvaria defects. Development *130*, 5269-5280.

Jerome,L.A. and Papaioannou,V.E. (2001). DiGeorge syndrome phenotype in mice mutant for the T-box gene, Tbx1. Nat. Genet. *27*, 286-291.

Jerome-Majewska,L.A., Jenkins,G.P., Ernstoff,E., Zindy,F., Sherr,C.J., and Papaioannou,V.E. (2005). Tbx3, the ulnar-mammary syndrome gene, and Tbx2 interact in mammary gland development through a p19Arf/p53-independent pathway. Dev. Dyn. *234*, 922-933.

Jezewski,P.A., Fang,P.K., Payne-Ferreira,T.L., and Yelick,P.C. (2009). Alternative splicing, phylogenetic analysis, and craniofacial expression of zebrafish tbx22. Dev. Dyn. *238*, 1605-1612.

Jezewski,P.A., Vieira,A.R., Nishimura,C., Ludwig,B., Johnson,M., O'Brien,S.E., Daack-Hirsch,S., Schultz,R.E., Weber,A., Nepomucena,B., Romitti,P.A., Christensen,K., Orioli,I.M., Castilla,E.E., Machida,J., Natsume,N., and Murray,J.C. (2003). Complete sequencing shows a role for MSX1 in non-syndromic cleft lip and palate. J. Med. Genet. *40*, 399-407.

Jiang,R., Bush,J.O., and Lidral,A.C. (2006). Development of the upper lip: morphogenetic and molecular mechanisms. Dev. Dyn. *235*, 1152-1166.

Jiang,R., Lan,Y., Chapman,H.D., Shawber,C., Norton,C.R., Serreze,D.V., Weinmaster,G., and Gridley,T. (1998). Defects in limb, craniofacial, and thymic development in Jagged2 mutant mice. Genes Dev. *12*, 1046-1057.

Jin,J.Z. and Ding,J. (2006). Analysis of cell migration, transdifferentiation and apoptosis during mouse secondary palate fusion. Development *133*, 3341-3347.

Jugessur,A., Farlie,P.G., and Kilpatrick,N. (2009). The genetics of isolated orofacial clefts: from genotypes to subphenotypes. Oral Dis. *15*, 437-453.

Jugessur,A. and Murray,J.C. (2005). Orofacial clefting: recent insights into a complex trait. Curr. Opin. Genet. Dev. *15*, 270-278.

Kaartinen,V., Voncken,J.W., Shuler,C., Warburton,D., Bu,D., Heisterkamp,N., and Groffen,J. (1995). Abnormal lung development and cleft palate in mice lacking TGF-beta 3 indicates defects of epithelial-mesenchymal interaction. Nat. Genet. *11*, 415-421.

Kalajzic,I., Kalajzic,Z., Hurley,M.M., Lichtler,A.C., and Rowe,D.W. (2003). Stage specific inhibition of osteoblast lineage differentiation by FGF2 and noggin. J. Cell Biochem. *88*, 1168-1176.

Kanno,K., Suzuki,Y., Yamada,A., Aoki,Y., Kure,S., and Matsubara,Y. (2004). Association between nonsyndromic cleft lip with or without cleft palate and the glutamic acid decarboxylase 67 gene in the Japanese population. Am. J. Med. Genet. A *127A*, 11-16.

Kantaputra,P.N., Sumitsawan,Y., Schutte,B.C., and Tochareontanaphol,C. (2002). Van der Woude syndrome with sensorineural hearing loss, large craniofacial sinuses, dental pulp stones, and minor limb anomalies: report of a four-generation Thai family. Am. J. Med. Genet. *108*, 275-280.

Kaplan,E.N. (1975). The occult submucous cleft palate. Cleft Palate J. *12*, 356-368.

Kassar-Duchossoy,L., Gayraud-Morel,B., Gomes,D., Rocancourt,D., Buckingham,M., Shinin,V., and Tajbakhsh,S. (2004). Mrf4 determines skeletal muscle identity in Myf5:Myod double-mutant mice. Nature *431*, 466-471.

Katagiri,T., Yamaguchi,A., Komaki,M., Abe,E., Takahashi,N., Ikeda,T., Rosen,V., Wozney,J.M., Fujisawa-Sehara,A., and Suda,T. (1994). Bone morphogenetic protein-2 converts the differentiation pathway of C2C12 myoblasts into the osteoblast lineage. J. Cell Biol. *127*, 1755-1766.

Kelly,R.G., Jerome-Majewska,L.A., and Papaioannou,V.E. (2004). The del22q11.2 candidate gene Tbx1 regulates branchiomeric myogenesis. Hum. Mol. Genet. *13*, 2829-2840.

Kelvin,D.J., Simard,G., and Connolly,J.A. (1989). FGF and EGF act synergistically to induce proliferation in BC3H1 myoblasts. J. Cell Physiol *138*, 267-272.

Kirk,E.P., Sunde,M., Costa,M.W., Rankin,S.A., Wolstein,O., Castro,M.L., Butler,T.L., Hyun,C., Guo,G., Otway,R., Mackay,J.P., Waddell,L.B., Cole,A.D., Hayward,C., Keogh,A., Macdonald,P., Griffiths,L., Fatkin,D., Sholler,G.F., Zorn,A.M., Feneley,M.P., Winlaw,D.S., and Harvey,R.P. (2007). Mutations in cardiac T-box factor gene TBX20 are associated with diverse cardiac pathologies, including defects of septation and valvulogenesis and cardiomyopathy. Am. J. Hum. Genet. *81*, 280-291.

Kispert,A. and Herrmann,B.G. (1993). The Brachyury gene encodes a novel DNA binding protein. EMBO J. *12*, 3211-3220.

Kispert,A., Koschorz,B., and Herrmann,B.G. (1995). The T protein encoded by Brachyury is a tissue-specific transcription factor. EMBO J. *14*, 4763-4772.

Klockars,T. (2007). Familial ankyloglossia (tongue-tie). Int. J. Pediatr. Otorhinolaryngol. *71*, 1321-1324.

Komori,T., Yagi,H., Nomura,S., Yamaguchi,A., Sasaki,K., Deguchi,K., Shimizu,Y., Bronson,R.T., Gao,Y.H., Inada,M., Sato,M., Okamoto,R., Kitamura,Y., Yoshiki,S., and Kishimoto,T. (1997). Targeted disruption of Cbfa1 results in a complete lack of bone formation owing to maturational arrest of osteoblasts. Cell *89*, 755-764.

Kondo,S., Schutte,B.C., Richardson,R.J., Bjork,B.C., Knight,A.S., Watanabe,Y., Howard,E., de Lima,R.L., Daack-Hirsch,S., Sander,A., Donald-McGinn,D.M., Zackai,E.H., Lammer,E.J., Aylsworth,A.S., Ardinger,H.H., Lidral,A.C., Pober,B.R., Moreno,L., rcos-Burgos,M., Valencia,C., Houdayer,C., Bahuau,M., Moretti-Ferreira,D., Richieri-Costa,A., Dixon,M.J., and Murray,J.C. (2002). Mutations in IRF6 cause Van der Woude and popliteal pterygium syndromes. Nat. Genet. *32*, 285-289.

Krapels,I.P., Rooij,I.A., Wevers,R.A., Zielhuis,G.A., Spauwen,P.H., Brussel,W., and Steegers-Theunissen,R.P. (2004a). Myo-inositol, glucose and zinc status as risk factors for non-syndromic cleft lip with or without cleft palate in offspring: a case-control study. BJOG. *111*, 661-668.

Krapels,I.P., van Rooij,I.A., Ocke,M.C., van Cleef,B.A., Kuijpers-Jagtman,A.M., and Steegers-Theunissen,R.P. (2004b). Maternal dietary B vitamin intake, other than folate, and the association with orofacial cleft in the offspring. Eur. J. Nutr. *43*, 7-14.

Krapels,I.P., van Rooij,I.A., Ocke,M.C., West,C.E., van der Horst,C.M., and Steegers-Theunissen,R.P. (2004c). Maternal nutritional status and the risk for orofacial cleft offspring in humans. J. Nutr. *134*, 3106-3113.

Krause,A., Zacharias,W., Camarata,T., Linkhart,B., Law,E., Lischke,A., Miljan,E., and Simon,H.G. (2004). Tbx5 and Tbx4 transcription factors interact with a new chicken PDZ-LIM protein in limb and heart development. Dev. Biol. *273*, 106-120.

Kreiborg,S. and Cohen,M.M., Jr. (1992). The oral manifestations of Apert syndrome. J. Craniofac. Genet. Dev. Biol. *12*, 41-48.

Krespi,Y.P., Husain,S., Levine,T.M., and Reede,D.L. (1987). Sublabial transseptal repair of choanal atresia or stenosis. Laryngoscope *97*, 1402-1406.

Kusch,T., Storck,T., Walldorf,U., and Reuter,R. (2002). Brachyury proteins regulate target genes through modular binding sites in a cooperative fashion. Genes Dev. *16*, 518-529.

LaBonne,C. and Bronner-Fraser,M. (1999). Molecular mechanisms of neural crest formation. Annu. Rev. Cell Dev. Biol. *15*, 81-112.

Lamolet,B., Pulichino,A.M., Lamonerie,T., Gauthier,Y., Brue,T., Enjalbert,A., and Drouin,J. (2001). A pituitary cell-restricted T box factor, Tpit, activates POMC transcription in cooperation with Pitx homeoproteins. Cell *104*, 849-859.

Lan,Y., Ovitt,C.E., Cho,E.S., Maltby,K.M., Wang,Q., and Jiang,R. (2004). Odd-skipped related 2 (Osr2) encodes a key intrinsic regulator of secondary palate growth and morphogenesis. Development *131*, 3207-3216.

Lander,E.S., Linton,L.M., Birren,B., Nusbaum,C., Zody,M.C., Baldwin,J., Devon,K., Dewar,K., Doyle,M., FitzHugh,W., Funke,R., Gage,D., Harris,K., Heaford,A., Howland,J., Kann,L., Lehoczky,J., Levine,R., McEwan,P.,

McKernan,K., Meldrim,J., Mesirov,J.P., Miranda,C., Morris,W., Naylor,J., Raymond,C., Rosetti,M., Santos,R., Sheridan,A., Sougnez,C., Stange-Thomann,N., Stojanovic,N., Subramanian,A., Wyman,D., Rogers,J., Sulston,J., Ainscough,R., Beck,S., Bentley,D., Burton,J., Clee,C., Carter,N., Coulson,A., Deadman,R., Deloukas,P., Dunham,A., Dunham,I., Durbin,R., French,L., Grafham,D., Gregory,S., Hubbard,T., Humphray,S., Hunt,A., Jones,M., Lloyd,C., McMurray,A., Matthews,L., Mercer,S., Milne,S., Mullikin,J.C., Mungall,A., Plumb,R., Ross,M., Shownkeen,R., Sims,S., Waterston,R.H., Wilson,R.K., Hillier,L.W., McPherson,J.D., Marra,M.A., Mardis,E.R., Fulton,L.A., Chinwalla,A.T., Pepin,K.H., Gish,W.R., Chissoe,S.L., Wendl,M.C., Delehaunty,K.D., Miner,T.L., Delehaunty,A., Kramer,J.B., Cook,L.L., Fulton,R.S., Johnson,D.L., Minx,P.J., Clifton,S.W., Hawkins,T., Branscomb,E., Predki,P., Richardson,P., Wenning,S., Slezak,T., Doggett,N., Cheng,J.F., Olsen,A., Lucas,S., Elkin,C., Uberbacher,E., Frazier,M., Gibbs,R.A., Muzny,D.M., Scherer,S.E., Bouck,J.B., Sodergren,E.J., Worley,K.C., Rives,C.M., Gorrell,J.H., Metzker,M.L., Naylor,S.L., Kucherlapati,R.S., Nelson,D.L., Weinstock,G.M., Sakaki,Y., Fujiyama,A., Hattori,M., Yada,T., Toyoda,A., Itoh,T., Kawagoe,C., Watanabe,H., Totoki,Y., Taylor,T., Weissenbach,J., Heilig,R., Saurin,W., Artiguenave,F., Brottier,P., Bruls,T., Pelletier,E., Robert,C., Wincker,P., Smith,D.R., Doucette-Stamm,L., Rubenfield,M., Weinstock,K., Lee,H.M., Dubois,J., Rosenthal,A., Platzer,M., Nyakatura,G., Taudien,S., Rump,A., Yang,H., Yu,J., Wang,J., Huang,G., Gu,J., Hood,L., Rowen,L., Madan,A., Qin,S., Davis,R.W., Federspiel,N.A., Abola,A.P., Proctor,M.J., Myers,R.M., Schmutz,J., Dickson,M., Grimwood,J., Cox,D.R., Olson,M.V., Kaul,R., Raymond,C., Shimizu,N., Kawasaki,K., Minoshima,S., Evans,G.A., Athanasiou,M., Schultz,R., Roe,B.A., Chen,F., Pan,H., Ramser,J., Lehrach,H., Reinhardt,R., McCombie,W.R., de la,B.M., Dedhia,N., Blocker,H., Hornischer,K., Nordsiek,G., Agarwala,R., Aravind,L., Bailey,J.A., Bateman,A., Batzoglou,S., Birney,E., Bork,P., Brown,D.G., Burge,C.B., Cerutti,L., Chen,H.C., Church,D., Clamp,M., Copley,R.R., Doerks,T., Eddy,S.R., Eichler,E.E., Furey,T.S., Galagan,J., Gilbert,J.G., Harmon,C., Hayashizaki,Y., Haussler,D., Hermjakob,H., Hokamp,K., Jang,W., Johnson,L.S., Jones,T.A., Kasif,S., Kaspryzk,A., Kennedy,S., Kent,W.J., Kitts,P., Koonin,E.V., Korf,I., Kulp,D., Lancet,D., Lowe,T.M., McLysaght,A., Mikkelsen,T., Moran,J.V., Mulder,N., Pollara,V.J., Ponting,C.P., Schuler,G., Schultz,J., Slater,G., Smit,A.F., Stupka,E., Szustakowski,J., Thierry-Mieg,D., Thierry-Mieg,J., Wagner,L., Wallis,J., Wheeler,R., Williams,A., Wolf,Y.I., Wolfe,K.H., Yang,S.P., Yeh,R.F., Collins,F., Guyer,M.S., Peterson,J., Felsenfeld,A., Wetterstrand,K.A., Patrinos,A., Morgan,M.J., de,J.P., Catanese,J.J., Osoegawa,K., Shizuya,H., Choi,S., and Chen,Y.J. (2001). Initial sequencing and analysis of the human genome. Nature *409*, 860-921.

Larsson,K.S. (1960). Studies on the closure of the secondary palate. II. Occurrence of sulpho-mucopolysaccharides in the palatine processes of the normal mouse embryo. Exp. Cell Res. *21*, 498-503.

Lassar,A.B., Davis,R.L., Wright,W.E., Kadesch,T., Murre,C., Voronova,A., Baltimore,D., and Weintraub,H. (1991). Functional activity of myogenic HLH proteins requires hetero-oligomerization with E12/E47-like proteins in vivo. Cell *66*, 305-315.

Laughon,A. (1991). DNA binding specificity of homeodomains. Biochemistry *30*, 11357-11367.

Lausch,E., Hermanns,P., Farin,H.F., Alanay,Y., Unger,S., Nikkel,S., Steinwender,C., Scherer,G., Spranger,J., Zabel,B., Kispert,A., and Superti-Furga,A. (2008). TBX15 mutations cause craniofacial dysmorphism, hypoplasia of scapula and pelvis, and short stature in Cousin syndrome. Am. J. Hum. Genet. *83*, 649-655.

Lekanne Deprez,R.H., Riegman,P.H., Groen,N.A., Warringa,U.L., van Biezen,N.A., Molijn,A.C., Bootsma,D., de Jong,P.J., Menon,A.G., Kley,N.A., et al. (1995). Cloning and characterization of MN1, a gene from chromosome 22q11, which is disrupted by a balanced translocation in a meningioma. Oncogene *10*, 1521-1528.

Leoyklang,P., Siriwan,P., and Shotelersuk,V. (2006). A mutation of the p63 gene in non-syndromic cleft lip. J. Med. Genet. *43*, e28.

Li,Q.Y., Newbury-Ecob,R.A., Terrett,J.A., Wilson,D.I., Curtis,A.R., Yi,C.H., Gebuhr,T., Bullen,P.J., Robson,S.C., Strachan,T., Bonnet,D., Lyonnet,S., Young,I.D., Raeburn,J.A., Buckler,A.J., Law,D.J., and Brook,J.D. (1997). Holt-Oram syndrome is caused by mutations in TBX5, a member of the Brachyury (T) gene family. Nat. Genet. *15*, 21-29.

Lian,J.B., Stein,G.S., Javed,A., van Wijnen,A.J., Stein,J.L., Montecino,M., Hassan,M.Q., Gaur,T., Lengner,C.J., and Young,D.W. (2006). Networks and hubs for the transcriptional control of osteoblastogenesis. Rev. Endocr. Metab Disord. *7*, 1-16.

Liao,J., Kochilas,L., Nowotschin,S., Arnold,J.S., Aggarwal,V.S., Epstein,J.A., Brown,M.C., Adams,J., and Morrow,B.E. (2004). Full spectrum of malformations in velo-cardio-facial syndrome/DiGeorge syndrome mouse models by altering Tbx1 dosage. Hum. Mol. Genet. *13*, 1577-1585.

Lie,R.T., Wilcox,A.J., and Skjaerven,R. (1994). A population-based study of the risk of recurrence of birth defects. N. Engl. J. Med. *331*, 1-4.

Lindsay,E.A., Vitelli,F., Su,H., Morishima,M., Huynh,T., Pramparo,T., Jurecic,V., Ogunrinu,G., Sutherland,H.F., Scambler,P.J., Bradley,A., and Baldini,A. (2001). Tbx1 haploinsufficieny in the DiGeorge syndrome region causes aortic arch defects in mice. Nature *410*, 97-101.

Lingbeek,M.E., Jacobs,J.J., and van Lohuizen,M. (2002). The T-box repressors TBX2 and TBX3 specifically regulate the tumor suppressor gene p14ARF via a variant T-site in the initiator. J. Biol. Chem. *277*, 26120-26127.

Little,J., Cardy,A., and Munger,R.G. (2004). Tobacco smoking and oral clefts: a meta-analysis. Bull. World Health Organ *82*, 213-218.

Liu,W., Lan,Y., Pauws,E., Meester-Smoor,M.A., Stanier,P., Zwarthoff,E.C., and Jiang,R. (2008). The Mn1 transcription factor acts upstream of Tbx22 and

preferentially regulates posterior palate growth in mice. Development *135*, 3959-3968.

Liu,W., Sun,X., Braut,A., Mishina,Y., Behringer,R.R., Mina,M., and Martin,J.F. (2005). Distinct functions for Bmp signaling in lip and palate fusion in mice. Development *132*, 1453-1461.

Louis,N., Evelegh,C., and Graham,F.L. (1997). Cloning and sequencing of the cellular-viral junctions from the human adenovirus type 5 transformed 293 cell line. Virology *233*, 423-429.

Lu,H., Jin,Y., and Tipoe,G.L. (2000). Alteration in the expression of bone morphogenetic protein-2,3,4,5 mRNA during pathogenesis of cleft palate in BALB/c mice. Arch. Oral Biol. *45*, 133-140.

Marcano,A.C., Doudney,K., Braybrook,C., Squires,R., Patton,M.A., Lees,M.M., Richieri-Costa,A., Lidral,A.C., Murray,J.C., Moore,G.E., and Stanier,P. (2004). TBX22 mutations are a frequent cause of cleft palate. J. Med. Genet. *41*, 68-74.

Mariani,T.J., Budhraja,V., Mecham,B.H., Gu,C.C., Watson,M.A., and Sadovsky,Y. (2003). A variable fold change threshold determines significance for expression microarrays. FASEB J. *17*, 321-323.

Martinez-Alvarez,C., Tudela,C., Perez-Miguelsanz,J., O'Kane,S., Puerta,J., and Ferguson,M.W. (2000). Medial edge epithelial cell fate during palatal fusion. Dev. Biol. *220*, 343-357.

Meester-Smoor,M.A., Vermeij,M., van Helmond,M.J., Molijn,A.C., van Wely,K.H., Hekman,A.C., Vermey-Keers,C., Riegman,P.H., and Zwarthoff,E.C. (2005). Targeted disruption of the Mn1 oncogene results in severe defects in development of membranous bones of the cranial skeleton. Mol. Cell Biol. *25*, 4229-4236.

Meyer,K.A., Werler,M.M., Hayes,C., and Mitchell,A.A. (2003). Low maternal alcohol consumption during pregnancy and oral clefts in offspring: the Slone Birth Defects Study. Birth Defects Res. A Clin. Mol. Teratol. *67*, 509-514.

Millard,D.R., Jr. and Latham,R.A. (1990). Improved primary surgical and dental treatment of clefts. Plast. Reconstr. Surg. *86*, 856-871.

Miloro,M., Ghali,G.E., Larsen,P.E., and Waite,P. (2004). Peterson's principles of oral and maxillofacial surgery. BC Decker Inc.

Milunsky,J.M., Maher,T.A., Zhao,G., Roberts,A.E., Stalker,H.J., Zori,R.T., Burch,M.N., Clemens,M., Mulliken,J.B., Smith,R., and Lin,A.E. (2008). TFAP2A mutations result in branchio-oculo-facial syndrome. Am. J. Hum. Genet. *82*, 1171-1177.

Minguillon,C. and Logan,M. (2003). The comparative genomics of T-box genes. Brief. Funct. Genomic. Proteomic. *2*, 224-233.

Minoux,M. and Rijli,F.M. (2010). Molecular mechanisms of cranial neural crest cell migration and patterning in craniofacial development. Development *137*, 2605-2621.

Molotkov,A., Deltour,L., Foglio,M.H., Cuenca,A.E., and Duester,G. (2002). Distinct retinoid metabolic functions for alcohol dehydrogenase genes Adh1 and Adh4 in protection against vitamin A toxicity or deficiency revealed in double null mutant mice. J. Biol. Chem. *277*, 13804-13811.

Moore,G.E., Ivens,A., Chambers,J., Farrall,M., Williamson,R., Page,D.C., Bjornsson,A., Arnason,A., and Jensson,O. (1987). Linkage of an X-chromosome cleft palate gene. Nature *326*, 91-92.

Moore,K.L. and Persaud,T.V.N. (2003). The Developing Human: Clinically Orientated Embryology. Saunders Elsevier Sciences.

Moretti,F., Marinari,B., Lo,I.N., Botti,E., Giunta,A., Spallone,G., Garaffo,G., Vernersson-Lindahl,E., Merlo,G., Mills,A.A., Ballaro,C., Alema,S., Chimenti,S., Guerrini,L., and Costanzo,A. (2010). A regulatory feedback loop involving p63 and IRF6 links the pathogenesis of 2 genetically different human ectodermal dysplasias. J. Clin. Invest *120*, 1570-1577.

Morita,H., Mazerbourg,S., Bouley,D.M., Luo,C.W., Kawamura,K., Kuwabara,Y., Baribault,H., Tian,H., and Hsueh,A.J. (2004). Neonatal lethality of LGR5 null mice is associated with ankyloglossia and gastrointestinal distension. Mol. Cell Biol. *24*, 9736-9743.

Morley,R.H., Lachani,K., Keefe,D., Gilchrist,M.J., Flicek,P., Smith,J.C., and Wardle,F.C. (2009). A gene regulatory network directed by zebrafish No tail accounts for its roles in mesoderm formation. Proc. Natl. Acad. Sci. U. S. A *106*, 3829-3834.

Morowati,S., Yasini,M., Ranjbar,R., Peivandi,A.A., and Ghadami,M. (2010). Familial ankyloglossia (tongue-tie): a case report. Acta Medica Iranica *48*, 123-124.

Moss,A.L., Piggott,R.W., and Jones,K.J. (1988). Submucous cleft palate. BMJ *297*, 85-86.

Mossey,P.A. and Little,J. (2002). Epidemiology of oral clefts: an international perspective. Cleft lip and palate: from origin to treatment. Wyszynski,D.F. ed. Oxford University Press, pp. 127-158.

Mossey,P.A., Little,J., Munger,R.G., Dixon,M.J., and Shaw,W.C. (2009). Cleft lip and palate. Lancet *374*, 1773-1785.

Muenke,M. (2002). The pit, the cleft and the web. Nat. Genet. *32*, 219-220.

Muller,C.W. and Herrmann,B.G. (1997). Crystallographic structure of the T domain-DNA complex of the Brachyury transcription factor. Nature *389*, 884-888.

Munger,R.G. (2002). Maternal nutrition and oral clefts. Cleft lip and palate: from origin to treatment. Wyszynski,D.F. ed. Oxford University Press, pp. 170-192.

Munger,R.G., Romitti,P.A., Daack-Hirsch,S., Burns,T.L., Murray,J.C., and Hanson,J. (1996). Maternal alcohol use and risk of orofacial cleft birth defects. Teratology *54*, 27-33.

Murray,J.C. (2002). Gene/environment causes of cleft lip and/or palate. Clin. Genet. *61*, 248-256.

Murray,J.C., Daack-Hirsch,S., Buetow,K.H., Munger,R., Espina,L., Paglinawan,N., Villanueva,E., Rary,J., Magee,K., and Magee,W. (1997). Clinical and epidemiologic studies of cleft lip and palate in the Philippines. Cleft Palate Craniofac. J. *34*, 7-10.

Murray,S.A., Oram,K.F., and Gridley,T. (2007). Multiple functions of Snail family genes during palate development in mice. Development *134*, 1789-1797.

Nabeshima,Y., Hanaoka,K., Hayasaka,M., Esumi,E., Li,S., Nonaka,I., and Nabeshima,Y. (1993). Myogenin gene disruption results in perinatal lethality because of severe muscle defect. Nature *364*, 532-535.

Naiche,L.A., Harrelson,Z., Kelly,R.G., and Papaioannou,V.E. (2005). T-box genes in vertebrate development. Annu. Rev. Genet. *39*, 219-239.

Naiche,L.A. and Papaioannou,V.E. (2003). Loss of Tbx4 blocks hindlimb development and affects vascularization and fusion of the allantois. Development *130*, 2681-2693.

Nakashima,K., Zhou,X., Kunkel,G., Zhang,Z., Deng,J.M., Behringer,R.R., and de Crombrugghe,B. (2002). The novel zinc finger-containing transcription factor osterix is required for osteoblast differentiation and bone formation. Cell *108*, 17-29.

Nemechek,A.J. and Amedee,R.G. (1994). Choanal atresia. J. La State Med. Soc. *146*, 337-340.

Ng,S.B., Bigham,A.W., Buckingham,K.J., Hannibal,M.C., McMillin,M.J., Gildersleeve,H.I., Beck,A.E., Tabor,H.K., Cooper,G.M., Mefford,H.C., Lee,C., Turner,E.H., Smith,J.D., Rieder,M.J., Yoshiura,K., Matsumoto,N., Ohta,T., Niikawa,N., Nickerson,D.A., Bamshad,M.J., and Shendure,J. (2010a). Exome sequencing identifies MLL2 mutations as a cause of Kabuki syndrome. Nat. Genet. *42*, 790-793.

Ng,S.B., Buckingham,K.J., Lee,C., Bigham,A.W., Tabor,H.K., Dent,K.M., Huff,C.D., Shannon,P.T., Jabs,E.W., Nickerson,D.A., Shendure,J., and Bamshad,M.J. (2010b). Exome sequencing identifies the cause of a mendelian disorder. Nat. Genet. *42*, 30-35.

Nie,X.G. (2005). Differential expression of Bmp2, Bmp4 and Bmp3 in embryonic development of mouse anterior and posterior palate. Chin Med. J. (Engl.) *118*, 1710-1716.

Noden,D.M. and Francis-West,P. (2006). The differentiation and morphogenesis of craniofacial muscles. Dev. Dyn. *235*, 1194-1218.

Nottoli,T., Hagopian-Donaldson,S., Zhang,J., Perkins,A., and Williams,T. (1998). AP-2-null cells disrupt morphogenesis of the eye, face, and limbs in chimeric mice. Proc. Natl. Acad. Sci. U. S. A *95*, 13714-13719.

Otto,F., Thornell,A.P., Crompton,T., Denzel,A., Gilmour,K.C., Rosewell,I.R., Stamp,G.W., Beddington,R.S., Mundlos,S., Olsen,B.R., Selby,P.B., and Owen,M.J. (1997). Cbfa1, a candidate gene for cleidocranial dysplasia syndrome, is essential for osteoblast differentiation and bone development. Cell *89*, 765-771.

Padmanabhan,R. and Ahmed,I. (1997). Retinoic acid-induced asymmetric craniofacial growth and cleft palate in the TO mouse fetus. Reprod. Toxicol. *11*, 843-860.

Papaioannou,V.E. (2001). T-box genes in development: from hydra to humans. Int. Rev. Cytol. *207*, 1-70.

Papapetrou,C., Edwards,Y.H., and Sowden,J.C. (1997). The T transcription factor functions as a dimer and exhibits a common human polymorphism Gly-177-Asp in the conserved DNA-binding domain. FEBS Lett. *409*, 201-206.

Park,K.W., Goo,J.H., Chung,H.S., Kim,H., Kim,D.H., and Park,W.J. (1998). Cloning of the genes encoding mouse cardiac and skeletal calsequestrins: expression pattern during embryogenesis. Gene *217*, 25-30.

Paulson,R.B., Hayes,T.G., and Sucheston,M.E. (1985). Scanning electron microscope study of tongue development in the CD-1 mouse fetus. J. Craniofac. Genet. Dev. Biol. *5*, 59-73.

Pauws,E., Hoshino,A., Bentley,L., Prajapati,S., Keller,C., Hammond,P., Martinez-Barbera,J.P., Moore,G.E., and Stanier,P. (2009a). *Tbx22*^{null} mice have a submucous cleft palate due to reduced palatal bone formation and also display ankyloglossia and choanal atresia phenotypes. Hum. Mol. Genet. *18*, 4171-4179.

Pauws,E., Moore,G.E., and Stanier,P. (2009b). A functional haplotype variant in the TBX22 promoter is associated with cleft palate and ankyloglossia. J. Med. Genet. *46*, 555-561.

Pauws,E. and Stanier,P. (2007). FGF signalling and SUMO modification: new players in the aetiology of cleft lip and/or palate. Trends Genet. *23*, 631-640.

Paxton,C., Zhao,H., Chin,Y., Langner,K., and Reecy,J. (2002). Murine Tbx2 contains domains that activate and repress gene transcription. Gene *283*, 117-124.

Peschiaroli,A., Figliola,R., Coltella,L., Strom,A., Valentini,A., D'Agnano,I., and Maione,R. (2002). MyoD induces apoptosis in the absence of RB function through a p21(WAF1)-dependent re-localization of cyclin/cdk complexes to the nucleus. Oncogene *21*, 8114-8127.

Peters,H., Neubuser,A., Kratochwil,K., and Balling,R. (1998). Pax9-deficient mice lack pharyngeal pouch derivatives and teeth and exhibit craniofacial and limb abnormalities. Genes Dev. *12*, 2735-2747.

Posch,M.G., Gramlich,M., Sunde,M., Schmitt,K.R., Lee,S.H., Richter,S., Kersten,A., Perrot,A., Panek,A.N., Al,K., I, Nemer,G., Megarbane,A., Dietz,R., Stiller,B., Berger,F., Harvey,R.P., and Ozcelik,C. (2010). A gain-of-function TBX20 mutation causes congenital atrial septal defects, patent foramen ovale and cardiac valve defects. J. Med. Genet. *47*, 230-235.

Prescott,N.J., Lees,M.M., Winter,R.M., and Malcolm,S. (2000). Identification of susceptibility loci for nonsyndromic cleft lip with or without cleft palate in a two stage genome scan of affected sib-pairs. Hum. Genet. *106*, 345-350.

Prescott,N.J., Winter,R.M., and Malcolm,S. (2001). Nonsyndromic cleft lip and palate: complex genetics and environmental effects. Ann. Hum. Genet. *65*, 505-515.

Proetzel,G., Pawlowski,S.A., Wiles,M.V., Yin,M., Boivin,G.P., Howles,P.N., Ding,J., Ferguson,M.W., and Doetschman,T. (1995). Transforming growth factor-beta 3 is required for secondary palate fusion. Nat. Genet. *11*, 409-414.

Pulichino,A.M., Vallette-Kasic,S., Couture,C., Gauthier,Y., Brue,T., David,M., Malpuech,G., Deal,C., Van Vliet,G., De,V.M., Riepe,F.G., Partsch,C.J., Sippell,W.G., Berberoglu,M., Atasay,B., and Drouin,J. (2003). Human and mouse TPIT gene mutations cause early onset pituitary ACTH deficiency. Genes Dev. *17*, 711-716.

Rahimov,F., Marazita,M.L., Visel,A., Cooper,M.E., Hitchler,M.J., Rubini,M., Domann,F.E., Govil,M., Christensen,K., Bille,C., Melbye,M., Jugessur,A., Lie,R.T., Wilcox,A.J., Fitzpatrick,D.R., Green,E.D., Mossey,P.A., Little,J., Steegers-Theunissen,R.P., Pennacchio,L.A., Schutte,B.C., and Murray,J.C. (2008). Disruption of an AP-2alpha binding site in an IRF6 enhancer is associated with cleft lip. Nat. Genet. *40*, 1341-1347.

Ramsden,J.D., Campisi,P., and Forte,V. (2009). Choanal atresia and choanal stenosis. Otolaryngol. Clin. North Am. *42*, 339-52.

Randall,P. (1965). A lip adhesion operation in cleft lip surgery. Plast. Reconstr. Surg. *35*, 371-376.

Rice,R., Spencer-Dene,B., Connor,E.C., Gritli-Linde,A., McMahon,A.P., Dickson,C., Thesleff,I., and Rice,D.P. (2004). Disruption of Fgf10/Fgfr2b-coordinated epithelial-mesenchymal interactions causes cleft palate. J. Clin. Invest *113*, 1692-1700.

Richardson,R.J., Dixon,J., Malhotra,S., Hardman,M.J., Knowles,L., Boot-Handford,R.P., Shore,P., Whitmarsh,A., and Dixon,M.J. (2006). Irf6 is a key determinant of the keratinocyte proliferation-differentiation switch. Nat. Genet. *38*, 1329-1334.

Rijli,F.M., Mark,M., Lakkaraju,S., Dierich,A., Dolle,P., and Chambon,P. (1993). A homeotic transformation is generated in the rostral branchial region of the head by disruption of Hoxa-2, which acts as a selector gene. Cell *75*, 1333-1349.

Riley,B.M., Mansilla,M.A., Ma,J., Daack-Hirsch,S., Maher,B.S., Raffensperger,L.M., Russo,E.T., Vieira,A.R., Dode,C., Mohammadi,M., Marazita,M.L., and Murray,J.C. (2007). Impaired FGF signaling contributes to cleft lip and palate. Proc. Natl. Acad. Sci. U. S. A *104*, 4512-4517.

Rinne,T., Brunner,H.G., and van Bokhoven,H. (2007). p63-associated disorders. Cell Cycle *6*, 262-268.

Rizzo,K.A., Kelly,M.F., and Lowry,L.D. (1989). Diagnosis and treatment of congenital choanal atresia. Trans. Pa Acad. Ophthalmol. Otolaryngol. *41*, 842-846.

Robson,E.J., He,S.J., and Eccles,M.R. (2006). A PANorama of PAX genes in cancer and development. Nat. Rev. Cancer *6*, 52-62.

Romitti,P.A., Lidral,A.C., Munger,R.G., Daack-Hirsch,S., Burns,T.L., and Murray,J.C. (1999). Candidate genes for nonsyndromic cleft lip and palate and maternal cigarette smoking and alcohol consumption: evaluation of genotype-environment interactions from a population-based case-control study of orofacial clefts. Teratology *59*, 39-50.

Rot-Nikcevic,I., Reddy,T., Downing,K.J., Belliveau,A.C., Hallgrimsson,B., Hall,B.K., and Kablar,B. (2006). Myf5-/- :MyoD-/- amyogenic fetuses reveal the importance of early contraction and static loading by striated muscle in mouse skeletogenesis. Dev. Genes Evol. *216*, 1-9.

Rudnicki,M.A., Braun,T., Hinuma,S., and Jaenisch,R. (1992). Inactivation of MyoD in mice leads to up-regulation of the myogenic HLH gene Myf-5 and results in apparently normal muscle development. Cell *71*, 383-390.

Rudnicki,M.A., Schnegelsberg,P.N., Stead,R.H., Braun,T., Arnold,H.H., and Jaenisch,R. (1993). MyoD or Myf-5 is required for the formation of skeletal muscle. Cell *75*, 1351-1359.

Ruffoli,R., Giambelluca,M.A., Scavuzzo,M.C., Bonfigli,D., Cristofani,R., Gabriele,M., Giuca,M.R., and Giannessi,F. (2005). Ankyloglossia: a morphofunctional investigation in children. Oral Dis. *11*, 170-174.

Russ,A.P., Wattler,S., Colledge,W.H., Aparicio,S.A., Carlton,M.B., Pearce,J.J., Barton,S.C., Surani,M.A., Ryan,K., Nehls,M.C., Wilson,V., and Evans,M.J. (2000). Eomesodermin is required for mouse trophoblast development and mesoderm formation. Nature *404*, 95-99.

Rutter,M., Wang,J., Huang,Z., Kuliszewski,M., and Post,M. (2010). Gli2 influences proliferation in the developing lung through regulation of cyclin expression. Am. J. Respir. Cell Mol. Biol. *42*, 615-625.

Ryan,A.K., Goodship,J.A., Wilson,D.I., Philip,N., Levy,A., Seidel,H., Schuffenhauer,S., Oechsler,H., Belohradsky,B., Prieur,M., Aurias,A., Raymond,F.L., Clayton-Smith,J., Hatchwell,E., McKeown,C., Beemer,F.A., Dallapiccola,B., Novelli,G., Hurst,J.A., Ignatius,J., Green,A.J., Winter,R.M., Brueton,L., Brondum-Nielsen,K., Stewart,F., van Essen,T., Patton,M., Paterson,J., Scambler,P.J. (1997). Spectrum of clinical features associated with interstitial chromosome 22q11 deletions: a European collaborative study. J. Med. Genet. *34*, 798-804.

Ryoo,H.M., Lee,M.H., and Kim,Y.J. (2006). Critical molecular switches involved in BMP-2-induced osteogenic differentiation of mesenchymal cells. Gene *366*, 51-57.

Sadler,T.W. (2004). Langman's Medical Embryology. Lippincott Williams & Wilkins.

Sakamoto,M.K., Nakamura,K., Handa,J., Kihara,T., and Tanimura,T. (1989). Morphogenesis of the secondary palate in mouse embryos with special reference to the development of rugae. Anat. Rec. *223*, 299-310.

Sartorelli,V. and Caretti,G. (2005). Mechanisms underlying the transcriptional regulation of skeletal myogenesis. Curr. Opin. Genet. Dev. *15*, 528-535.

Satokata,I. and Maas,R. (1994). Msx1 deficient mice exhibit cleft palate and abnormalities of craniofacial and tooth development. Nat. Genet. *6*, 348-356.

Scambler,P.J. (2000). The 22q11 deletion syndromes. Hum. Mol. Genet. *9*, 2421-2426.

Scapoli,L., Martinelli,M., Pezzetti,F., Carinci,F., Bodo,M., Tognon,M., and Carinci,P. (2002). Linkage disequilibrium between GABRB3 gene and nonsyndromic familial cleft lip with or without cleft palate. Hum. Genet. *110*, 15-20.

Schliekelman,P. and Slatkin,M. (2002). Multiplex relative risk and estimation of the number of loci underlying an inherited disease. Am. J. Hum. Genet. *71*, 1369-1385.

Schorle,H., Meier,P., Buchert,M., Jaenisch,R., and Mitchell,P.J. (1996). Transcription factor AP-2 essential for cranial closure and craniofacial development. Nature *381*, 235-238.

Schulte-Merker,S., Ho,R.K., Herrmann,B.G., and Nusslein-Volhard,C. (1992). The protein product of the zebrafish homologue of the mouse T gene is expressed in nuclei of the germ ring and the notochord of the early embryo. Development *116*, 1021-1032.

Schutte,B.C. and Murray,J.C. (1999). The many faces and factors of orofacial clefts. Hum. Mol. Genet. *8*, 1853-1859.

Scott,M.P., Tamkun,J.W., and Hartzell,G.W., III. (1989). The structure and function of the homeodomain. Biochim. Biophys. Acta *989*, 25-48.

Shamblott,M.J., Bugg,E.M., Lawler,A.M., and Gearhart,J.D. (2002). Craniofacial abnormalities resulting from targeted disruption of the murine Sim2 gene. Dev. Dyn. *224*, 373-380.

Shaw,G.M. and Lammer,E.J. (1999). Maternal periconceptional alcohol consumption and risk for orofacial clefts. J. Pediatr. *134*, 298-303.

Sherr,C.J. (1995). D-type cyclins. Trends Biochem. Sci. *20*, 187-190.

Shi,L., Reid,L.H., Jones,W.D., Shippy,R., Warrington,J.A., Baker,S.C., Collins,P.J., de,L.F., Kawasaki,E.S., Lee,K.Y., Luo,Y., Sun,Y.A., Willey,J.C., Setterquist,R.A., Fischer,G.M., Tong,W., Dragan,Y.P., Dix,D.J., Frueh,F.W., Goodsaid,F.M., Herman,D., Jensen,R.V., Johnson,C.D., Lobenhofer,E.K., Puri,R.K., Schrf,U., Thierry-Mieg,J., Wang,C., Wilson,M., Wolber,P.K., Zhang,L., Amur,S., Bao,W., Barbacioru,C.C., Lucas,A.B., Bertholet,V., Boysen,C., Bromley,B., Brown,D., Brunner,A., Canales,R., Cao,X.M., Cebula,T.A., Chen,J.J., Cheng,J., Chu,T.M., Chudin,E., Corson,J., Corton,J.C., Croner,L.J., Davies,C., Davison,T.S., Delenstarr,G., Deng,X., Dorris,D., Eklund,A.C., Fan,X.H., Fang,H., Fulmer-Smentek,S., Fuscoe,J.C., Gallagher,K., Ge,W., Guo,L., Guo,X., Hager,J., Haje,P.K., Han,J., Han,T., Harbottle,H.C., Harris,S.C., Hatchwell,E., Hauser,C.A., Hester,S., Hong,H., Hurban,P., Jackson,S.A., Ji,H., Knight,C.R., Kuo,W.P., LeClerc,J.E., Levy,S., Li,Q.Z., Liu,C., Liu,Y., Lombardi,M.J., Ma,Y., Magnuson,S.R., Maqsodi,B., McDaniel,T., Mei,N., Myklebost,O., Ning,B., Novoradovskaya,N., Orr,M.S., Osborn,T.W., Papallo,A., Patterson,T.A., Perkins,R.G., Peters,E.H., Peterson,R., Philips,K.L., Pine,P.S., Pusztai,L., Qian,F., Ren,H., Rosen,M., Rosenzweig,B.A., Samaha,R.R., Schena,M., Schroth,G.P., Shchegrova,S., Smith,D.D., Staedtler,F., Su,Z., Sun,H., Szallasi,Z., Tezak,Z., Thierry-Mieg,D., Thompson,K.L., Tikhonova,I., Turpaz,Y., Vallanat,B., Van,C., Walker,S.J., Wang,S.J., Wang,Y., Wolfinger,R., Wong,A., Wu,J., Xiao,C., Xie,Q., Xu,J., Yang,W., Zhang,L., Zhong,S., Zong,Y., and Slikker,W., Jr. (2006). The MicroArray Quality Control (MAQC) project shows inter- and intraplatform reproducibility of gene expression measurements. Nat. Biotechnol. *24*, 1151-1161.

Shi,L., Tong,W., Fang,H., Scherf,U., Han,J., Puri,R.K., Frueh,F.W., Goodsaid,F.M., Guo,L., Su,Z., Han,T., Fuscoe,J.C., Xu,Z.A., Patterson,T.A., Hong,H., Xie,Q., Perkins,R.G., Chen,J.J., and Casciano,D.A. (2005). Cross-platform comparability of microarray technology: intra-platform consistency and appropriate data analysis procedures are essential. BMC. Bioinformatics. *6 Suppl 2*, S12.

Shklover,J., Etzioni,S., Weisman-Shomer,P., Yafe,A., Bengal,E., and Fry,M. (2007). MyoD uses overlapping but distinct elements to bind E-box and tetraplex structures of regulatory sequences of muscle-specific genes. Nucleic Acids Res. *35*, 7087-7095.

Showell,C., Binder,O., and Conlon,F.L. (2004). T-box genes in early embryogenesis. Dev. Dyn. *229*, 201-218.

Shuler,C.F., Halpern,D.E., Guo,Y., and Sank,A.C. (1992). Medial edge epithelium fate traced by cell lineage analysis during epithelial-mesenchymal transformation in vivo. Dev. Biol. *154*, 318-330.

Singh,M.K., Petry,M., Haenig,B., Lescher,B., Leitges,M., and Kispert,A. (2005). The T-box transcription factor Tbx15 is required for skeletal development. Mech. Dev. *122*, 131-144.

Sinha,S., Abraham,S., Gronostajski,R.M., and Campbell,C.E. (2000). Differential DNA binding and transcription modulation by three T-box proteins, T, TBX1 and TBX2. Gene *258*, 15-29.

Sivertsen,A., Wilcox,A.J., Skjaerven,R., Vindenes,H.A., Abyholm,F., Harville,E., and Lie,R.T. (2008). Familial risk of oral clefts by morphological type and severity: population based cohort study of first degree relatives. BMJ *336*, 432-434.

Slovis,T.L., Renfro,B., Watts,F.B., Kuhns,L.R., Belenky,W., and Spoylar,J. (1985). Choanal atresia: precise CT evaluation. Radiology *155*, 345-348.

Smith,J.L. and Schoenwolf,G.C. (1997). Neurulation: coming to closure. Trends Neurosci. *20*, 510-517.

Snyder-Warwick,A.K., Perlyn,C.A., Pan,J., Yu,K., Zhang,L., and Ornitz,D.M. (2010). Analysis of a gain-of-function FGFR2 Crouzon mutation provides evidence of loss of function activity in the etiology of cleft palate. Proc. Natl. Acad. Sci. U. S. A *107*, 2515-2520.

Sozen,M.A., Suzuki,K., Tolarova,M.M., Bustos,T., Fernandez Iglesias,J.E., and Spritz,R.A. (2001). Mutation of PVRL1 is associated with sporadic, non-syndromic cleft lip/palate in northern Venezuela. Nat. Genet. *29*, 141-142.

Sperber,G.H., Gutterman,G.D., and Sperber,S.M. (2001). Craniofacial development, Volume 1. BC Decker Inc.

Stal,P.S. and Lindman,R. (2000). Characterisation of human soft palate muscles with respect to fibre types, myosins and capillary supply. J. Anat. *197 (Pt 2)*, 275-290.

Stal,S. and Hicks,M.J. (1998). Classic and occult submucous cleft palates: a histopathologic analysis. Cleft Palate Craniofac. J. *35*, 351-358.

Stanier,P., Forbes,S.A., Arnason,A., Bjornsson,A., Sveinbjornsdottir,E., Williamson,R., and Moore,G. (1993). The localization of a gene causing X-linked cleft palate and ankyloglossia (CPX) in an Icelandic kindred is between DXS326 and DXYS1X. Genomics *17*, 549-555.

Stanier,P. and Moore,G.E. (2004). Genetics of cleft lip and palate: syndromic genes contribute to the incidence of non-syndromic clefts. Hum. Mol. Genet. *13 Spec No 1*, R73-R81.

Stennard,F.A., Costa,M.W., Elliott,D.A., Rankin,S., Haast,S.J., Lai,D., McDonald,L.P., Niederreither,K., Dolle,P., Bruneau,B.G., Zorn,A.M., and Harvey,R.P. (2003). Cardiac T-box factor Tbx20 directly interacts with Nkx2-5, GATA4, and GATA5 in regulation of gene expression in the developing heart. Dev. Biol. *262*, 206-224.

Stennard,F.A., Costa,M.W., Lai,D., Biben,C., Furtado,M.B., Solloway,M.J., McCulley,D.J., Leimena,C., Preis,J.I., Dunwoodie,S.L., Elliott,D.E., Prall,O.W., Black,B.L., Fatkin,D., and Harvey,R.P. (2005). Murine T-box transcription factor Tbx20 acts as a repressor during heart development, and is essential for adult heart integrity, function and adaptation. Development *132*, 2451-2462.

Stoetzel,C., Riehm,S., Bennouna,G., V, Pelletier,V., Vigneron,J., Leheup,B., Marion,V., Helle,S., Danse,J.M., Thibault,C., Moulinier,L., Veillon,F., and Dollfus,H. (2009). Confirmation of TFAP2A gene involvement in branchio-oculo-facial syndrome (BOFS) and report of temporal bone anomalies. Am. J. Med. Genet. A *149A*, 2141-2146.

Stottmann,R.W., Bjork,B.C., Doyle,J.B., and Beier,D.R. (2010). Identification of a Van der Woude syndrome mutation in the cleft palate 1 mutant mouse. Genesis. *48*, 303-308.

Suter,V.G. and Bornstein,M.M. (2009). Ankyloglossia: facts and myths in diagnosis and treatment. J. Periodontol. *80*, 1204-1219.

Suzuki,K., Hu,D., Bustos,T., Zlotogora,J., Richieri-Costa,A., Helms,J.A., and Spritz,R.A. (2000). Mutations of PVRL1, encoding a cell-cell adhesion molecule/herpesvirus receptor, in cleft lip/palate-ectodermal dysplasia. Nat. Genet. *25*, 427-430.

Suzuki,S., Marazita,M.L., Cooper,M.E., Miwa,N., Hing,A., Jugessur,A., Natsume,N., Shimozato,K., Ohbayashi,N., Suzuki,Y., Niimi,T., Minami,K., Yamamoto,M., Altannamar,T.J., Erkhembaatar,T., Furukawa,H., Daack-Hirsch,S., L'heureux,J., Brandon,C.A., Weinberg,S.M., Neiswanger,K., Deleyiannis,F.W., de Salamanca,J.E., Vieira,A.R., Lidral,A.C., Martin,J.F., and Murray,J.C. (2009). Mutations in BMP4 are associated with subepithelial, microform, and overt cleft lip. Am. J. Hum. Genet. *84*, 406-411.

Tada,M. and Smith,J.C. (2001). T-targets: clues to understanding the functions of T-box proteins. Dev. Growth Differ. *43*, 1-11.

Tajbakhsh,S., Rocancourt,D., Cossu,G., and Buckingham,M. (1997). Redefining the genetic hierarchies controlling skeletal myogenesis: Pax-3 and Myf-5 act upstream of MyoD. Cell *89*, 127-138.

Takahara,S., Takigawa,T., and Shiota,K. (2004). Programmed cell death is not a necessary prerequisite for fusion of the fetal mouse palate. Int. J. Dev. Biol. *48*, 39-46.

Tam,P.P. and Beddington,R.S. (1992). Establishment and organization of germ layers in the gastrulating mouse embryo. Ciba Found. Symp. *165*, 27-41.

Tamarin,A. (1982). The formation of the primitive choanae and the junction of the primary and secondary palates in the mouse. Am. J. Anat. *165*, 319-337.

Tamura,T., Munger,R.G., Corcoran,C., Bacayao,J.Y., Nepomuceno,B., and Solon,F. (2005). Plasma zinc concentrations of mothers and the risk of nonsyndromic oral clefts in their children: a case-control study in the Philippines. Birth Defects Res. A Clin. Mol. Teratol. *73*, 612-616.

Thomason,H.A., Zhou,H., Kouwenhoven,E.N., Dotto,G.P., Restivo,G., Nguyen,B.C., Little,H., Dixon,M.J., van Bokhoven,H., and Dixon,J. (2010). Cooperation between the transcription factors p63 and IRF6 is essential to prevent cleft palate in mice. J. Clin. Invest *120*, 1561-1569.

Tollefson,T.T., Senders,C.W., and Sykes,J.M. (2008). Changing perspectives in cleft lip and palate: from acrylic to allele. Arch. Facial. Plast. Surg. *10*, 395-400.

Trotman,C.A., Hou,D., Burdi,A.R., Cohen,S.R., and Carlson,D.S. (1995). Histomorphologic analysis of the soft palate musculature in prenatal cleft and noncleft A/Jax mice. Cleft Palate Craniofac. J. *32*, 455-462.

Trowe,M.O., Maier,H., Schweizer,M., and Kispert,A. (2008). Deafness in mice lacking the T-box transcription factor Tbx18 in otic fibrocytes. Development *135*, 1725-1734.

Tzahor,E. (2009). Heart and craniofacial muscle development: a new developmental theme of distinct myogenic fields. Dev. Biol. *327*, 273-279.

van den Boogaard,M.J. (2004). *MSX1* and partial anodontia, orofacial clefting, and the Witkop syndrome. Inborn Errors of Development. The molecular basis of clinical disorders of morphogenesis. Epstein,J.C., Erickson,R.P., Wynshaw-Boris,A. ed. Oxford University Press, pp. 557-567.

van den Boogaard,M.J., Dorland,M., Beemer,F.A., and van Amstel,H.K. (2000). MSX1 mutation is associated with orofacial clefting and tooth agenesis in humans. Nat. Genet. *24*, 342-343.

van Bokhoven,H. and Brunner,H.G. (2002). Splitting p63. Am. J. Hum. Genet. *71*, 1-13.

Vanderas,A.P. (1987). Incidence of cleft lip, cleft palate, and cleft lip and palate among races: a review. Cleft Palate J. *24*, 216-225.

Vaziri,S.F., Hallberg,K., Harfe,B.D., McMahon,A.P., Linde,A., and Gritli-Linde,A. (2005). Fate-mapping of the epithelial seam during palatal fusion rules out epithelial-mesenchymal transformation. Dev. Biol. *285*, 490-495.

Vissers,L.E., van Ravenswaaij,C.M., Admiraal,R., Hurst,J.A., de Vries,B.B., Janssen,I.M., van der Vliet,W.A., Huys,E.H., de Jong,P.J., Hamel,B.C., Schoenmakers,E.F., Brunner,H.G., Veltman,J.A., and van Kessel,A.G. (2004). Mutations in a new member of the chromodomain gene family cause CHARGE syndrome. Nat. Genet. *36*, 955-957.

Wang,Q., Lan,Y., Cho,E.S., Maltby,K.M., and Jiang,R. (2005). Odd-skipped related 1 (Odd 1) is an essential regulator of heart and urogenital development. Dev. Biol. *288*, 582-594.

Wang,T., Tamakoshi,T., Uezato,T., Shu,F., Kanzaki-Kato,N., Fu,Y., Koseki,H., Yoshida,N., Sugiyama,T., and Miura,N. (2003). Forkhead transcription factor Foxf2 (LUN)-deficient mice exhibit abnormal development of secondary palate. Dev. Biol. *259*, 83-94.

Waterston,R.H., Lindblad-Toh,K., Birney,E., Rogers,J., Abril,J.F., Agarwal,P., Agarwala,R., Ainscough,R., Alexandersson,M., An,P., Antonarakis,S.E., Attwood,J., Baertsch,R., Bailey,J., Barlow,K., Beck,S., Berry,E., Birren,B., Bloom,T., Bork,P., Botcherby,M., Bray,N., Brent,M.R., Brown,D.G., Brown,S.D., Bult,C., Burton,J., Butler,J., Campbell,R.D., Carninci,P., Cawley,S., Chiaromonte,F., Chinwalla,A.T., Church,D.M., Clamp,M., Clee,C., Collins,F.S., Cook,L.L., Copley,R.R., Coulson,A., Couronne,O., Cuff,J., Curwen,V., Cutts,T., Daly,M., David,R., Davies,J., Delehaunty,K.D., Deri,J., Dermitzakis,E.T., Dewey,C., Dickens,N.J., Diekhans,M., Dodge,S., Dubchak,I., Dunn,D.M., Eddy,S.R., Elnitski,L., Emes,R.D., Eswara,P., Eyras,E., Felsenfeld,A., Fewell,G.A., Flicek,P., Foley,K., Frankel,W.N., Fulton,L.A., Fulton,R.S., Furey,T.S., Gage,D., Gibbs,R.A., Glusman,G., Gnerre,S., Goldman,N., Goodstadt,L., Grafham,D., Graves,T.A., Green,E.D., Gregory,S., Guigo,R., Guyer,M., Hardison,R.C., Haussler,D., Hayashizaki,Y., Hillier,L.W., Hinrichs,A., Hlavina,W., Holzer,T., Hsu,F., Hua,A., Hubbard,T., Hunt,A., Jackson,I., Jaffe,D.B., Johnson,L.S., Jones,M., Jones,T.A., Joy,A., Kamal,M., Karlsson,E.K., Karolchik,D., Kasprzyk,A., Kawai,J., Keibler,E., Kells,C., Kent,W.J., Kirby,A., Kolbe,D.L., Korf,I., Kucherlapati,R.S., Kulbokas,E.J., Kulp,D., Landers,T., Leger,J.P., Leonard,S., Letunic,I., Levine,R., Li,J., Li,M., Lloyd,C., Lucas,S., Ma,B., Maglott,D.R., Mardis,E.R., Matthews,L., Mauceli,E., Mayer,J.H., McCarthy,M., McCombie,W.R., McLaren,S., McLay,K., McPherson,J.D., Meldrim,J., Meredith,B., Mesirov,J.P., Miller,W., Miner,T.L., Mongin,E., Montgomery,K.T., Morgan,M., Mott,R., Mullikin,J.C., Muzny,D.M., Nash,W.E., Nelson,J.O., Nhan,M.N., Nicol,R., Ning,Z., Nusbaum,C., O'Connor,M.J., Okazaki,Y., Oliver,K., Overton-Larty,E., Pachter,L., Parra,G., Pepin,K.H., Peterson,J., Pevzner,P., Plumb,R., Pohl,C.S., Poliakov,A., Ponce,T.C., Ponting,C.P., Potter,S., Quail,M., Reymond,A., Roe,B.A., Roskin,K.M., Rubin,E.M., Rust,A.G., Santos,R., Sapojnikov,V., Schultz,B., Schultz,J., Schwartz,M.S., Schwartz,S., Scott,C., Seaman,S., Searle,S., Sharpe,T., Sheridan,A., Shownkeen,R., Sims,S., Singer,J.B., Slater,G., Smit,A., Smith,D.R., Spencer,B., Stabenau,A., Stange-Thomann,N., Sugnet,C., Suyama,M., Tesler,G., Thompson,J., Torrents,D., Trevaskis,E., Tromp,J., Ucla,C., Ureta-Vidal,A., Vinson,J.P., Von

Niederhausern,A.C., Wade,C.M., Wall,M., Weber,R.J., Weiss,R.B., Wendl,M.C., West,A.P., Wetterstrand,K., Wheeler,R., Whelan,S., Wierzbowski,J., Willey,D., Williams,S., Wilson,R.K., Winter,E., Worley,K.C., Wyman,D., Yang,S., Yang,S.P., Zdobnov,E.M., Zody,M.C., and Lander,E.S. (2002). Initial sequencing and comparative analysis of the mouse genome. Nature *420*, 520-562.

Welsh,I.C., Hagge-Greenberg,A., and O'Brien,T.P. (2007). A dosage-dependent role for Spry2 in growth and patterning during palate development. Mech. Dev. *124*, 746-761.

Weston,J.A., Yoshida,H., Robinson,V., Nishikawa,S., Fraser,S.T., and Nishikawa,S. (2004). Neural crest and the origin of ectomesenchyme: neural fold heterogeneity suggests an alternative hypothesis. Dev. Dyn. *229*, 118-130.

Wheeler,M.T., Snyder,E.C., Patterson,M.N., and Swoap,S.J. (1999). An E-box within the MHC IIB gene is bound by MyoD and is required for gene expression in fast muscle. Am. J. Physiol *276*, C1069-C1078.

Wide,K., Winbladh,B., and Kallen,B. (2004). Major malformations in infants exposed to antiepileptic drugs in utero, with emphasis on carbamazepine and valproic acid: a nation-wide, population-based register study. Acta Paediatr. *93*, 174-176.

Wilkie,A.O. and Morriss-Kay,G.M. (2001). Genetics of craniofacial development and malformation. Nat. Rev. Genet. *2*, 458-468.

Wilkinson,D.G. (1998). In Situ Hybridization: A Practical Approach. Oxford University Press.

Wilkinson,D.G., Bhatt,S., and Herrmann,B.G. (1990). Expression pattern of the mouse T gene and its role in mesoderm formation. Nature *343*, 657-659.

Wilson,D.I., Burn,J., Scambler,P., and Goodship,J. (1993). DiGeorge syndrome: part of CATCH 22. J. Med. Genet. *30*, 852-856.

Winograd,J., Reilly,M.P., Roe,R., Lutz,J., Laughner,E., Xu,X., Hu,L., Asakura,T., vander Kolk,C., Strandberg,J.D., and Semenza,G.L. (1997). Perinatal lethality and multiple craniofacial malformations in MSX2 transgenic mice. Hum. Mol. Genet. *6*, 369-379.

Wu,M., Li,J., Engleka,K.A., Zhou,B., Lu,M.M., Plotkin,J.B., and Epstein,J.A. (2008). Persistent expression of Pax3 in the neural crest causes cleft palate and defective osteogenesis in mice. J. Clin. Invest *118*, 2076-2087.

Wyszynski,D.F., Beaty,T.H., and Maestri,N.E. (1996). Genetics of nonsyndromic oral clefts revisited. Cleft Palate Craniofac. J. *33*, 406-417.

Wyszynski,D.F., Zeiger,J., Tilli,M.T., Bailey-Wilson,J.E., and Beaty,T.H. (1998). Survey of genetic counselors and clinical geneticists regarding recurrence risks for

families with nonsyndromic cleft lip with or without cleft palate. Am. J. Med. Genet. *79*, 184-190.

Xu,X., Han,J., Ito,Y., Bringas,P., Jr., Urata,M.M., and Chai,Y. (2006). Cell autonomous requirement for Tgfbr2 in the disappearance of medial edge epithelium during palatal fusion. Dev. Biol. *297*, 238-248.

Yaffe,D. and Saxel,O. (1977). Serial passaging and differentiation of myogenic cells isolated from dystrophic mouse muscle. Nature *270*, 725-727.

Yang,A., Schweitzer,R., Sun,D., Kaghad,M., Walker,N., Bronson,R.T., Tabin,C., Sharpe,A., Caput,D., Crum,C., and McKeon,F. (1999). p63 is essential for regenerative proliferation in limb, craniofacial and epithelial development. Nature *398*, 714-718.

Yazdy,M.M., Honein,M.A., and Xing,J. (2007). Reduction in orofacial clefts following folic acid fortification of the U.S. grain supply. Birth Defects Res. A Clin. Mol. Teratol. *79*, 16-23.

Yoshida,T., Vivatbutsiri,P., Morriss-Kay,G., Saga,Y., and Iseki,S. (2008). Cell lineage in mammalian craniofacial mesenchyme. Mech. Dev. *125*, 797-808.

Young,N.M., Wat,S., Diewert,V.M., Browder,L.W., and Hallgrimsson,B. (2007). Comparative morphometrics of embryonic facial morphogenesis: implications for cleft-lip etiology. Anat. Rec. *290*, 123-139.

Yu,L., Gu,S., Alappat,S., Song,Y., Yan,M., Zhang,X., Zhang,G., Jiang,Y., Zhang,Z., Zhang,Y., and Chen,Y. (2005). Shox2-deficient mice exhibit a rare type of incomplete clefting of the secondary palate. Development *132*, 4397-4406.

Zaragoza,M.V., Lewis,L.E., Sun,G., Wang,E., Li,L., Said-Salman,I., Feucht,L., and Huang,T. (2004). Identification of the TBX5 transactivating domain and the nuclear localization signal. Gene *330*, 9-18.

Zeiger,J.S., Hetmanski,J.B., Beaty,T.H., vander Kolk,C.A., Wyszynski,D.F., Bailey-Wilson,J.E., de Luna,R.O., Perandones,C., Tolarova,M.M., Mosby,T., Bennun,R., Segovia,M., Calda,P., Pugh,E.W., Doheny,K., and McIntosh,I. (2003). Evidence for linkage of nonsyndromic cleft lip with or without cleft palate to a region on chromosome 2. Eur. J. Hum. Genet. *11*, 835-839.

Zhang,L., Yoshimura,Y., Hatta,T., and Otani,H. (1999). Myogenic determination and differentiation of the mouse palatal muscle in relation to the developing mandibular nerve. J. Dent. Res. *78*, 1417-1425.

Zhang,X., Dowd,D.R., Moore,M.C., Kranenburg,T.A., Meester-Smoor,M.A., Zwarthoff,E.C., and MacDonald,P.N. (2009). Meningioma 1 is required for appropriate osteoblast proliferation, motility, differentiation, and function. J. Biol. Chem. *284*, 18174-18183.

Zhang,Z., Song,Y., Zhao,X., Zhang,X., Fermin,C., and Chen,Y. (2002). Rescue of cleft palate in Msx1-deficient mice by transgenic Bmp4 reveals a network of BMP and Shh signaling in the regulation of mammalian palatogenesis. Development *129*, 4135-4146.

Zhao,Y., Guo,Y.J., Tomac,A.C., Taylor,N.R., Grinberg,A., Lee,E.J., Huang,S., and Westphal,H. (1999). Isolated cleft palate in mice with a targeted mutation of the LIM homeobox gene lhx8. Proc. Natl. Acad. Sci. U. S. A *96*, 15002-15006.

Zhou,H.M., Wang,J., Rogers,R., and Conway,S.J. (2008). Lineage-specific responses to reduced embryonic Pax3 expression levels. Dev. Biol. *315*, 369-382.

Zimmerman,E.F. (1985). Role of neurotransmitters in palate development and teratologic implications. Prog. Clin. Biol. Res. *171*, 283-294.

Zucchero,T.M., Cooper,M.E., Maher,B.S., Daack-Hirsch,S., Nepomuceno,B., Ribeiro,L., Caprau,D., Christensen,K., Suzuki,Y., Machida,J., Natsume,N., Yoshiura,K., Vieira,A.R., Orioli,I.M., Castilla,E.E., Moreno,L., Arcos-Burgos,M., Lidral,A.C., Field,L.L., Liu,Y.E., Ray,A., Goldstein,T.H., Schultz,R.E., Shi,M., Johnson,M.K., Kondo,S., Schutte,B.C., Marazita,M.L., and Murray,J.C. (2004). Interferon regulatory factor 6 (IRF6) gene variants and the risk of isolated cleft lip or palate. N. Engl. J. Med. *351*, 769-780.

APPENDIX

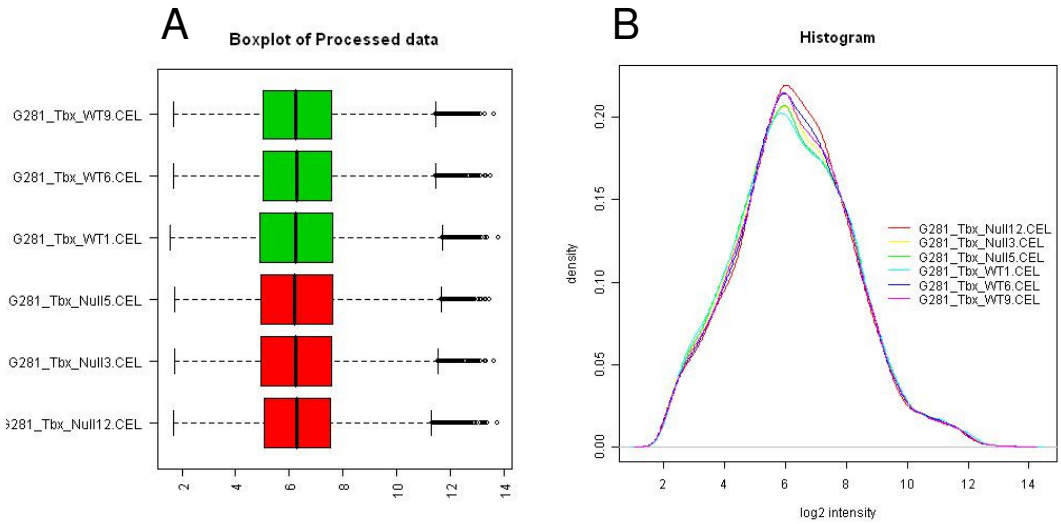
A
Boxplot of Processed data
G281_Tbx_WT9.CEL
G281_Tbx_WT6.CEL
G281_Tbx_WT1.CEL
G281_Tbx_Null5.CEL
G281_Tbx_Null3.CEL
G281_Tbx_Null12.CEL
2
4
6
8
10
12
14
B
Histogram
density
0.00
0.05
0.10
0.15
0.20
G281_Tbx_Null12.CEL
G281_Tbx_Null3.CEL
G281_Tbx_Null5.CEL
G281_Tbx_WT1.CEL
G281_Tbx_WT6.CEL
G281_Tbx_WT9.CEL
log2 intensity

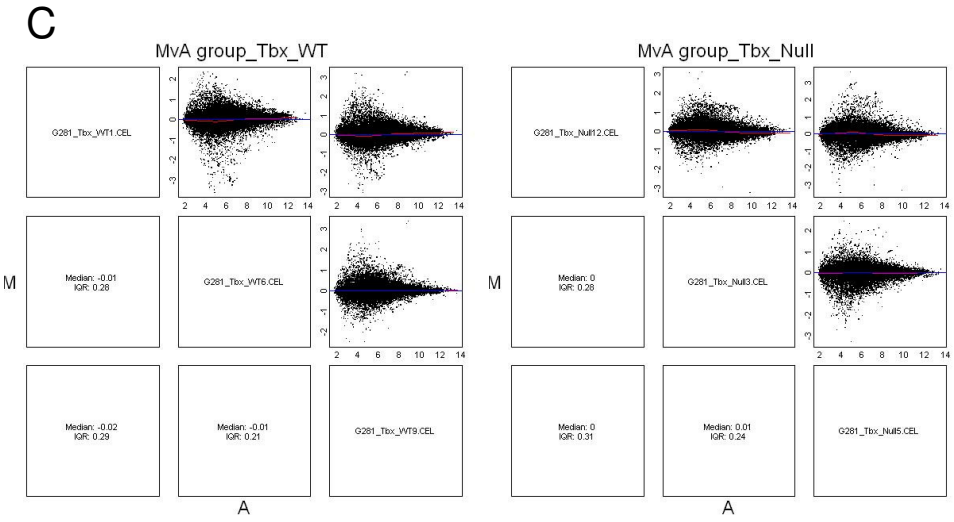
C
MvA group_Tbx_WT
MvA group_Tbx_Null
G281_Tbx_WT1.CEL
G281_Tbx_WT6.CEL
G281_Tbx_WT9.CEL
G281_Tbx_Null12.CEL
G281_Tbx_Null3.CEL
G281_Tbx_Null5.CEL
Median: -0.01
IQR: 0.28
Median: -0.02
IQR: 0.29
Median: -0.01
IQR: 0.21
Median: 0
IQR: 0.28
Median: 0
IQR: 0.31
Median: 0.01
IQR: 0.24
M
A

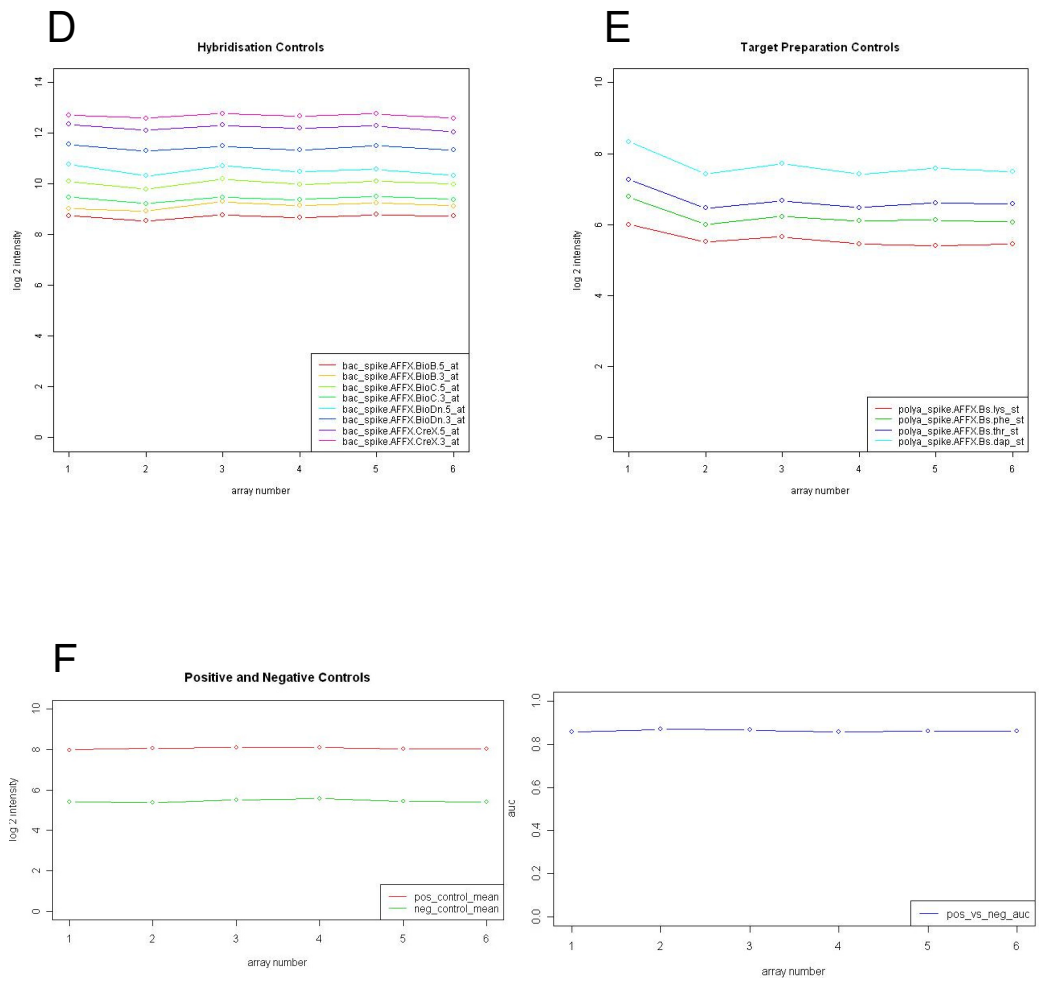

Appendix Figure 1.1 Affymetrix quality control analysis
Boxplots are used to identify any outliers (A). All the boxes looked similar indicating all the samples used had the same median and similar intensity range.

The density plot shows any differences in the distributions of the density of the probe intensities (B). Here, all intensity distributions representing each array (or sample) overlap well.

MvA plots allow a graphical view to see fold changes and fluorescence intensity, and are used to check the reproducibility of biological replicates (C). The x-axis is the average intensity of each probeset and the y-axis is the log2 fold change between the intensity value of each probeset. The graphs indicate good agreement between biological replicates.

Control probesets are used to identify problems with hybridisation and/or chip (Bac) and target preparation (PolyA+). Both Bac (D) and PolyA+ (E) probesets displayed the expected rank order of log2 intensity values for the six arrays. Also, signal value comparison between positive and negative controls as indicated by AUC (values between 0.8 and 0.9 are considered typical) showed good separation between positive and negative controls (F).

Cleft palate candidate genes

ID	Gene symbol	Gene description	Regulation	FC	p-value
10423654	*Osr2*	Odd-skipped related 2 (Drosophila)	up	1.14	0.14
10529651	*Msx1*	Homeobox, msh-like 1	up	1.09	0.69
10437055	*Sim2*	Single-minded homolog 2 (Drosophila)	up	1.05	0.35
10419261	*Bmp4*	Bone morphogenetic protein 4	up	1.05	0.38
10401673	*Tgfb3*	Transforming growth factor, beta 3	up	1.04	0.46
10553773	*Gabrb3*	Gamma-aminobutyric acid (GABA-A) receptor, subunit beta 3	up	1.04	0.54
10352815	*Irf6*	Interferon regulatory factor 6	up	1.03	0.71
10472707	*Gad1*	Glutamic acid decarboxylase 1	up	1.03	0.48
10502961	*Lhx8*	LIM homeobox protein 8	down	1.03	0.79
10568436	*Fgfr2*	Fibroblast growth factor receptor 2	down	1.03	0.60
10492689	*Pdgfc*	Platelet-derived growth factor, C polypeptide	down	1.02	0.65
10407350	*Fgf10*	Fibroblast growth factor 10	down	1.01	0.79
10402808	*Jag2*	Jagged 2	down	1.01	0.80
10504817	*Tgfbr1*	Transforming growth factor, beta receptor I	down	1.00	0.83
10597518	*Tgfbr2*	Transforming growth factor, beta receptor II	down	1.00	0.99

Ossification related genes

ID	Gene symbol	Gene description	Regulation	FC	p-value
10523701	*Ibsp* (Bone sialoprotein)	Integrin binding sialoprotein	up	1.12	0.83
10499363	*Bglap1* (*Osteocalcin*)	Bone gamma carboxyglutamate protein 1	up	1.09	0.62
10380419	*Col1a1*	Collagen, type I, alpha 1	up	1.06	0.55
10491699	*Fgf2*	Fibroblast growth factor 2	up	1.05	0.42
10536220	*Col1a2*	Collagen, type I, alpha 2	up	1.03	0.78
10517587	*Alpl*	Alkaline phosphatase, liver/bone/kidney	up	1.02	0.44
10476395	*Bmp2*	Bone morphogenetic protein 2	down	1.13	0.21
10409616	*Spock1* (*Osteonectin*)	Sparc/osteonectin, cwcv and kazal-like domains proteoglycan 1	down	1.11	0.17
10523717	*Spp1* (*Osteopontin*)	Secreted phosphoprotein 1	down	1.05	0.64
10433003	*Sp7* (*Osterix*)	Trans-acting transcription factor 7	down	1.02	0.86
10451061	*Runx2*	Runt related transcription factor 2	down	1.01	0.91

Appendix Table 1.1 Microarray data for the cleft palate candidate and ossification related genes
Some of the cleft palate candidate genes known to be important for normal palate development and genes related to ossification were compared between the wt and *Tbx22* null palatal shelves at E13.5, and tabulated with the Affymetrix Transcripts Cluster ID, gene symbol, gene description, regulation, fold change and p-values.

HEK 293T	Well	Firefly luciferase	*Renilla* luciferase	Firefly/*Renilla*
pGL3	A01	726	3036	0.24
pGL3-MyoD	A02	10972	2452	4.47
pGL3-MyoD/pcDNA3.1(-) 2.5 ng	A03	16036	3466	4.63
pGL3-MyoD/pcDNA3.1 (-) 10 ng	A04	15640	2938	5.32
pGL3-MyoD/wtTBX22 2.5 ng	A05	18822	5504	3.42
pGL3-MyoD/wtTBX22 10 ng	A06	10648	4564	2.33
pGL3-MyoD/GFP 2.5 ng	A07	15500	3146	4.93
pGL3-MyoD/GFP 10 ng	A08	7682	1588	4.84
pGL3	B01	466	2364	0.20
pGL3-MyoD	B02	9740	2396	4.07
pGL3-MyoD/pcDNA3.1(-) 2.5 ng	B03	9354	2382	3.93
pGL3-MyoD/pcDNA3.1 (-) 10 ng	B04	9660	2030	4.76
pGL3-MyoD/wtTBX22 2.5 ng	B05	10298	3916	2.63
pGL3-MyoD/wtTBX22 10 ng	B06	5564	2574	2.16
pGL3-MyoD/GFP 2.5 ng	B07	12308	2844	4.33
pGL3-MyoD/GFP 10 ng	B08	8512	1662	5.12
pGL3	C01	528	2544	0.21
pGL3-MyoD	C02	8122	2040	3.98
pGL3-MyoD/pcDNA3.1(-) 2.5 ng	C03	11486	2628	4.37
pGL3-MyoD/pcDNA3.1 (-) 10 ng	C04	11864	2326	5.10
pGL3-MyoD/wtTBX22 2.5 ng	C05	14650	3688	3.97
pGL3-MyoD/wtTBX22 10 ng	C06	5956	2858	2.08
pGL3-MyoD/GFP 2.5 ng	C07	9248	2352	3.93
pGL3-MyoD/GFP 10 ng	C08	7020	1488	4.72
pGL3	D01	538	2882	0.19
pGL3-MyoD	D02	6494	1414	4.59
pGL3-MyoD/pcDNA3.1(-) 2.5 ng	D03	7710	2076	3.71
pGL3-MyoD/pcDNA3.1 (-) 10 ng	D04	6176	1364	4.53
pGL3-MyoD/wtTBX22 2.5 ng	D05	10740	3382	3.18
pGL3-MyoD/wtTBX22 10 ng	D06	7540	2992	2.52
pGL3-MyoD/GFP 2.5 ng	D07	10070	2248	4.48
pGL3-MyoD/GFP 10 ng	D08	6646	1354	4.91

Appendix Table 1.2 Sample luciferase reporter assay (raw data)
The luciferase/*Renilla* ratio was calculated from the Firefly and *Renilla* luciferase raw values.

PUBLICATIONS PERTAINING TO THE WORK WITHIN THIS THESIS

1. Pauws,E., Hoshino,A., Bentley,L., Prajapati,S., Keller,C., Hammond,P., Martinez-Barbera,J.P., Moore,G.E., and Stanier,P. (2009). *Tbx22*^{null} mice have a submucous cleft palate due to reduced palatal bone formation and also display ankyloglossia and choanal atresia phenotypes. Hum. Mol. Genet. *18*, 4171-4179.

2. Kantaputra,P.N., Paramee,M., Kaewkhampa,A., Hoshino,A., Lees,M., McEntagart,M., Masrour,N., Moore,G.E., Pauws,E., and Stanier,P. (2011). Cleft lip with cleft palate, ankyloglossia, and hypodontia are associated with TBX22 mutations. J Dent Res – in press.

Human Molecular Genetics, 2009, Vol. 18, No. 21 ***4171–4179***
doi:10.1093/hmg/ddp368
Advance Access published on July 31, 2009

Tbx22^{null} mice have a submucous cleft palate due to reduced palatal bone formation and also display ankyloglossia and choanal atresia phenotypes

Erwin Pauws[1], Aya Hoshino[1], Lucy Bentley[1], Suresh Prajapati[2], Charles Keller[2], Peter Hammond[1], Juan-Pedro Martinez-Barbera[1], Gudrun E. Moore[1] and Philip Stanier[1,*]

[1]UCL Institute of Child Health, 30 Guilford Street, WC1N 1EH London, UK and [2]Greehey Children's Cancer Research Institute, The University of Texas Health Science Center, San Antonio, TX, USA

Received May 29, 2009; Revised and Accepted July 29, 2009

Craniofacial defects involving the lip and/or palate are among the most common human birth defects. X-linked cleft palate and ankyloglossia results from loss-of-function mutations in the gene encoding the T-box transcription factor TBX22. Further studies show that *TBX22* mutations are also found in around 5% of non-syndromic cleft palate patients. Although palate defects are obvious at birth, the underlying developmental pathogenesis remains unclear. Here, we report a *Tbx22*^{null} mouse, which has a submucous cleft palate (SMCP) and ankyloglossia, similar to the human phenotype, with a small minority showing overt clefts. We also find persistent oro-nasal membranes or, in some mice a partial rupture, resulting in choanal atresia. Each of these defects can cause severe breathing and/or feeding difficulties in the newborn pups, which results in ~50% post-natal lethality. Analysis of the craniofacial skeleton demonstrates a marked reduction in bone formation in the posterior hard palate, resulting in the classic notch associated with SMCP. Our results suggest that *Tbx22* plays an important role in the osteogenic patterning of the posterior hard palate. Ossification is severely reduced after condensation of the palatal mesenchyme, resulting from a delay in the maturation of osteoblasts. Rather than having a major role in palatal shelf closure, we show that *Tbx22* is an important determinant for intramembranous bone formation in the posterior hard palate, which underpins normal palate development and function. These findings could have important implications for the molecular diagnosis in patients with isolated SMCP and/or unexplained choanal atresia.

INTRODUCTION

Cleft palate (CP) is a common birth defect with an incidence of 1 : 1500 (1). CP may present either as an isolated congenital abnormality or in association with other clinical features, as part of a syndrome (2). Submucous cleft palate (SMCP) forms a clinically important sub-group, which may be at least as common as overt CP, with a reported incidence of 1 : 1250 (3) to 1 : 5000 (4). SMCP can be characterized as bifid uvula, a notch in the posterior hard palate and/or palatal muscle diastasis (5). In the latter, the palatine muscle inserts incorrectly onto the hard palate causing velopharyngeal insufficiency (VPI) (6). Whether muscle diastasis is caused by a defect in palate myogenesis, by a malformation of the posterior palatal bone, or both is currently not clear. When one or more of the characteristic anatomical features is present without VPI, the term occult SMCP is sometimes used. SMCP-related VPI is considered part of the clinical spectrum of CP and is a common cause of feeding difficulties, speech problems and otitis media-related hearing loss.

Human *TBX22* encodes a T-box protein containing transcriptional repressor activity and is mutated in X-linked cleft palate and ankyloglossia (CPX; MIM303400) (7–10). CPX is an X-linked semi-dominant craniofacial disorder affecting male patients and approximately one-third of female carriers (7). Ankyloglossia without a CP is seen in many carrier females and occasionally in males, indicating a partial penetrance (8,11). Similarly, a detectable ankyloglossia is not always present in CPX patients who are affected by a CP.

*To whom correspondence should be addressed. Tel: +44 2079052867; Fax: +44 2079052832; Email: p.stanier@ich.ucl.ac.uk

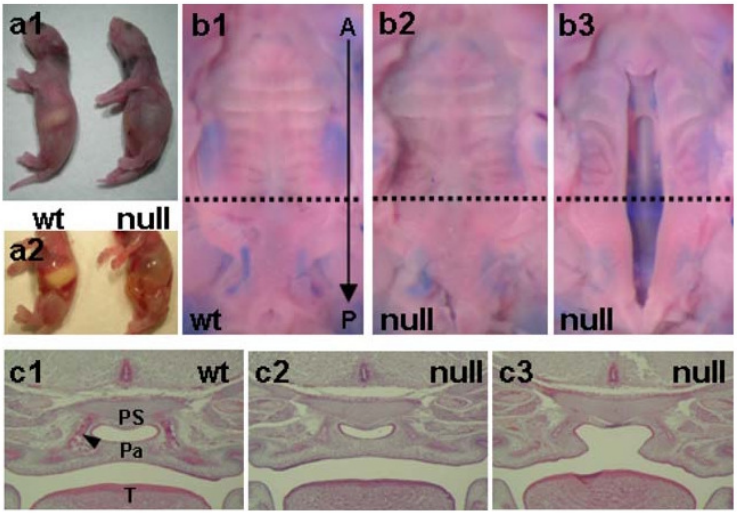

Figure 1. *Tbx22*^{null} mice show submucous cleft palate. (**A**) Approximately 50% of mutant animals die within 24 h post-partum, exhibiting breathing problems and inability to suckle. Their overall anatomy is grossly normal but with air rather than milk in the stomach. (**B**) Male hemizygous *Tbx22*^{null} (−/Y) and female homozygous animals (data not shown) are affected, displaying submucous (b2) or overt (b3) clefts. SMCP can be identified by the irregular and more widely spaced location of the rugae. (**C**) Submucous or overt cleft palate can be observed in E15.5 coronal sections through the posterior end of the hard palate (dotted line). Bone mineralization (pink osteoid) can be seen in the lateral parts of the wild-type fused palate (arrow), while in the SMCP and CP mice, ossification is severely reduced. Pa = palate, PS = pre-sphenoid, T = tongue, A = anterior, *P* = posterior.

In general, there is high inter- and intrafamilial phenotypic variation which ranges from ankyloglossia alone, SMCP, bifid uvula or cleft of the soft and hard palate, all with or without ankyloglossia (7–9,12). Loss-of-function mutations include frame shift, splice site and nonsense mutations, along with missense changes which have been shown to impair DNA binding and sumoylation (13). Sequence variation in the *TBX22* promoter has recently been associated as a risk factor for CP, but predominantly in patients with ankyloglossia (14), although coding region mutations are also found in 4–8% of non-syndromic cases of CP (8,9).

TBX22 is part of the TBX1 sub-family and shares a close evolutionary origin with TBX15 and TBX18 (15). Members of this gene family (*Tbx1*, *Tbx15*, *Tbx10*, *Tbx18* and *Tbx22*) are all expressed in the craniofacial area, and mutation of *Tbx1* and *Tbx10* results in CP phenotypes (16,17). Additionally, haploinsufficiency of the *TBX1* gene is the major gene responsible for DiGeorge syndrome, where one of the features is CP (DGS; MIM188400). Expression of *Tbx22* in mouse and chicken is seen in the posterior palate, caudal tongue, nasal mesenchyme, extra-ocular mesenchyme (Supplementary Material, Fig. S1) and early somites (12,18,19). This pattern correlates well with the phenotypic characteristics found in CPX patients but suggests additional roles for TBX22 in development. Although the defects associated with mutations in *TBX22* are obvious at birth, the underlying developmental pathogenesis remains unclear.

Here, we have created a *Tbx22*^{null} mouse, which has a SMCP, similar to the human phenotype. In addition to ankyloglossia, we find oro-nasal defects including choanal atresia. The latter defect causes post-natal lethality in ∼50% of mutant mice. Analysis of the craniofacial skeleton demonstrates a marked reduction in bone formation of the vomer and in the posterior hard palate, resulting in the classic notch associated with SMCP. Ossification is severely reduced after condensation of the palatal mesenchyme, resulting from a delay in the differentiation and/or maturation of osteoblasts. Rather than being involved in palatal shelf closure, we show that TBX22 is a major determinant for intramembranous bone formation in the posterior hard palate, which underpins both normal palate development and function.

RESULTS

Generation of mice lacking *Tbx22*

To study the molecular and cellular pathogenesis of CPX, we disrupted mouse *Tbx22* by gene targeting (Supplementary Material, Fig. S1). In brief, we introduced loxP sites flanking the first three exons to create a floxed line. *Tbx22*^{flox} animals did not show any phenotypic abnormalities. Subsequently, we removed the first three exons, including the start codon, the N-terminal repression domain, nuclear localization signal and part of the T-box domain, using a βactin-Cre deleter strain to create a *Tbx22*^{null} allele. This allele was bred onto a CD1 background. After initial inspection of *Tbx22*^{null} embryos (homozygous *Tbx22*$^{-/-}$ females or hemizygous *Tbx22*$^{-/Y}$ males) at embryonic day (E) 18.5 no palatal phenotype was immediately obvious. However, we then noticed a Mendelian imbalance in the survival of *Tbx22*^{null} pups after birth. Approximately 50% of these animals struggle to breathe and/or fail to suckle effectively resulting in death within 24 h. The stomach and intestine were filled with air rather than milk (Fig. 1A), similar symptoms to those described for other mouse models of CP (e.g. *Tgfb3*^{null}) (20). Close inspection of the orofacial morphology of

Tbx22^{null} embryos, showed an aberrant pattern of rugae in the posterior half of the hard palate, combined with an area of translucency in the posterior portion (Fig. 1B). A small number of *Tbx22*^{null} embryos (2/30) were identified with an overt CP (Fig. 1B). Detailed analysis of the secondary palate at E15.5 revealed that although fusion along the entire anterior–posterior axis was complete, the posterior hard palate was affected by severely reduced bone formation in all of the mutants analyzed ($n = 30$). This is illustrated by the lack of ossified bone matrix in haematoxylin and eosin (H&E) stained coronal sections of mutant compared with wild-type embryos (Fig. 1C).

Anomalies of the craniofacial skeleton

At E18.5, skeletal preparations of *Tbx22*^{null} mutants stained for bone and cartilage show an abnormal palatine process of the palatal bone and an under-developed vomer although the surrounding craniofacial skeleton is normal (Fig. 2). The palatine process provides the skeletal contribution to the posterior hard palate while the vomer sits anterior and rostral to the palate and is the supporting structure for the nasal cartilage and the secondary hard palate. The scale of bone loss can be seen in the bone surfaces generated from microCT scans of E18.5 embryos (Fig. 2B and Supplementary Material, Movies S1–S6). The mutant vomer is reduced in size and has not fused in the midline. Posterior palatal bone has formed in the dorsal–ventral direction but has not progressed in the lateral–medial direction. The total size of the vomer and palatine process is reduced by 74% (vomer) and 68% (palate) ($n = 4$). Together, these results are consistent with a SMCP phenotype.

Palatine bone deficiency results from a reduction in osteoblast maturation

To investigate the molecular mechanisms involving TBX22 in craniofacial development, we examined the expression of a number of genes known to play roles in palate development such as *Pax9*, *Snail*, *Msx1*, *Msx2*, *Bmp4*, *Osr1* and *Tgfb3*. With the exception of *Pax9* (discussed below) and a modest increase of *Msx2* in the posterior tongue, no significant differences in the levels or patterns of expression were detected in the developing craniofacial tissues of *Tbx22*^{null} embryos (Supplementary Material, Figs S2 and S3). Next, we investigated whether the resultant effect of TBX22 loss on palatine bone formation was through interference with the osteogenic process. Close inspection of coronal sections of the head at E15.5 shows a region of condensed mesenchyme in the mutant, but a complete lack of mineralized bone, as opposed to the wild-type control (Fig. 3A). This result implies that the impaired ossification is a direct result of osteoblasts failing to mature in the *Tbx22*^{null} mutant. Alkaline phosphatase activity, a marker for osteoblast activity is significantly reduced in the mutant palate, indicating that osteoblasts do not reach a mature enough status where they are capable of bone mineralization (Fig. 3B). The alkaline phoshatase activity in control sections shows that osteoblasts have differentiated and are actively involved in the ossification process. Although normal activity can be seen in the mutant's mandible, forming around Meckel's cartilage (Fig. 3B) and at anterior regions of the secondary palate (data not shown), only very low activity could be observed in the developing posterior palate.

To determine the effect of TBX22 loss on osteoblast differentiation, we analyzed the expression of *Runx2*, an early determinant of the osteoblast lineage from mesenchymal cells (21) in mutant animals. No difference in *Runx2* expression was observed at E13.5 between mutant and wild-type posterior palates (Supplementary Material, Fig. S3), while at E15.5 differences reflect the poor development of the bone matrix in *Tbx22*^{null} mutants (Fig. 3C). The area of expression is clearly smaller than the condensed mesenchyme weakly expressing alkaline phoshatase, indicating a reduced number of differentiated osteoblasts. Expression of *Runx2* in E15.5 *Tbx22*^{null} posterior palate resembles the *Runx2* expression pattern in E14.5 wild-type embryos (data not shown), indicating a delay of at least 1 day.

Tbx22^{null} mice have ankyloglossia and choanal atresia

Further comparative histological analysis of craniofacial structures between wild-type and *Tbx22*^{null} mouse embryos revealed a more anterior caudal attachment of the tongue to the mandible (Fig. 4A). This is similar to the shortened frenulum, frequently seen in human CPX patients with ankyloglossia. This feature was consistent in all mutant animals studied ($n = 30$), but does not extend to the tip of the tongue, representing a mild form of ankyloglossia. Another defect, this time not expected based on known CPX phenotypes, was choanal atresia. The choanae are located at the anterior end of the medial nasal prominence allowing air to flow from the nasal cavity into the oral pharynx, reaching the trachea. However, in *Tbx22*^{null} embryos, a persistent oro-nasal membrane (Fig. 4B), which narrows or blocks this passage, restricts nasal breathing. This defect is clearly illustrated in microCT scans of E18.5 embryos (Supplementary Material, Fig. S4). In severe cases, the choanae are blocked along their entire anterior–posterior length, although in milder cases only the posterior part of the choanae is obstructed. It is likely that the anterior position of the membrane will have a marked effect on the survival of the newborn pups. The most severe cases are incapable of nasal breathing, causing gasping for air and making suckling impossible for affected pups (Fig. 5A). Indeed, an investigation of *Tbx22*^{null} newborn pups suggests that the choanal phenotype is likely to be the main cause of the post-natal lethality. Choanal atresia was absent in all of the surviving male null animals analyzed but present in those that suffered a premature demise (Fig. 5B). In older, weaning stage animals, we observed that surviving mutants had a persistent notch in the posterior hard palate (Fig. 5C) indicating the SMCP, but with normal choanae. At E13.5, *Tbx22* expression is clearly detected in the medial and lateral nasal mesenchyme at the site where the oro-nasal fins occur (Supplementary Material, Figs S1 and 5D). In wild-type, *Pax9* expression overlaps in this region with *Tbx22*, although in the mutant the expression is both upregulated and the domain enlarged to span across the persistent oro-nasal membrane (Fig. 5D). These data are consistent with a possible role for PAX9 in the timely rupture of the oro-nasal membrane.

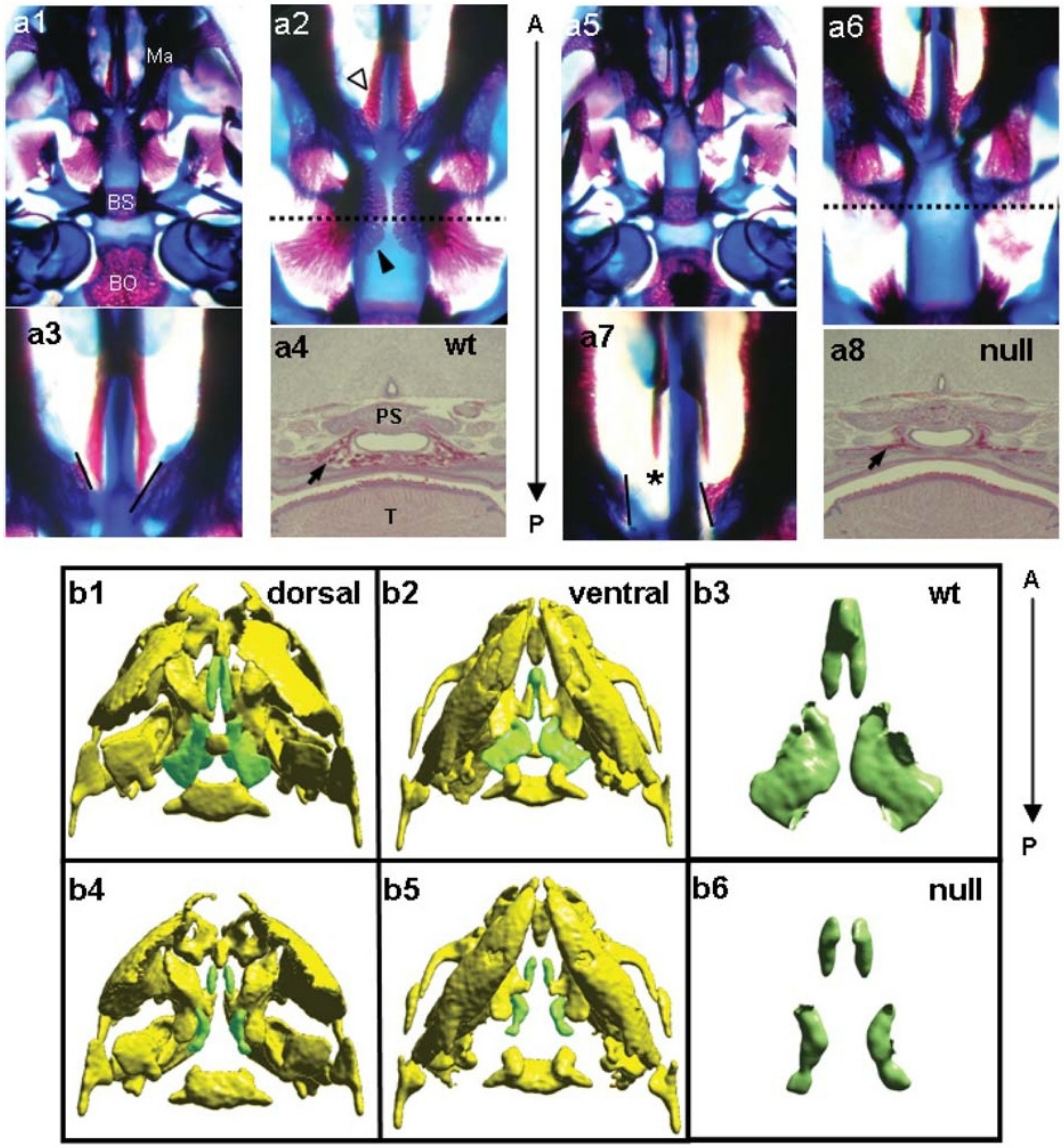

Figure 2. Loss of *Tbx22* causes bone phenotypes in the palate and vomer. (**A**) Ventral view of skeletal preparations with Alizarin Red (bone) and Alcian Blue (cartilage) of E18.5 embryos reveal reduced posterior palatal bones (black arrowhead), although anterior (maxillary) palatal bones (white arrowhead) are normal (a2,6). Additionally, the vomer is reduced (asterix in a7), visible after removing the maxillary palatine processes (black lines indicate cut surfaces). Coronal sections (a4,8; approximately at the level of the dotted lines in a2,6) stained with H&E show the mineralized palatine bone in wild-type embryos, although there is severely reduced mineralization in the $Tbx22^{null}$ embryo (black arrows). (**B**) Bone 3D surfaces generated from microCT scans of E18.5 day heads reveal the reduced size of the vomer and palatine bone (green). Occipital bone surfaces have been removed to facilitate dorsal view. BS = basisphenoid, BO = basoccipital, Ma = mandible, PS = presphenoid, T = tongue, A = anterior, *P* = posterior.

For all of the data presented in this study, the neo^{R} cassette is retained on the $Tbx22^{null}$ allele, however, no effects were attributable to its presence since identical phenotypes were also observed in mutants following *in vivo* excision with an Flp-deleter (data not shown). Similarly, the same spectrum of phenotypes and severity range was observed when the $Tbx22^{null}$ allele was crossed onto 129/SvJ and C57BL/6J strains and bred to >95% congenicity.

DISCUSSION

$Tbx22^{null}$ mice show multiple craniofacial defects that include submucous or overt CP, choanal atresia, reduced vomer and ankyloglossia, which are all consistent with its known expression pattern (12,18,19). Ankyloglossia was expected as it is a characteristic phenotype, frequently associated with CPX syndrome (8,9). Contrary to the variable penetrance in

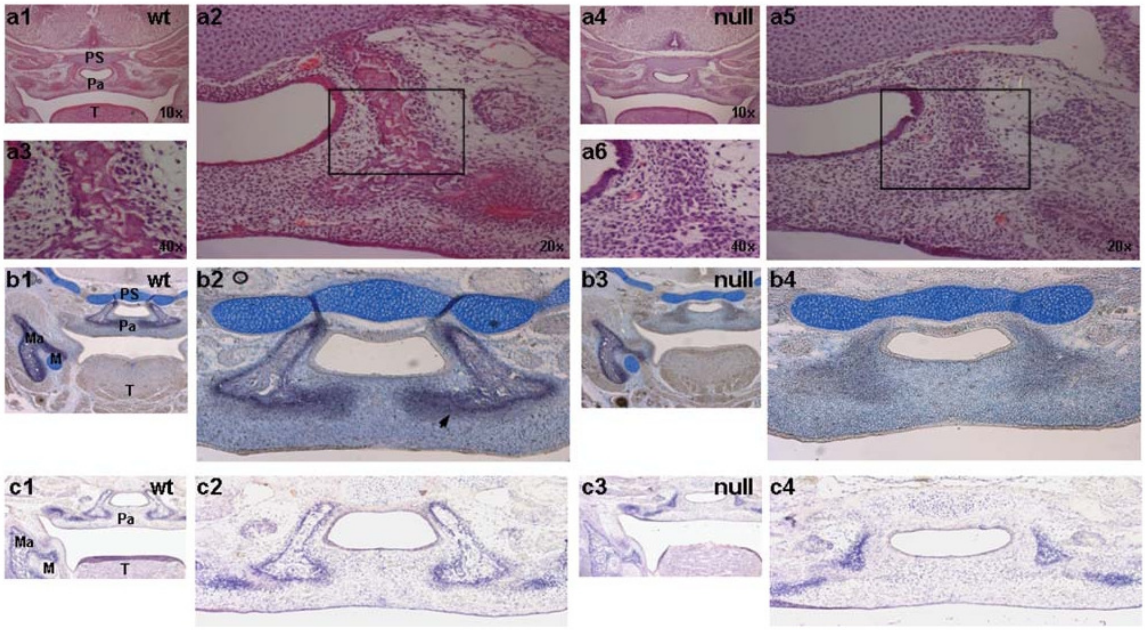

Figure 3. Reduced bone formation in the posterior hard palate is due to delayed maturation of osteoblasts. (**A**) H&E stained coronal sections of E15.5 embryos. In the wild-type, osteogenesis of the posterior palate is progressing normally with mineralized bone matrix visible (pink osteoid) on either end of the nasal passage (a1,2,3). In contrast, although condensation of mesenchyme can be observed in the *Tbx22*^{null}, mineralization is absent (a4,5,6). (**B**) Alkaline phosphatase activity assay on coronal sections of E15.5 embryos. In the wild-type, enzyme activity (purple) is observed in the osteoblasts on the edges of the posterior palatine osteogenic centre (arrow) (b1,2). In the *Tbx22*^{null}, alkaline phoshatase staining is severely reduced (b3,4). Sections are counter-stained with Alcian Blue. (**c**) *In situ* hybridization of coronal sections for *Runx2*. Expression can be detected in the developing mandible, palate and tooth buds in wild-type embryos (c1,2). *Tbx22*^{null} mutant embryos show reduced expression of *Runx2* in the posterior palate (c3,4). Ma = mandible, M = Meckel's cartilage, Pa = palate, PS = presphenoid, T = tongue.

CPX patients, this defect was detected in all *Tbx22*^{null} mice studied. The extent of the defect is variable but never as prominent or severe as that described in the *Lgr5* loss-of-function mutant (22). In these mice the defect is reported to be lethal, with null animals dying within 24 h of birth with empty, distended stomachs, filled with air. This is not unlike the *Tbx22*^{null} mice that fail to thrive except that the tongue defect is considerably milder. We suggest that other defects are more likely to be responsible for the prenatal demise observed.

Malformation of the vomer bone has not previously been discussed in relation to X-linked CP but has certainly been associated with both CP and SMCP. In a study of 30 patients undergoing surgery for SMCP, all were found to have vomerine malformations with the most frequently observed defect being a failure in vomer fusion with the rostral part of the palatal shelves (23). Similarly in a small series of fetuses the vomer was found to be poorly developed and also not fused in the region of the maxillary process in those with CP, which contrasted to the normal fetuses studied (24). We have not studied *Tbx22*^{null} mice at adult stages, but observations from around P12 also show the vomer to be severely underdeveloped. The vomer is thought to play a role in support of the secondary palate and also the development and separation of the choana. However, as choanal atresia is usually associated with a thickening of the vomer it may be more likely that these defects are independent (25). Nevertheless, the relevance of the vomer to SMCP and the pathology of VPI are currently unknown and in need of further investigation.

Our data, at least on the surviving *Tbx22*^{null} mice, suggests that they have an occult SMCP, where the palatal bone is affected, but the insertion of the palatine muscles into the aponeurosis, and the function of the palate, remains intact. Analysis of the posterior palatal bone has shown a distinct reduction of alkaline phoshatase in the development of the palatal bone, while expression of *Runx2* was intact at early stages, up to and including E14.5. Interestingly, TBX3 has recently been identified as a negative regulator of osteoblast differentiation in limb development with T-box binding sites identified in the regulatory regions of both *Runx2* and *Osterix* genes (26). Although we cannot exclude the possibility that the expression of *Runx2* is impaired by E15.5, the gross differences in palatal morphology between wild-type and mutant at this stage are already too large to make a direct comparison. These results therefore indicate a role for TBX22 in *Runx2*-independent and late differentiation of osteoblasts in the posterior palate. A delay of at least one embryonal day (as mirrored by the alkaline phoshatase expression) seems sufficient for a reduction in bone formation and function of the palate.

Whereas none of the craniofacial expressed genes we investigated were noticeably up or down regulated in *Tbx22*^{null} palates, we did observe an upregulation and broadening of the expression domain of *Pax9* throughout the persistent

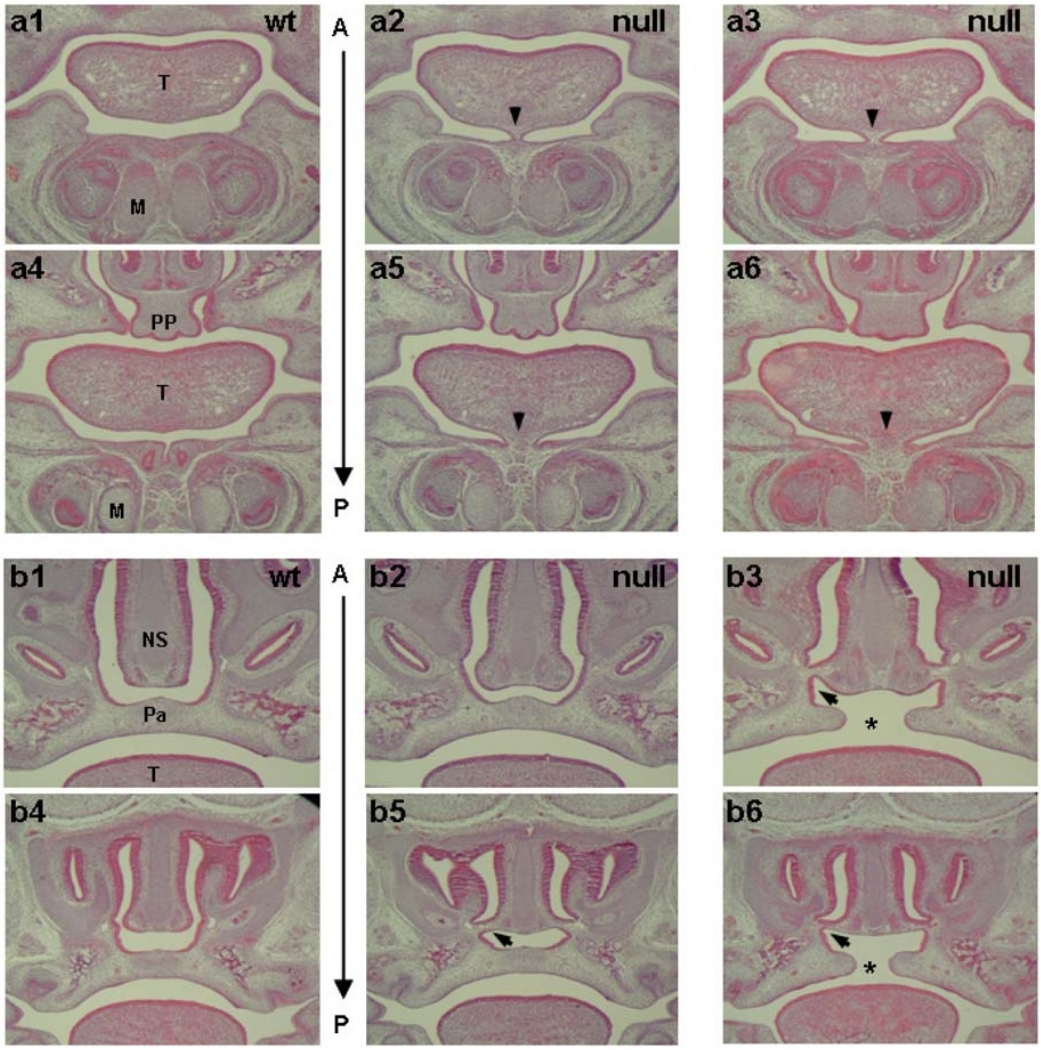

Figure 4. Phenotypic analysis of *Tbx22*^{null} mice. Embryos were collected at E15.5 and coronal sections were stained with H&E. (**A**) Ankyloglossia, or tongue-tie is observed in all mutant embryos (closed arrows in a2,3,5,6). In *Tbx22*^{null} mutants (a5,6), the tongue is usually attached caudally, at least as anteriorly as the incisive foramen, which is the transition between the primary and secondary palate, while at that point the tongue in the wild-type embryos is free (a4). (**B**) Choanal atresia is observed in mutant embryos with variable severity. In *Tbx22*^{null} embryos, a persistent oro-nasal membrane (arrows in b3,5,6) can be observed. M = Meckel's cartilage, NS = nasal septum, Pa = palate, PP = primary palate, T = tongue, A = anterior, *P* = posterior.

oro-nasal membrane. It is not yet clear if this is a direct effect, although both human and mouse *Pax9* promoters contain putative T-box binding sites in an area of sequence homology (>80%). Inappropriate expression of *Pax9* in the oro-nasal membrane could provide a possible explanation for its persistence since it is believed to promote cell survival, both by regulating the expression of genes involved in mediating cell proliferation and resistance to apoptosis (27). Although choanal atresia is not currently a recognized feature of CPX, this may in part be due to selection bias and will require specific investigation in the future. Choanal atresia has previously been described in combination with overt CP in CHARGE syndrome, which usually also includes other features such as coloboma, heart defects and growth restriction. About 60–80% of patients are estimated to be associated with haploinsufficiency of the gene *CHD7* (28) and mice mutant for this gene provides a useful model (29). Choanal atresia has also been described in the *Raldh3* null mouse mutant, which presents with a similar post-natal lethal respiratory distress phenotype, where the pups become cyanotic and die within 10 h (30). It is suggested that the persistence of the nasal fins may result from impairment to normal retinoic acid synthesis, which in turn down-regulates *Fgf8* expression in the nasal fins. The authors also demonstrate the prevention of choanal atresia using a maternal non-teratogenic dose of retinoic acid.

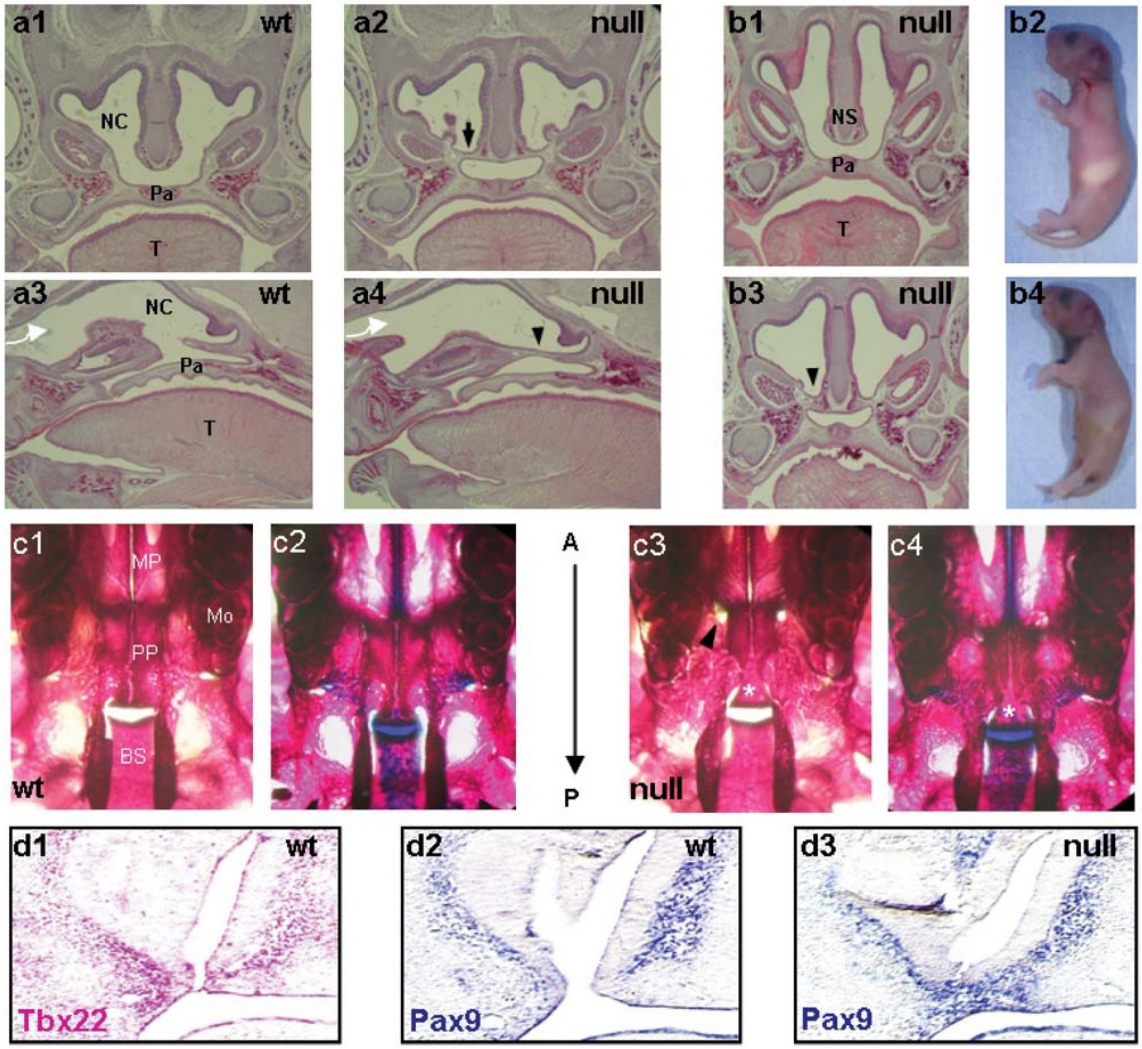

Figure 5. Choanal atresia is the likely cause of death in *Tbx22*^{null} mice. (**A**) In E18.5 embryos the choanal defect can be seen clearly in coronal (a1,2) as well as sagittal (a3,4) sections of the head. In the null animal (a2,4) the persistent oro-nasal membrane (black arrowhead) blocks the air-flow (white arrow) from the nostril into the oral pharynx and eventually the trachea. (**B**) When analyzing *Tbx22*^{null} littermates we observe that around half suckle successfully (b2), while the other half perish within 24 hours with breathing difficulties and air in the stomach (b4). (**C**) Skeletal preparations with Alizarin Red and/or Alcian Blue at postnatal day 12 in wild-type and *Tbx22*^{null} survivors show the extent of the submucous cleft as a notch in the posterior end of the hard palate at the cartilage between the basisphenoid and the presphenoid (asterisk). Palatine bone size is further reduced as is evident from the incomplete fusion with the maxillary part of the palatine bone (arrowhead). (**D**) *In situ* hybridizations showing expression of *Tbx22* (pink) and *Pax9* (blue) in lateral and medial nasal mesenchyme, either side of the choana. In *Tbx22*^{null} embryos, expression of *Pax9* can be observed in the persistent oro-nasal membrane. BS = basisphenoid, Mo = molar, MP = maxillary process, NC = nasal cavity, Pa = palate, PP = palatine process, T = tongue.

In contrast to many other CP mouse models where the specific genetic background had significant impact on either penetrance or severity, for example as described in the *Tgfb3* mutant (31), our analysis in CD1, 129Sv and C57Bl6 strains has shown similar phenotypes and with a similar penetrance for each. It is also interesting to note that unlike in the human, female heterozygote mutant mice are all unaffected whereas the null females are the same as male null animals. It will be interesting to determine whether these differences are due to additional genetic or environmental factors or differences in X-inactivation between mouse and human.

In summary, the *Tbx22*^{null} mouse has developmental defects similar to those found in patients with CPX and provides a new and unique model to understand the SMCP phenotype. Unlike overt clefts, this clinically recognizable form of SMCP has not been extensively studied in the mouse with only *Tshz1* and *Tgfbr2* mutants described with either cleft or premature truncation of the soft palate respectively (32,33). Both of these defects are restricted to soft palate development

and do not appear to involve the hard palate, which is a common cause of human SMCP. Since other mouse models for CP are frequently reported with less than 100% penetrance, our data suggests it might also be valuable to investigate the non-penetrant animals for intramembranous bone formation. The *Tbx22*^{null} model, clearly argues that SMCP is a continuous part of the same phenotypic spectrum. The precise molecular mechanism of the TBX22 transcriptional signaling cascade still remains to be determined but a failure in palatal osteoblast differentiation and maturation has been highlighted. A review of all CPX cases known to us suggests that SMCP is at least as common as overt CP (unpublished observations). This frequency might turn out to be even higher given a potential bias towards screening for *TBX22* mutations in overt CP cases. This study provides important new insight to further our understanding of common craniofacial birth defects and to initiate a proper exploration of the relationship between overt CP and SMCP.

MATERIALS AND METHODS

Generation of the *Tbx22*^{null} allele

The *Tbx22* targeting vector was generated by cloning genomic fragments, a loxP site and a loxP-frt-Neo-frt cassette into the pSP72 vector (Fig. 1A). The integrity of the targeting construct was confirmed by DNA sequencing. The vector was linearized and electroporated into 129/Sv embryonic stem (ES) cells (Kindly provided by E. Robertson). Successfully targeted G418 resistant clones were identified by PCR and confirmed by Southern blot analysis. Positive clones were used to generate chimera in C57BL/6J mice. Germline floxed mice (*Tbx22*$^{tm1(flox/exon0\text{-}2/NEO)Sta}$) were bred to β-actin-Cre mice to remove the first three exons and create a *Tbx22* deleted strain. This created the *Tbx22*$^{tm1.1(b\text{-}actin/Dexon0\text{-}2/NEO)Sta}$ allele, which we called *Tbx22*^{null}. Subsequently, mice were backcrossed onto CD1, 129/SvJ and C57BL/6J strains to >95% congenicity.

Histological analysis

Embryos were collected from *Tbx22*$^{+/-}$ females crossed with *Tbx22*$^{-/Y}$ males at different embryonic time points. Litters were dissected and fixed in 4% paraformaldehyde overnight. Embryos were paraffin-embedded, sectioned and stained with H&E. Alkaline phosphatase assay was performed by incubating deparaffinized sections with 0.5 mg/ml NBT/BCIP solution and counterstaining with Alcian Blue. Skeletal preparations were performed by removing the skin, fixing heads in 100% ethanol overnight, and staining in Alizarin Red and Alcian Blue solution, followed by clearing in 1% KOH for several days.

MicroCT imaging

Specimens were prepared and scanned as previously described (34). In brief, fixed fetuses were wrapped with a loose thin sponge and immersed in 1 × PBS in a plastic container then scanned on volumetric microCT scanner at 27 μm isometric voxel resolution using an eXplore Locus RS Small Animal MicroCT Scanner (GE Healthcare, London, ON, Canada). This volumetric scanner uses a 3500 × 1750 CCD detector for Feldkamp cone-beam reconstruction. The platform independent parameters of current, voltage and exposure time were kept constant at 450 μA, 80 kVP and 2000 ms, respectively. Additional scan parameters include 900 evenly spaced view angles (views) and 10 frames per view. Scan time was 400 min per sample. Images were reconstructed with the manufacturer's proprietary EVSBeam software. Images were analyzed and bone surfaces generated using Microview (version 2.0.29), ImageJ (version 1.41) and VAM (version 0.8.13).

In situ hybridization

For *in situ* hybridization, embryos were fixed overnight in 4% paraformaldehyde in PBS, dehydrated through graded alcohols, embedded in paraffin wax and sectioned at 8 μm thickness. Non-radioactive RNA *in situ* hybridization of tissue sections was performed as previously described (35). Dioxigenin-labeled *Tbx22* antisense riboprobe was generated with the *In vitro* Transcription kit (Roche Applied Science), and anti-digoxigenin-AP antibody (1 : 1000) (Roche Applied Science) was used to detect the hybridization signals.

URL

OMIM, http://www.ncbi.nlm.nih.gov/omim/.

SUPPLEMENTARY MATERIAL

Supplementary Material is available at *HMG* online.

ACKNOWLEDGEMENTS

We thank Massimo Signore (ES cell/chimera production service, UCL ICH), Zoe Webster and Jonathan Godwin (Transgenics and ES Cell laboratory, MRC/Imperial College London) for expert help with the generation of transgenic animals. We also thank Kit Doudney and James Grinham for technical assistance.

Conflict of Interest statement. None declared.

FUNDING

This work was supported by the Wellcome Trust [071494/Z/03/Z] and the Child Health Research Appeal Trust. Funding to pay the Open Access charge was provided by the Wellcome Trust.

REFERENCES

1. Murray, J.C. and Schutte, B.C. (2004) Cleft palate: players, pathways, and pursuits. *J. Clin. Invest.*, **113**, 1676–1678.
2. Stanier, P. and Moore, G.E. (2004) Genetics of cleft lip and palate: syndromic genes contribute to the incidence of non-syndromic clefts. *Hum. Mol. Genet.*, **13**, R73–R81.
3. Weatherley-White, R.C., Sakura, C.Y. Jr, Brenner, L.D., Stewart, J.M. and Ott, J.E. (1972) Submucous cleft palate. Its incidence, natural history, and indications for treatment. *Plast. Reconstr. Surg.*, **49**, 297–304.
4. Garcia, V.M., Ysunza, A., Hernandez, X. and Marquez, C. (1988) Diagnosis and treatment of submucous cleft palate: a review of 108 cases. *Cleft Palate J.*, **25**, 171–173.

5. Kelly, A.B. (1910) Congenital insufficiency of the palate. *J. Laryngol. Otol.*, **25**, 281–358.
6. Kaplan, E.N. (1975) The occult submucous cleft palate. *Cleft Palate J.*, **12**, 356–368.
7. Braybrook, C., Doudney, K., Marçano, A.C., Arnason, A., Bjornsson, A., Patton, M.A., Goodfellow, P.J., Moore, G.E. and Stanier, P. (2001) The T-box transcription factor gene TBX22 is mutated in X-linked cleft palate and ankyloglossia. *Nat. Genet.*, **29**, 179–183.
8. Marçano, A.C., Doudney, K., Braybrook, C., Squires, R., Patton, M.A., Lees, M.M., Richieri-Costa, A., Lidral, A.C., Murray, J.C., Moore, G.E. and Stanier, P. (2004) TBX22 mutations are a frequent cause of cleft palate. *J. Med. Genet.*, **41**, 68–74.
9. Suphapeetiporn, K., Tongkobpetch, S., Siriwan, P. and Shotelersuk, V. (2007) TBX22 mutations are a frequent cause of non-syndromic cleft palate in the Thai population. *Clin. Genet.*, **72**, 478–483.
10. Pauws, E. and Stanier, P. (2008) Epstein, C.J., Erickson, R.P. and Wynshaw-Boris, A. (eds), *Inborn Errors of Development*. Oxford University Press, New York, pp. 878–882.
11. Pauws, E. and Stanier, P. (2007) FGF signalling and SUMO modification: new players in the aetiology of cleft lip and/or palate. *Trends Genet.*, **23**, 631–640.
12. Braybrook, C., Lisgo, S., Doudney, K., Henderson, D., Marçano, A.C., Strachan, T., Patton, M.A., Villard, L., Moore, G.E., Stanier, P. and Lindsay, S. (2002) Craniofacial expression of human and murine TBX22 correlates with the cleft palate and ankyloglossia phenotype observed in CPX patients. *Hum. Mol. Genet.*, **11**, 2793–2804.
13. Andreou, A.M., Pauws, E., Jones, M.C., Singh, M.K., Bussen, M., Doudney, K., Moore, G.E., Kispert, A., Brosens, J.J. and Stanier, P. (2007) TBX22 missense mutations found in X-linked cleft palate (CPX) patients affect DNA binding, sumoylation and transcriptional repression. *Am. J. Hum. Genet.*, **81**, 700–712.
14. Pauws, E., Moore, G.E. and Stanier, P. (2009) A functional haplotype variant in the *TBX22* promoter is associated with cleft palate and ankyloglossia. *J. Med. Genet.*, **46**, 555–561.
15. Beaster-Jones, L., Horton, A.C., Gibson-Brown, J.J., Holland, N.D. and Holland, L.Z. (2006) The amphioxus T-box gene, AmphiTbx15/18/22, illuminates the origins of chordate segmentation. *Evol. Dev.*, **8**, 119–129.
16. Bush, J.O., Lan, Y. and Jiang, R. (2004) The cleft lip and palate defects in Dancer mutant mice result from gain of function of the Tbx10 gene. *Proc. Natl. Acad. Sci. U. S. A.*, **101**, 7022–7027.
17. Jerome, L.A. and Papaioannou, V.E. (2001) DiGeorge syndrome phenotype in mice mutant for the T-box gene, Tbx1. *Nat. Genet.*, **27**, 286–291.
18. Bush, J.O., Lan, Y., Maltby, K.M. and Jiang, R. (2002) Isolation and Developmental Expression Analysis of Tbx22, the Mouse Homolog of the Human X-linked Cleft Palate Gene. *Dev. Dyn.*, **225**, 322–326.
19. Haenig, B., Schmidt, C., Kraus, F., Pfordt, M. and Kispert, A. (2002) Cloning and expression analysis of the chick ortholog of TBX22, the gene mutated in X-linked cleft palate and ankyloglossia. *Mech. Dev.*, **117**, 321–325.
20. Proetzel, G., Pawlowski, S.A., Wiles, M.V., Yin, M., Boivin, G.P., Howles, P.N., Ding, J., Ferguson, M.W. and Doetschman, T. (1995) Transforming growth factor-beta 3 is required for secondary palate fusion. *Nat. Genet.*, **11**, 409–414.
21. Schroeder, T.M., Jensen, E.D. and Westendorf, J.J. (2005) Runx2: a master organizer of gene transcription in developing and maturing osteoblasts. *Birth Defects Res. C. Embryo. Today*, **75**, 213–225.
22. Morita, H., Mazerbourg, S., Bouley, D.M., Luo, C.W., Kawamura, K., Kuwabara, Y., Baribault, H., Tian, H. and Hsueh, A.J. (2004) Neonatal lethality of LGR5 null mice is associated with ankyloglossia and gastrointestinal distension. *Mol. Cell. Biol.*, **24**, 9736–9743.
23. Grzonka, M.A., Koch, K.H., Koch, J. and Glindemann, S. (2001) Malformation of the vomer in submucous cleft palate. *J. Craniomaxillofac. Surg.*, **29**, 106–110.
24. Hansen, L., Nolting, D., Holm, G., Hansen, B.F. and Kjaer, I. (2004) Abnormal vomer development in human fetuses with isolated cleft palate. *Cleft Palate Craniofac. J.*, **41**, 470–473.
25. Molina-Martinez, C., Guilemany-Toste, J.M., Cervera-Escario, J. and Bernal-Sprekelsen, M. (2009) Stucker, F., de Souza, C., Kenyon, G., Lian, T., Draf, W. and Schick, B. (Eds), *Rhinology and Facial Plastic Surgery*. Springer, Berlin Heidelberg, pp. 685–690.
26. Govoni, K.E., Linares, G.R., Chen, S.T., Pourteymoor, S. and Mohan, S. (2009) T-box 3 negatively regulates osteoblast differentiation by inhibiting expression of osterix and runx2. *J. Cell. Biochem.*, **106**, 482–490.
27. Robson, E.J.D., He, S.-J. and Eccles, M.R. (2006) A PANorama of PAX genes in cancer and development. *Nat. Rev. Cancer*, **6**, 52–62.
28. Vissers, L.E., van Ravenswaaij, C.M., Admiraal, R., Hurst, J.A., de Vries, B.B., Janssen, I.M., van der Vliet, W.A., Huys, E.H., de Jong, P.J., Hamel, B.C. *et al.* (2004) Mutations in a new member of the chromodomain gene family cause CHARGE syndrome. *Nat. Genet.*, **36**, 955–957.
29. Bosman, E.A., Penn, A.C., Ambrose, J.C., Kettleborough, R., Stemple, D.L. and Steel, K.P. (2005) Multiple mutations in mouse Chd7 provide models for CHARGE syndrome. *Hum. Mol. Genet.*, **14**, 3463–3476.
30. Dupe, V., Matt, N., Garnier, J.M., Chambon, P., Mark, M. and Ghyselinck, N.B. (2003) A newborn lethal defect due to inactivation of retinaldehyde dehydrogenase type 3 is prevented by maternal retinoic acid treatment. *Proc. Natl. Acad. Sci. U. S. A.*, **100**, 14036–14041.
31. Martinez-Sanz, E., Del, R.A., Barrio, C., Murillo, J., Maldonado, E., Garcillan, B., Amoros, M., Fuerte, T., Fernandez, A., Trinidad, E. *et al.* (2008) Alteration of medial-edge epithelium cell adhesion in two Tgf-beta3 null mouse strains. *Differentiation*, **76**, 417–430.
32. Core, N., Caubit, X., Metchat, A., Boned, A., Djabali, M. and Fasano, L. (2007) Tshz1 is required for axial skeleton, soft palate and middle ear development in mice. *Dev. Biol.*, **308**, 407–420.
33. Xu, X., Han, J., Ito, Y., Bringas, P. Jr, Urata, M.M. and Chai, Y. (2006) Cell autonomous requirement for Tgfbr2 in the disappearance of medial edge epithelium during palatal fusion. *Dev. Biol.*, **297**, 238–248.
34. Vasquez, S.X., Hansen, M.S., Bahadur, A.N., Hockin, M.F., Kindlmann, G.L., Nevell, L., Wu, I.Q., Grunwald, D.J., Weinstein, D.M., Jones, G.M. *et al.* (2008) Optimization of volumetric computed tomography for skeletal analysis of model genetic organisms. *Anat. Rec. (Hoboken)*, **291**, 475–487.
35. Wilkinson, D.G. (1998) *In Situ Hybridization: A Practical Approach*. IRL Press, Oxford.